UNIVERSITY OF LATVIA

FACULTY OF PHYSICS, MATHEMATICS AND
OPTOMETRY

INTERFACE SMEARING AND GRAVITY EFFECTS ON MAGNETIC MICRO-CONVECTION

Lāsma Puķina-Slava

A thesis presented for the degree of
Doctor of Physics

Thesis advisors: Prof. Andrejs Cēbers, Dr. Guntars Kitenbergs

Riga, 2023

ABSTRACT

In this study an active mixing with a magnetic micro-convection of two miscible fluids: water and water based magnetic fluid in a vertical microfluidics chip is investigated. The magnetic micro-convection is a finger-like instability occurring on the interface between magnetic and non-magnetic fluid exposed to an external magnetic field above a certain threshold. A ponderomotive force of the non-homogeneous self-magnetic field of the magnetic fluid causes this instability. In this work, the magnetic micro-convection is induced by two different experimental setups with different directions of the external magnetic field.

The properties of this instability can be easily manipulated by altering experimental components. This makes the magnetic micro-convection interesting for fundamental studies as some behaviors and their contributors of this instability are yet to be found. In addition, the magnetic micro-convection can enhance the mixing in microfluidics and lab-on-a-chip devices where normally laminar fluid flows and slow diffusion processes are typical.

In this work, the information about various parameters governing and characterizing the instability is collected: the critical magnetic fields, the mixing dynamics and enhancement, the wavelength of the finger-like instabilities and the form of the fingers of the instability, the interface thickness at the beginning of an experiment between both fluids, the characteristic size of used microfluidics chips as well as various magnetic and hydrodynamic properties of the used magnetic fluids. The relevance and influence of these parameters on the dynamics of the micro-convection are deduced and compared experimentally.

Here, the influence of magnetic and gravitational fields in the stabilization of the magnetic micro-convection is investigated, quantifying how the magnetic field is governing and the gravity is stabilizing the instability. The dynamics of the magnetic micro-convection in horizontal and vertical external magnetic fields are compared with each other. The study is mostly experimental, the experimental results are discussed and compared to theoretical predictions and numerical simulations done by colleagues. The comparison is done qualitatively by comparing video and images in addition to quantitative representation using two dimensionless quantities- magnetic and gravitational Rayleigh numbers. The experimental results are in agreement with the numerical simulations.

The results show that the magnetic micro-convective mixing is restricted by the amount of initial smearing. The mixing enhancement due to the magnetic micro-convection is smaller for a larger initial interface thickness, while the mixing can be amplified by increasing the magnetic field. Also, the shape and thickness of the micro-channel affect the

results. The properties of magnetic fluids significantly influence the mixing dynamics. It is demonstrated that gravity minimizes the magnetic micro-convection by using magnetic fluids with different densities. Also it is demonstrated that the direction of the external magnetic field affects the shape of the instability fingers and the effectiveness of the mixing. For the same values of the external magnetic field the fingers of the instability grow taller in horizontal magnetic field that is perpendicular to the microfluidics chip than in the vertical magnetic field that is parallel to the microfluidics chip.

ANOTĀCIJA

Šajā disertācijā tiek pētīta aktīvā samaisīšanās ar magnētisko mikrokonvekciju vertikālā mikrofluīdikas čipā starp diviem sajaukties spējīgiem šķidrumiem- ūdeni un ūdens bāzes magnētisko šķidrumu. Magnētiskā mikrokonvekcija ir pirkstveida nestabilitāte, kas veidojas robežvirsmā starp magnētisku un nemagnētisku šķidrumu, ja tie ir pakļauti ārējam magnētiskam laukam, kas ir lielāks par kādu kritisko vērtību. Šo nestabilitāti izraisa nehomogēna pašmagnētiska lauka izraisītais spēks magnētiskajā šķidrumā. Šā darba ietvaros magnētiskā mikrokonvekcija tiek ierosināta divās dažādās eksperimentālās sistēmas modifikācijās ar atšķirīgu ārējā magnētiskā lauka virzienu.

Magnētiskās mikrokonvekcijas raksturlielumi ir viegli manipulējami, pamainot eksperimentālas komponentes. Tādēļ magnētiskā mikrokonvekcija ir ērta fundementāliem zinātniskiem pētījumiem, kuros iespējams atrast kādas jaunas likumsakarības starp magnētisko mikrokonvekciju un tās ierosinātajiem. Magnētiskā mikrokonvekcija var uzlabot maisīšanos mikrofluīdikas iekārtās, kurās parasti šķidrumu maisīšanās ir lēna un plūsmas ir lamināras.

Šajā darbā apkopota plaša informācija par dažādiem šo nestabilitāti raksturojošiem un regulējošiem eksperimentālajiem parametriem,tādiem kā piemēram, kritiskie magnētiskie lauki, maisīšanās dinamika un pienesums, nestabilitāti raksturojošais viļņa garums un pirkstu forma, sākuma samaisīšanās joslas platums, raksturīgie mikrofluīdikas čipu izmēri un citas magnētiskās un hidrodinamiskās magnētisko šķidrumu īpašības. Šo parametru ietekme uz magnētisko mikrokonvekcijas dinamiku tiek salīdzināta dažādiem eksperimentiem.

Tiek salīdzināta magnētisko un gravitācijas lauku ietekme uz magnetiskās mikrokonvekcijas stabilizāciju, aprēķinot kā magnētiskais lauks ierosina un gravitācija stabilizē šo nestabilitāti. Magnētiskās mikrokonvekcijas attīstības dinamika tiek savstarpēji salīdzināta starp eksperimentiem vertikālā un horizontālā ārējā magnetiskajā laukā. Šajā darbā aprakstītais pētījums lielākoties ir eksperimentāls, taču eksperimentālie rezultāti tiek salīdzināti ar kolēģu veiktajām teorētiskajām prognozēm un skaitliskaiem modeļiem. Tiek veikts gan kvalitatīvs salīdzinājums, izmantojot nestabilitāti raksturojošos videomateriālus un attēlus, gan kvantitatīvs salīdzinājums, izmantojot divus bezdimensionālus lielumus-magnētisko un gravitācijas Releja skaitļus. Eksperimentālajos un skaitlisko modeļu rezultātos vērojama laba savstarpējā atbilstība.

Darbā apkopotie rezultāti apliecina, ka magnētisko mikrokonvekciju ierobežo šķidrumu savstarpējā sajaukšanās pirms eksperimenta. Samaisīšanās pienesums ir mazāks, ja sākotnēji šķidrumi sajaukušies vairāk. Maisīšanos var pastiprināt, palielinot ārējo magnētisko lauku. Izvēlētā mikrofluīdikas kanāla biezums un forma maina rezultātus. Magnētisko mikrokonvekciju ietekmē arī izvēlētā magnētiskā šķidruma īpašības. Šajā darbā ir de-

monstrēts kā gravitācija ierobežo maisīšanos ar magnētisko mikrokonvekciju, izmantojot magnētiskos šķidrumus ar dažādiem blīvumiem. Kā arī darba rezultāti apliecina, ka ārējā magnētiskā lauka virziens ietekmē gan nestabilitātes raksturīgo formu, gan samaisīšanās efektivitāti. Vienāda stripruma ārējā magnētiskajā laukā nestabilitātes pirksti izaug garāki, ja magnētiskais lauks ir horizontāls un perpendikulārs mikrofluīdikas čipam, nevis vertikāls un paralēls mikrofluīdikas čipam.

Atslēgvārdi: Magnētiskie šķidrumi, Mikrokonvekcija, Nestabilitātes, Gravitācija, Mikrofluīdika

ACKNOWLEDGEMENTS

This dissertation would not have been completed without help and support of my colleagues, family, and friends whom I want to thank here.

I want to thank my thesis advisors Dr. Guntars Kitenbergs and Prof. Andrejs Cēbers who guided this study from its very beginning to the finish. Special thanks to Dr. Guntars Kitenbergs for proposing me this research direction.

I also want to thank my colleagues for both practical and emotional support during my PhD studies. I thank Dr. Delphine Talbot (PHENIX lab, Sorbonne University in Paris, France) and Dr. Oksana Petričenko for the magnetic fluids used within this study. Thanks to Dr. Andrejs Tatuļčenkovs for theoretical results, Dr. Ivars Driķis for an Android based synchronization solution for microfluidics pumps, and Michail Maiorov (IPUL) for magnetic measurements. My gratitude goes to Dr. Gökhan Ergin for the opportunity to work with 3D micro-PIV system in Dantec Dynamics, Denmark.

Thanks for general support and fruitful discussions to my colleagues: Dr. Viesturs Šints, Dr. Andris P. Stikuts, Dr. Aigars Langins, Dr. Jānis Cīmurs. For fun, mental support and useful tips thanks to my dear steministas Dr. Tija Sīle, Maija Sjomkāne, Malvīne N. Strakova, Līga Jasulaņeca and my best friend Marta Berķe.

Another level of gratitude I express to my emotional, technical and every-other-way possible support, my husband Eduards Puķins-Slava.

And at last I also want to thank myself for believing in myself and bringing this personal project to completion (see fig. 1.).
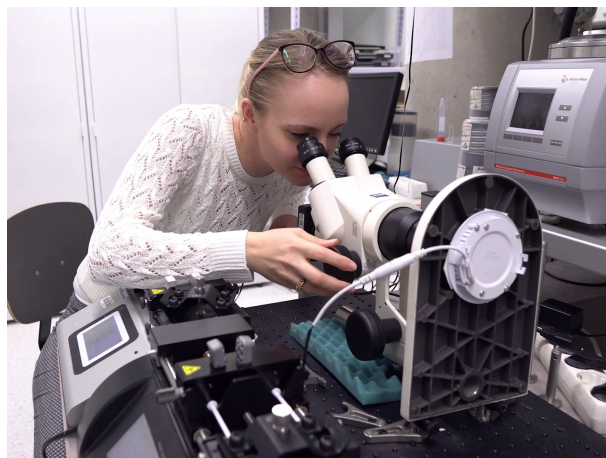
1. Figure: A picture of me looking at magnetic micro-convection through a microscope

CONTENTS

INTRODUCTION

In this dissertation, two different types of instabilities on the interface between two miscible fluids- water and water based magnetic fluid are investigated experimentally. Magnetic fluid is a colloidal solution of magnetic nano-sized particles suspended in a carrier fluid [1, 2]. Magnetic fluids possess both magnetic and hydrodynamic properties therefore making them a compelling research subject [3].

The instabilities in this work are initiated and can be regulated by external magnetic field. When exposed to magnetic fields, various instabilities emerge on the interface between magnetic and nonmagnetic fluids [1, 2, 4–6]. Two of these instabilities are broadly investigated in this study. As the characteristic size of the instability is in the scale of microns, these instabilities are termed magnetic micro-convection. Magnetic micro-convection is a finger-like instability occurring on an interface between magnetic and non-magnetic fluid, caused by a pondermotive force acting on the magnetic fluid in an applied homogeneous magnetic field [7, 8]. Magnetic micro-convection enhances the mixing between the fluids in the experimental system investigated here. This mixing enhancement-mixing length due to magnetic micro-convection is one of the main parameters explored.

The spatial parameters of the system under the study are also in the scale of microns as the mixing fluids are investigated in a Hele-Shaw cell-like microfluidics chip. Therefore the term microfluidics is in the title of this work. This leads to the fact that different fields of physics are combined within this study.

Magnetic micro-convection in vertically placed various microfluidics chips is induced in two different experimental setups within the scope of this study. In one of the setups the external magnetic field is horizontal and perpendicular to the microfluidics chip whereas in the other one the external magnetic field is vertical and parallel to the microfluidics chip.

Although the systems of interest are in the scale of microns, gravity plays a role restricting the growth of the patterns of the magnetic micro-convection. The significance of gravity in small systems and also particularly for this instability has been proposed before [9]. The influence of magnetic and gravitational fields with a set of other experimental parameters on the dynamics of micro-convection is investigated in detail in this study. This work is mostly an experimental study, the experimental results are compared to theoretical predictions and numerical simulations carried out by colleagues. The comparison is done both qualitatively by visual materials of the instability as well as quantitatively. For a quantitative comparison two dimensionless quantities- magnetic and gravitational Rayleigh numbers are used, quantifying how the magnetic field is governing and the gravity is stabilizing the magnetic micro-convection.

The magnetic fluids and hydrodynamic instabilities related to this topic have been studied for a considerable time as the terms magnetic fluid or ferrofluid have been defined already in the 1970's [1, 10]. Meanwhile, the microfluidics is a relatively newer topic that has been studied interdisciplinary, especially in life sciences [11, 12] and in search for different solutions for micro-mixers [13–15]. As microfluidics handle liquids within sub-millimeter ranges, small Reynolds numbers are typical. This means that flows in microfluidics are mostly laminar and despite many studies, one of the challenges that still is being addressed in the field of microfluidics are the physical limitations for mixing, as by itself it happens as a slow diffussion process. One way to enhance this mixing rapidly in a contact-less manner is to use magnetic materials and fields [14] as done in this work.

The magnetic mixing in the scope of microfluidics proposes various research topics, as many different instabilities on the interface between magnetic and non-magnetic fluids can be induced [1, 2, 6]. The nature of the patterns formed by these instabilities depends upon many factors. For example a shape of the interface between the fluids, the direction of the magnetic field, the dimensions of the microfluidics-chip and others [16–18]. Most of these properties can be easily manipulated by altering experimental components, as it is done in this study by using various magnetic fluids with different magnetic and hydrodynamic properties as well as by changing the orientation of the external magnetic field and using differently sized microfluidics chips.

Over the years magnetic fluids have had several practical applications in industry and medicine [1, 2, 19–21], but the magnetic micro-convection itself, besides promising applications in the fluid mixing, has aroused an interest as an academic research topic, both experimentally [6, 22] and theoretically [6, 23, 24]. This work was motivated mostly by this academic curiosity to better understand the dynamics of the magnetic micro-convection and the impact of the factors that affect it.

Goal of thesis and set tasks

For this study the following goal and tasks have been formulated.

Goal

Investigate how the dynamics and size characteristics of the magnetic micro-convection on the interface between two miscible fluids is affected by various factors- gravity, the strength and intensity of the external magnetic field, the thickness of the already pre-mixed interface between two fluids, the thickness of the micro-channel and the properties of the magnetic fluid.

Hypotheses

During this thesis following hypotheses were formed:

- Micro-convective mixing in horizontal magnetic field will be more effective than mixing in a vertical magnetic field as the fingers of this instability have more active character in a horizontal magnetic field.

- The total mixing length that consists of micro-convective mixing and diffusive mixing can be achieved by a specific value of external magnetic field and does not depend on the thickness of the pre-mixed layer between the fluids.

- The value of the critical magnetic field for a certain amount of the initial smearing of the interface between the mixing fluids is the same value of the magnetic field that must be applied to obtain total mixing length equal this initial smearing.

Tasks

To achieve the goal of this thesis following tasks were formed:

1. Characterize the existing experimental system for experiments in horizontal, external magnetic field perpendicular to the microfluidics chip. Perform the experiments using this experimental system to observe the magnetic micro-convection in flowing fluids.

2. Improve and modify the experimental system for observing the magnetic micro-convection for initially stagnant fluids in two different orientations of external magnetic field; characterize the experimental system.

3. Perform the experiments to observe the magnetic micro-convection for initially stagnant fluids both in horizontal and vertical external magnetic field.

4. Collect the data of the various factors that govern and characterize magnetic micro-convection during the experiments and write the software code to process this data.

5. Analyze the magnetic micro-convection on a miscible fluid interface. Find out how gravity, pre-mixed interface thickness and the orientation of the external magnetic field affect the mixing efficiency due to the magnetic micro-convection.

6. Compare the experimental results of this work with the theory and numerical simulations done by colleagues as well as give the possible reasons for the differences between these results.

All of these tasks were accomplished. The results are presented in this thesis in the 4 chapters with complementary information in appendices. The experimental results of this work have been presented in 7 reports in international conferences, published in one paper [25], and two papers that includes the results presented in the §3.2. [26] and §3.3. are prepared for publishing. The results of this work confirmed the first and the second

hypotheses. The third hypothesis was confirmed qualitatively for instability in a horizontal magnetic field. Results show some correlation between the critical magnetic field for a certain initial smearing with the total mixing length within such magnetic field. But whether total mixing length does depend on the thickness of the pre-mixed layer between the fluids is inconclusive for the results in the vertical magnetic field due to data dispersion and this phenomenon should be investigated further.

The experimental work of this thesis was carried out in the Laboratory of Magnetic Soft Materials in University of Latvia in Riga, except for a brief experimental investigation of the fluid flows in a horizontal microfluidics chip with stereo micro-PIV system that was carried out in Dantec Dynamics in Denmark. All of the experimental results collected in §3. are obtained and processed by the author of this thesis. The experimental system is manipulated, the microfluidics chips are produced and flow simulation in the microfluidics chip as described in §2. also are done by the author of this thesis. The theoretical predictions and numerical simulations presented in §4. are carried out by colleagues in MMML and found in the literature, but the comparison with the experimental data is carried out by the author of this thesis. Brief information about the chapters is given further in the structure of the thesis.

Structure of thesis

- The theoretical concepts that are important for this study along with the corresponding literature review are presented in chapter §1.. In §1.1. information about the unit systems used within this work is briefly described. §1.2. reviews the concepts and challenges in microfluidics. The topic of magnetic fluids is explored in §1.3. with subsections that explore deeper the concepts of colloidal stability in §1.3.1., preparation of magnetic fluids in §1.3.2., various properties of magnetic fluids are reviewed in §1.3.3. and the magnetic nano-particle diffusion in magnetic fluid is described in §1.3.4.. The theory of magnetic micro-convection is reviewed in §1.4. with theoretical concepts of Particle image velocimetry in §1.4.1.. The review of the previous studies about magnetic micro-convection that have led to the forming of this work is presented in §1.4.2..

- In chapter § 2. the magnetic fluids used within this study, experimental setup and data processing are described. Tasks 1, 2 and 4 are partially addressed here. In §2.1. the properties of the magnetic fluids used within this study are explored. The experimental systems used to characterize the magnetic fluids are briefly reviewed in §2.1.1. and §2.1.2.. The experimental system used for 3-dimensional velocity field measurements to explore the flow of the fluids with different densities in a horizontally placed microfluidics chip is described in §2.2.. The section §2.3. reviews the fabrication methods and properties of the microfluidics chips used within this

work. Various experimental setups used within this work to explore the magnetic micro-convection are thoroughly described in §2.4. and its three subsections: §2.4.1. setup variation for experiments with continuous fluid flow, §2.4.2. for experiments with initially stagnant fluids in a horizontal magnetic field and §2.4.3. for experiments in vertical magnetic field.

- The results of the 4th and 5th tasks with the experimental observations are collected in chapter §3. that is divided in 5 sections. The experimental observations and results from experiments with continuous fluid flow are collected in §3.1. that addresses a part of the first task. Also the results from this section are published in [25]. Experiments carried out with the improved experimental system for initially stagnant fluids are reviewed in §3.2., hence undertaking the 3rd task of these thesis. A publication about the results presented within this section is prepared [26]. Next the effect of the thickness of the premixed interface layer between the mixing fluids on the magnetic micro-convection is explored. The results of the experiments in a horizontal external magnetic field are collected in §3.3., thus addressing part of the 3rd task. Another publication about the results presented within this section is also prepared. The results of the experiments in a vertical external magnetic field addressing the 4th task are reviewed in §3.4.. Within these sections the magnetic micro-convection with respect to various experimental parameters is investigated. The critical magnetic field for the instability to emerge, characteristic size of the instability, mixing enhancement due to magnetic micro-convection, effects of the thickness of the microfluidics chip are explored here. And in the last section §3.5. results collected from stereo micro-PIV system are collected. This part of the research was carried out in Dantec Dynamics, Denmark. The velocity field of the fluid flow in a horizontally placed microfluidics chip was investigated here.

- The 5th and 6th tasks are carried out in the discussion in §4.. Here the results of this thesis are compared with each other as well as with theoretical predictions and numerical simulations carried out by colleagues.

- The chapters of this work are followed by conclusions in that are are arranged in four groups according to the four main experimental sections that explore magnetic micro-convection.

- In appendices a complementary information to this thesis is provided.

PARTIAL GLOSSARY

Characteristic quantity

χ Magnetic susceptibility

η Viscosity

μ Magnetic permeability

ϕ Volume fraction

ρ Density

B Magnetic induction

c Concentration

H Magnetic field strength — magnetic intensity

Ra_{g} Gravitational Rayleigh number

Ra_{m} Magnetic Rayleigh number

Re Reynolds number

Physical constants

ϵ_0 Electric constant — vacuum permittivity

μ_0 Magnetic constant — vacuum magnetic permeability

g Standard gravity

k_B Boltzmann constant

Abbreviations

DLS Dynamic Light Scattering

MF Magnetic fluid

PIV Particle image velocimetry

ROI Region of interest

VSM Vibrating sample magnetometer

Denotations of experimental quantities

2δ Mixing length

δ_0 Initial smearing thickness

δ_{MC} Mixing thickness due to the magnetic micro-convection

t_0 Dimensionless initial smearing time

1. Chapter

Theoretical concepts

1.1. Systems of units in this work

Within this study different unit systems are used: depending on the convenience either SI unit system and its conjunction units or the Gaussian unit system- sometimes referred as CGS system for centimeter, gram and second. The Gaussian system is used within this work for some of the experimental data to simplify comparison between the experimental results of this work to the theoretical predictions and numerical simulations done by colleagues. The Gaussian unit system is favored in the theoretical physics community accordingly as well as by colleagues in the Laboratory of Magnetic Soft Materials, who work in the theoretical field. In this unit system no base units for vacuum in electromagnetism are necessary, in other words, the ϵ_0 and μ_0 constants are equal to 1 [27], unlike in the SI unit system due to the different definitions of electric current and a charge [28].

The literature [27, 28] tells a rather eventful story about a bit chaotic historic evolution of the various unit systems in electromagnetism and then sometimes confusing transition from one unit system to another one. The conversion of units in mechanics between the SI and the Gaussian unit systems is rather simple differing only by some factor of ten. The situation is a bit more difficult when converting quantities in electromagnetism, especially when using dimensionless quantities.

Bellow in the table 1.1. of magnetic quantities used within this work the conversion formulas for these quantities between the Gaussian unit system and SI unit system are collected.

Quantity	Conversion
Magnetic induction	$B^{\mathrm{CGS}}[\mathrm{G}] = 10^4 B^{\mathrm{SI}}[\mathrm{T}]$
Magnetic field strength/ Magnetic intensity	$H^{\mathrm{CGS}}[\mathrm{Oe}] = \frac{4\pi}{10^3} H^{\mathrm{SI}}\left[\frac{\mathrm{A}}{\mathrm{m}}\right]$
Magnetization (=moment per volume)	$M^{\mathrm{CGS}}[\mathrm{Oe}]$ or $\left[\frac{\mathrm{emu}}{\mathrm{cm}^3}\right] = 10^{-3} M^{\mathrm{SI}}\left[\frac{\mathrm{A}}{\mathrm{m}}\right]$
Magnetic permeability	$\mu^{\mathrm{CGS}} = \frac{\mu^{\mathrm{SI}}}{\mu_0}$
Magnetic susceptibility	$\chi^{\mathrm{CGS}} = \frac{1}{4\pi}\chi^{\mathrm{SI}}$
	$B^{\mathrm{SI}}[\mathrm{T}] \rightarrow \mu_0 H\left[\frac{\mathrm{A}}{\mathrm{m}}\right] \rightarrow 10^4 B^{\mathrm{CGS}}[\mathrm{G}] \rightarrow 10^4 H^{\mathrm{CGS}}[\mathrm{Oe}]$

1.1. Table: Conversion of magnetic units between the Gaussian (CGS) unit system and SI unit system

1.2. Microfluidics

Microfluidics is the science of manipulating and controlling fluids of small volumes, where one or all of the spatial dimensions are in the scale of microns. Microfluidics can miniaturize many laboratorial fluid manipulation processes like filtration, mixing, reaction, rheometric measurements and others [29]. It is widely implemented in various science fields, for example, biotechnology, chemistry, engineering or physics [30–33]. Due to the wide range of multidisciplinary applications of the microfluidics, it has been for some time and still is an active research topic [34–36].

There are many practical advantages to microfluidical devices, for example, only a small amount of reagents is necessary for microchemical reactors, the possibility of numerical geometry optimizations, smaller inertial effects, optical access and a direct characterization of the fluid-flow dynamics and others [29].

Microfluidics devices can be fabricated from various materials depending on the application of the device. Common materials are silicon, metal, polydimethylsiloxane (PDMS) and other polymer materials. Advantages of the polymer material based microfluidics device include relatively simple production, optical transparency to visible light, durability and chemical inertness just to mention a few. Though their shortcomings include low thermal stability and high compressebility. PDMS is the most commonly used elastomer in the production of microfluidics devices as it offers relatively simple fabrication and good sealing to various materials, low cost and biocompatibility, and versatility. The production steps of PDMS microfluidics devices has been widely described in literature [29, 35]. Microfluidics-chips used within this study are made from PDMS or from Parafilm M® spacer and glass. Effective, precise and reproducible microfluidics chip fabrication methods like soft lithography requires cleanroom and lithography tools [29, 35]. Within this study microfluidics chips are produced effectively with cheaper and easier method, albeit this limits reproducibility. The production and characterization of the used microfluidics-chips

is described in detail in §2.3..

Fluid flow at micro scale differs from the one at macro scale. As the geometric scale of the flow is reduced down to microns, the viscous forces increases over the inertial forces. A way to measure the interaction between these two forces is the Reynolds number [29, 37]. Reynolds number is a dimensionless parameter defined as a relation between the inertial and viscous forces and can be expressed as:

$$\text{Re} = \frac{\rho \bar{v} L}{\eta}, \tag{1.1}$$

where ρ is the density of the fluid, $\bar{v}$ is the average velocity, L is the characteristic length of the micro-channel and η is the viscosity of the fluid. For small Reynolds number flows usually are laminar and the prevailing mechanism for transport is diffusion. For large Reynolds number flows are turbulent and viscous effects can be neglected except close to walls. In turbulent flows the dominant mechanism of transport is convection [29]. The critical value of Reynolds number above which the flow is expected to be turbulent is around 2300 on the macroscale [13].

For typical microfluidics flows the Reynolds number varies between 10^{-6} and 1. So the viscous forces typically dominate over inertial forces. Therefore, the flow in microfluidics devices can be considered laminar [29].

Considering the experimental setup of this study the typical value of the Reynolds number here can be estimated. The thickness of the most used microfluidics chip in this study is $h_1 = 0.135$ mm and the width of the channel might vary up to 2 mm, giving the cross-section of 0.27 mm^2. A typical flowrate of the experiments described in the chapter §3.1. is $Q = 1$ μL/min giving the average velocity $\bar{v} = 6.2 \cdot 10^{-5}$ m/s. By using the thickness of the microfluidics chip as the characteristic length $L = 1.35 \cdot 10^{-4}$ m and density and viscosity of water ($\rho = 1000$ kg/m^3, $\eta = 0.001$ Pa $\cdot$ s) the acquired value of the Reynolds number is Re ≈ 0.008.

As the typical flow in the microfluidics device is strongly laminar, mixing happens only as a result of the slow diffusion process. Despite the typically laminar flows, rapid mixing is essential in many applications of the microfluidics systems and devices. Few application examples where accelerated mixing in microfluidics systems is strongly desirable include biochemistry analysis, drug delivery, lab-on-a-chip platforms for chemical reactions and others. Passive and active mixing can be used as a mechanism for speeding up the mixing of fluids in microfluidics devices [13, 37]. Passive micromixers do not require external energy. The mixing process in microfluidics systems with passive mixing relies entirely on diffusion or chaotic advection. In passive micromixers the contact surface between the different fluids is increased and the diffusion path between them is decreased by splitting, curving, introducing rips and grooves and otherwise manipulating the geometries of micro-

channels [38].

Opposed to passive micromixers, active micromixers for the mixing process use disturbances generated by an external field. Active mixers can be categorized by the types of this external field. If magnetic materials and fields are used (just as in this study) mixing can be conveniently enhanced in a contact-less manner. A part of active mixers that are based on magnetic materials and fields, has opened a sub-field called micro-magnetofluidics or magneto-hydrodynamic active micromixers [13]. One way to accelerate the mixing in microfluidics is by external magnetic field creating instability. There are multiple realizable ways for mixing with magnetic elements, like incorporation of the magnetic fluids or using magnetic micro-beads that are driven by stationary or alternating magnetic fields that generate Lorentz forces [14]. One way to accelerate the mixing in microfluidics is by external magnetic field creating instability- magnetic micro-convection [39, 40]. This is explored more within this work. The information about the effects of the magnetic micro-convection on the fluid mixing with respect to various experimental parameters is collected in sections §3.1., §3.2., §3.3., §3.4. and §4..

1.3. Magnetic fluids

By composition magnetic fluids are artificially made stable colloidal suspensions consisting of a carrier fluid and magnetic particles dispersed in it. A colloid is a suspension of finely divided particles in a continuous medium. The terms magnetic fluid and ferrofluid were defined in the 1970's [1, 2].

After magnetic fluids became available, many uses of these liquids were recognized [1, 3]. Actual commercial usage of the magnetic fluids includes novel zero- rotary shaft seals used in computer disk drives, pressure seals for compressors and blowers, magnetic liquid cooled loudspeakers and more [1, 41, 42]. Magnetic fluids have also proved to have possible applications in medicine, for example, drug delivery or a tracer of blood flow [1, 43–45].

Variety of different carrier fluids can be used. The first magnetic fluids were made with oil or organic carrier fluids. Depending on the purpose of the application of the magnetic fluid the carrier fluid can be oils, various organic solvents or even water which is convenient if the intended application is biological [1]. In this study water based magnetic fluids are investigated. Their properties are explored in detail in §2.1..

Magnetic particles of the magnetic fluid are nano-sized. If the magnetic particles are larger (in the scale of micrometers) then the "magnetic fluid" is magneto-rheological fluid [46] or clutch magnetic fluids [1]. The clutch magnetic fluids may solidify in the external magnetic field, but colloidal magnetic fluids retain liquid flowability even in strong external magnetic fields. In this study only colloidal magnetic fluids with nano-sized magnetic particles are considered. There has been an interest in magnetic fluids also by looking at magnetic nano-particles as individual elements; several uses in biomedicine have

been proposed contrast agents for magnetic resonance imaging, magnetic hyperthermia for cancer treatment and others [20, 47, 48].

1.3.1. Colloidal stability of magnetic fluids

As magnetic fluids are colloids they might stratify due to sedimentation in a gravitational field (or due to other external external forces, for example, centrifugal). Although a small concentration gradient can establish itself after a long exposure to external force field, a true magnetic fluid does not settle out [1].

The sedimentation can be minimized by finding the particle size at which the forces governing sedimentation and Brownian motion are at the equilibrium. For magnetic particles of the magnetic fluids typically the gravitational energy is smaller than thermal energy (see eq. 1.2 of the gravitational stability condition bellow) if the magnetic particles have a diameter smaller than 20 nm.

$$\Delta\rho V g h \leq k_{\mathrm{B}} T \tag{1.2}$$

In this inequality $\Delta\rho$ is the density difference between the magnetic particles and the carrier fluid, V is the volume of a spherical magnetic particle, g is the standard gravity, h is a height in which the concentration of the magnetic particles has decreased e times, k_{B} is the Boltzmann constant and T is the absolute temperature [2].

Another factor that might affect the stability of magnetic fluids is the aggregation of the magnetic particles. In order to avoid the aggregation particles must be far enough from each other by some short-range repulsive effect on the particles to disregard van der Waals attraction force or magnetic dipole-dipole interaction [3]. To avoid aggregation magnetic particles can be coated with a layer of surfactant, then referred as surfactant stabilized or sterically stabilized magnetic fluids [1]. This method is older and is used for organic solvent or oil based magnetic fluids. Aggregation can also be escaped by electrostatic interaction when each magnetic particle have a superfacial charge with the same polarity. Thus electrostatic repulsion between the magnetic particles is ensured. In order to achieve electrostatic neutrality of the magnetic fluid counter-ions are added to the carrier fluid-water. Therefore each magnetic particle becomes an ion or macro-ion and the charge of the particles is controlled during the synthesis of the magnetic fluid. Magnetic fluids that are stabilized this way are referred as ionic magnetic fluids. All of the magnetic fluids investigated within this study are ionic ones produced with Massart's method [49].

1.3.2. Preparation of magnetic fluids

As all of the magnetic fluids used within this study have water as a carrier fluid only a method for water based magnetic fluids are reviewed.

The Massart method is a field standard for making electrically stabilized water based

magnetic fluids. Magnetic fluids produced by this method are stable at a normal pH 7, which together with the fact that they are water based is a requirement for them to be compatible for bio-medical applications. Advantage of the method is that electrostatic repulsion between the magnetic particles can be controlled and magnetic fluids synthesised this way remain stable over a wide range of temperatures and concentrations of magnetic particles [3]. Maghemite γ-Fe_2O_3 and magnetite Fe_3O_4 particles can provide all of them necessary requirements for application in bio-medicine and bio-engineering [50].

For the magnetic fluids used within this study the first stage of the synthesis is obtaining of magnetic particles consisting of γ-maghemite γ-Fe_2O_3 crystals by precipitation from a mixture of ferrous and ferric salts in an alkaline solution [3]. In this step the size of the magnetic particles can be regulated by the ratio of these salts. In order to obtain magnetic particles and ensure the stability of the colloid, sodium citrate is often used to create a functional stabilisation of the nanoparticles. This way stable colloid solutions with biocompatible pH values can be obtained [50]. Citrate ions from dissolved trisodium citrate salt are adsorbed on the particle surface. Thus magnetic nanoparticles with surface charge are obtained. The negative charge is neutralized in the solution by the free sodium ions [51].

By increasing the number of the ions during the synthesis of magnetic fluid and thus weakening the electrostatic repulsion between the particles a phase separated magnetic fluid can be created. The colloidal solution separates into two discrete liquid phases with different magnetic particle concentration [3]. This property can be used to limit the particle size range in suspensions as phase separation occurs more easily in the presence of large particles.

1.3.3. Properties of magnetic fluids

Precise properties of the used magnetic fluids must be known in order for the experimental results to be reproducible or comparable to theoretical predictions. Essential properties for magnetic fluids include: ionic strength I, osmotic pressure Π, volume fraction Φ, size distribution and polidispersity of the magnetic particles, saturation magnetization M_s and magnetic susceptibility χ. The last two properties will be explored more later below in the section about magnetic properties. Ionic strength and osmotic pressure can be fixed during magnetic fluid preparation. The volume fraction can be measured by weight measurements with analytical balance [50] as it is done during this study. The densities of the magnetic particle material ρ_{mat} and the solvent ρ_{solv} must be known. In the case of this work, the solvent is water. Then a known volume V_{MF} of the magnetic fluid in interest must be weighted in order to calculate the density ρ_{MF} of this fluid. Then volume

fraction can be calculated with the following expression:

$$\Phi = \frac{\rho_{\mathrm{MF}} - \rho_{\mathrm{solv}}}{\rho_{\mathrm{mat}} - \rho_{\mathrm{solv}}} \tag{1.3}$$

This method is quick and handy to check if the particle volume fraction has not changed, as sometimes for longer set of experiments the solvent of the magnetic fluid might evaporate thus changing ρ_{MF}. Another complimentary method for measuring Φ is magnetization measurements described further below from which the particle volume fraction value can be obtained.

When characterizing the size of the magnetic particles for simplicity they are considered to be perfectly spherical. The diameter d of the particle can be described with a log-normal distribution. The probability density then is defined as [52]:

$$P(d; d_0; \sigma) = \frac{1}{\sqrt{2\pi}\sigma d} e^{-\frac{\left(\ln \frac{d}{d_0}\right)^2}{2\sigma^2}} \tag{1.4}$$

where d_0 is a characteristic diameter of the magnetic particle and $\ln d_0$ is the average value of $\ln d$, and σ is polydispersity factor. These parameters can be found with multiple methods [53], but within this study dynamic light scattering described further was used.

Particle characterization with Dynamic Light Scattering

Dynamic Light Scattering (DLS) is a measurement technique for the characterization of particle sizes in suspensions and emulsions. The method is convenient and fast. A laser beam is shot in the sample. When light hits the small particles it scatters in all directions. Due to the Brownian motion of the colloidal particles the distance between the scattering intensity in the solution is constantly changing with time. The scattering signal fluctuations are related with the Brownian motion [54]. The scattering signal is measured in a position that is defined with a scattering vector q [55]:

$$q = \frac{4\pi n}{\lambda}\sin\frac{\Theta}{2}, \tag{1.5}$$

where λ is the wavelength of the laser, n is the refractive index of the studied medium and Θ is the angle between the direction of laser beam and the direction of the scattering observation. The dynamic information of the particles then is derived from the autocorrelation of the measured signal $I(t)$ and a delay time τ. After averaging multiple measurements the normalized intensity and electric field autocorrelation functions are calculated. A colloid is always at least slightly polydispersed. A common simplification of an autocorrelation function for a polydisperse suspension is the method of cumulants [56], which is valid for a narrow monomodal distribution and includes information about the diffusion coefficient.

Thus the size of the particles can be determined using Stokes-Einstein relation for the diffusion coefficient [57]:

$$D = \frac{k_\text{B}T}{3\pi\eta d_\text{H}} \tag{1.6}$$

where k_B is the Boltzmann constant, T is the temperature, η is the viscosity of the base fluid and d_H is the hydrodynamic diameter of a particle [56]. The mean diffusion coefficient $\overline{D}$ gives the value of the mean hydrodynamic diameter $\overline{d_\text{H}}$, which is also known as *z-average*.

DLS method also provides information of the size distribution of the particles with a polydispersity index PDI. PDI is proportional to the ratio of the standard deviation σ_H and mean hydrodynamic diameter $\overline{d_\text{H}}$ squared [56]:

$$\text{PDI} = \left(\frac{\sigma_\text{H}}{d_\text{H}}\right)^2 \tag{1.7}$$

PDI is not the same as already mentioned polidispersity factor σ from equation 1.4, but it is related by parameters σ_H and $\overline{d_\text{H}}$ with equation:

$$\sigma = \sqrt{\ln\left(1 + \left(\frac{\sigma_\text{H}}{d_\text{H}}\right)^2\right)} = \sqrt{\ln\left(1 + \text{PDI}\right)}. \tag{1.8}$$

And the characteristic diameter d_0 from equation 1.4 is related to mean hydrodynamic diameter $\overline{d_\text{H}}$:

$$\ln d_0 = \ln \overline{d_\text{H}} - \frac{\sigma^2}{2}. \tag{1.9}$$

Magnetic properties and magnetization measurements

Magnetic properties of the magnetic fluid depend on the properties of its magnetic particles. The magnetic particles are made of ferromagnetic materials. Ferromagnetism is exhibited by iron, nickel, cobalt, many of their alloys and some other materials. Magnetic fluids explored within this study are made of maghemite (γ-Fe_2O_3) nano-particles. Ferromagnetic ordering of the material disappears at the Curie temperature [1]. Meaning at this certain temperature, which is different for various materials, the material loses its permanent magnetic properties.

The small size of the magnetic particles within the scale of few nanometers ensures that the particles are single domain, meaning that per particle magnetic moments of individual atoms are oriented in the same fixed direction. The particles can be described as magnetic dipoles. Each magnetic particle has a permanent magnetic moment m that is directly proportional to the volume V of the magnetic particle. If the particles are assumed to be

spherical, the magnetic moment of a single particle is [1]:

$$m = m_s V = \frac{m_s \pi d^3}{6},$$ (1.10)

where m_s is the saturation magnetization of the material of the particles and d is the diameter of the magnetic particle.

There is no macroscopic magnetization M of the magnetic fluid as the magnetic particles are oriented randomly and chaotically within the carrier fluid if there is no external magnetic field applied. If the external magnetic field is applied the magnetic nano-particles become aligned accordingly.

Magnetic fluids have paramagnetic properties and their magnetic susceptibility χ is relatively large. Paramagnetism is a form of magnetism in which material has a tendency of molecular moments to align with the applied magnetic field, but the material does not have a long-range order. Sometimes magnetic fluids are described as superparamagnetic as their magnetization curve does not have a hysteresis [3]. Superparamagnetism is similar to paramagnetism, only the magnetization of the material in low-to-moderate magnetic fields is much larger than in paramagnetic materials [1].

The magnetization M of the magnetic fluid can be described by Langevin's law if the dipole interaction between the colloidal particles is negigible (for example for magnetic fluids with a rather low particle concentration) [2]:

$$M = M_s \left(\coth \xi - \frac{1}{\xi} \right),$$ (1.11)

where $M_s = \Phi_M \cdot m_S$ is saturation magnetization of the magnetic fluid if the applied external magnetic field $H \to \infty$, where Φ_M is the magnetic volume fraction of the magnetic fluid. M_s can be read approximately from the magnetization curve if the magnetic fluid is exposed to large enough magnetic field. The quantity in parentheses is also known as Langevin's function and the parameter ξ is the argument of the Langevin's function and is defined as:

$$\xi = \mu_0 \frac{\overline{m} H}{k_\mathrm{B} T},$$ (1.12)

where μ_0 is the vacuum magnetic permeability, $\overline{m}$ is the average magnetic moment of the colloidal magnetic particle, H is the intensity of the external magnetic field, k_B is the Boltzmann's constant and T is the absolute temperature [1].

Previously mentioned magnetic susceptibility χ characterizes the magnetization M in external magnetic field H:

$$\chi = \frac{\partial M}{\partial H}.$$ (1.13)

Then by deriving equation 1.11 relation for magnetic susceptibility χ in magnetic field H

is:

$$\chi = M_s \left(\frac{1}{\xi H} - \frac{\xi}{H} \cdot \frac{1}{(\sinh \xi)^2} \right), \tag{1.14}$$

where M_s is saturation magnetization of the magnetic fluid and parameter ξ is described earlier by equation 1.12. If the external magnetic field is small enough the magnetization curve is rather linear. Then for this range of magnetic field values magnetic susceptibility χ can be obtained as a gradient of the magnetization curve as it is done for the experiments within this study (see §2.1.2.).

Typically magnetic measuremens for magnetic fluids can be carried out with a Vibrating Sample Magnetometer (VSM). In VSM, a small sample of the magnetic fluid is vibrated between large coils producing homogeneous magnetic field. VSM measures magnetic properties based on Faraday's Law of Induction. The magnetization of the sample induces a proportional voltage in detection coils, which is measured and converted to magnetization [58].

Magnetization curve obtained with VSM is a composition of many magnetization curves of individual magnetic particles as the magnetic fluid particles are polydispersed. Therefore information about particle size distribution can be obtained from magnetization curves. Magnetization of a polydispersed magnetic fluid can be found by relation [59]:

$$M(H) = \Phi m_s \frac{\int_0^\infty L(d, m_s, T, H) P(d; d_0; \sigma) d^3 \mathrm{d}d}{\int_0^\infty P(d; d_0; \sigma) d^3 \mathrm{d}d}, \tag{1.15}$$

where Φm_s corresponds to the saturation magnetization M_s, $L(d, m_s, T, H)$ is the Langevin's function M/M_s that could be extracted from equation 1.11 and $P(d; d_0; \sigma)$ the size probability density defined in equation 1.4. The parameter d^3 is necessary for proper weighting as magnetic properties are volume dependent.

1.3.4.   The diffusion of the magnetic particles

Diffusion is a thermal motion of a random character exhibited by particles at temperatures above absolute zero [60].

As mentioned previously in this study magnetic fluids that are water based and have nano-sized magnetic particles dispersed in them are investigated. The investigated system can be considered as an incompressible Newtonian fluid [53] and the viscoelastic contributions are disregarded. Water molecules with the magnetic particles change their their position and direction due to thermal motion, leading to what is referred to as rotational and translational diffusion. [60]. Translational diffusion is reviewed further as it limits magnetic micro-convection [53].

The random movement of a magnetic particle in a carrier fluid can be described by a random walk- sequence of random steps. The average displacement squared is

linearly proportional to the movement time, and the proportionality coefficient is diffusion coefficient D and the number of directions [57]. From here it can be derived that the distance a particle travelled due to diffusion on average is proportional to $\sqrt{(t)}$. Within this work 2-dimensional Hele-Shaw model is used, where the particle could travel back and forward in 2 dimensions. The diffusion coefficient describes the particle's ability move around in a certain time period, and larger diffusion coefficient means that typically this particle will explore a larger area. The diffusion coefficient is affected by the size of the particles and the properties of the carrier fluid. The diffusion coefficient can be expressed via Stokes-Einstein equation (see eq. 1.6) [57] already reviewed before.

When a group of particles diffuses, meaning they change their positions, then particle concentration changes accordingly and it may be visible even macroscopically. If the initial particle concentration has some pattern, as it happens in this work due to magnetic micro-convection, the diffusion smears out the pattern over time.

The diffusion coefficient characterizing magnetic particles may be affected by external magnetic field[58], but it is disregarded within this study. For concentration gradient the process of particle diffusion can be described with the second Fick's law [61]:

$$\frac{\partial c}{\partial t} = D\Delta c \tag{1.16}$$

where Δ is the Laplacian operator, c is the concentration and D is the diffusion coefficient of the diffusing particles and t is for time.

Experimentally within this work magnetic fluid and water are filled in a thin microfluidics chip that can be described by a Hele-Shaw cell. The interface between the fluids are considered to be sharp when they meet and if the fluids are let to mix it is expected that the diffusion of magnetic particles can be observed until the magnetic particle concentration equalizes over whole volume of the mixing fluids. This situation can be described by one-dimensional case of a step-like initial concentration pattern [61]. The initial conditions in the case where magnetic fluid is placed beneath the water are the following: $c = c_0$ for $x \leq 0$ and $c = 0$ for $x > 0$ at $t = 0$ as also demonstrated in figure 1.1.. The position $x = 0$ corresponds to the interface between the fluids. The boundary conditions are: $\frac{\partial c}{\partial x}|_{x=-\infty,t=0} = 0$; $\frac{\partial c}{\partial x}|_{x=+\infty,t=0} = 0$

An analytical expression for concentration value $c(x,t)$ can be found by solving the Fick's law from equation 1.16 with just mentioned initial and boundary conditions [61]:
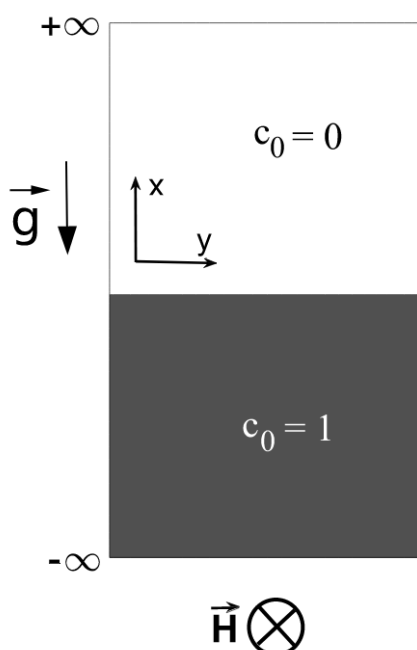
$$c(x,t) = \frac{c_0}{2}\left[1 - \text{erf}\left(\frac{x}{2\sqrt{Dt}}\right)\right], \tag{1.17}$$

where erf is an error-function defined as:

$$\mathrm{erf}(x) = \frac{2}{\sqrt{\pi}} \int_0^x e^{-2t^2} \mathrm{d}t. \tag{1.18}$$

Diffusion length δ that gives a measure for the propagation of the diffusion can be defined as [53]:

$$\delta = 2\sqrt{Dt}. \tag{1.19}$$

1.1. Figure: A schematic illustration of the Hele-Shaw cell at the beginning of the experiment. The magnetic fluid is placed beneath the water and The external magnetic field H is normal to the Hele-Shall cell.

1.4.   Magnetic micro-convection

Magnetic fluids as explained before have magnetic properties and as fluids have hydrodynamic properties. Therefore magnetic fluids respond to an applied magnetic field and modify the external field. At a critical point, there is typically an abrupt change that results in a new equilibrium state. This change often leads to an instability [8]. Various different instabilities can be observed in magnetic fluids [2]. The most common is the normal-field instability (also called Rosensweig instability). In this instability a regular, hexagonal pattern of peaks and valleys sometimes referred to as "a hedgehog like" forms on the surface of the liquid if it is subjected to vertical magnetic field [1]. This pattern is the outcome of the interaction between the forces exerted by gravity and surface tension

and magnetic forces [3].

The instability explored in the scope of this study is magnetic micro-convection. The magnetic micro-convection is a finger-like instability that happens on an interface between magnetic and non-magnetic fluid, first found by M. Maiorov and A. Cēbers in 1980s [7]. The instability is a result of the ponderomotive force exerted on the magnetic fluid in a uniform magnetic field. This force is proportional to both the concentration of magnetic particles in the fluid and the local gradient of the magnetic field. In turn the self-magnetic field of the magnetic fluid creates the local gradient of the magnetic field [2]. If the magnetic field is higher than some critical value, a flow is created by any concentration perturbation that disturbs the collinearity of the concentration gradient and magnetic field gradient [8]. A finger-like pattern emerges as a result of these induced flows.

The theoretical model used for the description of the phenomena that is experimentally researched within this study is described by a set of equations, which includes the Brinkman equation, the continuity and convection-diffusion equation [25, 62, 63]:

$$-\nabla p - \frac{12\eta}{h^2}\vec{v} - \frac{2M(c)}{h}\nabla\psi_m(c) + \eta\Delta\vec{v} + \Delta\rho c\vec{g} = 0, \tag{1.20}$$

$$\nabla\vec{v} = 0, \tag{1.21}$$

$$\frac{\partial c}{\partial t} + (\vec{v}\cdot\nabla)c = D\nabla^2 c. \tag{1.22}$$

Differential operators Laplacian Δ and Nabla ∇ expands as: $\Delta = \frac{\partial^2}{\partial x^2} + \frac{\partial^2}{\partial y^2}$ and $\nabla = \left(\frac{\partial^2}{\partial x}, \frac{\partial^2}{\partial y}\right)$ for two-dimensional problem. In these equations p stands for pressure, η is the viscosity of the fluid (the viscosity of the two fluids is asumed to be equal), h is the thickness of the Hele-Shaw cell, $\vec{v} = (v_x(x,y), v_y(x,y))$ is the depth averaged velocity, $M(c)$ is the magnetization and c is the concentration of the magnetic fluid normalized by its value far from the interface between the mixing fluids. $M(c)$ is taken to be proportional to the concentration of the magnetic fluid c: $M = M_0 c$, where M_0 is the initial magnetization of the magnetic fluid far from the interface between the mixing fluids. ψ_m is the magnetostatic potential. Next $\Delta\rho = \rho_{\mathrm{MF}} - \rho_{\mathrm{H_2O}}$ is the density difference between the mixing fluids, or in our case, density of the magnetic fluid ρ_{MF} and water $\rho_{\mathrm{H_2O}}$. And lastly $\vec{g}$ is the gravity vector and D is the isotropic constant diffusion coefficient.

Brinkman equation (eq. 1.20) is the modification of the usual Darcy law, which would be the equation without the last two terms. The term $\eta\Delta\vec{v}$ in the equation 1.20 also called the Brinkman term is account for transitional flow between boundaries and the last term accounts for the gravity effects.

The magnetostatic potential ψ_m on the boundary of the Hele-Shaw cell is given by [64, 65]:

$$\psi_m(\vec{r}, t) = M_0 \int c(\vec{r'}, t)K(\vec{r} - \vec{r'}, h)\mathrm{d}S', \tag{1.23}$$

where the integration is performed over the boundary of the Hele-Shaw cell: $K(\vec{r}, h) = 1/|\vec{r}| - 1/\sqrt{|\vec{r}|^2 + h^2}$.

To get the dimensionless form of the Brinkman model (from earlier equations 1.20-1.22) that the colleagues in MMML lab are using for theoretical exploration of the magnetic micro-convection, non-dimensional quantities, such as, the magnetic Rayleigh Ra_m and gravitational Rayleigh Ra_g numbers are introduced. Ra_m is expressed as a ratio between the characteristic time of the diffusion $\tau_D = h^2/D$ and the characteristic time of motion that is driven by non-homogeneous self-magnetic field of the fluid $\tau_M = 12\eta/M_0^2$, and reads as:

$$\text{Ra}_m = M_0^2 h^2 / 12\eta D. \tag{1.24}$$

Ra_g is the ratio between the characteristic time of the diffusion τ_D and the characteristic time of motion due to the gravitational field $\tau_G = 12\eta/\Delta\rho g h$:

$$\text{Ra}_g = \Delta\rho g h^3 / 12\eta D, \tag{1.25}$$

where $\Delta\rho = \rho_{\text{MF}} - \rho_{\text{H}_2\text{O}}$ is the density difference between the denser magnetic fluid below and less dense water above and g is the standard gravity. Other scaling factors to make the equations dimensionsless are the thickness of the Hele-Shaw cell h for length, h^2/D for time, D/h for velocity, $12\eta D/h^2$ for pressure, $M_0 h$ for magnetostatic potential. The fluid viscosity is assumed to be equal across the fluid. Then non-dimensional forms of the Brinkman, the continuity and convection-diffusion equations read [25]:

$$-\nabla p - \text{v} - \text{Ra}_m c \nabla \psi_\text{m}(c) + \frac{\Delta\text{v}}{12} - \text{Ra}_g c e_\text{x} = 0, \tag{1.26}$$

$$\nabla\vec{v} = 0, \tag{1.27}$$

$$\frac{\partial c}{\partial t} + (\text{v} \cdot \nabla)c = \nabla^2 c. \tag{1.28}$$

As it will be visible further in this study the development of the micro-convection is affected by both: magnetic Rayleigh number and gravitational Rayleigh number, which characterizes gravity influence on a miscible fluid interface due to the density difference between the fluids.

Convenient method for measuring microconvection and flows in general is Particle Image Velocimetry (PIV), briefly described in next section.

1.4.1. Particle image velocimetry- general principles

Particle image velocimetry (PIV) is an imaging method for quantifying the velocity field of liquid or gas flows [66]. Micro-PIV (µPIV) is a tool for measuring the velocity profile in a microfluidics device. Stereo-µPIV enables to visualize the flow in three dimensions using stereo microscope and two digital cameras in a double-frame mode that capture

images simultaneously [67]. The cameras are mounted on the stereo microscope. Stereo microscopes typically use light reflected from the surface of an object contrary to a method transmitting light through it.

Two cameras are necessary for depth perception, recording two simultaneous, but different views of the same object. This double camera setting mimics binocular vision. Using the combination of the two views and specific algorithms a third (depth) dimension is reconstructed [68].

Also necessary elements for stereo-μPIV (or μPIV in general) measurements are filter-set for fluorescence imaging, a double-pulse laser, light-shaping optics, a programmable timing unit for synchronization of the components, a computer for data acquisition. Also small fluorescent tracer particles are added to the fluids in order to make the motion of the fluid observable [67, 69]. Fluorescent light is emitted from the tracer particles after the illumination from the laser. The tracer particles must be small enough and in low concentration so that they would move with the fluid flow, but would not change it. Also the particles in the images should be clear and sharp.

Two or more consecutive images with a set delay time of the moving particles are captured and analyzed. Typically, the two particle image fields are subdivided into uniformly spaced interrogation regions [69]. The local velocity of the tracer particles is measured from the average displacement of the particles in an interrogation region over a set delay time. Typically the motion of these particles within each interrogation region is determined using cross correlation algorithms [29, 70]. The Brownian motion can cause errors in the velocity measurements especially for slower flows [29, 69].

1.4.2. Review of the previous studies

Over the years and also recently various fingering instabilities have been investigate both for immiscible fluids [71–75] and miscible fluids[22, 25, 76–78]. Here in this study the focus is on the instability between two miscible fluids. Also the focus is on magnetic instabilities. In this section the methods and results of some studies about magnetic micro-convection carried out by others over the years are summarized. The first experimental evidence of the finger-like instability for miscible fluids in a plane layer was delivered already in 1980 by M. Maiorov and A. Cēbers [8]. Though, despite the relatively long time since the phenomenon was first observed the first experiments the first detailed experimental investigation of the fingering instability caused by the magnetic micro-convection in miscible fluids was carried out only in 2007 by C.-Y. Wen and his colleagues [79, 80]. Within Wen's study experimental results of labyrinthine instabilities in a miscible interface of mineral oil based magnetic fluid and non-magnetic fluid subjected to a normal magnetic field were explored. The studied interface was circular as the magnetic drop was investigated in a horizontally placed Hele-Shaw type microfluidics chip. Wen's research showed that after

removing external magnetic field diffusive effects smoothed off fine fingering structures rapidly thus accelerating the mixing of both fluids. One of the main findings was that the fingers of the instability cluster in secondary wave bundles and the wave number of these secondary waves can be regulated by the thickness of the Hele-Shaw layer. Also the prominence of the instability fingers were confirmed to be affected by magnetic field strength and the thickness of the microfluidics device.

A development and an emergence of the magnetic micro-convection instability is set by a mix of various parameters. Over the years several studies have been conducted to quantify the effects of these parameters. There has been investigation of the phenomenon both experimental and theoretical. Though the theoretical branch of the study has been more active. The detailed study of these PhD thesis will nicely compliment the experimental research field of the phenomena, as without experimental studies theoretical models can not be verified.

To review relatively recent development of the research in the scope of this study investigation of the instability in a Hele-Shaw model is explored further. In the 2002 the role of an initially diffused concentration distribution for the magnetic micro-convection in a Hele-Shaw cell was explored numerically by a linear stability analysis [62, 81, 82].

It has been found out that the magnetic micro-convection depends significantly on the initial concentration gradient as well as the local viscosity of the mixing interface [16, 81]. Studies of numerical simulations for various geometries have been carried out [83–85]. Also more complex model with Kortweg stress was developed during these studies. After the first detailed experimental study with the circular interface between the mixing fluids [79, 80] magnetic micro-convection on a straight interface for miscible fluids was explored in 2008 [17]. During this experimental study the characteristic size of the instability for various microfluidics chip thicknesses was measured. The results showed that the wavelength of the instability is approximately equal to the thickness of the microfluidics chip. Within that study the dependence of this wavelength and the critical magnetic fields was discussed and explored as well. Another study [86] explored a hybrid instability, where peak and labyrinthine-finger patterns coexists in a droplet of magnetic fluid. The droplet was immersed in a thin layer of a nonmagnetic fluid, and subjected to a uniform perpendicular magnetic field. The normal-field instability proved to be initially dominant.

Extensive study of magnetic microconvection in a horizontally placed Hele-Shaw type microfluidics chip exposed to homogeneous, vertical magnetic field had been carried out by G. Kitenbergs in his PhD thesis [53] in 2015, which were accompanied by several publications [39, 40, 87]. The micro-convective flows were measured for the first time and the significance of gravity for this instability in a Hele-Shaw cell was proposed in one of them [39], but in [87] the theoretical description of magnetic micro-convection in a Hele-Shaw cell was improved by introducing a Brinkman term. During Kitenbergs

research the critical magnetic fields an magnetic Rayleigh numbers for the instability to appear on interface between two miscible fluids- water based magnetic fluid and water were found. The research was mainly experimental complimented by numerical simulations based on Darcy and Brinkman models. During Kitenbergs research it was found out that due to the small density difference of the mixing fluids gravity driven convective motion appeared during which a bit denser magnetic fluid slipped under the water causing an additional smearing of the interface. The process resembled a diffusive process. This was concluded at the end phase of the research so investigation of magnetic micro-convection without parasitic gravity driven convective motion is still necessary. Numerical simulations presented in the study indicated that a convective motion appears immediately after the interface formation. It forces the denser magnetic fluid to flow under the water. The concentration profile across the cell, averaged over the depth of the cell, smears in time and therefore resembles a diffusive behavior. Although it has been general assumption that gravity effects can be neglected in microfluidics devices [29] it was proved during Kitenberg's research that gravity effects can not be neglected even in thin cells, if miscible fluids have slightly different densities. An attempt was made to measure this convective flow with stereo-μPIV during the research of these thesis, the results are collected in § 3.5..

The parasitic gravity driven convective motion can be escaped if thinner channels are used [88] or the microfluidics chip is placed vertically so that a bit denser magnetic fluid is placed beneath the water. The next step should be to continue the investigation of the magnetic micro-convection and to improve the description of this instability and its governing factors. This was done by MMML lab scientists, including the author of this thesis, and the results were published in [25]. There the experimental system from [53] was turned sideways and slightly denser magnetic fluid was placed underneath water. The experiments were carried out in a continuous flow mode in Y-shaped micro-channel. But the theoretical model of the magnetic micro-convection, based on the Brinkman equation, was improved to better describe a case in which both of the mixing fluids are initially stagnant. Within this paper mixing by magnetic micro-convection considering gravity effects was explored. The results of this paper are more broadly explored in the result section of these thesis in § 3.1.. Afterwards magnetic micro-convection in horizontal magnetic field is explored more in § 3.2. of this thesis for initially stagnant fluids. In § 3.3. the effect of the initial interface smearing between the mixing fluids is explored.

A different type of instability emerges if the magnetic field is parallel [89–91] not perpendicular to the microfluidics chip as investigated further in §3.4. of this work. If sufficient vertical external magnetic field is applied to a pool of magnetic fluid lying horizontally perpendicular to the free surface of the magnetic fluid normal-field instability emerges. The description of the instability is complex due to the 3D nature of this

instability. Simpler version of normal-field instability in a 2D system is investigated theoretically in [5] by quantifying impact of the elastic interface. There a Hele-Shaw cell is subjected to a uniform magnetic field acting perpendicular to the initially flat ferrofluid-nonmagnetic fluid boundary. External magnetic field applied there is in the plane of the vertical, rectangular Hele-Shaw cell. The research focuses on the inter-facial elastic effects between the immiscible viscous fluids. In the study of this work the mixing fluids are miscible.

An experimental as well as numerical study with miscible fluids in a similar setup was investigated by M.S. Krakov and his coleagues [6]. Within the study by Krakov *et al.* surfactant stabilized magnetic fluid and its carrier fluid (kerosene) are used. Magnetic fluid is placed below the nonmagnetic carrier fluid in a vertical microfluidics chip with thickness $h \approx 100 \ \mu m$. During the numerical simulations of the study by Krakov *et al.* it was concluded that edge effects influence the instability to a distance of eight layer thickneses. As this study explores similar setup and comparable thickness of the used microfluidics chip, the results are explored broader and compared to the results of these thesis within §3.4..

Despite the long history there still is a lot to study about the magnetic micro-convection and other inter-facial instabilities as they are affected by various configurable parameters. Within this work many of them are explored in detail. The gravity- one of these parameters is explored here via gravitational Rayleigh number for various experimental modifications. The gravity effects are acknowledged in small systems also by other authors [9], though in a different setup. Recent publications [92] show that instabilities on an interface between two miscible fluids are a current research topic.

2. Chapter

Materials and Experimental methods

2.1. Magnetic fluids used in experimental work

In this study magnetic micro-convection with four different magnetic fluids was explored: D107, KTF11-1, KTF09-9 and FF21-5. The magnetic fluid D107 was made in the PHENIX laboratory in Paris, but the other three in the MMML laboratory in Riga. All of the used magnetic fluids are water based with maghemite (γ-Fe_2O_3) nanoparticles produced with previously described Massart's method [49]. All of these magnetic fluids are electrically stabilized with citrate ions ($C_3H_5O(COO)_3{}^{3-}$), so the magnetic particles have a negative surface charge. As the citrate ions are from dissolved trisodium citrate salt ($Na_3C_6H_5O_7$) the solution has free sodium ions that neutralize the negative surface charge of the magnetic particles [50, 51].

The properties of the magnetic fluid D107 vith various methods are explored in great detail in [53]. Most important properties of all of these magnetic fluids for this work are collected in the table 2.1.. For some of the magnetic fluids the original magnetic fluid was diluted with distilled water in different ratios to vary the density and particle concentration. In the table 2.1. this is noted as the "dilution ratio" and the percentage describes the fraction of the original magnetic fluid in this magnetic fluid-water dilution. As can be noted in the table, some of the properties are indicated separately exactly for those dilutions. For example, as the original magnetic fluid is diluted its magnetic properties as well as its density decrease. If the property is written for whole magnetic fluid (starting from ϕ_M and below) this property was measured for the original 100% concentrated magnetic fluid. And if it applies, as for the magnetic susceptibility χ it must be calculated for each dilution separately. Further in the text to excel a specific dilution of the magnetic fluid a subscript will be used, for example, D107$_{66\%}$ describes magnetic fluid D107 that is diluted with distilled water to the volume ratio 2 : 1.

In following rows the value of Ra_g for experiments in microfluidics chips with different thicknesses h calculated from equation 1.25 is collected. If a particular combination of

the microfluidics chip and a specific dilution ratio was not explored in this work, then the corresponding cell is left empty. The results demonstrated in sectiopns §3.1. and §3.2. were carried out only with magnetic fluid D107 in microfluidics chip with single layer Parafilm® spacer. During this stage of the study the spacer was measured and determined to be $h = 0.13$ mm thick, but later for sections §3.3. and §3.4. a complete microfluidics chip was measured and the micro-channel thickness was determined to be $h = 0.135 \pm 0.005$ mm. As the thickness of the microfluidics chip affects the values of $\mathrm{Ra_g}$ (see eq. 1.25), during the first phase of this study the colleagues carrying out the theoretical analysis used the $\mathrm{Ra_g}$ values written in the parenthesis in table 2.1..

In the next row the densities of the magnetic fluids ρ are collected. The density is calculated from a weight measurement with an analytic balance (KERN) for a known volume, taken with a pipette (Gilson). $\Delta\rho = \rho_{\mathrm{MF}} - \rho_{\mathrm{H_2O}}$ is the density difference between the magnetic fluid and the distilled water. This quantity is necessary for quantifying the gravity effects on magnetic micro-convection via $\mathrm{Ra_g}$. Φ_{Vol} is the volume fraction of the magnetic particles found by weighting.

Parameters in the following rows are measured for the original magnetic fluids (undiluted). Φ_M is the volume fraction, χ is magnetic susceptibility found from the magnetization curve as showed in §2.1.2. further for the concentrated magnetic fluid. For diluted magnetic fluids the susceptibility can be calculated from the dilution factor:

$$\chi_{\mathrm{dil}} = \frac{\chi_{\mathrm{conc}}\phi_{\mathrm{dil}}}{\phi_{\mathrm{conc}}}. \tag{2.1}$$

M_s is saturation magnetization of the magnetic fluid found from magnetization curve at large magnetic field H values. d_{M} is the particle diameter from magnetization measurements.

Hydrodynamic diameter d_{H} and polydispersity index are measured with DLS. It is expected that the hydrodynamic diameter d_{H} measured by DLS will show larger value than the particle diameter from magnetization measurements d_{M}, because of stabilizing citrate ions surrounding the magnetic particles [50]. However $d_{\mathrm{H}} = 81.3$ nm of the magnetic fluid FF21-5 seems suspiciously large and suggests that there might be some agglomerated particles in the sample.

In the last row the information of the diffusion D is collected. All diffusion coefficients except for the fluid D107 were obtained from DLS measurements. Diffusion coefficient for magnetic fluid D107 has been measured with various methods by G. Kitenbers in his PhD Thesis [53] and here I am choosing to work with the value that was chosen by the author as the best one and agreed for several methods.

Viscosity η not included in the table were considered to be equal with the one of the water $\eta = 1$ P for all magnetic fluids represented here.

	D107				KTF11-1			FF09-9			FF21-5
Dilution ratio	100%	66%	50%	33%	100%	66%	100%	66%	50%	33%	100%
$\mathrm{Ra_g}$, $h = 0.050$ mm	—	—	—	—	—	—	—	—	—	—	—
$\mathrm{Ra_g}$, $h_1 = 0.135$ mm	5214 (4657)	3395 (3031)	2491 (2225)	1581 (1412)	10 740	4000	3650	16 640	2170	—	80 050
$\mathrm{Ra_g}$, $h_2 = 0.257$ mm	35 970	—	—	—	74 120	27 620	25 170	—	14 980	5930	552 300
$\mathrm{Ra_g}$, $h_3 = 0.399$ mm	—	—	—	—	—	—	—	—	—	—	—
ρ, g/cm^3	1.143	1.091	1.066	1.040	1.041	1.003	1.013	1.002	1.000	0.988	1.219
$\Delta\rho$, g/cm^3	0.148	0.096	0.071	0.045	0.061	0.023	0.033	0.022	0.020	0.008	0.239
ϕ_{Vol}, %	2.8	1.9	1.4	0.9	0.66	0.44	0.87	0.58	0.44	0.29	5.0
ϕ_{M}, %		2.9				0.49			0.67		3.9
χ		0.016				0.008			0.007		0.079
M_s, G		8.4				2.1			2.45		18.6
d_{M}, nm		7.1				12.5			11.2		8.5
d_{H}, nm		17.2				42.9			30.0		81.3
PDI, nm		0.13				0.18			0.11		0.29
D, cm^2/s		$5.7{\cdot}10^{-7}$				$1.15{\cdot}10^{-7}$			$1.83{\cdot}10^{-7}$		$6.8{\cdot}10^{-8}$

2.1. Table: Properties of the magnetic fluids used in experiments

As noted earlier, used magnetic fluids were characterized by DLS and VSM measurements described bellow.

2.1.1. Magnetic fluid characterization with DLS

DLS experiments to characterize the magnetic fluids within this study were done with Malvern Zetasizer Nano ZS ($\theta = 173°$, $\lambda = 633$ nm) in MMML lab in Riga. The liquid under study is put in a disposable cuvette before inserting it in the apparatus. So in order for a sufficient amount of the light to go through the sample the particle concentration (Φ less than few%) must be small or moderate. Therefore magnetic fluids were diluted with water before the measurements. The measurements in the apparatus are combined with Malvern software that automatically guides the data collection and performs analysis to get the information of particle sizes. The theoretical concepts of the method are reviewed in §1.3.3..

2.1.2. Magnetic fluid characterization with VSM

Magnetization measurements for all the magnetic fluids used within this study were done by M.M.Maiorov at the Institute of Physics of the University of Latvia. Measurements were carried out with *Lake Shore 7400* VSM. The theoretical concepts of the method are reviewed in §1.3.3.. An example of the magnetization curve obtained from VSM for magnetic fluid FF09-9 is demonstrated in figure 2.1.. By fitting this line linearly from $H = -200$ Oe till $H = 200$ Oe the value of the magnetic susceptibility $\chi_{\text{FF09-9}} = 0.007$ as the slope of the linear fit from relation in equation 1.13 is obtained.
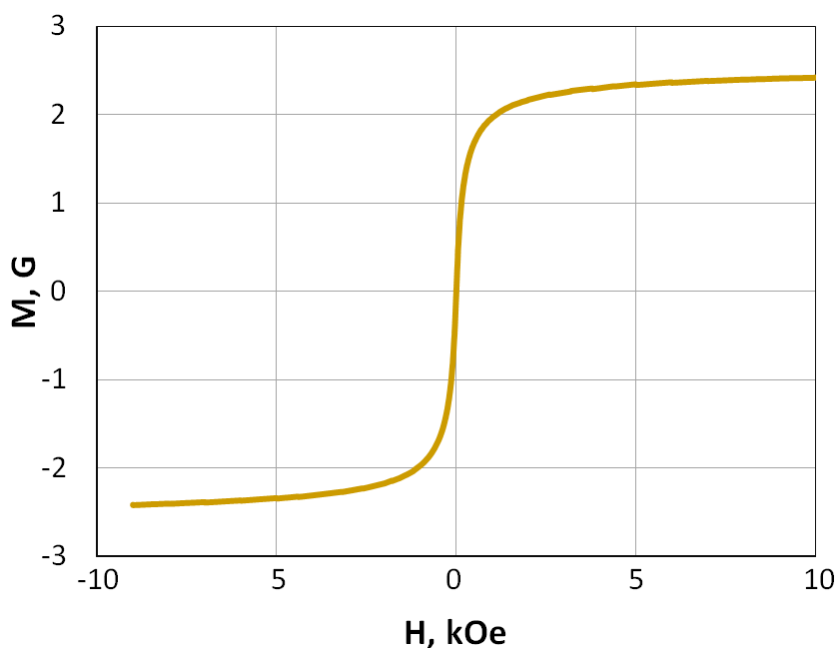
2.1. Figure: Magnetization curve of the magnetic fluid FF09-9.

2.2. Stereo-micro-PIV

The results carried out with the experimental system described here are collected in §3.5. and the theoretical principles of PIV method are described in §1.4.1.. For all of the measurements with stereo μPIV system magnetic fluid FF09-9$_{33\%}$ and distilled water were used. The measurements were carried out in a horizontally placed microfluidics chip with Y-shaped micro-channel. Thickness of the micro-channel was $h_1 = 0.135$ mm and width of the micro-channel was $d \approx 1.62$ mm.

The stereo-micro-PIV system at Dantec Dynamics consists of following elements listed below:

- Stereo microscope with a control unit: *Leica M165FC*;

- Two cameras: *Dantec FlowSense EO 4M*;

- LED illumination for calibration: *Dantec Pulsed Microstrobe for Stereomicroscope*;

- Nd:YAG laser illumination for measurement: *Dantec DualPower 50-20 PIV laser*;

- Calibration kit;

- System computer and synchronizer: *Dantec Performance synchronizer*;

- Software for experiment management and data analysis: *Dynamic Studio 7.4*;

- Syringe pump: *Chemix syringe pump; Y-shaped*;

- Microfluidics chip with tubing for fluid handling.

The experimental setup is demonstrated in figure 2.3.. The microfluidics chip was placed horizontally bellow the microscope objective as visible in figure 2.3.b with tubing for fluids facing downwards. With the available equipment it might have been that for some experiments the microfluidics chip was slightly tilted as some results suggest that. The stereo-microscope and other parts of the experimental system is demonstrated in figure 2.3.a. A control unit enables to easily manipulate the position of the microscope. The microscope can also be manipulated using Dynamic Studio 7.4 software.

Before the experiments the experimental system is calibrated using calibration kit. Camera calibration is necessary and is used for the reconstruction of particle displacements in 3D space [70]. The calibration kit consists of a checkerboard calibration target and a calibration pool. Calibration process and the image of the checkerboard calibration target are demonstrated in figure 2.2..

Due to the light refraction in the microfluidics chip the calibration pool is filled with distilled water as the measurements are carried out in water and water based magnetic

fluid. The cover glass installed in the calibration pool is the same type as the one used for the assembly of the microfluidics chip. Calibration process is long and meticulous and it was especially capricious here as the used cover glass was relatively thick and some optical artifacts appeared in the calibration images. The stereoscopic calibration is described in greater detail in [93].

During the calibration stage LED illumination is used. But later, during the flow measurements, experiment is illuminated by Nd:Yag laser. For visualisation purposes fluorescent tracer particles (FluoSpheres® carboxylate modified micro-spheres with diameter $d = 0.1$ µm) were added to the fluids in ratio 0.1 ml particle solution to 20 ml water or magnetic fluid. Reflected light from the laser is filtered off and only the fluorescent particles are captured by cameras.
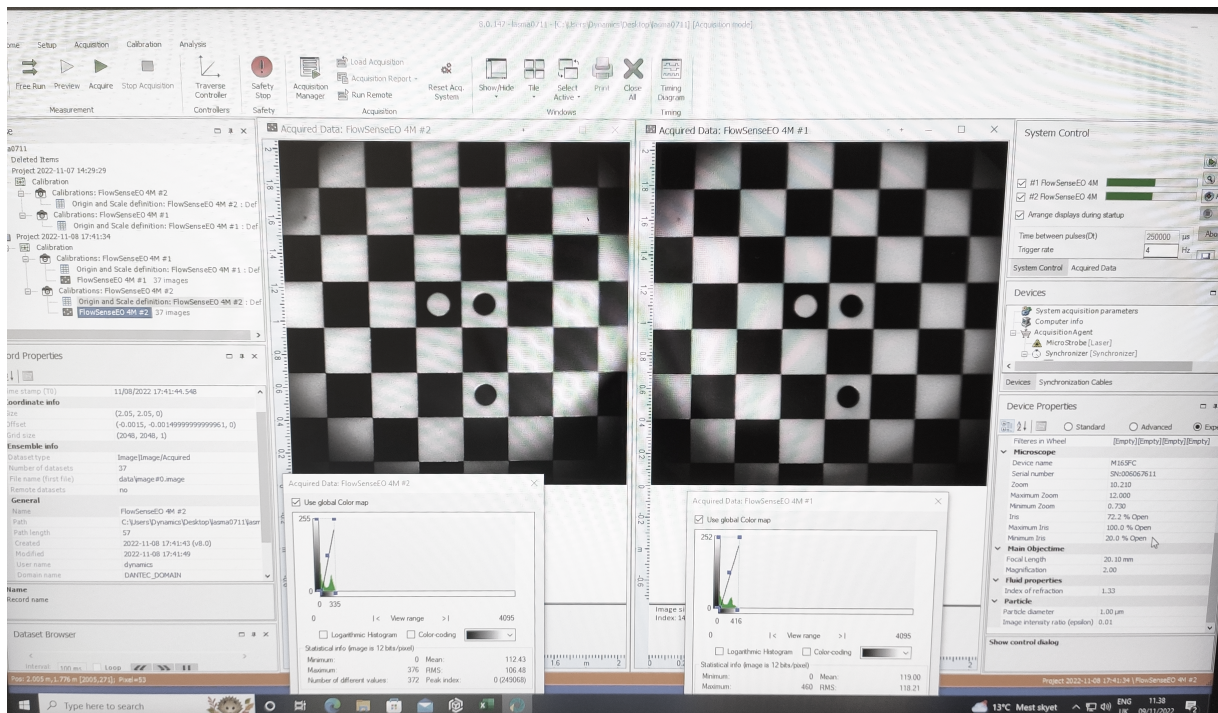
2.2. Figure: Dynamic Studio 7.4 software window during the calibration of the stereo µPIV system. The checkerboard calibration target is visible on the screen.

The following system and image acquisition settings were set: single rate mode image acquisition with 16 Hz time characteristic between laser pulses which corresponds to the trigger rate 62.5 ms. For the depth direction the correlation depth was 17.3 µm and the depth of field was 5.36 µm.

In contrast to experimental setup used in [53] where 2D micro-PIV system was used with a light source positioned above the sample and camera filming bellow the sample, here the light does not go through the sample. The microfluidics chip is exposed with laser beam from above and the cameras are capturing the fluorescence of the tracer particles

also from above. This way the recorded image does not have obviously separated regions dark (corresponding to magnetic fluid) and light (corresponding to water) as in [53].
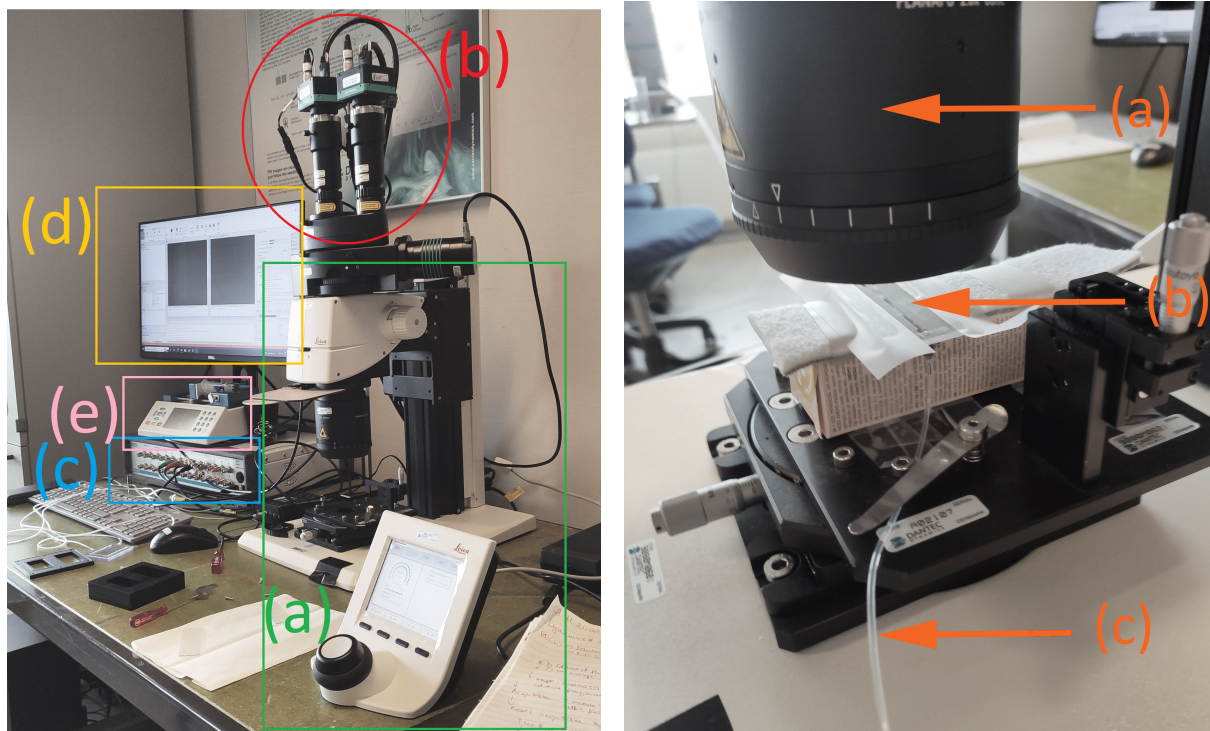
(a) Stereo µPIV system.
(a): Stereo microscope with control unit, *(b)*: Two cameras, *(c)*: Synchronizer; *(d)*: System computer with necessary software, *(e)*: Syringe pump.

(b) Placement of the microfluidics chip.
(a): Microscope objective, *(b)*: Horizontally placed microfluidics chip, *(c)*: Tubing for fluid handling connected to a syringe pump.

2.3. Figure: An experimental setup of the stereo µPIV system used within this work.

Therefore it is not possible to separate the flows of the two mixing fluids visually as it was done in [53] using a special image processing algorithm described and developed in [94]. So it can not be known for sure which velocity vectors of the vector field are tracing the magnetic fluid and which water.

However, some assumptions about the fluid placement can be made from raw images of the experiment demonstrated in figure 2.4.. There is an intensity difference of the tracking particles visible while the fluids are pumped, as the magnetic fluid absorbs the light that the tracer particles emit. It is demonstrated in figure 2.4.a where the upper darker part of the field of view corresponds to the magnetic fluid and the lower part to distilled water. Therefore the initial position of the interface between the fluids can be estimated. Once the pumping of the fluids is stopped, this intensity difference gradually disappears, as the particles start to sink in both fluids and also it is expected that the magnetic fluid is flowing underneath the water. This is shown in figure 2.4.b, which was captured 20 s

after the flow had been stopped. Here the contrast between the water and magnetic fluid region is barely noticeable.
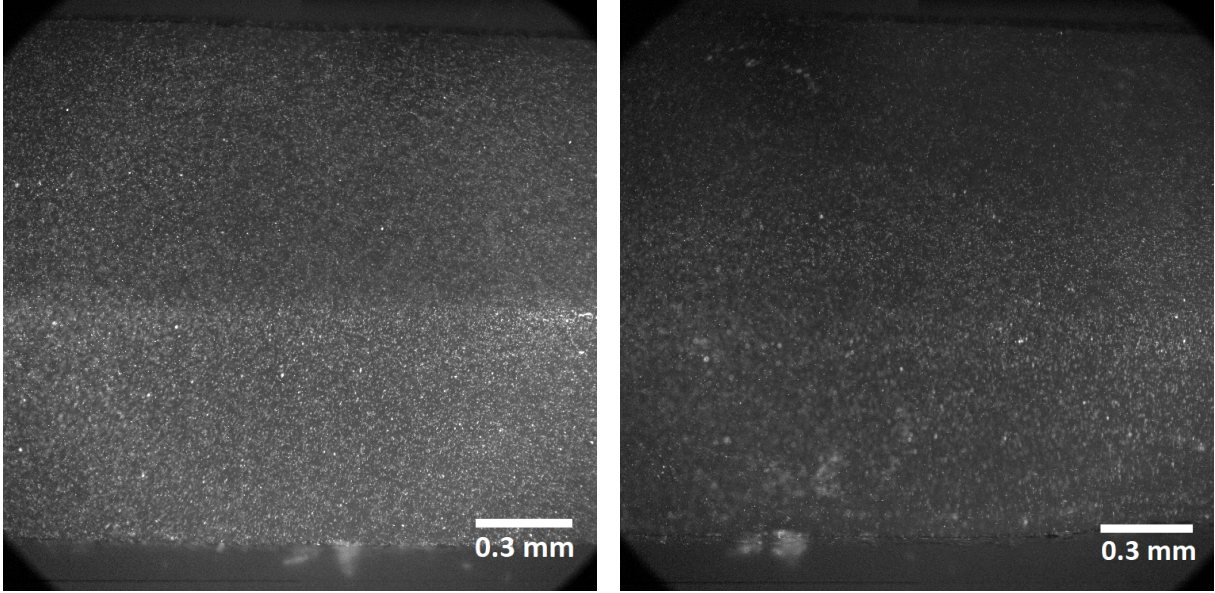
(a) Fluid flow: $Q = 0.02$ ml/min.   (b) 20 s after stopping the flow of the fluids.

2.4. Figure: Raw images of the fluorescent tracker particles captured by one of the µPIV system cameras before the image processing. The images represent 1.87 mm × 1.87 mm.

After capturing raw images of the experiment, they are masked to neglect unnecessary information. During a single experiment, burst of several image pairs is captured. Contrast of raw particle images is enhanced by performing a background subtraction using the minimum pixel value found in the ensemble of this picture burst as described in [93]. All image processing steps have been performed using Dynamic Studio software.

2.3.   Microfluidics chips

The Hele-Shaw cell or as further referred in this experimental study the microfluidics chips used here are mostly made from two microscope cover glasses separated with Parafilm M® spacer. One chip that was not successful for the experiments intended here as later observed in the section §3.3. was made from PDMS. Parafilm M® chips were made with three different thicknesses: $h_1 = 0.135 \pm 0.005$ mm, consisting of one Parafilm M® layer, $h_2 = 0.257 \pm 0.025$ mm and $h_3 = 0.399 \pm 0.015$ mm consisting of two and three Parafilm M® layers accordingly. The measurements of the layer thickness were made with micrometer, measuring the microfluidics chips and then subtracting the thickness of the glass slides. PDMS microfluidics chip was made by colleague, so its production will not be described in detail here; the thickness of this microfluidics chip was $h_{PDMS} = 0.050$ mm.

The steps for fabricating Parafilm M® microfluidics chips are are demonstrated in figure 2.5. and listed below:

1. First the desired shape of the microfluidics channel is chosen and cut in the spacer with a paper knife as shown in fig. 2.7.a;

2. Three holes are drilled in the top glass with drill bits coated with diamod dust (see fig. 2.7.b). For the best results the pressure of the drill must be applied slowly and the drill tip must be submerged in water while drilling (see fig. 2.5.c), and the glass slide must be placed on flat, easily penetrable surface, like organic glass;

3. The inlets and outlets of the microfluidics chip for the fluids are made from syringe tips, that are glued into the holes of the top glass as shown in fig. 2.5.d;

4. The glasses must be dry and clean. Then the spacer with the cutout micro-channel is placed between the glasses (see fig. 2.5.e) and the microfluidics chip is heated on a hotplate at $68° - 75°$ for few minutes to weld cover glasses as it can be seen in fig. 2.5.f. The chip might be slightly squeezed together during this step to push out some air bubbles.

After this the chip is ready for use.

Within this study quickly drying UV resin was used within the third step. The glasses were washed with acetone, and distilled water before the last step so there would not be any oils or dust settled on them. One must be careful not to over-squeeze the chips during the last step as that might affect the homogeneity of the thickness of the microfluidics chip. Also as the Parafilm M® spacer is very soft during this step it is easy to deform the edges of the micro-channel by squeezing the microfluidics chip.

This method of producing microfluidics chips is fast and inexpensive, however it is not possible to make two exactly identical micro-channels. Also as the micro-channels are cut out by hand, the minimal width of the channel and precision is restricted.
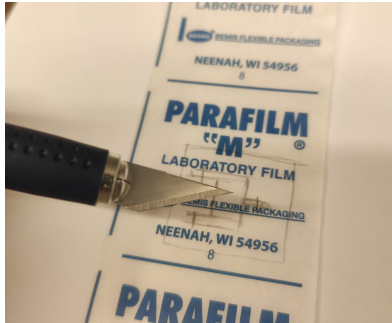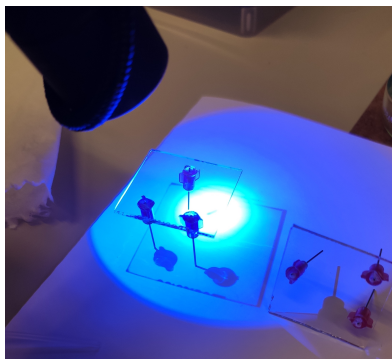
(a) Desired shape of the micro-channel drawn on the Parafilm M® spacer, ready to be cut out.
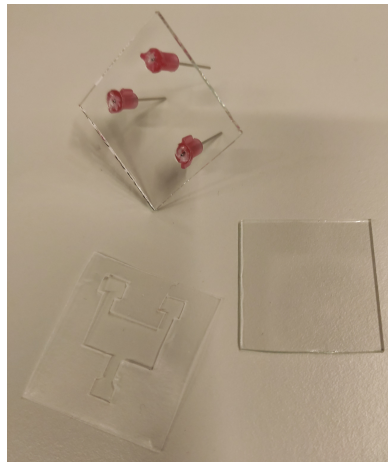

(b) A glass cutter, diamond dust coated jewellery drill bits (in the yellow case) and a box of used microscope glass slides.
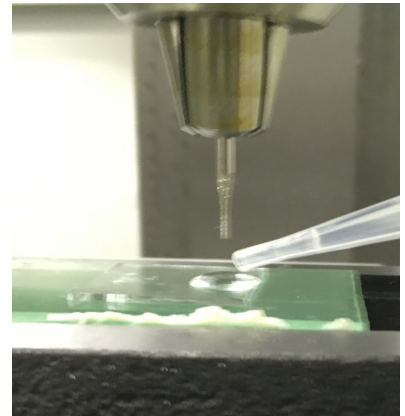
(c) Drilling a hole in the top glass through a water droplet.

(d) Gluing of the syringe tips into the top glass with glue that quickly hardens under UV light.

(e) Cleaned top and bottom glasses and the Parafilm M® spacer with the cut-out micro-channel just before putting them together.

(f) Heating of the microfluidics chip with a hot plate (Biosan MSH-300). This is last step of the preparation.

2.5. Figure: Preparation steps of a microfluidics chip with Parafilm M® spacer.

The Parafilm M® spacer is a very stretchy material that sometimes sticks to the paper knife so it is hard to create sharp angles of the micro-channel with this method. Also it must be noted that Parafilm M® can come off the glass if being exposed to warmer temperatures for a prolonged period of time. This was important during the experiments, as the electromagnet coils heated up.

Microfluidics chips with several different shapes of micro-channels were created (see §2.4.2.). Experiments with continuous fluid flow described in §3.1. were carried out in chips with Y-shaped channel. The magnetic micro-convection was filmed in the middle of the chip a little further from the Y-junction as a velocity distortion around the tip is

created as the fluids have friction with the walls. An average velocity in the channel after the Y-junction can be estimated as:

$$\overline{v} = \frac{2Q}{h \cdot w},$$

(2.2)

where Q is the flow-rate of fluids, which are controlled by the syringe pump, h is the channel thickness and w is its width. Y-shaped channels were produced only with one layer of Parafilm M® spacer with thickness $h_1 = 0.135$ mm. If a micro-channel with width $w = 3$ mm is chosen and the syringe pump is pumping each fluid in one of the Y-junction branches with flow-rate $Q = 1$ µl/min the average velocity $v = 2 \cdot 1 \cdot \frac{1}{60}/(0.135 \cdot 3) \approx 0.08$ mm/s in the micro-channel is obtained.

To verify this estimation a numerical 2D simulation of the micro-channel geometry was performed in COMSOL Multiphysics® software. A Hele-Shaw cell approximation was used. This is demonstrated in figure 2.6. for several Y-junction micro-channels. The characteristic velocity away from the Y-junction is in agreement with the previous estimation.
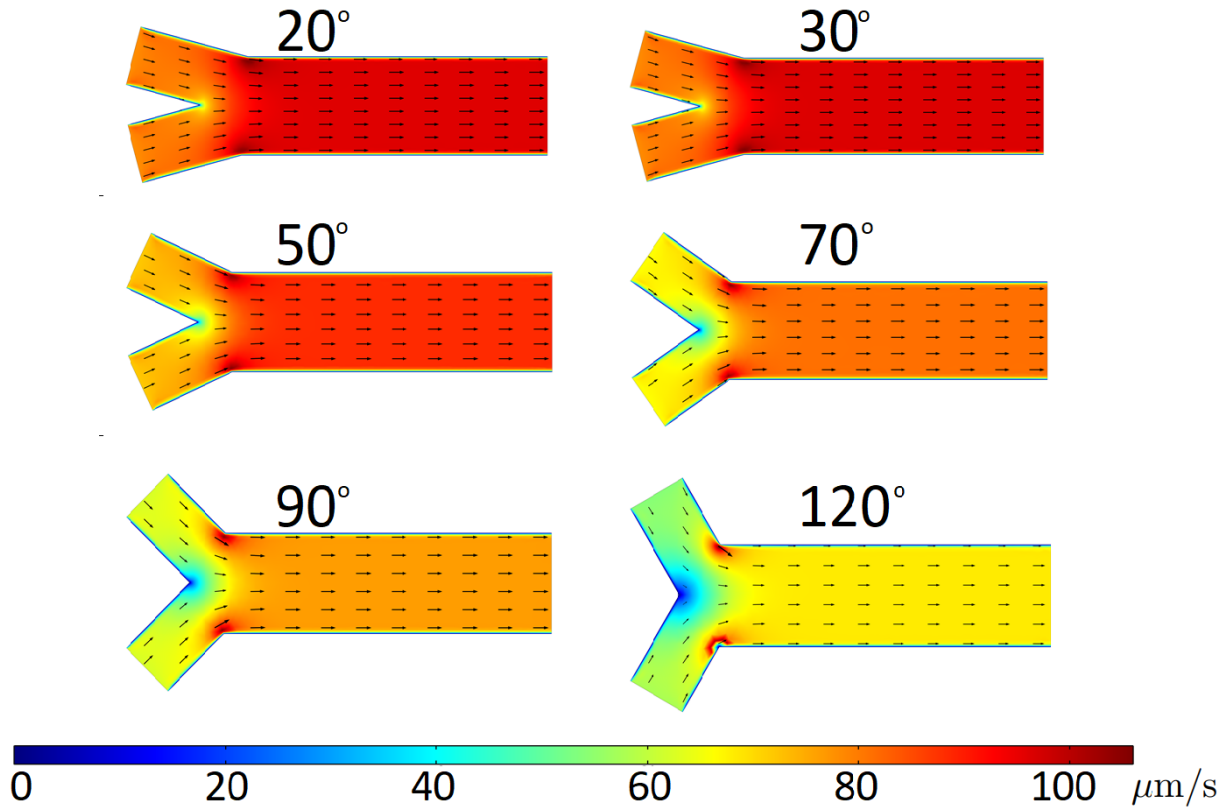
2.6. Figure: Velocity plot in Y-shaped micro-channels with various angles between Y-branches. Numerical simulation was carried out with the COMSOL Multiphysics® software using Hele-Shaw flow. The width of the channel was chosen to be 3 mm for the tail and 1.5 mm for each Y-branch. Input flow-rate was fixed at $Q = 1$ $\mu l/min$ for each fluid.

As visible from fig. 2.6. a velocity distortion appears after the Y-junction and it depends

on the angle between the Y-branches and is smaller for smaller angles. Velocity around the tip is smaller, especially if the Y-junction has larger angle. But it is harder to cut out channels with small angles between the Y-branches due to the stickiness and stretchability of the Parafilm M® spacer.

Even if the angle between the branches is small, as the micro-channels are cut out by hand so the Y-tip is not perfectly sharp and the fluid flow is distorted around the tip even more. A velocity plot example in a real microfluidics chip is demonstrated in figure 2.7.. But as it can be noted by figures 2.6. and 2.7. slightly away from the tip and in the middle of the chip the velocity field of the fluids is homogeneous enough.

(a) A photography of a micro-channel through microscope.

(b) A numerical simulation (COMSOL Multiphysics®) of a velocity plot in the particular micro-channel using Hele-Shaw flow.
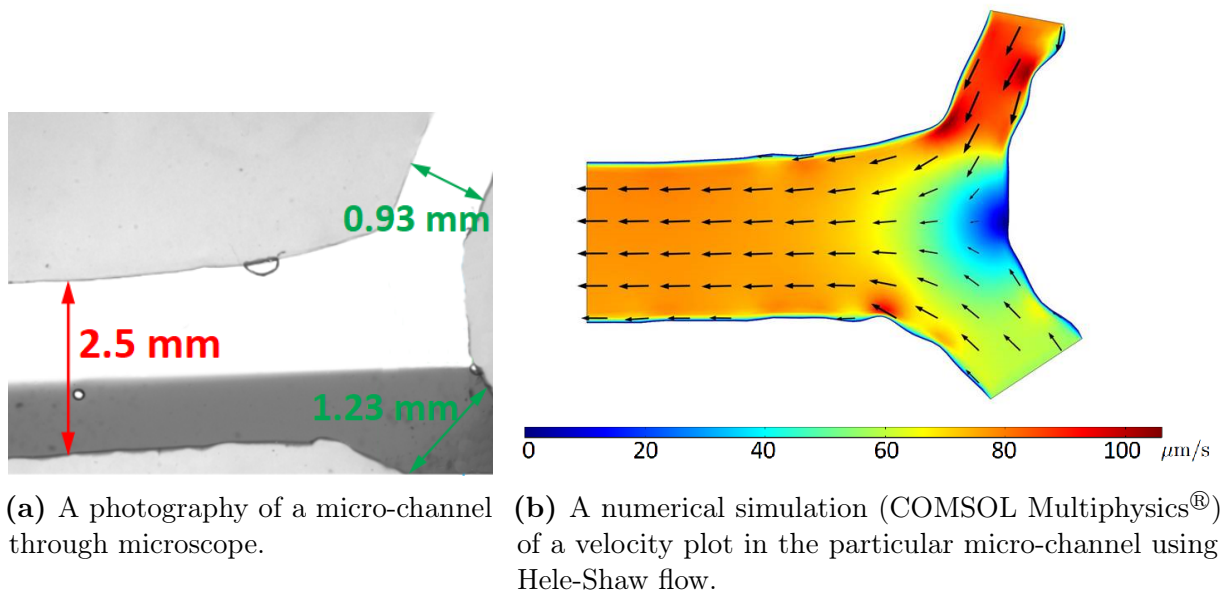
2.7. Figure: An example of Y-shaped micro-channel near the tip, cut out by hand. Thickness of the particular micro-channel is $h_1 = 0.135$ mm.

The position of the interface in the channel depends on the viscosity of both fluids. Here the viscosity of the magnetic fluid is considered to be the same of the water, although in reality magnetic fluids reviewed here are a bit more viscous than water. In a hypothetical case for two immiscible flowing fluids the interface between them would be positioned proportionally to the ratio of their viscosity:

$$\frac{\eta_1}{\eta_2} = \frac{w_1}{w_2},$$ (2.3)

where w_1 and w_2 are the widths in the channel of to two fluids with viscosity η_1 and η_2 accordingly. In the experimental system within this work the initial interface position depends on the position of the tip of Y-junction. Also the interface can fluctuate due to pressure changes or bubbles within the system.

Micro-channel with a wide rectangular pool was used in the rest of the experiments

(§3.2., §3.3. and §3.4.). An example of microfluidics chips used in experiments with Y-shaped and "rectangular pool"-shaped micro-channels is demonstrated in figure 2.8..
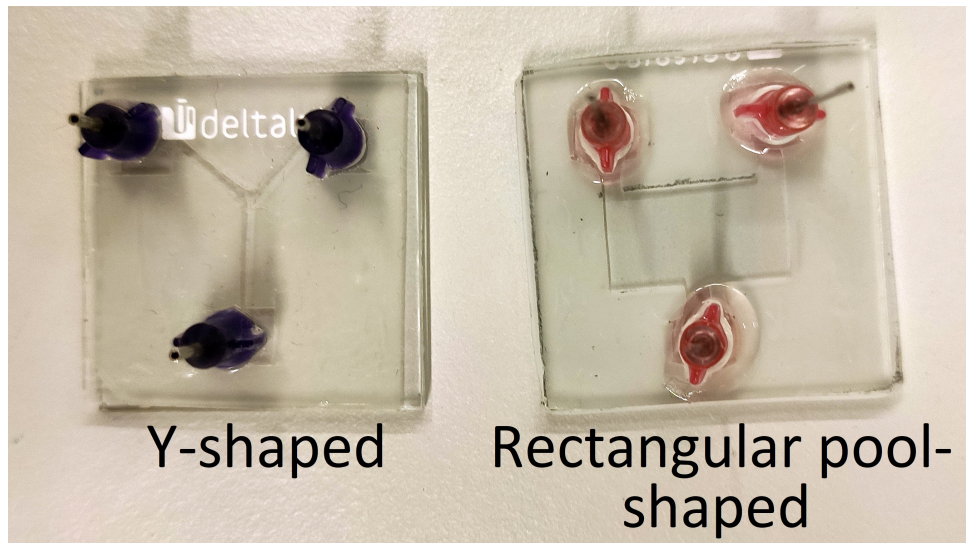
2.8. Figure: Picture of microfluidics chips with the two used micro-channel shapes during this research. On the left Y-shaped micro-channel is visible and on the right micro-channel with rectangular pool is demonstrated.

The particular shape of the microfluidics channel was chosen in an empirical way among several others hypothesised to be effective for magnetic micro-convection measurements with initially stagnant fluids. It was found out that the "rectangular pool" shaped one was the most effective one to minimize the parasitic flows that exist after pumps have been stopped and the magnetic field is turned on.

2.4.   Experimental setups

The concept of the experimental system already existed from the research described in [53]. However some improvements were necessary. Previously microfluidics chip was placed horizontally, therefore gravity caused a convective motion in which a bit denser magnetic fluid slipped underneath the water during the experiments. This complicated the tests and interpretation of the results.

Within the study of these thesis the experimental system was improved to exclude the mentioned parasitic convection by studying the magnetic micro-convection in a vertically placed microfluidics chip.

Conceptually the same experimental system with three small variations was used in this study. The differences in the setup for experiments with flowing fluids, initially stagnant fluids and experiments in a vertical magnetic field are described further.

Simplified schematic illustration oh the experimental system is demonstrated in figure 2.9.. In general experimental system consists of:

- Microfluidics chip and tubing;

- Electromagnet and its holder;

- LED panel: *Visional®, 4 W, 400 lm, 3000 K*;

- Microscope: *Zeis Stemi 2000-C*;

- Camera: *Lumenera Lu165c, 15 Hz*;

- Computer with necessary software;

- One or two syringe pumps: *Harvard Aparatus PHD Ultra* and *KD Scientific Legato 210P*.
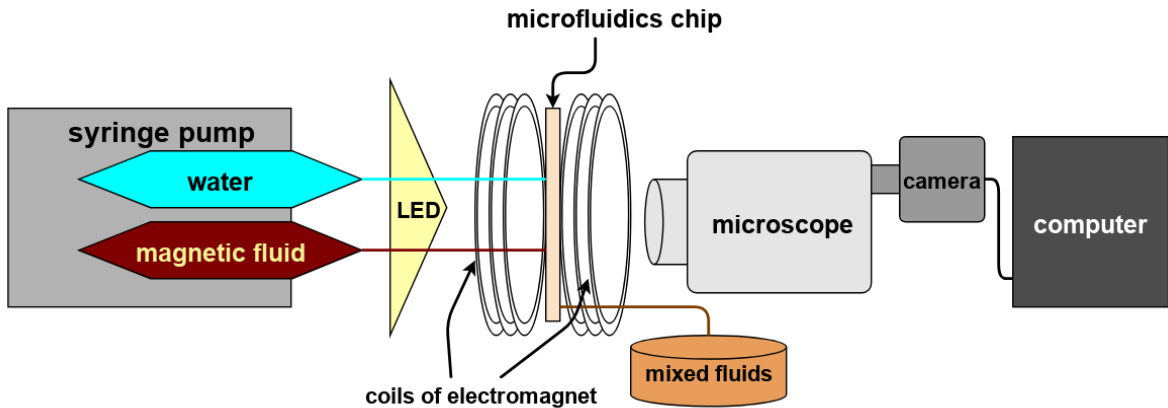
2.9. Figure: A schematic illustration of the experimental setup.

The microscope is put sideways as can be seen in figure 2.10. and the camera is filming the experiments through it. If two syringe pumps are used, they are connected with Android based synchronizer. This allows to start and stop the flow from both pumps simultaneously. The electromagnet is made from two identical coils and can create a homogeneous magnetic field up to $H = 200$ Oe. The coils consist of 200 turns of copper wire with a diameter $d = 0.7$ mm. Inner and and outer diameters are $d_{\mathrm{in}} = 45$ mm and $d_{\mathrm{out}} = 57$ mm, and the height of a coil is 19 mm. The coils are powered by a power supply (TENMA 72-2930) in a constant current mode. Experiments with higher magnetic fields must be kept short (< 1 min) as the air can cool the coils only if currents smaller than 1 A are used, which corresponds to magnetic field $H \approx 60$ Oe. Overheating affects the experiment in two ways: chaotic movement of the particles increases and the microfluidics chip may come apart if exposed to temperatures above 40 °C for prolonged periods of time. The latter especially affects the continuous flow experiments as the higher flow-rates of the syringe pump add extra pressure within the chip.
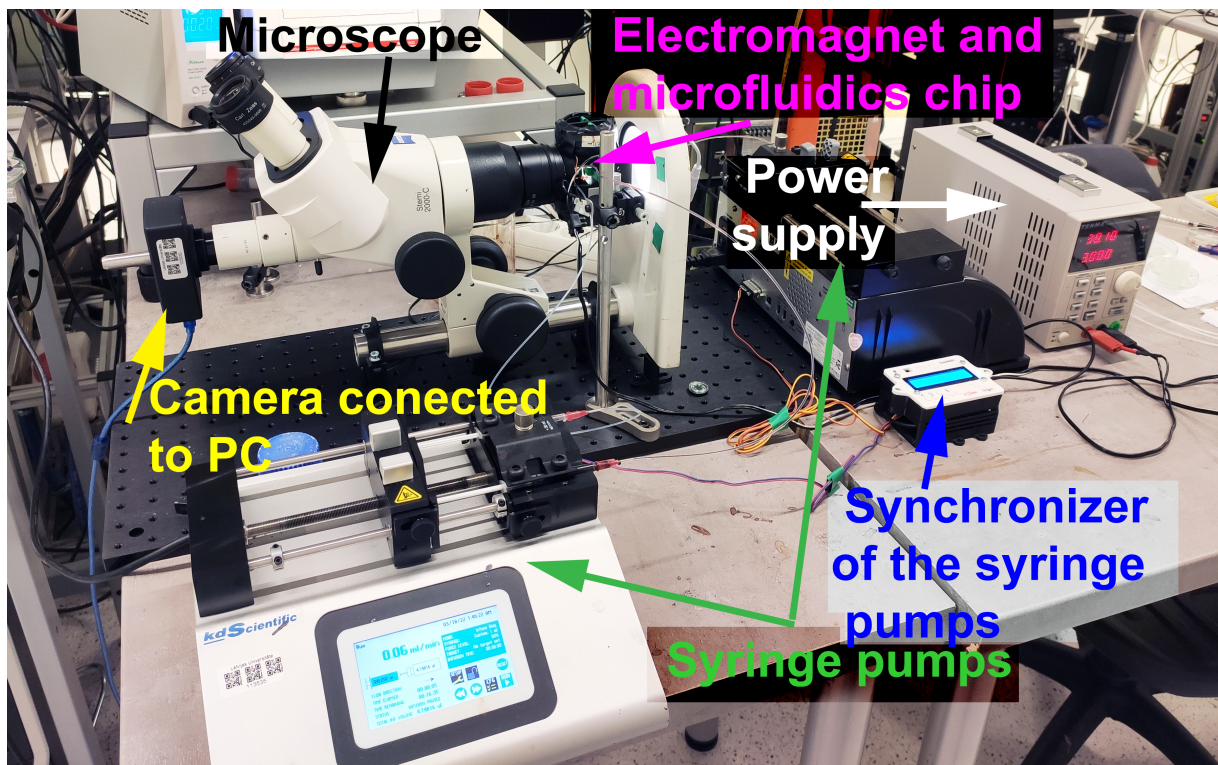
2.10. Figure: A photography of the experimental setup for experiments in vertical magnetic field

The microfluidics chip is vertically fixed in the center of the electromagnet by a 3D printed holder (Materieal: PLA filament; 3D printer: Mass Portal Pharaoh XD 20). Depending on the type of the experiments carried out two different coil holders are used as showed in figure 2.11.a.

(a) Coils with the holder for experiments with horizontal magnetic field that is perpendicular to the microfluidics chip.

(b) Coils with the holder for experiments with vertical magnetic field that is parallel to the microfluidics chip.

2.11. Figure: Coils of the electromagnet with 3D printed holder and microfluidics chip.

The data is collected by custom made program written in LabView® by colleagues for previous research [53]. The program conveniently saves each image with title corresponding to the time since the beginning of the experiment. Afterwards the data is processed mostly using MATLAB® software.

Magnetic micro-convection experiments are performed with distilled water and various magnetic fluids. For liquid handling, 1 ml syringes that are connected to the micro-chip with FEP tubing (IDEX, $\varnothing_{\text{ID}} = 0.76$ mm, $\varnothing_{\text{OD}} = 1.59$ mm) are used. Magnetic fluid is denser than water. Therefore its tubing is connected to the lower inlet of the micro-chip, while water is connected to the upper inlet. If one syringe pump is used, then the outlet of the micro-channel is left open and the mixed fluids drip into a waste container. If two syringe pumps are used, then the second pump is connected to the outlet.

2.4.1. Experimental setup for continuous flow experiments

In this section the variation of experimental setup for continuous flow experiments (that are reviewed in § 3.1.) is explored.

Within this part of the study microfluidics chips with Y-shaped micro-channel were used. Only one syringe pump was used for pumping in the fluids of interest and the outlet was left open. Microfluidics chip was placed in the center of the coils of the electromagnet so that the magnetic field is perpendicular to the plane of the chip as demonstrated in figure 2.12..
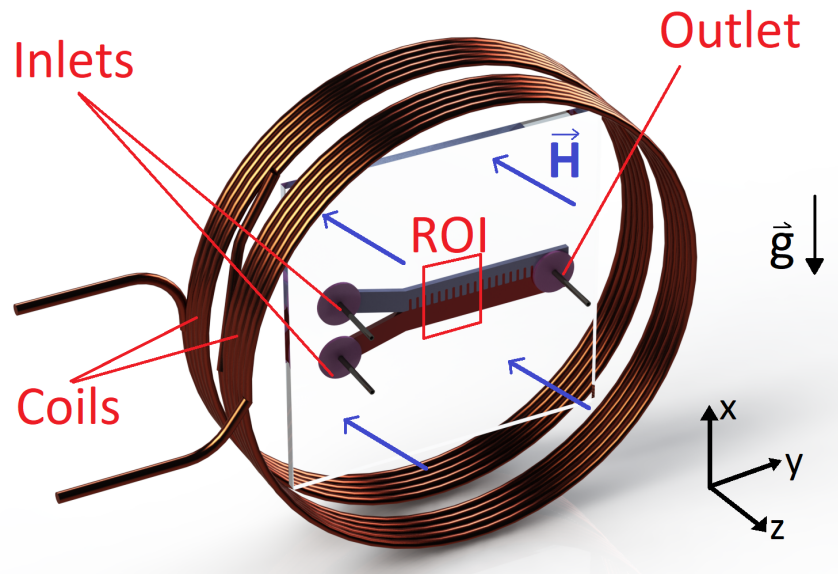
2.12. Figure: An illustration of the Y-shaped microfluidics chip. The microfluidics chip is placed vertically between the coils of an electromagnet. The chip has the horizontal Y-shaped channel cut in the Parafilm M® spacer. The chip has two inlets- the upper one for distilled water and the lower one for magnetic fluid as well as one outlet for mixed fluids. Coils provide a homogeneous magnetic field H, perpendicular to the chip. Region of interest (ROI) indicates the field of view of the camera. The axis in the picture are the same as used in data analysis.

The desired flow-rate was chosen and the fluids were let to flow for a few moments before the experiment for the interface to stabilize. Then the magnetic field was applied. The experiments are timed and recorded from the moment the magnetic field is switched on. Magnetic field is not changed during all of the experiment.

It was found out during the study that by this setup it is not possible to carry out experiments with initially stagnant fluids, as after turning on the magnetic field a parasitic longitudinal motion of magnetic fluid along the y-axis of the micro-channel appeared although syringe pump was not working. The nature of the parasitic flows is not clear. Probably, they arise due to the local differences of the demagnetizing field.

So the experimental setup was once again modified as described in the next section §2.4.2. to acquire experimental data of magnetic micro-convection if the mixing fluids are not flowing.

2.4.2. Experimental setup for experiments with initially stagnant fluids

In this section a variation of experimental setup designed for experiments with initially stagnant fluids is explored. The experimental results made with this experimental setup are collected in §3.2. and in §3.3. where the effects of initially smeared interface are explored.

The thickness of the interface smearing between the miscible fluids is varied by letting the fluids to diffuse for various periods of time. Although the diffusion length δ should depend on time alone (see eq. 1.19), experimentally it is not the case. As the interface between the fluids fluctuates a bit after the syringe pumps are switched off, a small interface smearing is created. Therefore it is not possible to set a specific smearing thickness just by a specific amount of time. So large amount of experimental data was obtained in order to get several experiments with the same initial interface smearing to draw some conclusions about the instability. In the literature [6], specific magnetic field was applied before the experiment to get the desired initial interface smearing, but as authors note, this method was also unpredictable.

An example of the obtained initial smearing lengths δ_0 for various waiting times is collected in table 2.2. for magnetic fluid KTF11-1$_{100\%}$ in microfluidics chip with thickness $h_1 = 0.135$ mm. For each waiting time represented here, 15 experiments were carried out, minimal $\delta_{0,\min}$, maximal $\delta_{0,\max}$ and average $\overline{\delta_0}$ values of the initial smearing thickness as well as standard deviation σ_{δ_0} for the measurement set is represented.

These experimental values are compared with theoretical diffusion curve using equation 1.19 in figure 2.13. and diffusion coefficient of the magnetic fluid KTF11-1 from table 2.1..

t, s	$\delta_{0,\min}$, mm	$\delta_{0,\max}$, mm	$\overline{\delta_0}$, mm	σ_{δ_0}, mm
0	0.08	0.20	0.12	0.03
60	0.13	0.17	0.15	0.02
120	0.17	0.23	0.20	0.02
150	0.14	0.27	0.20	0.04
300	0.18	0.28	0.23	0.02

2.2. Table: Initial smearing δ_0 dependence of the waiting time before the experiment.

Experimental data is represented by the round marker with one standard deviation for error and the theoretical curve is represented by the dashed line. As it is visible here, experimentally the initial smearing values are larger than theoretical values expected due to diffusion. Small interface fluctuations occur during pumping the fluids as well as after stopping the flow. The small interface fluctuations are also the reason why it is not possible to create an experiment with perfectly sharp initial interface.

After the interface between the fluids has stabilized or the desired amount of pre-mixing is obtained, the magnetic field to create the instability is applied. The experiment is timed and recorded from this moment.
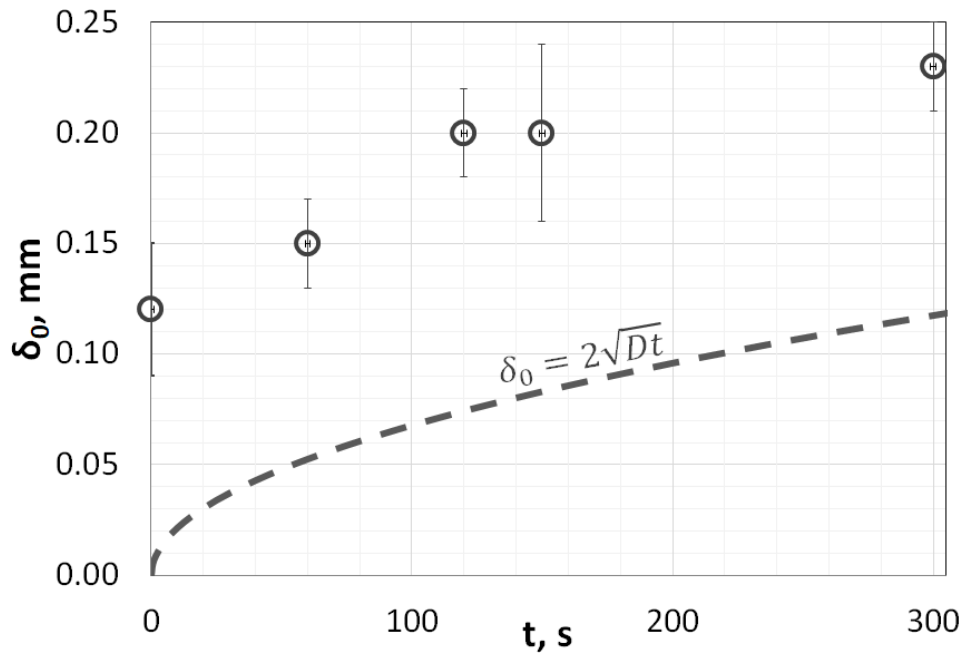
2.13. Figure: Initial smearing δ_0 dependence of the waiting time before the experiment.

There are two innovations as compared with the setup described in the previous section § 2.4.1. in order to obtain initially stagnant fluids. Two syringe pumps instead of one are used. The shape of the micro-channel for this experimental setup is chosen with a wide rectangular pool as shown in fig. 2.14.. The micro-channel has two inlets, that are connected to one syringe pump and one outlet which is connected to the other syringe pump. The pumps are connected electronically with a switch, so that they can operate synchronously. The pumps start and stop working at the same time, so that the same amount of fluid is pumped in and out of the micro channel. This allows to rapidly stop the flow. Also the closed system decreases the effects of the parasitic longitudinal flow after the application of the external magnetic field. Fresh fluids are pumped in before each experiment. The flow-rate of the pumps must be set fast enough so the interface between the fluids would be smooth and straight but slow enough so the chip would not come apart.

The shape of the micro-channel for this experimental setup was chosen in empirical way amongst several others. It was noticed during the experiments with Y-shaped channel that it is possible to carry out experiments with initially stagnant fluids if the outlet was blocked by accidental air bubble. So the first guess was to create micro-channels where air bubbles might be created and trapped. Extra inlet in the microfluidics chip for the air to come in was created as visible in figure 2.15. for microfluidics chips a and b. The air bubble was created by syringe regulated with second syringe pump. The outlet was still left open. It turned out that it is too hard to control the input, size as well as the position within the micro-channel of the air bubbles with the available equipment.
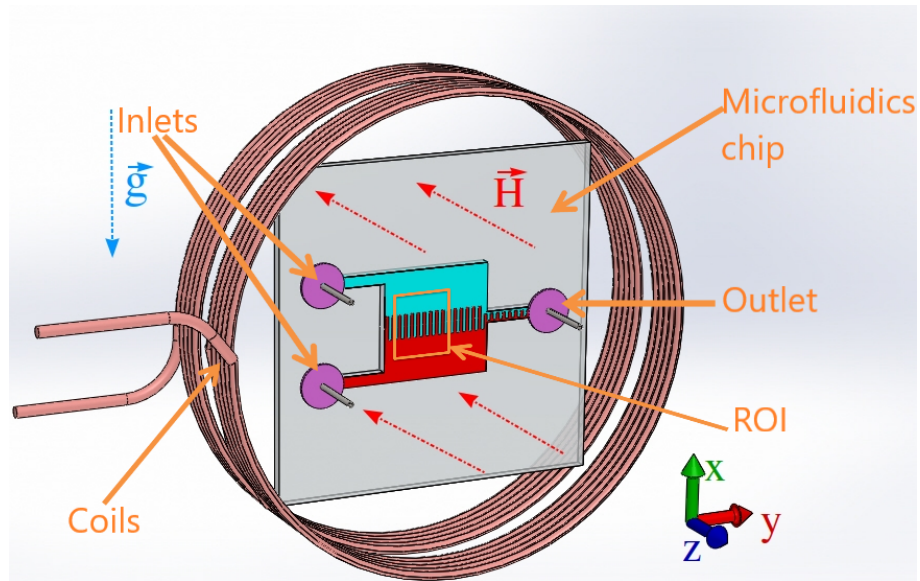
2.14. Figure: An illustration of the microfluidics chip within an electromagnet. The chip has two inlets and one outlet connected to syringe pumps. The lower inlet is for the denser magnetic fluid, while the upper inlet is for water. Coils provide a homogeneous magnetic field H, perpendicular to the chip. Region of interest (ROI) indicates the field of view of the camera.
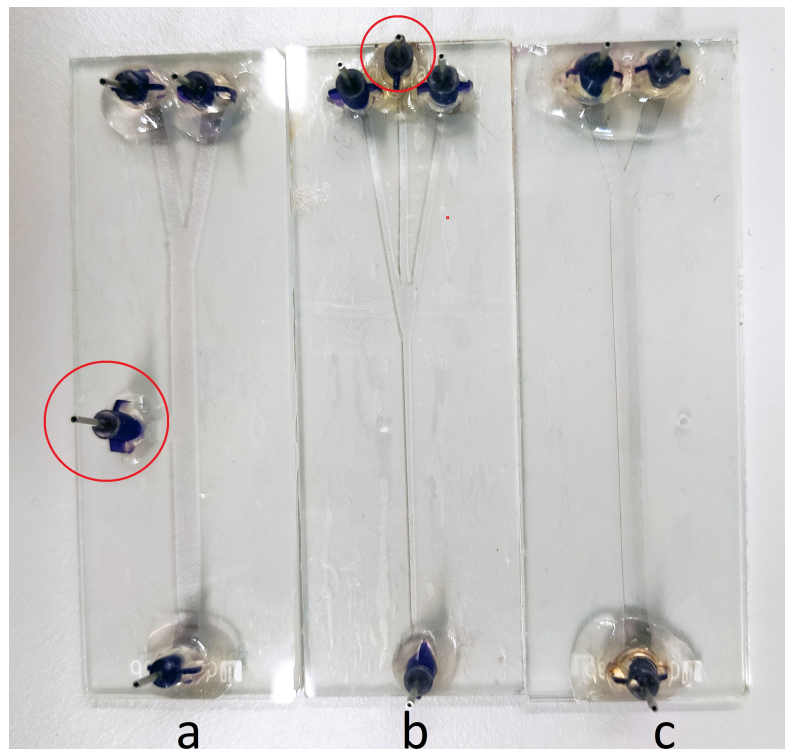

2.15. Figure: A picture of microfluidics chips with various micro-channels. *(a)*: Micro-channel with extra inlet for air bubble at the side; *(b)*: Micro-channel with extra inlet for air bubble at the beginning; *(c)*: Y- shaped micro-channel with long tail. Inlet for air is circled with red line.

Then it was hypothesised that long enough micro-channel might be sufficient (see fig. 2.15..c) as the parasitic longitudinal motion first appears near the outlet and affects the beginning of the chip only after some moments. Alas this solution also was not good enough. It was noticed that amongst several geometries tested, the best results minimizing the parasitic longitudinal flows that exist after pumps have been stopped and the magnetic field is turned on were achieved with micro-channels with rectangular pool in the middle with inlet channels at right angle.

2.4.3. Vertical external magnetic field

In this section the variation of experimental setup for experiment in vertical external magnetic field is explored. The experimental results made with this experimental setup are collected in §3.4.. Similarly as for the experiments in horizontal magnetic field, the thickness of the interface smearing between the miscible fluids is varied by letting the fluids to diffuse for various periods of time before the experiment. Before each experiment, fresh fluids are pumped in using syringe pumps. Then the flow is stopped for a certain amount of time after which the magnetic field is applied. An experiment is timed and recorded from the moment the magnetic field is applied.

Within this part of the study, the microfluidics chip was placed within the coils so that that magnetic field would be parallel to the microfluidics chip as showed in figure 2.16.. Microfluidics chips with a rectangular-pool shaped micro-channel is used.
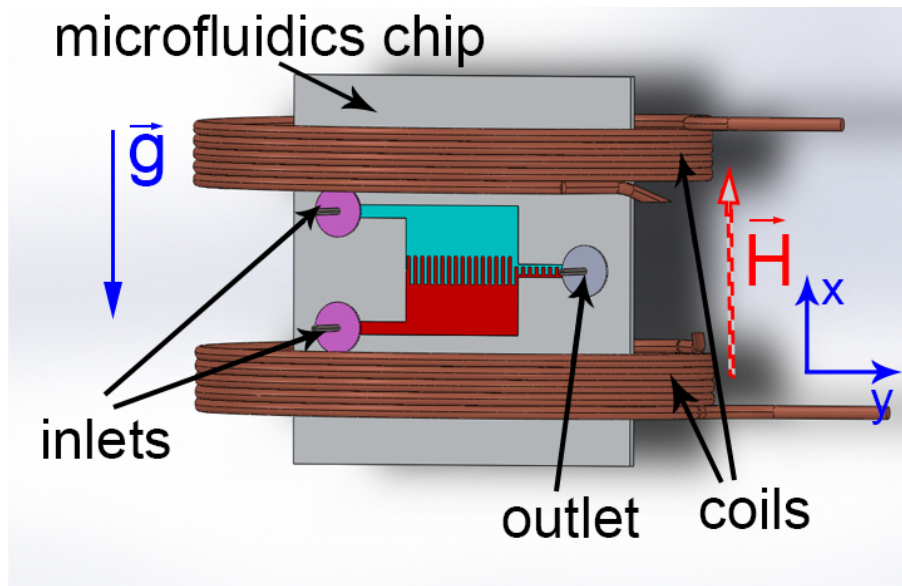
2.16. Figure: An illustration of the microfluidics chip within an electromagnet with vertical magnetic field.

The same coils as in previous experimental setups were used, but new coil holder was 3D printed to hold the coils and microfluidics chip as demonstrated in figure 2.17.. The holder was made so that it would be possible to capture the experimental data with the

current microscope objective, so that was the main limit for the distance between the coils.
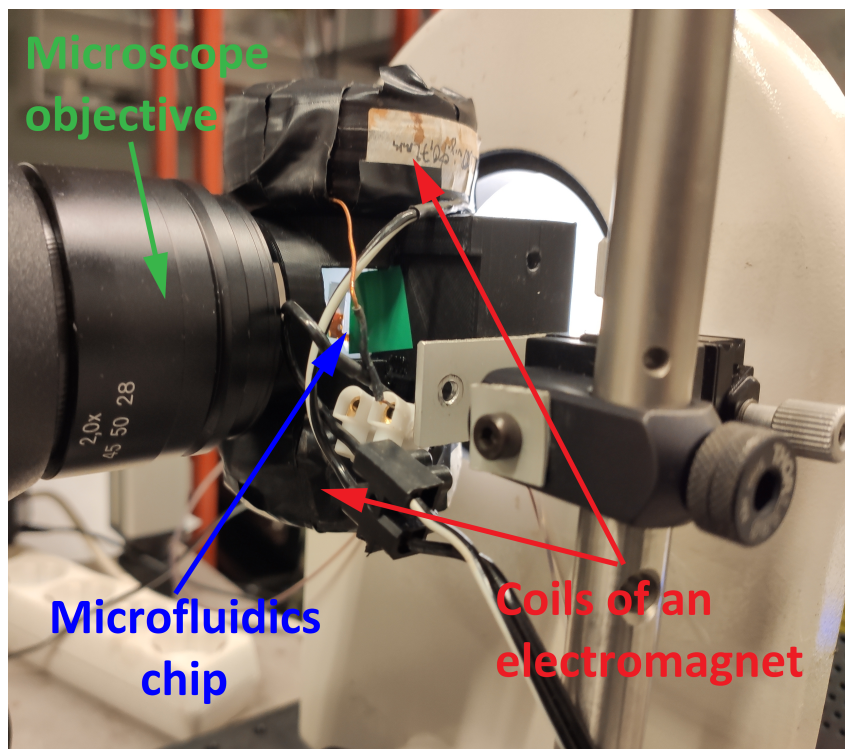
2.17. Figure: A photography of the coil holder with microfluidics chip placed in the middle between the coils of the electromagnet.

As with this setup the coils are further away from each other, the magnetic field for set electric current was measured again using FW Bell 5180 Gauss Meter. Also as the microfluidics chip is not tightly sandwiched between the coils the experiments can be run for longer periods of time before the microfluidics chip would come apart. The strength of magnetic field is still restricted aproximately the same, so the electrical insulation of the coils would not start to melt.

2.5. Processing of the experimental data

In this section the steps from an experiment to visualized and perceivable results are addressed.

2.5.1. Acquisition of the mixing length

Once the experiment starts the development of the mixing of two fluids is recorded as image series over time (15 frames per second) with a microscope camera. The camera is connected to the computer and the data is collected using LabView® based program that saves each image with milliseconds since the beginning of the experiment as title. The recorded image series are analyzed for a manually selected area- region of interest (ROI) with x and y axes as shown in fig. 2.18.. Each particular ROI is chosen so, that all of the mixing is captured (fingers of the instability are well visible and are not cropped) during

all of the experiment. The mixing length (2δ) characterizes the height of the fingers of the instability. And single δ is diffusion length defined by equation 1.19.
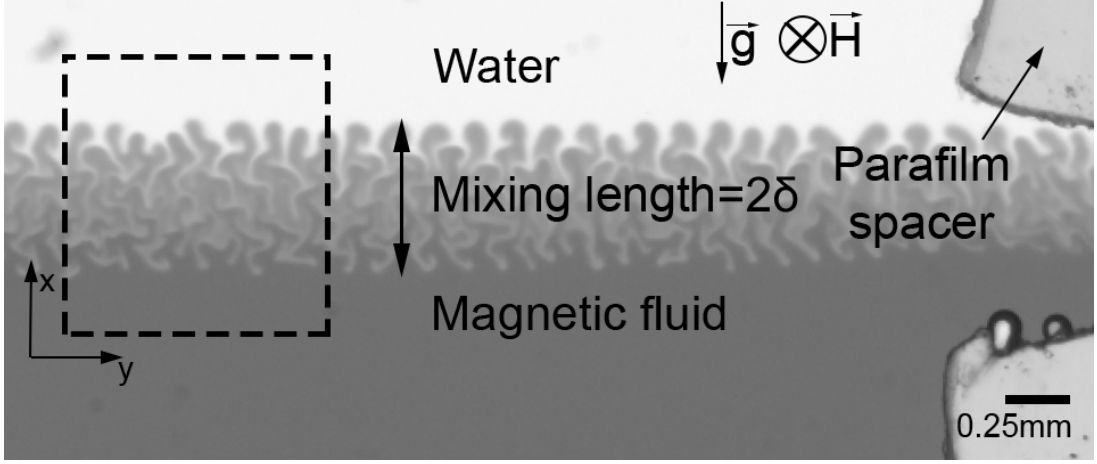
2.18. Figure: A recorded image of the magnetic micro-convection for a magnetic fluid D107 100% and water, in an external magnetic field $H = 89$ Oe, at $t = 5$ s. The area of analysis is indicated by the dashed line.

The data processing steps described further are done using MATLAB®, to get a quantitative information from the image series. The core idea of the processing steps described here are already used in [53], but here some steps and the corresponding MATLAB® code is improved to be more convenient and to fit better for the aims of this thesis (see §A.2).

An example of the next three steps is demonstrated in figure 2.19.. The camera records color images that are first converted to 8-bit gray-scale images (see fig. 2.19.a). The camera acquires images as intensity plots $I_t(i,j)$, where i and j are spatial indexes and t is the time passed in the experiment (time of the image acquisition). However theory for the magnetic micro-convection is based on the magnetic particle concentration. As the illuminated light in the experiments is transmitted through the microfluidics chip- the experimental recording of the magnetic micro-convection complies with the bright field microscopy. Magnetic fluid absorbs light more effectively than water so the contrast of the images is generated by this light absorption difference. The Beer-Lambert law states that there is a linear relationship between the concentration and the absorbance of the solution [95, 96], so concentration of a solution can be calculated by measuring its absorbance. Here the intensity data is converted to a normalized concentration plot $c_t(i,j)$ via Beer-Lambert law, which is normalized to an initial concentration [87]:

$$c_t(i,j) = \frac{\log I_t(i,j) - \log I_{H_2O}}{\log I_{MF} - \log I_{H2O}}, \tag{2.4}$$

where I_{MF} and I_{H2O} are the intensities of initial concentrations (when $t = 0$) for magnetic fluid and water accordingly. This way an initial concentration of magnetic fluid is set to

$c_0 = 1$ and of clear water to $c_{0,H_2O} = 0$. An example of this can be seen in figure 2.19.b. The real concentration of magnetic fluid can be calculated by multiplying the real initial concentration with the normalized concentration: $\phi_t(i,j) = \phi_0 \cdot c_t(i,j)$, where ϕ_0 is the initial volume fraction of the magnetic fluid [53].
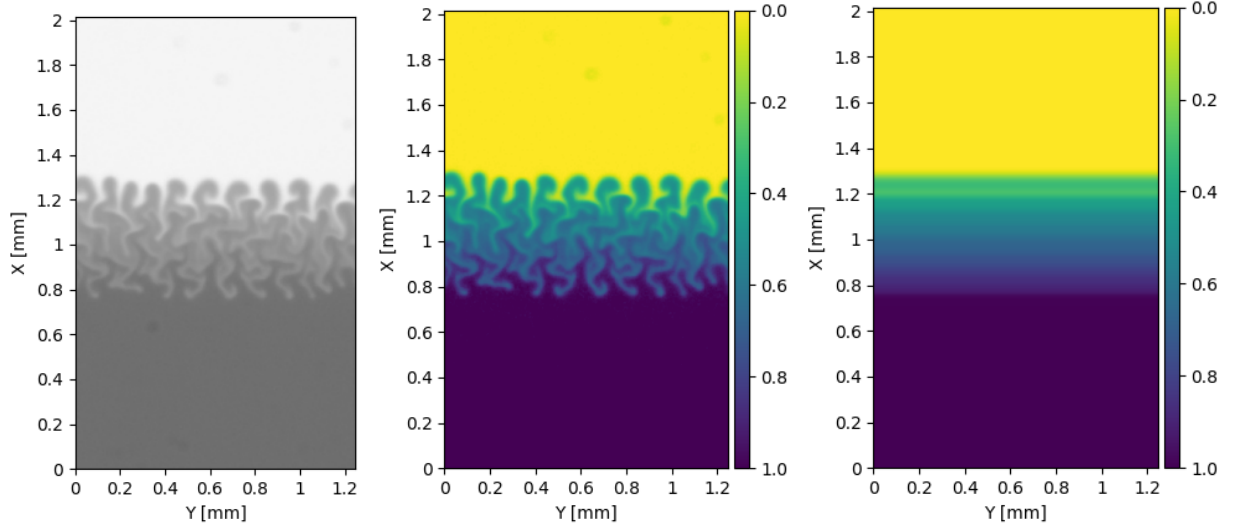

(a) An intensity plot— a gray-scale original image of the experiment.

(b) A normalized concentration plot.

(c) An averaged concentration profile along the vertical x-axis.

2.19. Figure: An experiment with initially stagnant fluids at $t = 5$ s in $H = 89$ Oe horizontal magnetic field with magnetic fluid $D107_{100\%}$. A gray-scale original image of the experiment is converted to normalized concentration plot, where $c = 1$ corresponds to concentrated magnetic fluid and $c = 0$ to clean distilled water and then averaged along the vertical x-axis.

After this step the concentration of each image is averaged along the y-axis (see fig. 2.19.c). A spatially averaged concentration is calculated from the concentration data:

$$\overline{c_t}(i,j) = \frac{1}{N} \sum_{j=1}^{N} c_t(i,j), \tag{2.5}$$

where N is the total length of spatial index i in pixels. As a result the average concentration depending on the vertical direction (x- axis) giving $\overline{c}(x)$. X-axis is converted from pixels to millimeters using a scaling factor determined for the microscope using calibration kit. By plotting how this averaged concentration changes regarding the coordinate x, one gets a line of the average concentration profile $\overline{c}(x)$. This is demonstrated for an experiment in horizontal magnetic field with initially stagnant fluids in figure 2.20. with red circles. Due to fingers of the instability this line might have a wavy look as it does here.
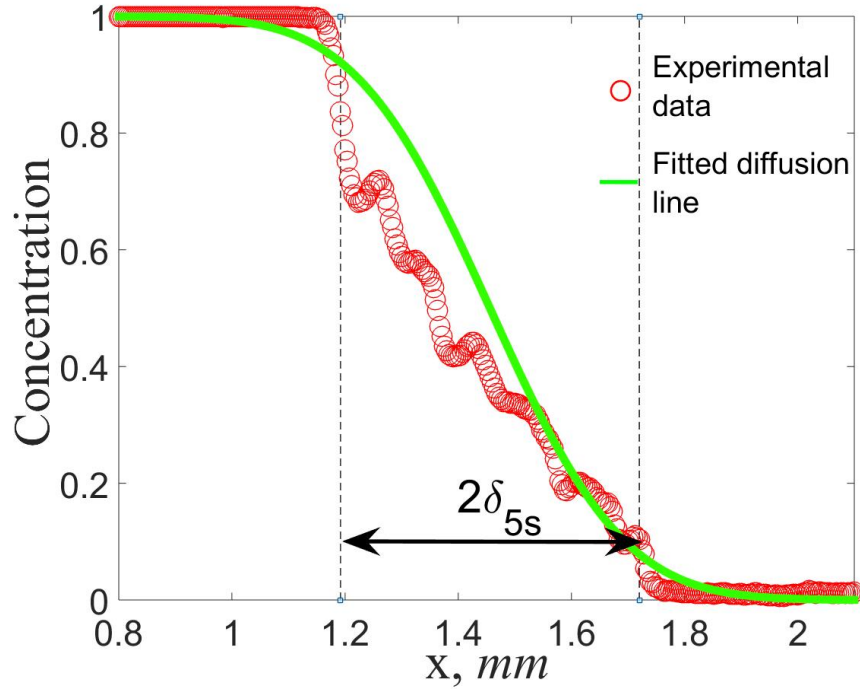
2.20. Figure: An average concentration profile (red circles) for time moment $t = 5$ s in an experiment with initially stagnant fluids with the magnetic fluid D107$_{100\%}$, in horizontal external magnetic field $H = 89$ Oe in microfluidics chip with $h_1 = 0.135$ mm. And the fitted diffusion curve using Fick's law solution (green line). The mixing length at that moment is represented by an arrow as doubled diffusion length 2δ.

The figure 2.20. corresponds to just one time-point in a single experiment. To characterize the whole experiment, these last steps must be repeated for all the time-points of the experiment.

Then for all of the time points this averaged concentration profile $\bar{c}(x)$ is fitted with the diffusion curve (green line in fig. 2.20.), according to Fick's law solution:

$$c(x) = \frac{1}{2}\left(1 - \text{erf}\left(\frac{x - x_0}{\delta}\right)\right), \tag{2.6}$$

where diffusion length $\delta = 2\sqrt{Dt}$ is equal to half of the mixing length (see fig. 2.18. and fig.2.20.) and it was defined in §1.3.4. with equation 1.19 and erf is the error function and x_0 is the coordinate of the symmetry center and gives a degree of freedom for the fit.

The next step is to obtain the dynamics of the mixing length over time for a particular experiment. It is done, by reprocessing lines of the average concentration profile for all the time-frames of each experiment. Mixing length for several experiments in horizontal magnetic field with initially stagnant fluids is demonstrated in figure 2.21.. As it is visible here, larger values of the mixing length over time are achieved if the fluids are exposed to stronger magnetic fields.
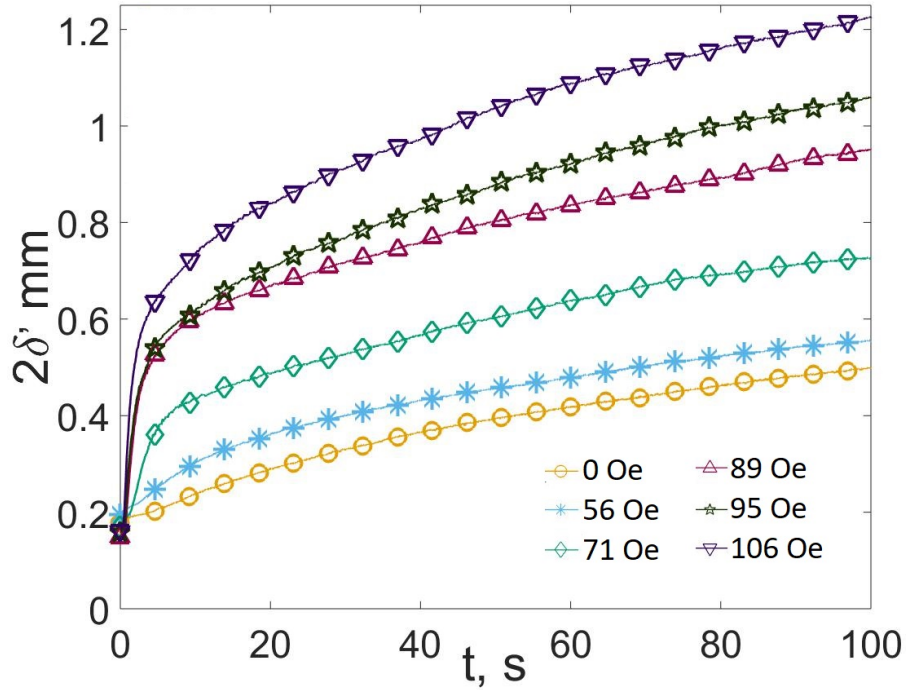
2.21. Figure: Dynamics of the mixing between both fluids in experiments with initially stagnant fluids in horizontal magnetic field. A change of a mixing length over time for the magnetic fluid D107$_{100\%}$ in various magnetic fields. Microfluidics chip $h_1 = 0.135$ mm.

The equation for diffusion length can be rewritten as $\delta^2/4 = Dt$. Thus the quantity $\frac{\delta^2}{4}$ is directly proportional to the time t the experiment has been happening and the proportionality constant is the particle diffusion coefficient D.
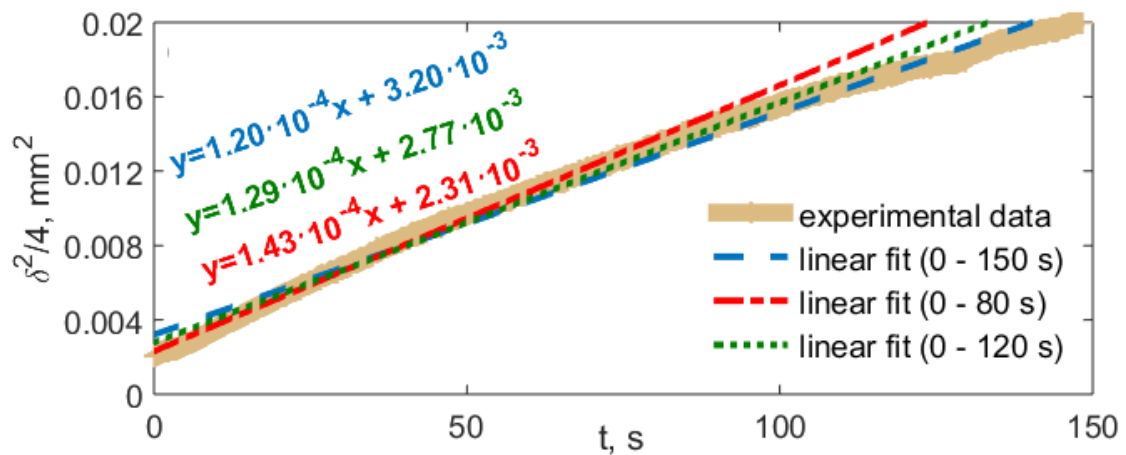
2.22. Figure: Dynamics of the mixing between D107$_{100\%}$ and water as $\frac{\delta^2}{4}$. The diffusion without magnetic field $H = 0$ Oe is shown by a beige line. The blue, green and red lines are linear fit of the experimental data for different time regions (150 s, 120 s and 80 s accordingly). Microfluidics chip $h_1 = 0.135$ mm.

Therefore to identify the diffusive behavior it is useful to plot dynamics of the mixing between both fluids as $\frac{\delta^2}{4}(t)$.

If there is no external magnetic field and the mixing between both fluids is due to diffusion only, then $\frac{\delta^2}{4}$ is directly proportional to the diffusion time t. Therefore the mixing dynamics should look like a straight line. This assumption is used to find the diffusion coefficient D_{exp} for experimental analysis of the data as described further.

$\frac{\delta^2}{4}$ as a function of time is linearly fitted line for for several experiments at $H = 0$ Oe to get the value of D_{exp}. Theoretically $\delta^2/4$ as a function of time at $H = 0$ Oe should look like a perfectly straight line, as only the diffusion process should be present. Experimentally it is not the case, as it can be seen in figure 2.22.. Here magnetic fluid D107$_{100\%}$ is mixing with water. The experimental data (beige line) does not look perfectly linear. To approach this fact the experimental data is linearly fitted with multiple straight lines. The fitting regions are chosen in an according pattern- the first line fits the data from the start of the experiment (when the pumping of the fluids is stopped at $t = 0$ s) till the end of the experiment ($t = 250$ s), the next line fitted the experiment from the start, but the fit was 10 s shorter and so on. Sometimes when there is some interface fluctuations after switching off the syringe pump, the fits are started a bit later, for example, at $t = 10$ s. Here in fig. 2.22., as an example, three different linear fits over different time intervals are demonstrated with three different slope coefficients, which should correspond to the diffusion coefficient. Then these values of the slope of all these linear fits for all the experiments where $H = 0$ Oe for each of the magnetic fluids are averaged. This averaged value of slope is referred as the experimental diffusion coefficient D_{exp}. Range of valid D_{exp} values for each magnetic fluid is obtained.

This way the following experimental diffusion coefficient values were found: $D_{\text{exp, D107}} = (1.25\pm0.23)\cdot10^{-6}$ cm^2/s is found for magnetic fluid D107 used in §3.2. and later by repeating the experiments without magnetic field for §3.4., the values of $D_{\text{exp, D107}}$ fluctuated from $4.9 \cdot 10^{-5}$ cm^2/s to $7.2 \cdot 10^{-5}$ cm^2/s. For other magnetic fluids used within this study values $D_{\text{exp, FF21-5}} \approx 6.9 \cdot 10^{-5}$ cm^2/s, $D_{\text{exp, FF09-9}} \approx 3.0 \cdot 10^{-5}$ cm^2/s and $D_{\text{exp, KTF11-1}} \approx 2.8 \cdot 10^{-5}$ cm^2/s were obtained. These values differ a bit from the ones collected in tab. 2.1. from the DLS measurements, but the order of magnitude is the same for all fluids except FF21-5, which might have agglomerated particles judging from magnetic and hydrodynamic particle diameter measurements.

2.5.2. Quantifying mixing due to magnetic micro-convection

For the experiments in a magnetic field where the micro-convection is present, the quantity $\frac{\delta^2}{4}$ is not linearly proportional to the time any more. The line that represents the relationship $\frac{\delta^2}{4}(t)$ has a steep increase at the beginning, but eventually acquires a linear shape. An example can be seen in figure 2.23., where the experiment in $H = 56$ Oe horizontal

magnetic field (blue line in fig. 2.21.) is represented in corresponding coordinates. The linearity of the relationship between $\frac{\delta^2}{4}$ and time characterizes the diffusion process, but the initial rise is due to the micro-convective instability.

The fitting range of the linear fit is different for each experiment. For example, the fingers of the instability reach their maximal size and the character of the instability stabilises faster in weaker magnetic fields- then the linear fit can be attached earlier. Similarly as with experiments without magnetic field, here also several linear fits were used. Only at this step of the data processing the fit is started from the end of the experiment until approaching some specific time value with 10 s step. This specific time value is determined both visually from experiments, when the fingers of the instability have reached their maximal height and start to smear out due the diffusion as well as by the slope value of the linear fits, when it reaches the value range of D_{exp}. This information is also included when to determining the errors of of the linear fit.

The influence of the micro-convection within this thesis is characterized by a parameter δ_{MC}— mixing length due to magnetic micro-convection. This parameter can be obtained, by considering the function of the mixing dynamics as a sum of both diffusion and micro-convection. Therefore $\delta_{\mathrm{MC}}{}^2/4$ is expressed from the difference between the linearly fitted line and the curved one from experiments represented as graphs of $\delta^2/4$ with respect to time.

Mathematically the situation is simple for the experimental results collected in §3.2.. The magnetic field is applied and the experiment is started a short time after the syringe pumps are switched off. Small fluctuation of the interface between the fluids happens, thus creating slight initial interference smearing. But it is included within the value of the error, therefore the initial interface between the fluids is considered to be sharp, so that the initial smearing of the interface $\delta_0 \approx 0$. So the mixing length due to magnetic micro-convection δ_{MC} within these experiments can be expressed simply from the intercept of the vertical axis at $t = 0$ s of the linear fit from the graph of $\frac{\delta^2}{4}$ over time. This is demonstrated in figure 2.23.. The blue line represents the experimental data. At first the data line is curved as the magnetic micro-convection is governing the mixing, but after some time the line seems to have become straight. The tail of this line is fitted by a straight line (dashed black line in fig. 2.23.) in the range from $t = 60$ s to $t = 150$ s. This line crosses vertical axis at $\frac{\delta^2}{4}|_{t=0} = 0.0074$ mm^2. The linearly fitted line should have a diffusion coefficient for a slope. So it means if at $t = 0$ the magnetic field would not have been turned on, the diffusion process would look like a straight line parallel to the fitted one and starting from the coordinate $(0; 0)$. The rise between these two straight lines comes from the contribution of the magnetic micro-convection. Therefore if the initial smearing is $\delta \approx 0$ then the intercept of the vertical axis at $t = 0$ s of the linear fit comes from the magnetic micro-convection and agrees with $\frac{\delta^2_{\mathrm{MC}}}{4}$ (denoted by the pink brace in

fig. 2.23.), where δ_{MC} is mixing length due to the magnetic micro-convection. Here, in fig. 2.23. this quantity is $\delta_{\mathrm{MC}} \approx 0.17$ mm.
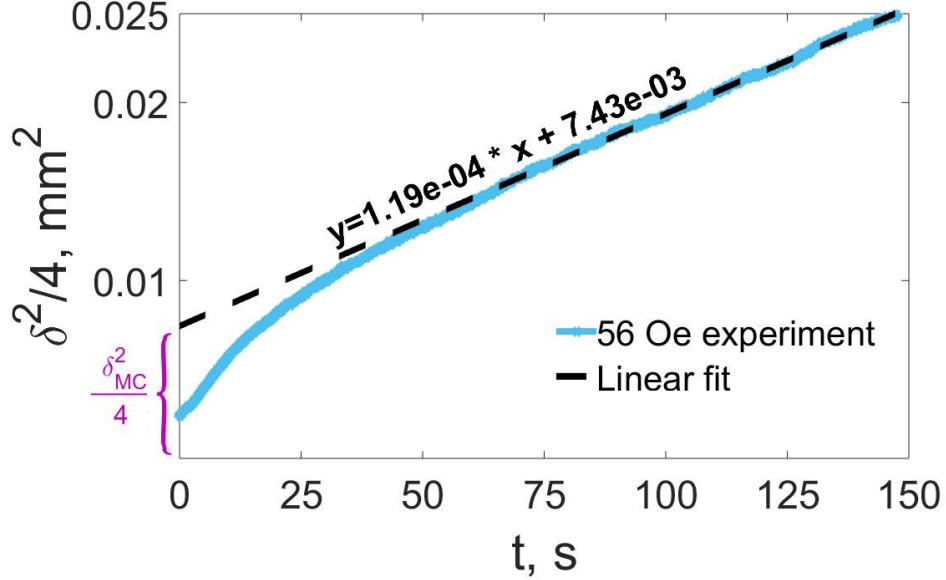
2.23. Figure: Dynamics of the mixing between water and magnetic fluid D107$_{100\%}$ in an experiment with initially stagnant fluids in a horizontal magnetic field $H = 56$ Oe. microfluidics chip $h_1 = 0.135$ mm. The black dashed line is a linear fit from $t = 60$ s to $t = 150$ s. $\delta_{\mathrm{MC}}{}^2/4$ is the y-intercept of the Linear fit line. The value of initial interface smearing (value of $\delta^2/4$ at $t = 0$ s) is taken into consideration when calculating errors. For this experiment $\delta_{\mathrm{MC}}{}^2/4 = 7.4 \cdot 10^{-3}$ mm^2.

The value of $\delta_{\mathrm{MC}}^2/4$ at $H = 0$ Oe is also included in the error estimation, as the value of $\delta_{\mathrm{MC}}^2/4$ without external magnetic field must be non-existent, because there is no magnetic micro-convection present.

This method of expressing δ_{MC} is not fit for experiments with varied initial interface smearing. Within chapters §3.3. and §3.4. both fluids diffuse for some time before the experiment, resulting in mixed interface with some mixing length 2δ before the magnetic field. Using the steps described for fig. 2.20. the initial smearing parameter δ_0 is expressed as $\delta_0 = \frac{2\delta}{2}|_{t=0}$, where $t = 0$ is the moment when the magnetic field is applied, thus also the start of the experiment. To compare the initial smearing thickness δ_0 with the theoretical predictions, a dimensionless time parameter t_0 is used:

$$t_0 = \left(\frac{\delta_0}{2h} \right)^2 = \frac{D \cdot t_{0,\mathrm{exp}}}{h^2}, \tag{2.7}$$

where h is the thickness of the used microfluidics chip, D is the diffusion coefficient of the magnetic nano-particles, $t_{0,\mathrm{exp}} = \frac{\delta_0^2}{4D}$ is the time, that should have been waited experimentally, to obtain the specific initial mixing δ_0.

In coordinates $\delta^2/4$ with respect to time the initial smearing is visible as initial rise of the experimental data, as it is demonstrated in figure 2.24. and this value corresponds to $\delta_0^2/4$. Here, $\frac{\delta_0^2}{4} = 0.0025$ mm^2, therefore accordingly $\delta_0 = 0.10$ mm. Several linear fits are showed in fig. 2.24., they cross vertical axis ($t = 0$) at value $y \approx 0.0075$ mm^2. Here, the mixing due to micro-convection is expressed as $\delta_{\mathrm{MC}} = \sqrt{4y} - \sqrt{4 \cdot \frac{\delta_0^2}{4}}$. So here $\delta_{\mathrm{MC}} = 0.17 - 0.10 = 0.07$ mm.
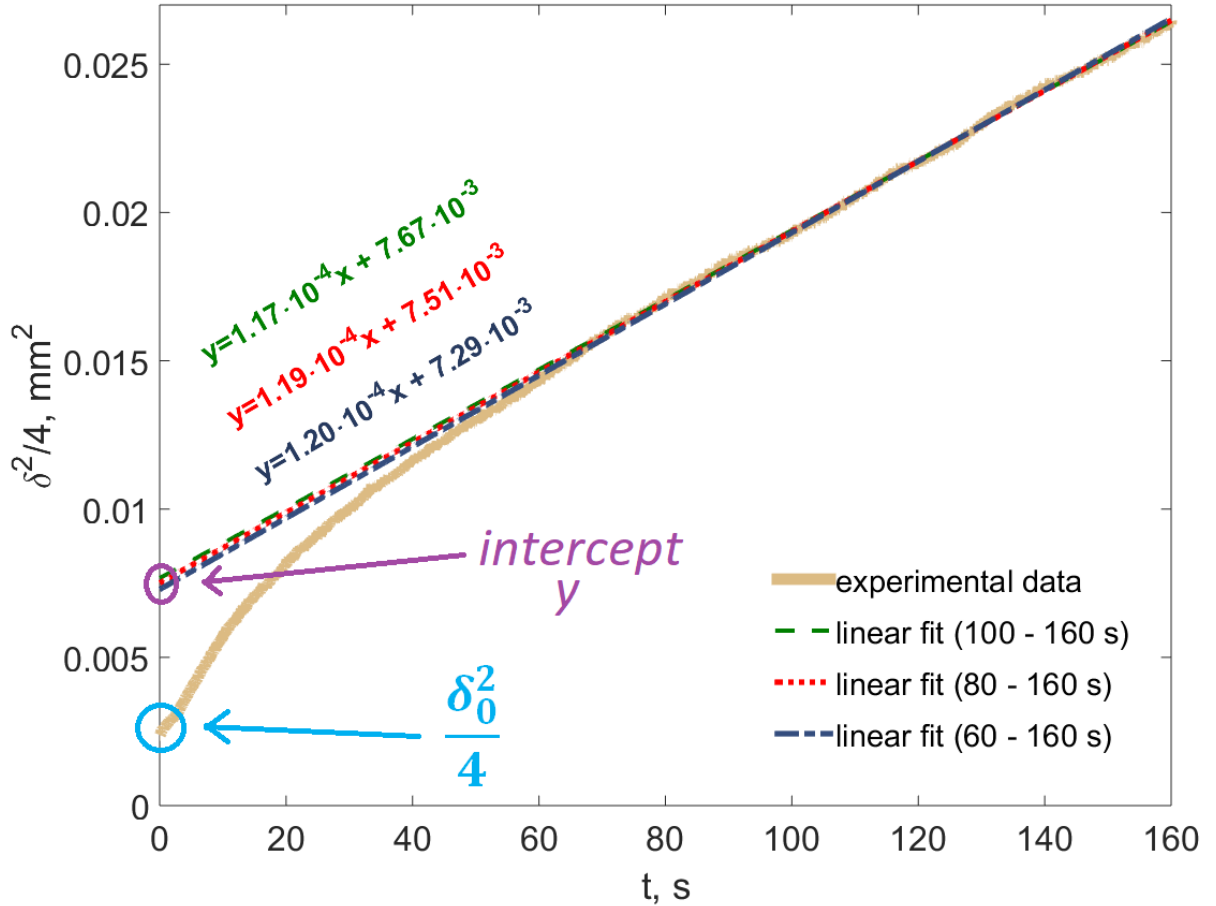
2.24. Figure: Dynamics of the mixing between water and magnetic fluid D107$_{100\%}$ in horizontal magnetic field $H = 56.2$ Oe with initially smeared interface. Experimental data is shown by a beige line. The blue, green and red lines are linear fits of the experimental data for different time regions. Thickness of the used microfluidics chip: $h_1 = 0.135$ mm.

Some of the experiments, mostly the ones carried out in stronger magnetic fields, did not reach the linear region in coordinates $\frac{\delta^2}{4}(t)$ over the recorded time period. The recording time was too short for the diffusive behavior to take the upper hand. The values of the slope for the linear fit for experiments with initially stagnant fluids (see §3.2.) are collected in figure 2.25.. As it is visible in the graph, for some linear fits the slope did not reach the value range for D_{exp} as the experiment did not reach the linear regime for such fit to be appropriate. Here, the experiments that did not reach the linear regime or were too short for the linear fit are represented by empty markers.
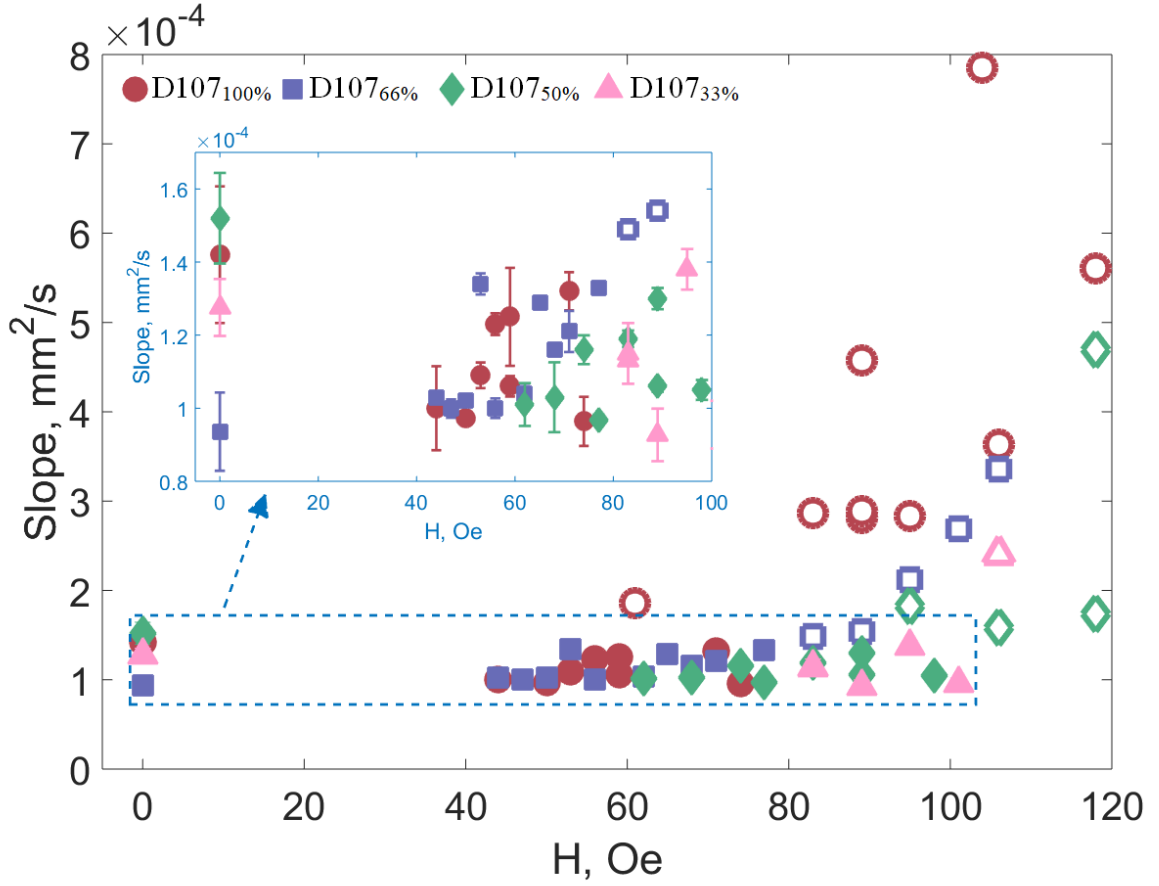
2.25. Figure: The slope of the linearly fitted line for $\frac{\delta^2}{4}$ as a function of time for magnetic fluid D107. Experiments are carried out in rectangular-pool shaped micro-channel in horizontal magnetic field. The empty markers represent that $\delta^2/4$ as function of time has not reached a linear regime for this experiment. The error-bars represent one standard deviation σ of the data for the particular experiment. Microfluidics chip $h_1 = 0.135$ mm.

To estimate δ_{MC} in such a case, a straight line with a slope D_{exp} was attached at the end of the graph as presented in the figure 2.26.. As it is visible here the linear fit of the experimental data (black dashed line) does not agree with the estimated diffusion coefficient $D_{\mathrm{exp}} = 1.25 \cdot 10^{-4}$ mm^2/s. Although, judging by the eye, the tail of the experimental data (beige line) might seem already linear, it is possible, that a longer experiment would lead to a flatter curve. It was not possible to record longer videos of these experiments, due to the heating of the coil. For this particular experiment the magnetic field was relatively strong: $H = 103.5$ Oe. Therefore a straight line with a slope of D_{exp} is attached at the end of the graph (orange dashed line). Therefore it can be concluded that the $\delta_{\mathrm{MC}}^2/4$ should be at least the value of the intercept with the vertical axis of the attached line. Further in the thesis, if not mentioned otherwise these experiments graphically are represented by empty markers and are referred to as experimental results from "attachment method". In the experiment demonstrated in fig. 2.26. the estimated $\frac{\delta_{\mathrm{MC}}^2}{4} \geq 6.65 \cdot 10^{-2}$ mm^2 and

accordingly $\delta_{\mathrm{MC}} \geq 0.51$ mm.
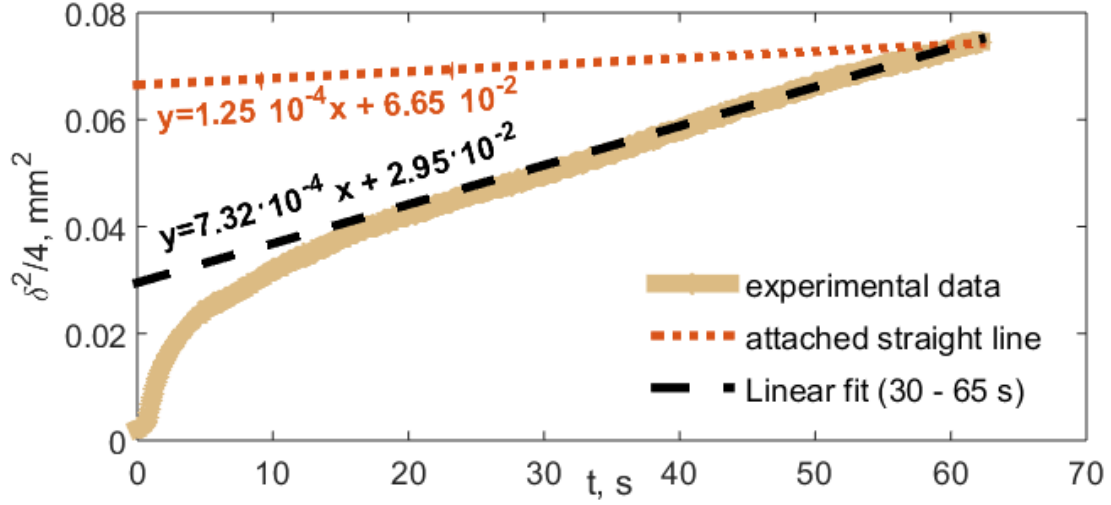
2.26. Figure: Dynamics of the mixing between D107$_{100\%}$ and water as $\frac{\delta^2}{4}$ in horizontal magnetic field $H = 103.5$ Oe with initially stagnant fluids. The experimental data is shown by a beige line. The black dashed line is a linear fit from $t = 35$ s to $t = 65$ s and the orange dotted line with a slope D_{exp} is attached to the graph at $t = 65$ s. Microfluidics chip with thickness $h_1 = 0.135$ mm is used here.

An example how well the δ_{MC} values estimated with "attachment method" fits in with other experiments are demonstrated in figure 2.27.. Here, experiments in a vertical magnetic field with magnetic fluid FF21-5 are visualized. Information of the mixing due magnetic micro-convection δ_{MC} for various values of the initial smearing δ_0 between the fluids before the experiment in various values of magnetic field is collected. Experiments carried out in the same magnetic field are represented by the same marker shape and color, but experimental data obtained using "attachment method" is demonstrated with empty markers. As it is visible in fig. 2.27. that the empty and filled markers of the same shape and color agree within the margin of the error.

Next step of the data processing is to collected the information about δ_{MC} with respect to various quantities: initial smearing thickness δ_0, external magnetic field H intensity and orientation, various parameters of the magnetic fluids and the thickness of the microfluidics chip h. These relationships are described in detail in results section (§3.2., §3.3. and §3.4.).

To compare experimental value of δ_{MC} with theoretical predictions, non-dimensional magnetic micro-convective mixing length $\delta_{\mathrm{MC, ND}}$ is calculated:

$$\delta_{\mathrm{MC, ND}} = \frac{\delta_{\mathrm{MC}}}{h}, \tag{2.8}$$

where h is the thickness of the microfluidics chip used and δ_{MC} is the magnetic micro-convective mixing obtained experimentally. In the numerical simulations carried out by

colleagues and reviewed in §4. δ_{MC} is obtained similarly as in experiments described here from graphs $\frac{\delta^2}{4}(t)$ using linear fit.
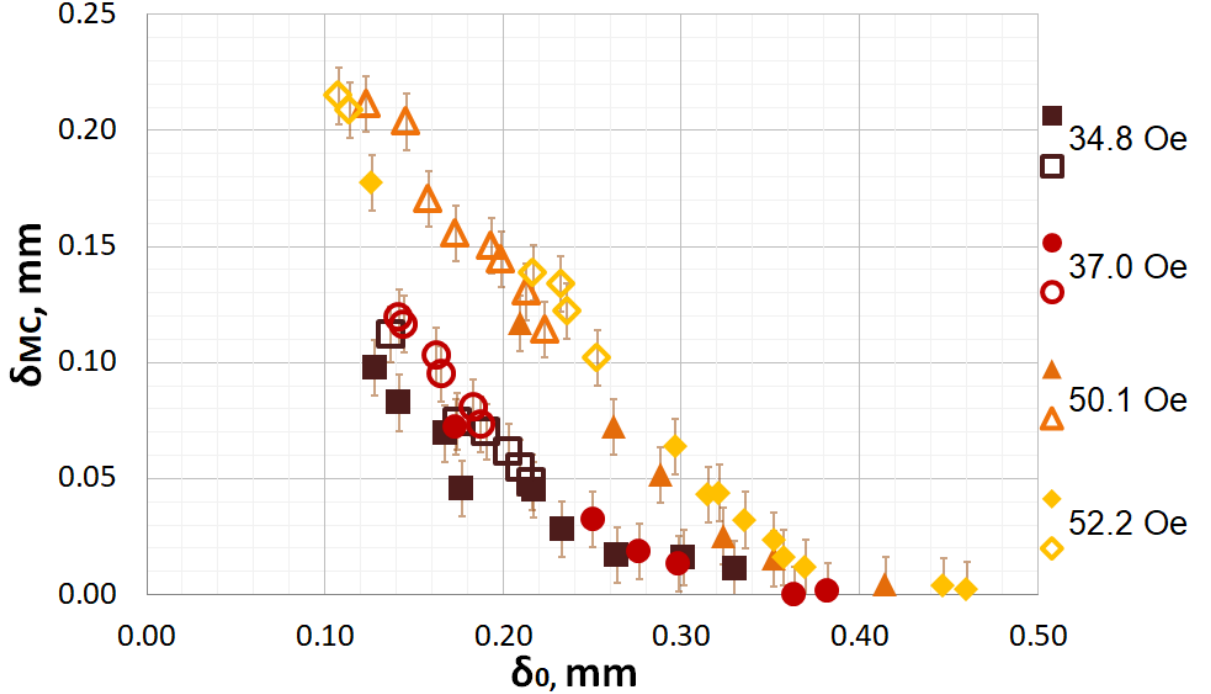
2.27. Figure: Mixing due to magnetic micro-convection δ_{MC} in vertical external magnetic field with respect to initial smearing δ_0 between the fluids. Magnetic fluid: FF21-5, Microfluidics chip: $h_1 = 0.135$ mm. The color of the markers becomes lighter as the value of the magnetic field increases.
Empty markers represent data obtained with attachment method.

2.5.3. Characteristic wavelength determination

Another property that the magnetic micro-convection can be characterized by, is the characteristic wavelength λ. It describes the spacial periodicity of the instability. Within the experiments of this study λ was measured once the fingers of the magnetic micro-convection emerged at their base. All fingers grow out straight at first, and then if the external magnetic field is high enough, they bend and branch. Therefore acquired λ values for the same experiment might differ in time and in position especially for experiments in stronger magnetic fields.

Experimentally the images of the initial instability are used and the fingers are counted at their base. This can be done manually by visually counting the fingers. Also Fourier transform to find a characteristic frequency can be used and then the characteristic wavelength can be calculated as described in [25]. Within error, both methods show the same results. Errors in both methods might occur as not always fingers are perfectly uniform in their width especially when they first appear as demonstrated in figure 2.28.. Here two finger formations are pointed out by arrows where the finger is thicker than the

usual finger of this instability and it might split in two afterwards. If the base of the fingers (red line in fig. 2.28.) is used to determine the characteristic wavelength of the instability, 7 fingers might be counted within this image. Thus knowing the size of the image, the characteristic wavelength (average size of one finger and one space) is $\lambda = 0.19$ mm. If the position of the upper green line in fig. 2.28. is used to count the fingers, the as the thicker finger positioned above the arrow b is split in two the characteristic wavelength is $\lambda = 0.16$ mm for the same experiment.
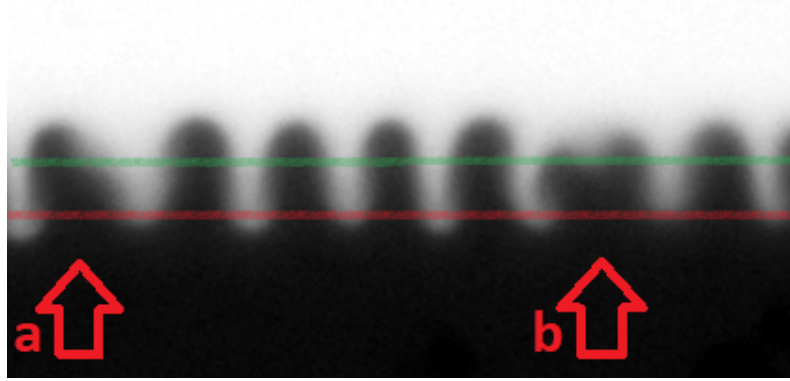
2.28. Figure: Hardships measuring the characteristic wavelength of the magnetic micro-convection. Experiment with initally stangant fluids. Magnetic fluid: D107$_{50\%}$, Horizontal magnetic field magnetic field: $H = 118$ Oe, Time in experiment $t = 3$ s. Region represented by this image 1.3 mm $\times$0.7 mm.

To compare the experimental results with the theoretical ones, dimensionless wave-number is used:

$$k = \frac{2\pi}{\lambda} \cdot h, \tag{2.9}$$

where h is the thickness of the used microfluidics chip.

2.5.4. Determination of the critical magnetic field

Experiments are performed for various magnetic field values and the information about the critical magnetic field H_c is collected. Critical magnetic field is the value of the external magnetic field at which the instability first emerges. Experiments are usually recorded starting from the stronger magnetic fields. Magnetic field is decreased by approximately 5.7 Oe each next experiment. When the fingers of the instability are barely visible this step is reduced to approximately 2.8 Oe. The critical value of the magnetic field then it is determined visually by recording experiment using larger magnification of the microscope and by increasing the contrast of the images.

Critical magnetic fields are determined for all magnetic fluids used within this research for various initial smearing thicknesses δ_0 and also for both orientations of the magnetic field (horizontal and vertical).

To compare H_c with the theoretical predictions critical magnetic Rayleigh number is

used via eq. 1.24. But to express the gravity effects and gravitational Rayleigh number is used (via eq. 1.25) to compare magnetic fluids with different dilution ratios, therefore different densities.

2.6.   Experimental difficulties

As it is to be expected, during experimental work different kind of difficulties may appear. Here some of the problems are summarized. Already mentioned ones previously are: appearance of longitudinal parasitic flow after turning on the magnetic field and restricted precision of the handmade microfluidic chips.

Another experimental artifact is pulses created by syringe pumps from moving mechanical part connected to the fluid that results in uneven flow of the fluids and unwanted interface smearing. This can be limited by using syringes with smaller diameters. The interface may fluctuate also if the tubing is moved. therefore the tubing must be carefully fixed during the experiment.

Sometimes some air bubbles get stuck in the micro-channel, thus distorting the fluid flow and damaging the accuracy of the results. To minimize the development of the bubbles it is advised first to rinse the microfluidics chips with distilled water. It was observed that air bubbles get stuck more if the microfluidics chip was completely dry before the experiment. Also the tubing can be filled with fluid completely before attaching the tubes to the microfluidics chips, thus minimizing appearance of new air bubbles from empty tubing. Shaking of the fluid keeping containers should be avoided just before the experiment.
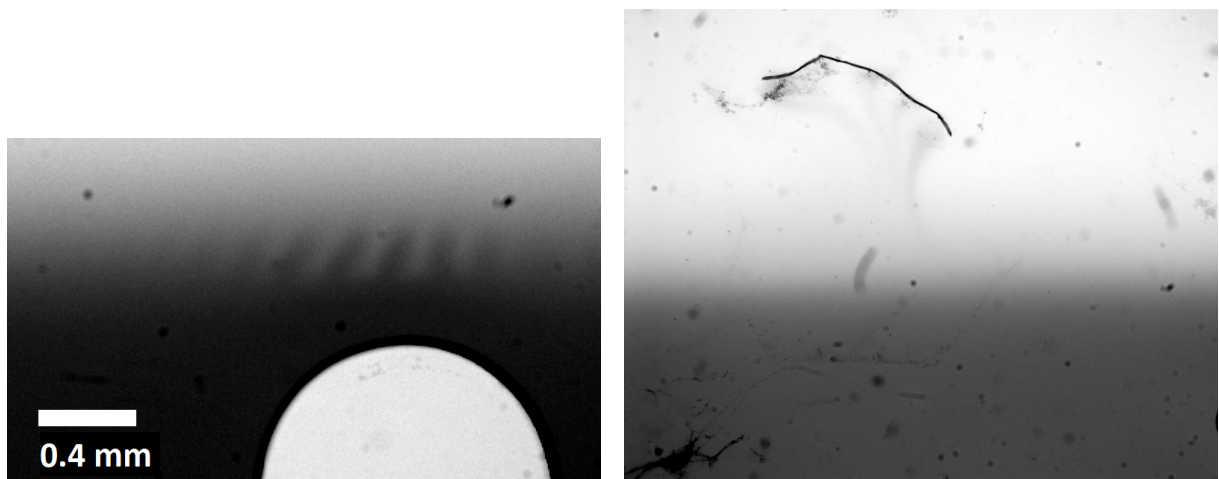
(a) Stuck air bubble. Region represented by this image 2.6 mm ×1.3 mm.

(b) Stuck dirt. Region represented by this image 4 mm ×3 mm.

2.29. Figure: Physical impediments of the experiments.

An example of experiment with air bubble stuck in the micro-channel is shown in figure 2.29.a. Here, an experiment with initially smeared interface with magnetic fluid

KTF11-1$_{100\%}$ in horizontal magnetic field $H = 83$ Oe is carried out in microfluidics chip with thickness $h_1 = 0.135$ mm. As it is visible in the figure, the fingers have appeared in the region above the air bubble, while no fingers are visible elsewhere, as the critical value of the magnetic field for this experimental setup has not been reached.

Another type of physical inconvenience is dirt that get stuck in the micro-channel over time. This dirt is made of dust or sometimes agglomerated particle cluster as in case working with magnetic fluid FF21-1. The dust might settle also on the outside surface of the microfluidics chip and that complicates data processing. An example of dirty microfluidics chip after measuring several experiments is shown in figure 2.29.b. The problem with dirt that is stuck inside the chip, is that it is almost impossible to get it out, so once the micro-channel gets too dirty a new one must be made.

3. Chapter

Experimental observations and results

In this chapter the experimental observations and results are collected. The chapter is divided in five sections. Experiments in continuous flow setup are reviewed in §3.1.. Experiments with initially stagnant fluids are explored in §3.2., the effects of initially smeared interface between the fluids is explored in §3.3. ,and the instability in vertical magnetic field is explored in §3.4.. Additionally, stereo μPIV measurements and observations are collected in §3.5..

3.1. Magnetic micro-convection in flowing fluids

In this section of the work mixing by magnetic micro-convection in a vertically placed microfluidics chip in an experimental setup described in §2.4.1. is explored. Experiments here were carried out in a continuous flow mode. The magnetic field was directed horizontally and perpendicular to the microfluidics chip. Part of the results collected in this section are published in publication [25].

All experiments within this section are carried out in Y-shaped microfluidics chip with thickness $h_1 = 0.135 \pm 0.005$ mm. As microfluidics chips are heat sensitive, some chips came apart during experiments in stronger magnetic fields with stronger flow created by syringe pump. Therefore several chips were used during these experiments with various channel widths. The comparison of experiments with various flow rates (Q, μl/min) was carried out for the same microfluidics chip as the velocity (v, mm/s) of the fluids on the interface differs for chips with different channel width (see eq. 2.2).

In these experiments magnetic fluid D107 with four different dilution ratios (100%, 66%, 50% and 33%) was used thus exploring gravity effects on the instability. For each dilution, the experiments were carried out for different flow-rates set by syringe pump and in different values of the magnetic field.

Denser magnetic fluid is placed bellow the distilled water as showed in figure 3.1. for all experiments. Each experiment is timed from the moment the magnetic field is applied. Before that a syringe pump is pumping both fluids for some time for the flow to stabilize.

Within short moment after the application of the magnetic field the fingers of the instability emerge across all of the interface.
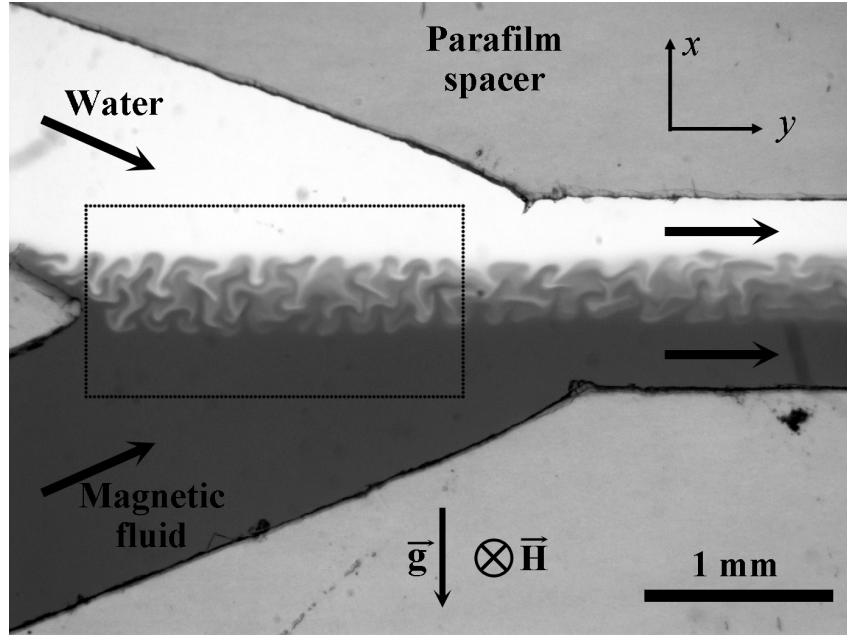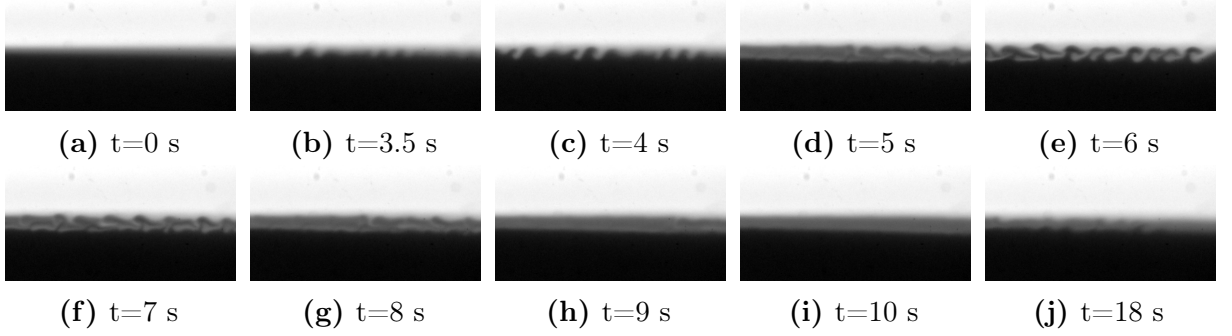

3.1. Figure: An image of Y-shaped microfluidics chip. Micro-convection is observed while both fluids are being pumped. The dotted rectangle in the picture represents the area used in further analysis (ROI). Magnetic fluid: D107$_{50\%}$; Flow rate: $Q = 1$ μl/min; Magnetic field: $H = 100$ Oe. *Fig.2. from [25]*

An experiment is filmed for some time for the fingers to develop fully. At some time in the experiment the fingers have reached their maximal height and are not growing taller anymore. The constant flow of the fluids is mixing the fingers. Fingers have the same height all across the interface, even when they have reached their maximal height. As the fluids are flowing out of the micro-channel the fresh fingers forming near the Y-junction instantly have the same height (see fig. 3.1., where Y-junction and the straight micro-channel are visible). After each experiment the magnetic field is turned off. When a sufficient time has passed and the fluids form the initial no-field situation, the next experiment with the next field value is proceeded.

An example of the micro-convection while both fluids are being pumped for the most concentrated magnetic fluid D107$_{100\%}$ in various magnetic fields is shown in figures 3.2., 3.3. and 3.4. for experiments with flow-rate $Q = 1$ μl/min for both fluids. Additional figures of experiments are collected in Appendix §A.1.1.

Within these experiments micro-channel with $w = 1$ mm width was used. Using equation 2.2 the average velocity of the fluids in the micro-channel is found to be $\bar{v} \approx 15$ mm/min $= 0.25$ mm/s. Comparing these figures, it is visible that fingers of the instability emerge earlier if the magnetic field is stronger. In magnetic field $H = 53$ Oe extremely tiny fingers appear around $t \approx 2$ s and become easily visible at $t = 3.5$ s since the

application of the magnetic field (see fig. 3.2.b). In stronger magnetic field $H = 0.75$ Oe the fingers have appeared already at $t = 0.7$ s (see fig. 3.3.b) and in even stronger magnetic field $H = 124$ Oe the fingers are visible even at $t = 0.2$ s (see fig. 3.4.b).
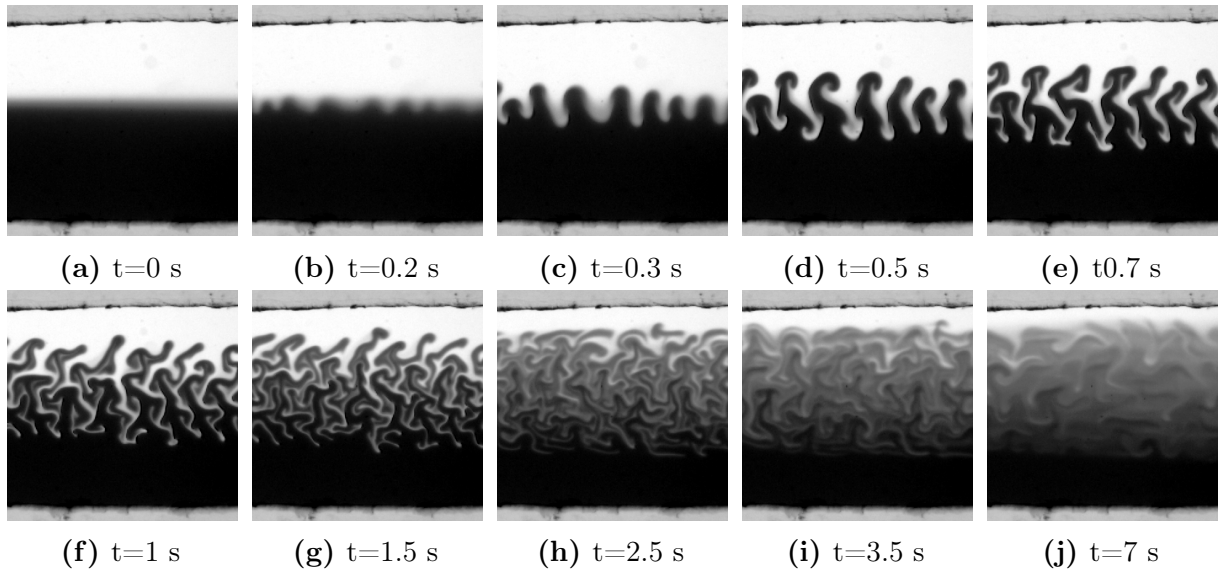

(a) t=0 s   (b) t=3.5 s   (c) t=4 s   (d) t=5 s   (e) t=6 s

(f) t=7 s   (g) t=8 s   (h) t=9 s   (i) t=10 s   (j) t=18 s

3.2. Figure: Image series of magnetic micro-convection dynamics in time in Y-shaped micro-channel. Magnetic fluid: D107$_{100\%}$, Magnetic field: $H = 53$ Oe. Flow-rate of the syringe pump for each fluid: $Q = 1$ µl/min. Width of the micro-channel: $w = 1$ mm. Average velocity of the fluids: $\overline{v} \approx 0.15$ mm/min $= 0.25$ mm/s. Size of a region represented by a singular image is 1.5 mm × 0.7 mm. The contrast of the images is changed, for displaying purpose.


(a) t=0 s   (b) t=0.7 s   (c) t=1 s   (d) t=1.5 s   (e) t=2 s

(f) t=2.5 s   (g) t=3 s   (h) t=4 s   (i) t=5 s   (j) t=6 s
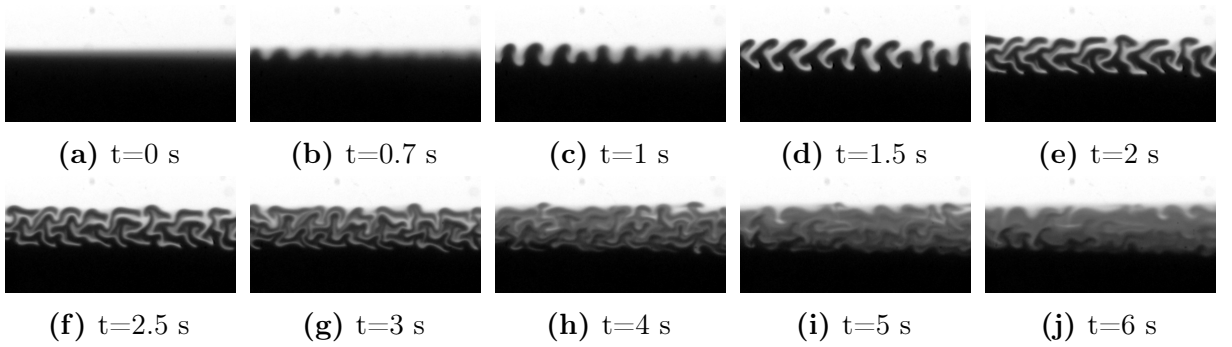
3.3. Figure: Image series of magnetic micro-convection dynamics in time in Y-shaped micro-channel. Magnetic fluid: D107$_{100\%}$, Magnetic field: $H = 75$ Oe. Flow-rate of the syringe pump for each fluid: $Q = 1$ µl/min. Width of the micro-channel: $w = 1$ mm. Average velocity of the fluids: $\overline{v} \approx 0.15$ mm/min $= 0.25$ mm/s. Size of a region represented by a singular image is 1.5 mm × 0.7 mm. The contrast of the images is changed, for displaying purpose.

The fingers not only emerge earlier, but also reach their maximal height faster in stronger magnetic fields. The maximal height of the fingers is taller in stronger magnetic fields. Comparing these three experiments the fingers have reached their maximum height:

- $\delta_{\text{fing}} \approx 0.15$ mm at $t = 6$ s in $H = 53$ Oe (fig. 3.2.e);

- $\delta_{\text{fing}} \approx 0.33$ mm at $t = 4$ s in $H = 75$ Oe (fig. 3.3.h);

- $\delta_{\text{fing}} \approx 0.62$ mm at $t = 2.5$ s in $H = 124$ Oe (fig. 3.4.h).

(a) t=0 s	**(b)** t=0.2 s	**(c)** t=0.3 s	**(d)** t=0.5 s	**(e)** t0.7 s
(f) t=1 s	**(g)** t=1.5 s	**(h)** t=2.5 s	**(i)** t=3.5 s	**(j)** t=7 s

3.4. Figure: Image series of magnetic micro-convection dynamics in time in Y-shaped micro-channel. Magnetic fluid: D107$_{100\%}$, Magnetic field: $H = 124$ Oe. Flow-rate of the syringe pump for each fluid: $Q = 1$ μl/min. Width of the micro-channel: $w = 1$ mm. Average velocity of the fluids: $\overline{v} \approx 0.15$ mm/min = 0.25 mm/s. Size of a region represented by a singular image is 1.2 mm × 1.2 mm. The contrast of the images is changed, for displaying purpose.

When the maximal height of the fingers have been reached, the character of the flow stabilizes. For the experiment in the lowest magnetic field $H = 53$ Oe it means that the interface between the fluids is blurred (see fig. 3.2.h and 3.2.i) with smearing thickness the same as the maximal height of the fingers, and from time to time some distinguishable finger structures appears (see fig. 3.2.g and 3.2.j) that are flowing to outlet of the micro-channel along with the fluid flow. For experiments in higher magnetic fields the finger shapes are distinguishable all the time, but fingers are heavily mixed together and blurred due to the longitudinal flow (see fig. 3.3.j and 3.4.j). The instability is still continuously forming on the fresh interface on the left side as the flow is going from left to right. And these freshly grown fingers quickly smears on the way to the right side.

From these experiments it is also visible that it would not be convenient to use this specific microfluidics chip for measurements in stronger magnetic field with the same flow-rate ($Q = 1$ $\mu l/min$ for each fluid) as the fingers are almost reaching walls of the micro-channel when fully developed if magnetic field is $H = 124$ Oe (see fig. 3.4.i).

Comparing experiments carried out with diluted magnetic fluids, instability emerges later, if the magnetic fluid is diluted. Also the maximal height of the fingers is smaller for experiments with more diluted magnetic fluids.

Next the effect of the fluid flow-rate on the magnetic micro-convection is explored. An example of dynamics equilibrium state images of magnetic micro-convection in various external magnetic field strengths for various flow-rates of the fluids is demonstrated in

figure 3.5.. Here the experiments are carried out with magnetic fluid D107$_{100\%}$ for various magnetic fields. Each row represents a different flow-rate that is increasing downwards. And each column represents a different value of the external magnetic field increasing from left to right. The pattern of magnetic micro-convection emerges only if a sufficient magnetic field, known as the critical magnetic field H_c, is applied. Here in fig. 3.5. the critical magnetic field has not been reached for some experiments as there are no fingers visible. It is visible that the flow-rate affects the critical magnetic field, for higher flow-rates stronger magnetic field must be applied to induce the magnetic micro-convection.
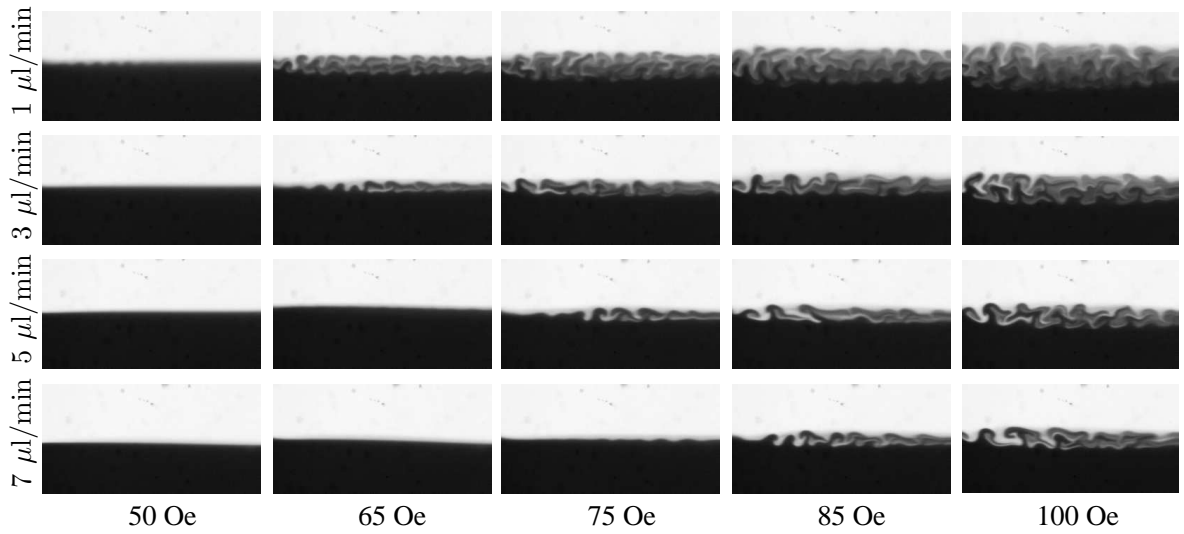
3.5. Figure: Dynamics equilibrium state images of magnetic micro-convection for various flow rates and magnetic fields. Magnetic fluid: D107$_{66\%}$. Each image is 1.0×2.0 mm large. *Fig.6. from [25]*

How flow-rate stabilizes magnetic micro-convection is explored in finer detail in figure 3.6.. Here magnetic micro-convection with half diluted magnetic fluid D107$_{50\%}$ in $H = 118$ Oe strong magnetic field is explored in four different flow-rates. $H = 118$ Oe is relatively strong magnetic field for this experimental system and fingers appear early in all flow-rates. But the equilibrium state of the instability is reached faster in experiments with stronger flow-rates. As it is visible here in fig. 3.6. for faster flow-rates ($Q = 5$ µl/min and $Q = 7$ µl/min) the fingers have reached their maximal height and the character of the flow is not changing much already after $t \approx 3$ s. However for the slowest flow-rate ($Q = 1$ µl/min) the fingers reach their maximal height and the character of the flow stabilizes only after $t = 7$ s. Also it is clearly visible that fingers grow taller for slower flow-rates. For example, here the maximal height of the fingers is $\delta_{\text{fing}} \approx 0.38$ mm for the experiment in the weakest flow-rate ($Q = 1$ µl/min), $\delta_{\text{fing}} \approx 0.24$ mm and $\delta_{\text{fing}} \approx 0.19$ mm for experiments in flow-rates $Q = 3$ µl/min and $Q = 5$ µl/min accordingly and only $\delta_{\text{fing}} \approx 0.14$ mm for the experiment in the strongest flow-rate ($Q = 7$ µl/min).
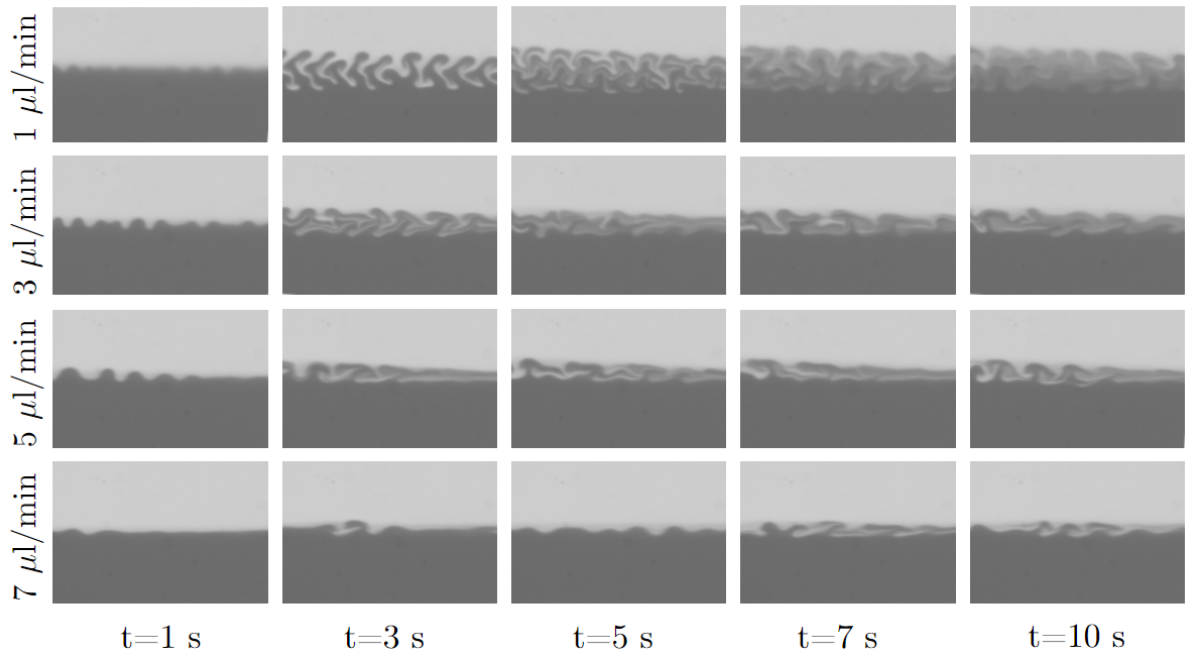
3.6. Figure: Image series of magnetic micro-convection dynamics in time in Y-shaped micro-channel for various flow-rates. Magnetic fluid: D107$_{50\%}$, Magnetic field: $H = 118$ Oe. Flow-rate of the syringe pump for each fluid: $Q = 1$ µl/min. Size of a region represented by a single image is 1.5×1.0 mm.

One of the desired aims of this study was to find the critical values of the external magnetic field at which the instability emerges if both fluids are stagnant at the beginning of the experiment and syringe pump is switched off. During these experiments it was found out that the current setup was not suitable for measuring initially stagnant fluid experiments, as after the application of the external magnetic field a parasitic flow along the channel (y- direction) appeared and flushed away the fluids. This was resolved later in the next series of experiments with altered experimental setup and those results are collected in the next section § 3.2..

An example of this parasitic motion is showed in figure 3.7. for diluted D107$_{50\%}$ magnetic fluid, in magnetic field $H = 118$ Oe, additional examples are reviewed in Appendix §A.1.1. The contrast of the images here is increased for easier perception. In this example the fingers grow out normal at the beginning of the experiment and the parasitic flows appears suddenly and rapidly after 15 seconds since the application of the magnetic field (see fig. 3.7.c). Within few seconds this flow completely mix the fingers so that there are no distinguishable fingers at $t = 22$ s only 6 seconds after the emergence of the flow (see fig. 3.7.e although the magnetic field is still applied. It was observed that the parasitic flow appears earlier for concentrated liquids and it seemed to be stronger in stronger magnetic fields.
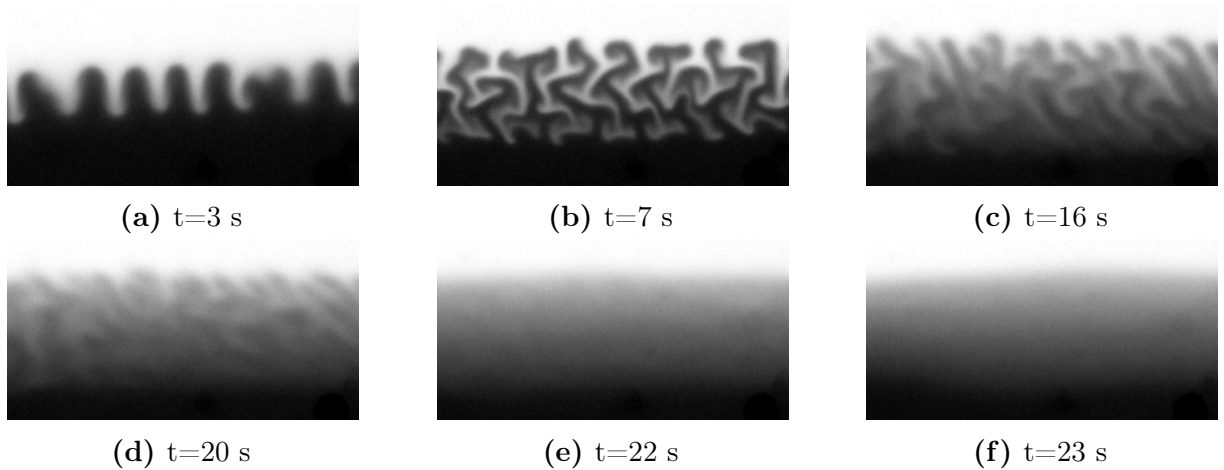
(a) t=3 s   **(b)** t=7 s   **(c)** t=16 s

(d) t=20 s   **(e)** t=22 s   **(f)** t=23 s

3.7. Figure: Image series of magnetic micro-convection dynamics in time in Y-shaped microfluidics chip with syringe pump turned off. Magnetic fluid: $D107_{50\%}$, Magnetic field: $H = 118$ Oe. Size of a region represented by a singular image is 1.3×0.7 mm.

Although it was not possible to acquire experiments with initially stagnant fluids during this stage of this study, the estimation of the critical magnetic fields for the magnetic micro-convection to emerge for initially stagnant fluids was made. The critical magnetic field for various flow-rates was measured for all four magnetic fluid dilutions. An example of visual detection of the critical magnetic field is demonstrated in fig.3.8.. Here the magnetic fluid $D107_{66\%}$ at flow-rate $Q = 1$ μl/min is explored. It is visually detectable that in magnetic fields stronger than $H = 50$ Oe pronounced fingers of the instability have emerged and that in magnetic field $H = 45$ Oe the interface between the fluids is straight and undisturbed. A slight initial disturbance of the interface between the fluids appear when the magnetic field is increased to 47.5 Oe, thus the critical magnetic field for this flow-rate is determined as this value.

45.0 Oe   47.5 Oe   50.0 Oe   52.5 Oe   55.0 Oe
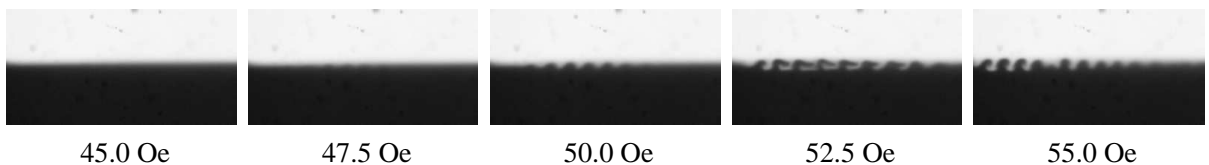
3.8. Figure: Visual detection of the critical magnetic field for a magnetic fluid $D107_{66\%}$ and a flow-rate $Q = 1$ μl/min. Critical field is $H = 47.5$ Oe, as small interface perturbations can be seen. Each image is 1.0×2.0 mm large. *Fig.7. from [25]*

For each of the dilutions these tiny interface perturbations are found and the critical values of the magnetic field for the magnetic micro-convection to emerge are found. By diluting magnetic fluids the critical values of the magnetic field decreases for each tested flow-rate. By diluting magnetic fluids the density difference $\Delta\rho$ between the magnetic fluid and the water decreases. Thus the gravitational Rayleigh number (see eq. 1.25), which is directly proportional to this density difference decreases as well. Another factor

that must be considered is that by diluting a magnetic fluid it's particle volume fraction ϕ_{Vol} changes as well proportionally to the dilution ratio from the original value of the concentrated magnetic fluid. This affects the magnetic properties of the magnetic fluid and the magnetic susceptibility χ decreases by diluting magnetic fluid. So the magnetic Rayleigh number $\mathrm{Ra_m}$ (see eq. 1.24) is affected as well as $\mathrm{Ra_m} \sim \chi^2$. This is reviewed more in discussion §4.1. where experimental and theoretical results are compared.

An information about the critical fields for the different dilutions of the magnetic fluid is collected and the summary is visible in the figure 3.9.. The red crosses mark the experimental data points of the concentrated magnetic fluid D107$_{100\%}$, blue diamonds mark slightly diluted magnetic fluid D107$_{66\%}$, green circles are for the half-diluted magnetic fluid D107$_{50\%}$ and cyan triangles are for the most diluted magnetic fluid D107$_{33\%}$. It is visible that stronger magnetic fields are necessary to induce the magnetic micro-convection in experiments with more diluted magnetic fluids as data points describing these experiments are above the ones for experiments with concentrated magnetic fluid (see fig. 3.9.). From this graph it is also visible quantitatively that the flow-rate restricts the instability as for stronger flow-rates higher values of magnetic field are necessary to induce the fingering.
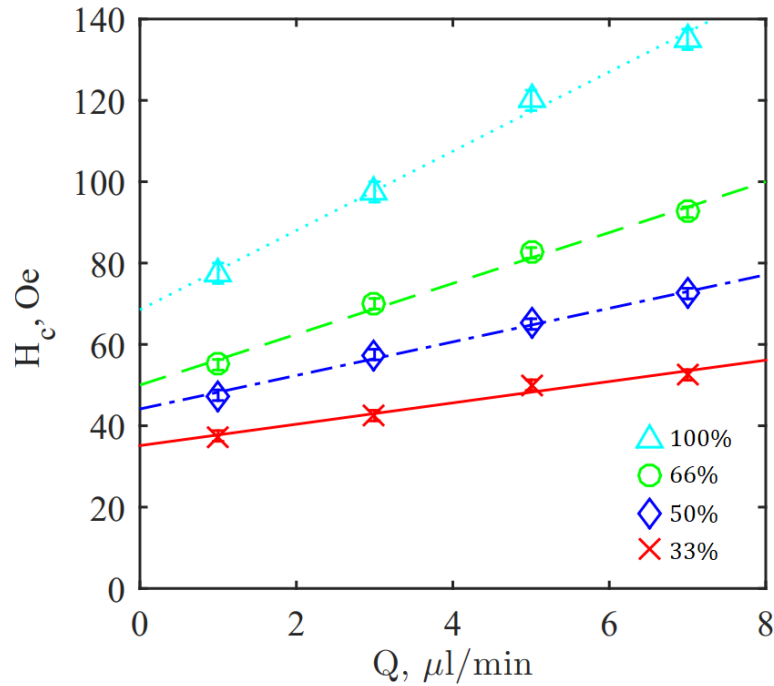
3.9. Figure: Critical magnetic fields for various flow-rates and different dilutions of magnetic fluid D107. Lines correspond to linear fits that are used to extrapolate the critical magnetic field values at $Q = 0$ μl/min.

Another conclusion can be made from fig. 3.9.. It seems that the critical field can be approximated by a linear relationship depending on the flow-rate. Thus by fitting the experimental data points linearly using the least-squares method a y-intercept at

$Q = 0$ µl/min can be found. So the estimation of the critical field with initially stagnant fluids (situation where the syringe pump is not working) can be estimated. This is done here, and the critical values for the magnetic fluids used in this part of the study are collected in table 3.1..

Magnetic fluid	$H_c \pm \Delta H_c$, Oe
D107$_{100\%}$	35 ± 2
D107$_{66\%}$	44 ± 1
D107$_{50\%}$	50 ± 2
D107$_{33\%}$	69 ± 2

3.1. Table: Estimated values of the critical magnetic field with initially stagnant fluids.

Also the characteristic size of the instability was investigated during this part of the study. The characteristic wavelengths were found for all of the experiments above the critical magnetic field and with distinctive finger pattern. No clear dependence on the flow-rate was found as the error is larger than the measurement difference between various flow-rates. So it could be hypothesised that the characteristic wavelength would be the same also for initially stagnant fluid ($Q = 0$ µl/min) case.
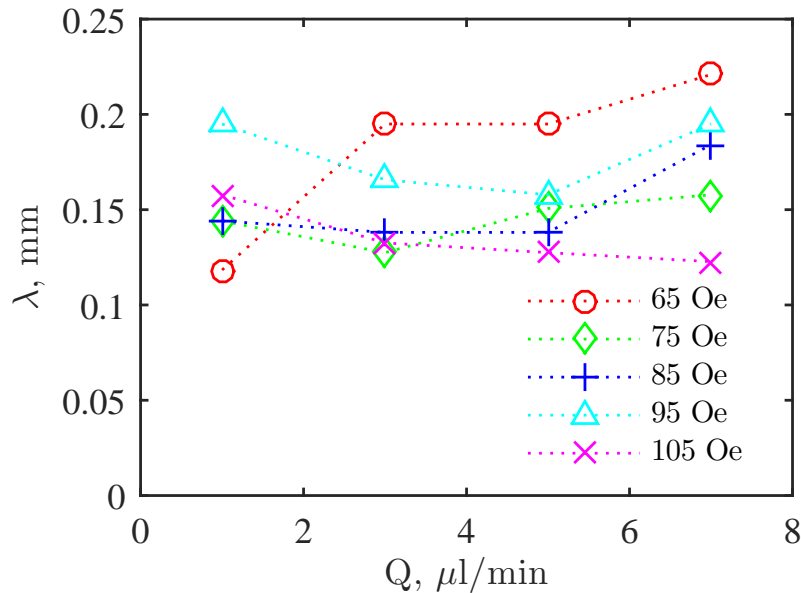
3.10. Figure: Characteristic wavelength of the initial instability at different magnetic fields measured for various flow-rates. Magnetic fluid: D107$_{100\%}$. The measurement error is larger than the differences measured ($\sigma = 0.03$ mm). *Fig.10. from [25]*

An example of the characteristic wavelength distribution for the concentrated magnetic fluid D107$_{100\%}$ in various magnetic fields is demonstrated in figure 3.10.. For all four

dilutions of the magnetic fluid D107 the average characteristic wavelength for all the measured experiments were found:

- $\overline{\lambda}_{D107_{100\%}} \pm \Delta\lambda = 0.15 \pm 0.05$ mm;

- $\overline{\lambda}_{D107_{66\%}} \pm \Delta\lambda = 0.19 \pm 0.03$ mm;

- $\overline{\lambda}_{D107_{50\%}} \pm \Delta\lambda = 0.22 \pm 0.04$ mm;

- $\overline{\lambda}_{D107_{33\%}} \pm \Delta\lambda = 0.23 \pm 0.04$ mm.

It is hard to tell whether the dilution ratio affects the characteristic wavelength of the instability due to the high data dispersion.

3.1.1. Summary

Within this section it was showed that the flow-rate restricts the magnetic micro-convection in a continuous flow mode. Stronger magnetic field must be applied in order to create an instability in experiments with stronger flow-rates. At some time in the experiment fingers reach their maximal height and do not grow taller.

Critical magnetic field for the instability to emerge was measured for four dilutions of magnetic fluid D107 for various flow-rates. Using this information, the critical magnetic field for initially stagnant fluids was estimated.

Characteristic wavelength of the instability was measured for all of the experiments above the critical magnetic field and with distinctive finger pattern. No obvious relationship between the dilution ratio of the magnetic fluid, the flow-rate of the fluids or the value of the external magnetic field and the characteristic wavelength of the instability was found.

3.2. Magnetic micro-convection in initially stagnant fluids

In this section of the work mixing by magnetic micro-convection in a vertically placed microfluidics chip in an experimental setup described in §2.4.2. is explored. Experiments described here were carried out with initially stagnant fluids in a vertically placed microfluidics chip with rectangular pool-shaped micro-channel with thickness $h_1 = 0.135$ mm. A publication is prepared for publishing about the results collected in this section [26].

In this part of the study magnetic fluid D107 with four different dilution ratios (100%, 66%, 50% and 33%) was used. For each dilution, the experiments were carried in different values of the magnetic field. The magnetic field was directed horizontally and perpendicular to the microfluidics chip. The aim of this part of the study was to quantify some parameters of the magnetic micro-convection (critical magnetic field H_c, the characteristic size of the instability, contribution to the mixing) and using dimensionless Rayleigh numbers quantify how the gravity restricts the instability if the mixing fluids are initially stagnant. This was done by carrying out experiments without any flow applied from syringe pumps in contrast to the results described in previous section §3.1..

The timing and recording of an experiment begins when the magnetic field is applied. After that the experiment is filmed for some time. Due to the heating of the coils of the electromagnet experiments in stronger magnetic fields are recorded for shorter periods of time. Before each experiment syringe pumps are used to pump in fresh material in the micro-channel. The pumps are pumping both fluids with a high flow-rate for a short time, to get a smooth interface between the fluids. Then the flow is stopped already before the beginning of the experiment for a short time, to stabilize the interface between the fluids. As after switching of the syringe pumps the interface of the fluids sometimes fluctuates. This results in an initial smearing $\overline{\delta_{t=0s}} = 0.08 \pm 0.02$ mm (error is one standard deviation) of the interface already before the experiments. However during this part of the experiments the initial interface between the fluids was considered to be sharp when calculating part of the mixing created by magnetic micro-convection δ_{MC}. Nevertheless the small initial smearing was taken into account when expressing error-bars for δ_{MC} for these experiments.

If parasitic longitudinal flow appears during the experiment then it is not analyzed. Sometimes it is hard to determine whether parasitic flow has appeared at the end of the experiment. If it happens, the fingers bend specifically in the flow. When both fluids are considerably mixed there are no apparent fingers left for clues.

During this part of the study $D_{\text{exp}} = (1.25 \pm 0.23) \cdot 10^{-6}$ cm^2/s for magnetic fluid D107 was found by method described in §2.5.. This value of the diffusion coefficient was used as a slope for a straight line to fit the experimental data in coordinates $\frac{\delta^2}{4}(t)$ describing the part of the experiment where the diffusive mixing becomes dominant. This linear fit is important to obtain the information about the mixing due to magnetic micro-convection.

The value for δ_{MC} is is calculated from the intercept of this linear fit with the vertical axis $\frac{\delta^2}{4}$ when $t = 0$. Some of the experiments, mostly the ones carried out in stronger magnetic fields did not reach this linear regime in coordinates $\frac{\delta^2}{4}(t)$ over the recorded time period. The analysis of those experiments is described in detail in §2.5. and graphically they will be represented by empty markers.

When a magnetic field is applied, an instability gradually develops across all the interface. However this happens only if the intensity of the magnetic field is above a critical value H_c. The fingers continue to grow until they reach some maximum height. After appearing all fingers of the instability grow at the same rate. Therefore, at a specific time-point all fingers have approximately the same height. An example of this can be observed in figure 3.11. where the dynamics of the instability over time are explored for the most concentrated magnetic fluid D107$_{100\%}$ in magnetic field $H = 89$ Oe. First the instability appears as small waves over the interface between the fluids ($t = 0.5$ s in fig. 3.11.). Then small straight fingers appear and if the magnetic field is strong enough they start to bend ($t = 1$ s in fig. 3.11.) and curl ($t = 2$ s in fig. 3.11.). In stronger magnetic fields the fingers even start to branch after some time ($t = 4$ s in fig. 3.11.). When the fingers have reached their maximal height they still move and swirl but the diffusion slowly takes over as the edges of the fingers start to blur ($t = 10$ s in fig. 3.11.).
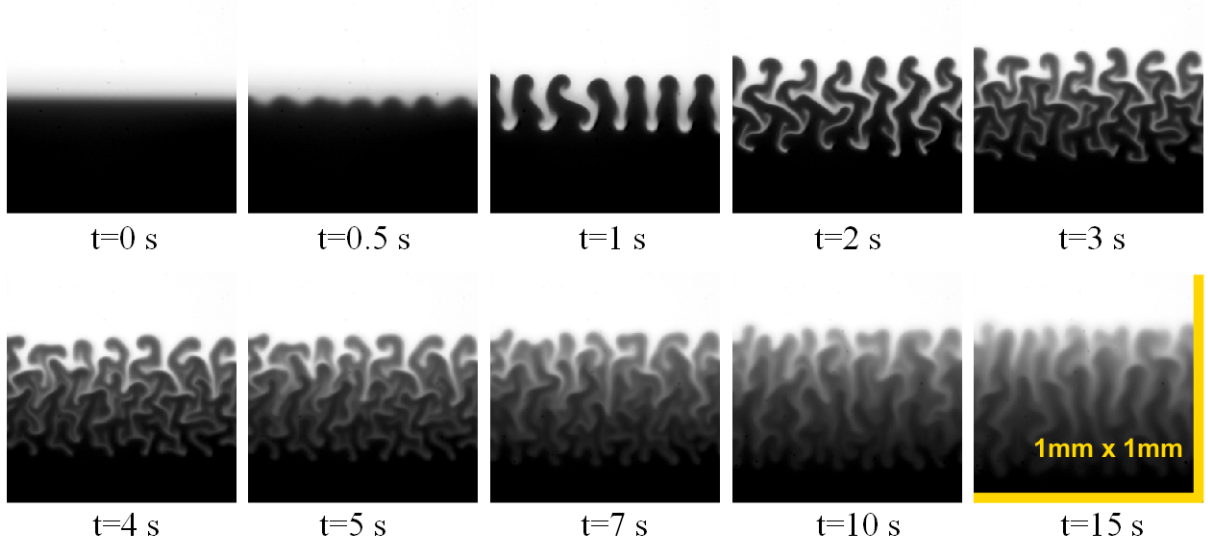
3.11. Figure: An image series of the magnetic micro-convection dynamics with magnetic fluid D107$_{100\%}$ in $H = 89$ Oe. A single image represents 1.0×1.0 mm region.

Dynamics of the magnetic micro-convection over time for several values of magnetic field is demonstrated in figure 3.12. for the most concentrated magnetic fluid and in figures A.3, A.4, and A.5 in Appendix §A.1.2 for other dilutions of magnetic fluid D107. The vertical axis represents the time period since the beginning of the experiment. The time is

increasing in upwards direction. The horizontal axis represents the value of the external magnetic field. One column represents a particular experiment in time.

It is visible that the behavior of the fingers is strongly affected by the value of the external magnetic field. In all four of these figures it is clearly visible that the fingers appear earlier in experiment if the magnetic field is stronger. For example, in experiments with magnetic fluid $D107_{100\%}$ (see fig. 3.12.) barely visible fingers of the instability appear only after 15 seconds if the magnetic field is $H = 41.4$ Oe, but already 0.18 mm tall fingers are visible at $t = 5$ s if the magnetic field is $H = 53.2$ Oe or even already at $t = 1$ s if the magnetic field is $H = 82.8$ Oe.
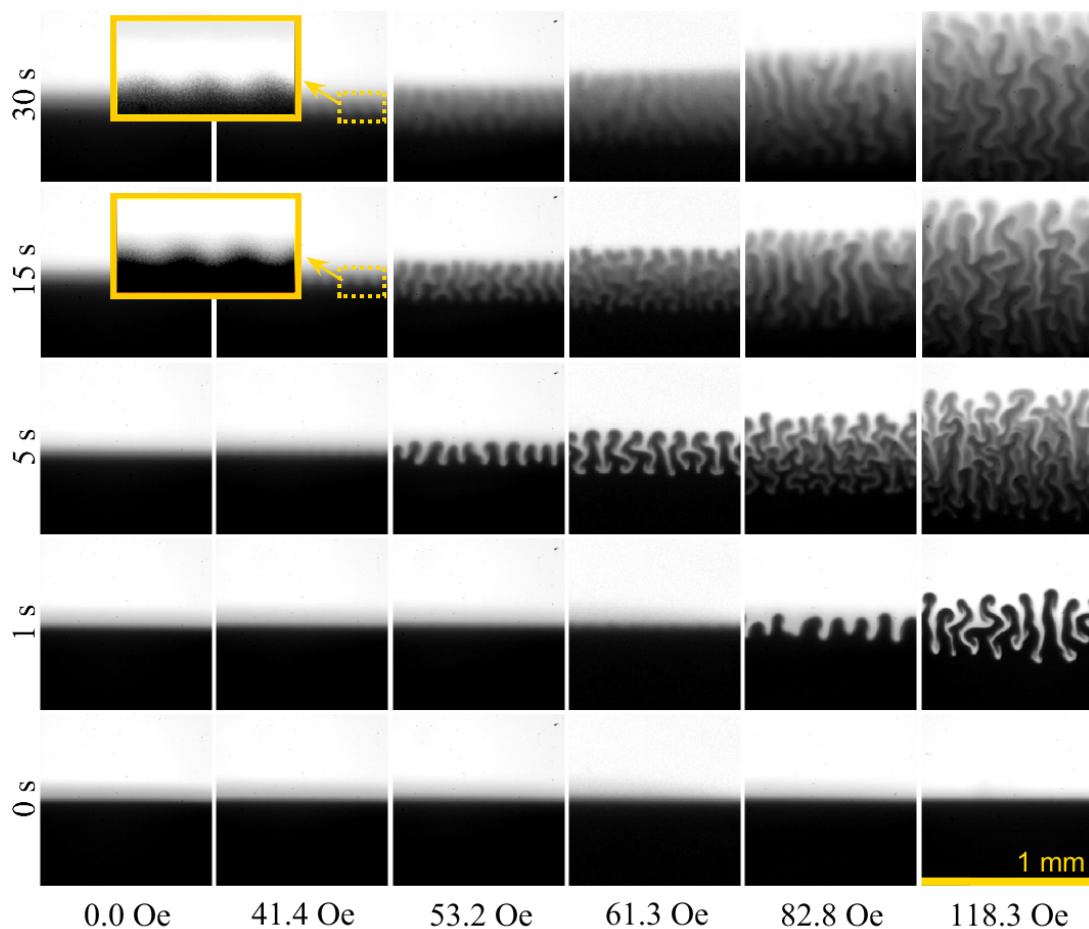
3.12. Figure: Image series of the magnetic micro-convection dynamics with magnetic fluid with $D107_{100\%}$ in various magnetic fields. Each image represents 1×1 mm region.

A similar situation unfolds in experiments with other dilutions of the magnetic fluid, but the fingers appear later. For the same values of the magnetic fields, the fingers grow out shorter in more diluted magnetic fluids. The concentrated magnetic fluid has a higher magnetic susceptibility and is denser. For the diluted fluids, the intensity of the magnetic field must be higher, in order to observe the micro-convection. As a result, a higher current must be used and the coils of an electromagnet heat up faster. To avoid overheating of

the system, shorter experiments are performed for the diluted fluids.

An interesting note to keep in mind that not only fingers appear later in experiments in weaker magnetic fields, but also as the fingers are appearing latter the interface between the fluids has started to diffuse. And as it will be demonstrated in the next section §3.3. the fingers of the instability appear even later if the interface between the fluids is smeared. For example, when the fingers finally appear at $t = 15$ s in magnetic field 50.3 Oe for diluted magnetic fluid D107$_{66\%}$ (see fig. A.3) the fluids already have been diffusing for 15 seconds.

Also the fingers not only appear earlier but also grow out to be taller in stronger magnetic fields. For example, in experiments with magnetic fluid D107$_{100\%}$ (see fig. 3.12.) fingers grow out to be 0.26 mm tall in $H = 53.2$ Oe strong magnetic field, but they grow almost two times taller 0.41 mm in a bit stronger magnetic field $H = 61.3$ Oe and in even stronger magnetic field $H = 82.8$ Oe the fingers reach 0.64 mm. In experiments with slightly diluted magnetic fluid D107$_{66\%}$ (see fig. A.3) fingers grow out to be a bit shorter. For example:

- $\delta_{\text{fing}} = 0.15$ mm in $H = 50.3$ Oe;

- $\delta_{\text{fing}} = 0.20$ mm in $H = 53.2$ Oe;

- $\delta_{\text{fing}} = 0.30$ mm in $H = 65.0$ Oe;

- $\delta_{\text{fing}} = 0.44$ mm in $H = 71.0$ Oe;

- $\delta_{\text{fing}} = 0.51$ mm in $H = 88.7$ Oe.

In experiments with half diluted magnetic fluid D107$_{50\%}$ (see fig. A.4) the fingers are even more restricted in size as listed bellow:

- $\delta_{\text{fing}} = 0.10$ mm in $H = 62.2$ Oe;

- $\delta_{\text{fing}} = 0.27$ mm in $H = 76.9$ Oe;

- $\delta_{\text{fing}} = 0.40$ mm in $H = 88.7$ Oe;

- $\delta_{\text{fing}} = 0.62$ mm in $H = 118.3$ Oe.

In stronger magnetic fields although the fingers have reached their maximum height, the convective motion is still present and the fingers continue to bend and grow branches. This is common for experiments at high magnetic fields. Once the finger has fully grown, the shape of it stays the same. When the fingers have reached their maximum height, the mixing of the fluids still continues: the edges of the fingers blur gradually due to the diffusion as the time passes. This happens until only diffusion remains.

Another property that is affected by the magnetic field and the dilution ratio is the form of the fingers. If the intensity of the magnetic field is relatively small, the fingers stay straight and do not branch, not even after some time has passed. This is demonstrated in figure 3.13. for the most concentrated magnetic fluid D107$_{100\%}$ in magnetic field $H = 47$ Oe, and in Appendix §A.1.2 in figure A.5 for the most diluted magnetic fluid D107$_{33\%}$ in magnetic field $H = 82.8$ Oe.
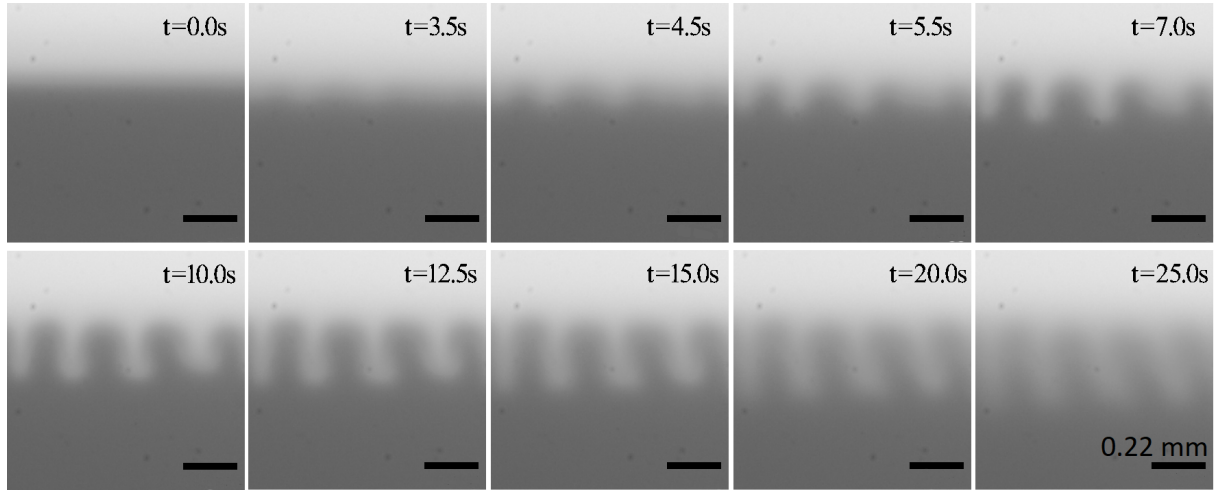
3.13. Figure: An mage series of magnetic micro-convection dynamics over time with magnetic fluid D107$_{100\%}$ in $H = 47$ Oe magnetic field. Each image represents 0.45×0.45 mm large area. The scale bar is 0.1 mm long.

In a bit stronger magnetic field the fingers already grow considerably taller and start to curl after some time, or already start to grow out wavy as it can be seen in figure 3.12. for magnetic fluid D107$_{100\%}$ in experiments with magnetic fields $H = 53.2$ Oe and $H = 61.3$ Oe. The fingers grow out branches, if the magnetic field is even stronger as it is visible in fig. 3.12. in $H = 82.8$ Oe and $H = 118.3$ Oe for magnetic fluid D107$_{100\%}$. Not as impressive, but the branching behavior was captured for D107$_{66\%}$ and D107$_{50\%}$ magnetic fluids as well (see $H = 100.5$ Oe in fig. A.3 and $H = 118.3$ Oe in fig. A.4 accordingly). The branching of the fingers was not observed in experiments with the most diluted magnetic fluid D107$_{33\%}$ for the magnetic field value range tested.

The dilution ratio affects the form of the fingers in a sense that stronger magnetic fields must be applied to obtain curled and branched finger forms for more diluted magnetic fluids. The fingers continue to mix for considerably longer period of time, if both the intensity of the magnetic field and the dilution ratio of the magnetic fluid are higher. The fingers grow more rapidly for more concentrated magnetic fluid. Magnetic micro-convection in $H = 106$ Oe strong magnetic field is compared between magnetic fluids D107$_{100\%}$ and D107$_{66\%}$ in figures 3.14. and 3.15. accordingly.
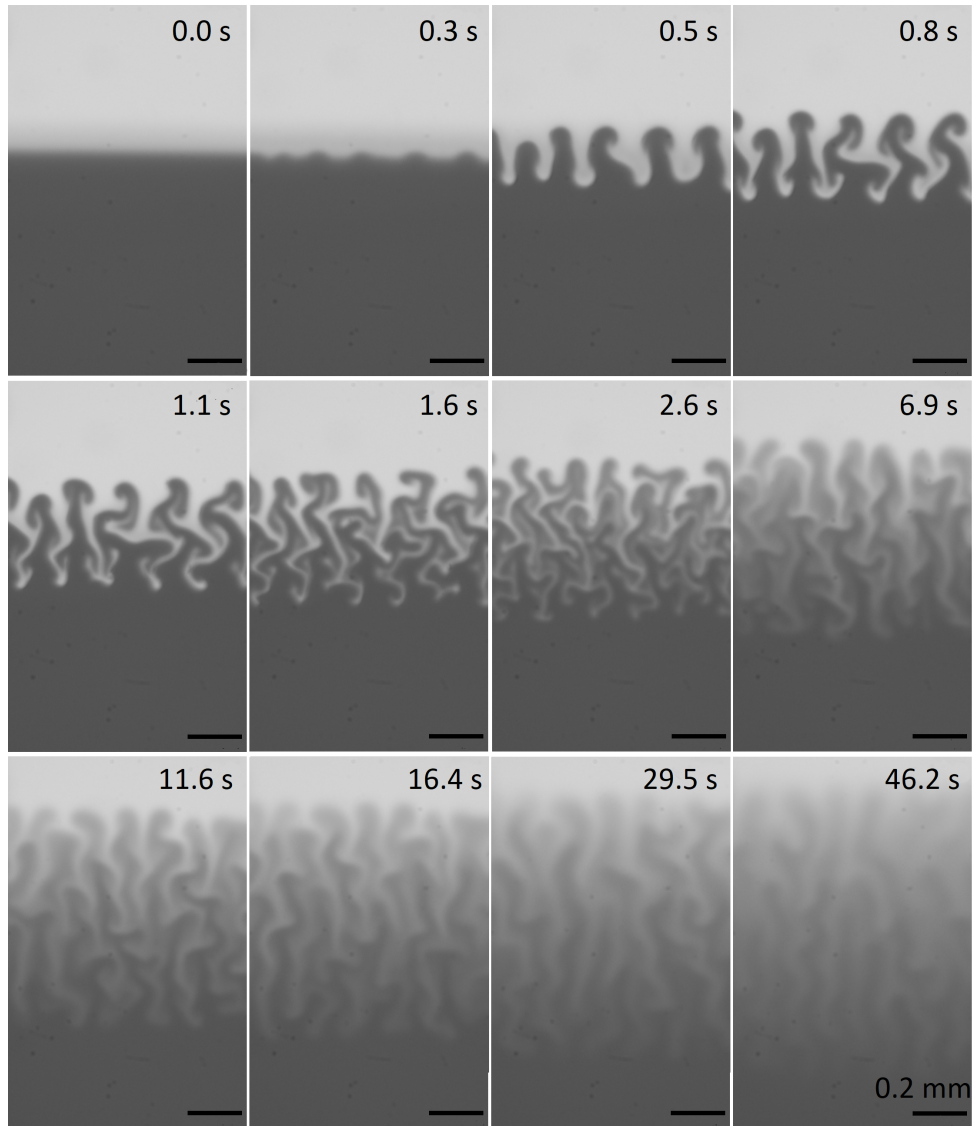
3.14. Figure: An mage series of magnetic micro-convection dynamics over time with magnetic fluid D107$_{100\%}$ in $H = 106$ Oe magnetic field. Each image represents 0.9×1.4 mm large area. The scale bar is 0.2 mm long.

The interface disturbance is visible already at $t = 0.3$ s for the concentrated magnetic fluid D107$_{100\%}$ and slightly later at $t = 0.5$ s for a diluted magnetic fluid D107$_{66\%}$. But for the concentrated fluid at $t = 0.5$ s already distinguished fingers have formed. The fingers have started to form branches already within the first second of the experiment with the concentrated magnetic fluid. Similar fingers are visible at $t = 2.4$ s for the diluted magnetic fluid. At $t = 2.6$ s for the concentrated magnetic fluid the fingers are already actively bending and branching further. Although the instability character seems very similar in both of these experiments, the fingers grow taller and faster in the experiment with magnetic fluid D107$_{100\%}$. At the end of these experiments, the fingers have reached their maximal height of the micro-convection. Nevertheless the mixing length continues to increase, as the diffusion is still present.
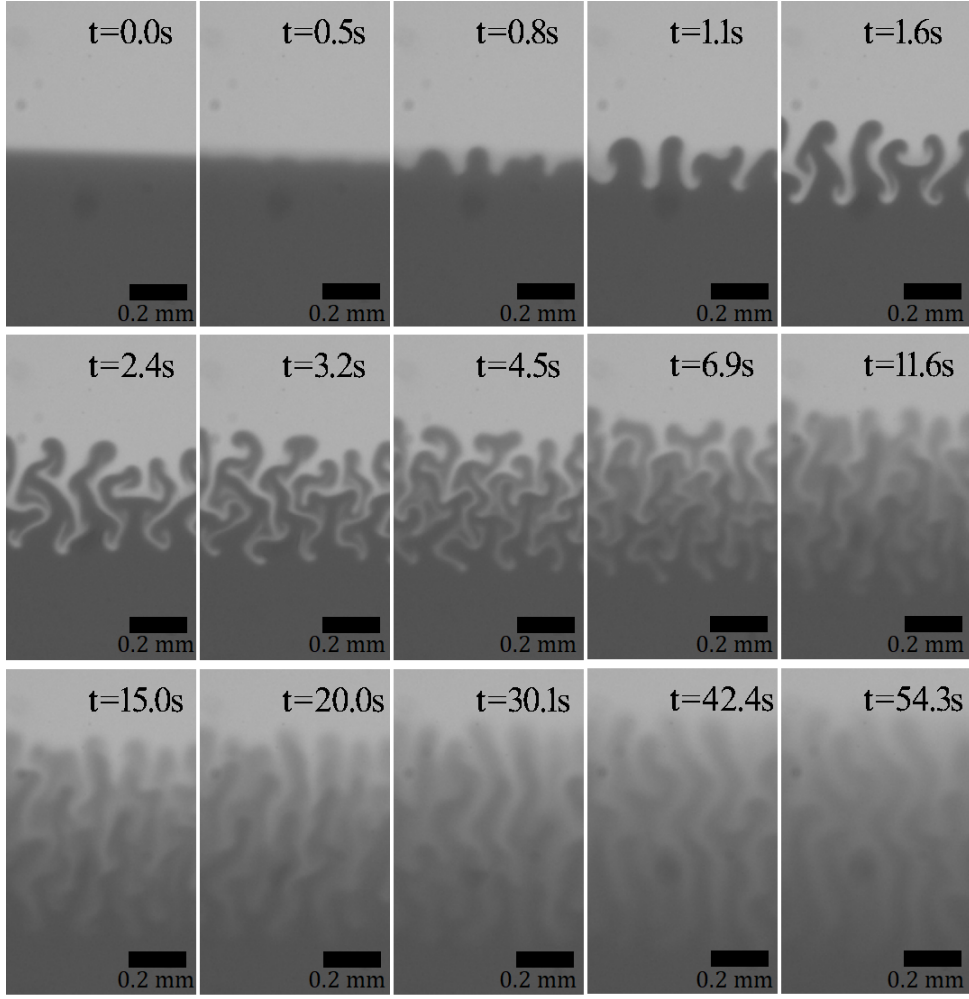
3.15. Figure: An mage series of magnetic micro-convection dynamics over time with magnetic fluid D107$_{66\%}$ in $H = 106$ Oe magnetic field. Each image represents 0.7×1.2 mm region.

During this stage of the study magnetic field and dilution ratio effect on the magnetic micro-convection was explored. As the density of the magnetic fluid changes, by diluting it, the gravitational Rayleigh number is affected. Thus the gravitational effects on the micro-convection can be quantified, as it is done later in §4.2. where the experimental results are compared with numerical simulations. Here, the experimental dependency of the mixing length due to magnetic micro-convection δ_{MC} on the intensity of the magnetic field H is reviewed in figure 3.16. for all explored dilutions of the magnetic fluid D107. The empty markers correspond to the data gained from graphs with "attachment method" where $\delta^2/4$ as a function of time has not reached linear regime. The filled markers represent data gained from the graphs where the linear part of $\delta^2/4$ as a function of time corresponds to D_{exp} within error limits, accordingly. The errors of the experiments are mostly created by the initial interface smearing. The red circles represent experiments with magnetic fluid D107$_{100\%}$, the blue squares are for slightly diluted magnetic fluid D107$_{66\%}$, the green diamonds represent half diluted magnetic fluid D107$_{50\%}$ and the pink triangles are for the

81

most diluted magnetic fluid D107$_{33\%}$. δ_{MC} increases with the intensity of the magnetic field, but is smaller for more diluted magnetic fluids in the same magnetic field. As it can be noted from the graph that at the same values of magnetic field, the triangle markers are bellow all others and the circle markers are above all others.
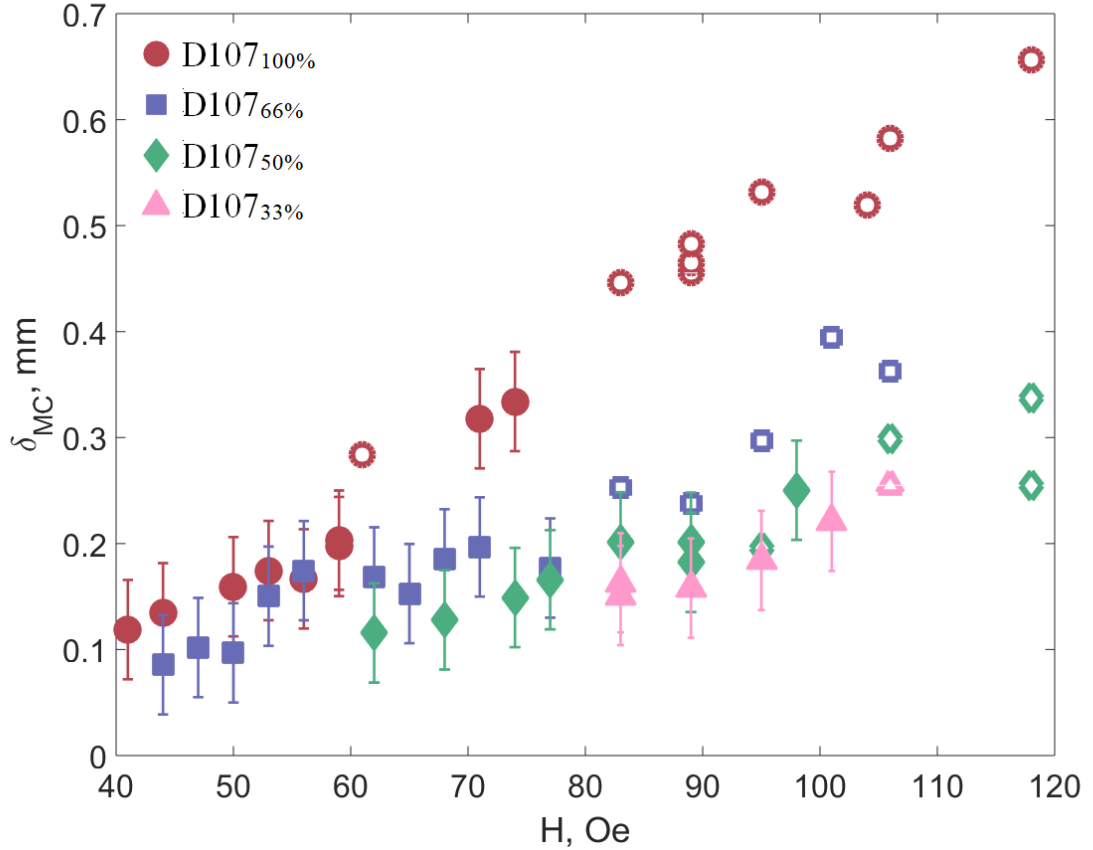
3.16. Figure: δ_{MC} with respect to the magnetic field H. The empty markers represent δ_{MC} obtained with attachment method.

Characteristic size of the instability was measured for all experiments where distinguishable fingers appeared. Just the same as with the flowing experiments, the size of the fingers was measured at their base. The fingers were measured once they appeared as well as after some time since the beginning of the experiment ($t = 5$ s, $t = 10$ s, and $t = 30$ s). As the fingers were growing their wavelength at their base was not affected. The results did not show any dependency on the dilution ratio. The average characteristic wavelength of the fingers in the beginning of the instability experimentally was found to be $\overline{\lambda} = 0.12 \pm 0.02$ mm.

The critical magnetic field H_c for the instability to emerge was found as well. The estimation of H_c experimentally is affected by the initial smearing as the fingers appear at higher magnetic fields if the initial smearing is larger. This effect is demonstrated in figure 3.17..

(a)	(b)	(c)	(d)
H=38.4 Oe	H=41.4 Oe	H=41.4 Oe	H=44.4 Oe
$\delta_{t=0\ s}$=0.092 mm	$\delta_{t=0\ s}$=0.112 mm	$\delta_{t=0\ s}$=0.098 mm	$\delta_{t=0\ s}$=0.092 mm
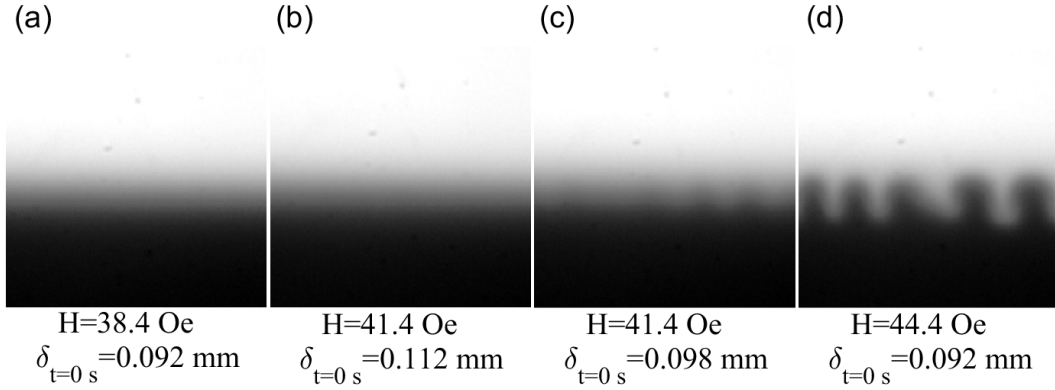
3.17. Figure: The evaluation of the critical magnetic field H_c for magnetic fluid D107$_{100\%}$. The pictures are taken at $t = 10$ s since the beginning of the experiment. Each image represent 0.7×0.7 mm large area.

The critical magnetic field here is estimated to be $H_c = 41.4$ Oe, as in this magnetic field the fingers are visible (see fig. 3.17..c). But the fingers can not be seen in the fig. 3.17..b, although the magnetic field and explored magnetic fluid is the same ($H = H_c$, D107$_{100\%}$). The initial smearing between the fluids $\delta_{t=0\ s} = 0.11$ mm is larger for experiment in fig. 3.17..b than for the experiment in fig. 3.17..c,, where it is $\delta_{t=0\ s} = 0.10$ mm. Although this difference is minimal, it still has affected the value of the critical magnetic field.

The critical magnetic fields for all four dilutions of the magnetic fluid were found:

- D107$_{100\%}$: $H_c = 41.4 \pm 2.5$ Oe;

- D107$_{66\%}$: $H_c = 44.4 \pm 2.5$ Oe;

- D107$_{50\%}$: $H_c = 59.1 \pm 2.5$ Oe;

- D107$_{33\%}$: $H_c = 79.4 \pm 2.5$ Oe.

As expected the critical magnetic field is stronger if the magnetic fluid is more diluted. The errors written here are the size of the step the magnetic field was changed when searching the critical magnetic field during the experiments. Experimentally the value of H_c is estimated visually from experiments, H_c is the lowest magnetic field at which the fingers are visible. However fingers might appear even at smaller magnetic fields, if the interface between both fluids was sharper at the beginning of the experiment.

3.2.1. Summary

During the experiments collected in this section it was demonstrated that the fingers of the instability appear earlier and grow more rapidly in experiments with a higher intensity of the applied magnetic field. Also the fingers emerge only in magnetic fields higher than the critical one. Depending on the strength of the magnetic field the fingers have

3 characteristic shapes: straight, curvy or branched. Fingers bend and branch if the magnetic field is high enough. Once the fingers have grown, they do not grow taller and the shape of them stays the same. But they might still swirl in stronger magnetic fields. The edges of the fingers blur gradually due to the diffusion as the time passes.

The instability is affected by the dilution ratio of the magnetic fluid. Fingers grow faster and taller as well as appear earlier in the same magnetic field if the magnetic fluid is more concentrated. But the fundamental character of the instability stays the same for all of the used fluids. The critical values of the magnetic field were collected for all four dilutions of the magnetic fluid D107. Information about the critical wavelength was gathered as well.

3.3. Magnetic micro-convection in fluids with initially smeared interface between the mixing fluids

In this section of the work the results of the dynamics of the magnetic micro-convection in experiments with initially smeared interface between the mixing fluids are collected. The aim of this part of the study is to find out how the magnetic micro-convection is affected by the interface between both fluids and how the instability changes if this interface is not sharp, but already pre-mixed. It has been showed in the literature [81] that the initial smearing affects the instability and here it is explored more. A publication is prepared about the results collected in this section.

The thickness of the smeared layer δ_0 between both fluids is set and varied by letting the magnetic fluid and water to diffuse over different periods of time. As described in §2.4.2. the syringe pumps are used to pump in the fresh material for each experiment. Then the pumps are switched of and magnetic fluid and water diffuse for some set period of time. After that the external magnetic field is applied and the experiment is timed and recorded from this exact moment.

In these experiments three different magnetic fluids were used: D107, KTF11-1 and FF09-9. Similar as in the previous experimental series the magnetic fluids were diluted to various concentrations (100%, 66%, 50% and 33%) using distilled water. The diffusion coefficient D is not altered by diluting magnetic fluids, but the particle volume fraction and density becomes smaller. Therefore the dimensionless quantities $\mathrm{Ra_g}$ and $\mathrm{Ra_m}$ that are used for resut comparison are affected as well.

In addition to diluting the magnetic fluids with water the experimental parameters were varied also by using micro-channels with four different thicknesses ($h = 0.050$ mm; $h_1 = 0.135 \pm 0.005$ mm; $h_2 = 0.257 \pm 0.025$ mm and $h_3 = 0.399 \pm 0.015$ mm). By changing the thickness of the micro-channel $\mathrm{Ra_g}$ and $\mathrm{Ra_m}$ also change. As can be noted from equations 1.25 and 1.24: $\mathrm{Ra_g} \sim h^3$ and $\mathrm{Ra_m} \sim h^2$.

The smallest microfluidics chip ($h = 0.050$ mm) was made from PDMS. Only few experiments were made to qualitatively observe the nature of magnetic-micro-convection in the smallest microfluidics chip as it was too hard to manipulate the fluids by syringe pumps with existing experimental setup in a chip this miniature. The interface between the fluids tended to fluctuate and change position with respect to a vertical direction during the experiments in this microfluidics chip due to some changes of the pressure in the system. As the micro-channel was small enough, the effect of the pressure changes was too visible and affected the results of the experiments as the fluctuation of the interface affected the mixing rate. The pressure changes in the experiments could arise due to some bubbles in the syringes and tubing and due to the fact that the used experimental system is not completely rigid. In thicker micro-channels the interface fluctuation during the experiments was not observed. Few successful experiments of the magnetic micro-convection

in this microfluidics chip were recorded and one of them is demonstrated below in fig. 3.18..
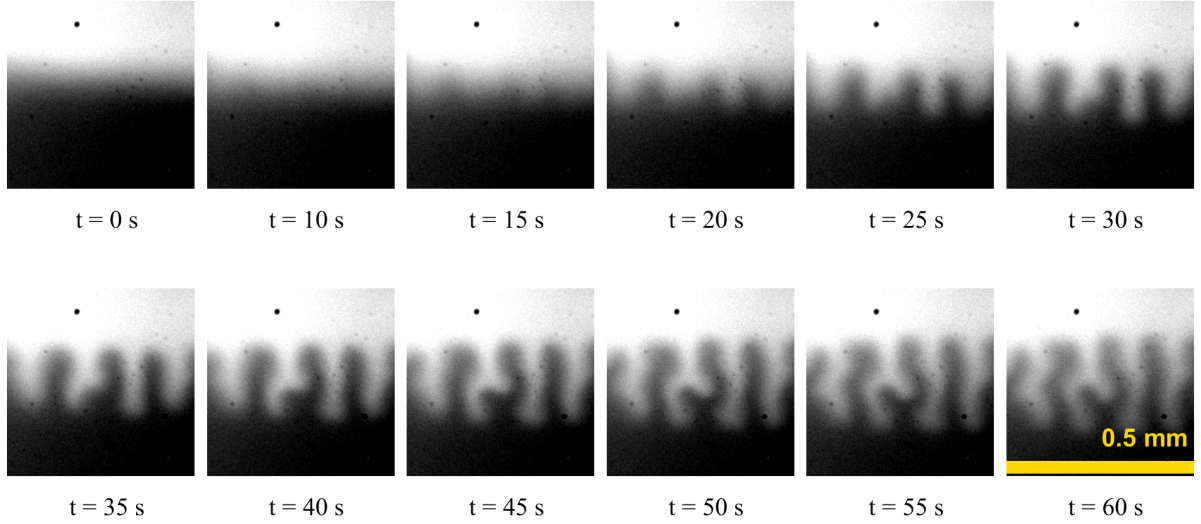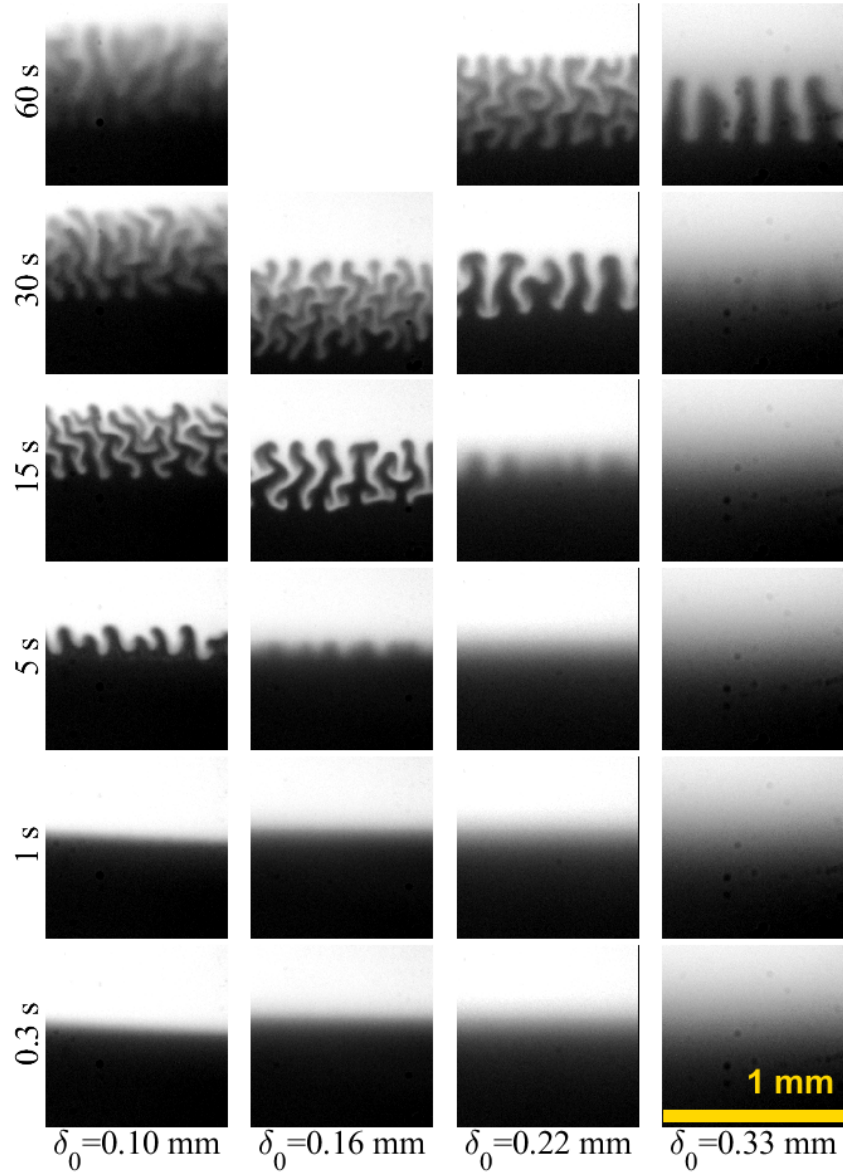

3.18. Figure: Image series of magnetic micro-convection dynamics in time in micro-channel with thickness $h = 0.050$ mm. Magnetic fluid: KTF11-1$_{100\%}$, Magnetic field: $H = 71$ Oe, Initial smearing thickness: $\delta_0 = 0.07$ mm. Size of a region represented by a single image is 0.5×0.5 mm.

Visually the set of the experiments with initially smeared interface between the mixing fluids is demonstrated by image series in figures 3.18., 3.19. and 3.20.. The contrast of the images is increased for easier perception. The time values in these figures represent the time since the beginning of the experiment or in other words, how much time has passed since the application of the external magnetic field.

In the fig. 3.18. the development of the magnetic micro-convection in time of a single experiment with magnetic fluid KTF11-1$_{100\%}$ is shown. The experiment is carried out in the micro-channel with the smallest thickness $h = 0.050$ mm. The initial smearing thickness for this experiment is $\delta_0 = 0.07$ mm and the value of the external magnetic field is $H = 71$ Oe. The fingers of the instability start to form around $t \approx 10$ s. As the time passes the fingers become taller. After some time (at $t \approx 35$ s) they start to bend and even branch. The characteristic wavelength of this instability in this micro-channel is $\lambda \approx 0.125$ mm at the beginning of the instability.

In the fig. 3.19. the visual effects of various initial smearing thicknesses δ_0 on magnetic micro-convection in micro-channel with $h_1 = 0.135$ mm is demonstrated. The external magnetic field is the same ($H = 82.8$ Oe) for all of the demonstrated experiments and the used magnetic fluid in the demonstrated experiments is KTF11-1$_{100\%}$. One column of images represents a singular experiment in time. Similar as in experiments with sharp interface between the mixing fluids represented in §3.2., the fingers start to grow out

straight, then if the magnetic field is high enough they bend and branch. After some time the fingers reach their maximum height and stop growing. After a long enough period of time the edges of fingers become less prominent and they fuse together due to the diffusion.

3.19. Figure: Image series of magnetic micro-convection dynamics with different initial smearing thicknesses δ_0 in a constant magnetic field $H = 82.8$ Oe in micro-channel with thickness $h_1 = 0.135$ mm. Magnetic fluid: KTF11-1$_{100\%}$. Size of a region represented by a single image is 1.0×1.0 mm.

It can be seen in fig. 3.19. that the fingers of the instability appear latter in time and form slower for experiments with higher values of δ_0. As follows the fingers at a set time-point are shorter and less wavy for experiments with higher values of δ_0. For example, the fingers of the instability appear already at $t = 5$ s for the experiment with $\delta_0 = 0.16$ mm. After 10 seconds at $t = 15$ s they are already relatively tall and have

started bending. But for the experiment placed next to it with $\delta_0 = 0.22$ mm the fingers start to form around $t = 15$ s. And although both experiments look quite similar the moment the fingers have appeared, the experiment with higher $\delta_0 = 0.22$ mm has not reached the finger length even in 15 seconds at $t = 30$ s that was reached in 10 seconds in the experiment with shorter $\delta_0 = 0.16$ mm. The maximum height of the fingers in the same external magnetic field also is smaller in experiments with higher δ_0. When the fingers appear they are visually more blurred out in experiments with larger δ_0. This effect is visible, for example, for experiment with $\delta_0 = 0.33$ mm at $t = 30$ s in the fig. 3.19. as the fingers are almost indistinguishable.

h, mm	MF	H, Oe	δ_0, mm	λ, mm	observation
0.050	KTF11-1$_{100\%}$	71.0	0.07	0.125	
0.135	KTF11-1$_{100\%}$	82.8	0.10	0.14	λ increases as δ_0 increases
			0.16	0.17	
			0.22	0.17	
			0.33	0.20	
	KTF11-1$_{66\%}$	71.0	0.04	0.14	λ increases as δ_0 increases
			0.13	0.20	
			0.21	0.20	
		82.8	0.04	0.14	λ increases as δ_0 increases
			0.13	0.15	
			0.16	0.20	
			0.18	0.18	
			0.25	0.20	
0.257	KTF11-1$_{100\%}$	88.7	0.10	0.15	λ increases as δ_0 increases
			0.12	0.22	
			0.20	0.22	
	KTF11-1$_{66\%}$	88.7	0.18	0.18	λ increases as δ_0 increases
			0.23	0.22	
			0.26	0.20	

3.2. Table: Characteristic wavelength of the magnetic micro-convection in experiments with the magnetic fluid KTF11-1

It is not conclusive whether the initial smearing thickness affects the characteristic size of the instability. According to [62] the characteristic wavelength λ should increase if the initial smearing thickness δ_0 increases. The effects of smearing thickness and the thickness of micro-channel on the characteristic wavelength of the magnetic micro-convection for the

magnetic fluid KTF11-1 are collected in tables 3.2.. There it is visible that λ increases as the initial smearing between the mixing fluids is increased, as expected from the theoretical predictions [62]. For other used magnetic fluids the results were statistically inconclusive due to the data dispersion, and the results are visible in Appendix §A.1.3 in table A1.. For all of the experiments collected in the tables 3.2. and A1. the fingers were counted as soon as the instability emerged at the base of the fingers. So if some of the fingers branched or split later in time it was not accounted for.

Another effect that we can observe from the data in the tables 3.2. and A1. is that by increasing the thickness of the micro-channel, the average characteristic λ of the instability increases as well, which agrees with the literature [17], where the authors found a linear relationship between the wavelength and the thickness of the microfluidics chip if the thickness of the chip is larger than 12 μm, but smaller than 250 μm. Here such conclusion about the relationship between the thickness of the micro-channel and the wavelength can not be made , but the overall tendency agrees with the results of [17].

The effect of the strength of the magnetic field on the magnetic micro-convection is visible in the fig. 3.20. for the same initial smearing thickness $\delta_0 = 0.18$ mm for magnetic fluid KTF11-1$_{100\%}$. One column represents a single experiment in time. The magnetic field $H = 59.1$ Oe is the critical field for the instability for experiments with this δ_0. The fingers are almost indistinguishable (blurred and short) and they appear only after a minute since the beginning of the experiment. The same as for the experiments with a sharp interface between the mixing fluid presented in §3.2., the external magnetic field affects the form of the fingers of the instability. For smaller fields the fingers are short and straight, as here it is visible for the experiment in $H = 65.0$ Oe. In larger fields the fingers become wavy or even posses zig-zag look-a-like shape, also the grow out longer. For example, here, the fingers at 1 minute are approximately 0.15 mm tall in magnetic field $H = 65.0$ Oe; but they are 5 times larger at the same time in the magnetic field $H = 88.7$ Oe. For even larger fields the fingers become branched. Also the instability itself emerges earlier in higher magnetic fields, for example, there are already visible fingers already at $t = 15$ s in the experiment in the magnetic field $H = 88.7$ Oe, whereas in $H = 65.0$ Oe fingers are visible only at $t \approx 60$ s. On the other hand it is visible that miniature fingers have started to form already at $t = 5$ s in the magnetic field $H = 100.5$ Oe.

Although magnetic field sets the shape of the fingers at the end of the instability magnetic field does not affect the characteristic wavelength at the beginning of the instability. In all of the demonstrated experiments in the fig. 3.20. there are six fingers in a picture once the instability emerges. Each picture here represents 1.0×1.0 mm region in a real life, thus for all of these experiments $\lambda = 0.17$ mm.

All of the fingers start growing out straight in the first moments of the instability regardless of the shape they will become. The branching and bending of the fingers

appears relatively fast and it continues even for some time after the fingers have reached their maximum height. The stronger the magnetic field, the faster the fingers will start to branch (if they are going to do so).
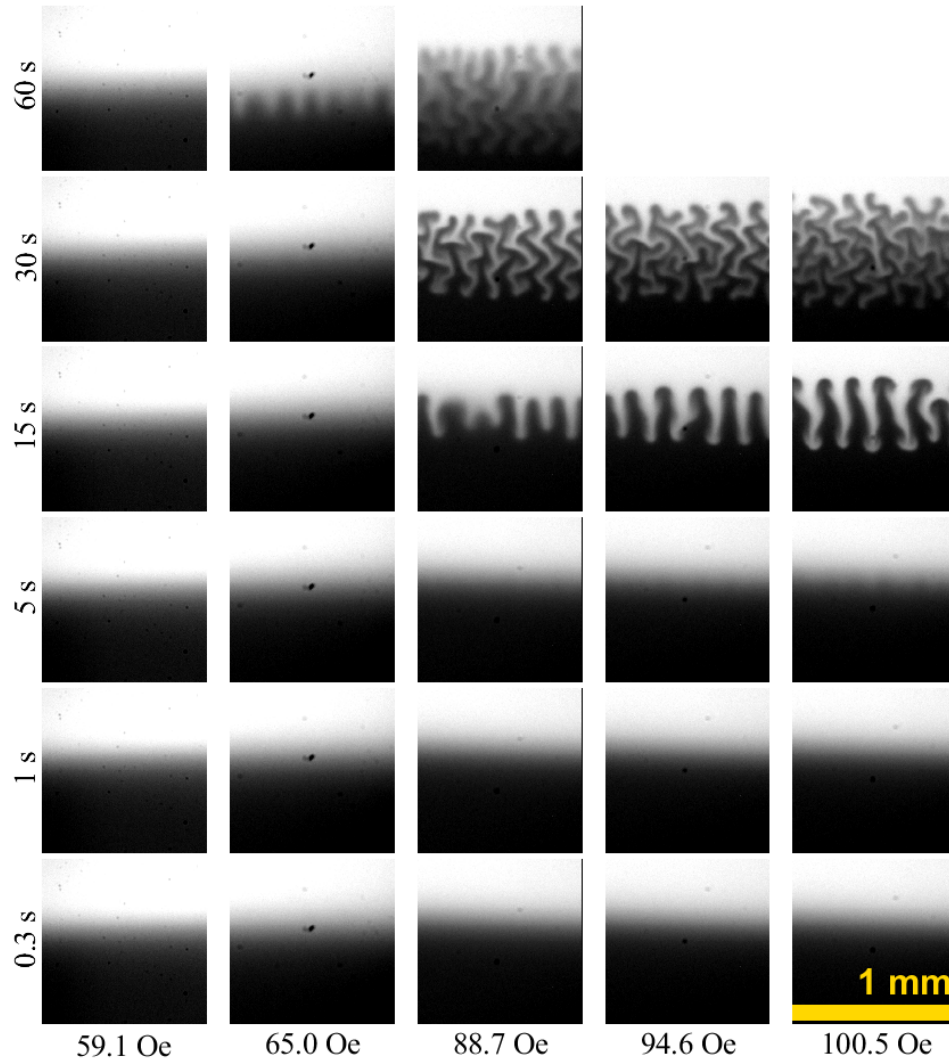
3.20. Figure: Image series of magnetic micro-convection dynamics in various magnetic fields with a constant initial smearing thickness $\delta_0 = 0.18$ mm in micro-channel with thickness $h_1 = 0.135$ mm. Magnetic fluid: KTF11-1$_{100\%}$. Size of a region represented by a single image is 1.0×1.0 mm.

The value of the magnetic field at which the fingers change their nature can be approximately measured experimentally. The minimal values of the magnetic field in which the fingers grow out to become either wavy or branched are collected collected for magnetic fluids HTF11-1 and FF09-9. For the experiments with magnetic fluids KTF11-1$_{66\%}$ in the micro-channel with thickness $h_1 = 0.135$ mm and FF09-9$_{50\%}$ the fingers started to branch or become wavy only for small enough values of initial smearing thickness. For higher values of δ_0 the fingers stay either straight or wavy till the end of the experiment even if

the determined threshold value of the magnetic field has been reached. For the rest of the experiments the fingers changed their nature after the mentioned threshold magnetic field for all of the collected values of the initial smearing thickness up to $\delta_0 \approx 0.3$ mm. So it can be concluded that the initial smearing affects the form of the fingers.

The threshold values of the magnetic field for the fingers to become or grow out wavy in the micro-channel with thickness $h_1 = 0.135$ mm are:

- KTF11-1$_{100\%}$: $H = 60$ Oe;

- KTF11-1$_{66\%}$: $H = 60$ Oe;

- FF09-9$_{100\%}$: $H = 47$ Oe;

- FF09-9$_{50\%}$: $H = 77$ Oe, only if $\delta_0 \leq 0.15$ mm.

In thicker micro-channel with $h_2 = 0.257$ mm the fingers become wavy in following fields:

- KTF11-1$_{100\%}$: $H = 71$ Oe;

- KTF11-1$_{66\%}$: $H = 83$ Oe;

- FF09-9$_{50\%}$: $H = 77$ Oe, only if $\delta_0 \leq 0.15$ mm.

During the experiment the fingers of the instability start to branch in the micro-channel with thickness $h_1 = 0.135$ mm if the following values of the external magnetic field are reached:

- KTF11-1$_{100\%}$: $H = 71$ Oe;

- KTF11-1$_{66\%}$: $H = 83$ Oe;

- FF09-9$_{100\%}$: $H = 65$ Oe.

But for brancing to be observable in thicker micro-channel with thickness $h_2 = 0.257$ mm magnetic fields must be higher:

- KTF11-1$_{100\%}$: $H = 83$ Oe;

- KTF11-1$_{66\%}$: $H = 89$ Oe, only if $\delta_0 \leq 0.13$ mm;

- FF09-9$_{50\%}$: $H = 83$ Oe, only if $\delta_0 \leq 0.13$ mm.

It is visible that the minimal value of the magnetic field for the fingers to change their character (straight $\rightarrow$ wavy $\rightarrow$ branched) is larger if the magnetic fluid is diluted. The magnetic field must be stronger for the fingers to change character also if the thickness of the micro-channel is larger.

3.3.1. Mixing with magnetic micro-convection with respect to the external magnetic field

In this section the results of the dynamics of the magnetic micro-convection with respect to the external magnetic field grouped by the initial smearing thickness are collected.

The quantitative influence of the initial smearing thickness δ_0 of the interface between the magnetic fluid and water on the mixing by magnetic micro-convection δ_{MC} is presented in figure 3.21. for the magnetic fluid FF09-9$_{100\%}$ in a micro-channel with thickness $h_1 = 0.135$ mm. For experiments with other magnetic fluids and various micro-channel thicknesses the additional figures are collected in Appendix §A.1.3.

One data point in a graph represents one experiment in a constant external magnetic field with a set initial smearing thickness δ_0 as shown in the legend. The results are grouped by initial smearing thickness and the colors of markers are chosen to easily perceive the effect of the δ_0 on the mixing by magnetic micro-convection δ_{MC} as they become lighter as the δ_0 increases. It is apparent that micro-convective mixing is more effective for sharper interfaces (smaller δ_0) between the mixing fluids as the darker markers are above the lighter ones. Meaning that with the same value of external magnetic field greater mixing due to micro-convection can be achieved if the fluids in interest have not been mixed yet.
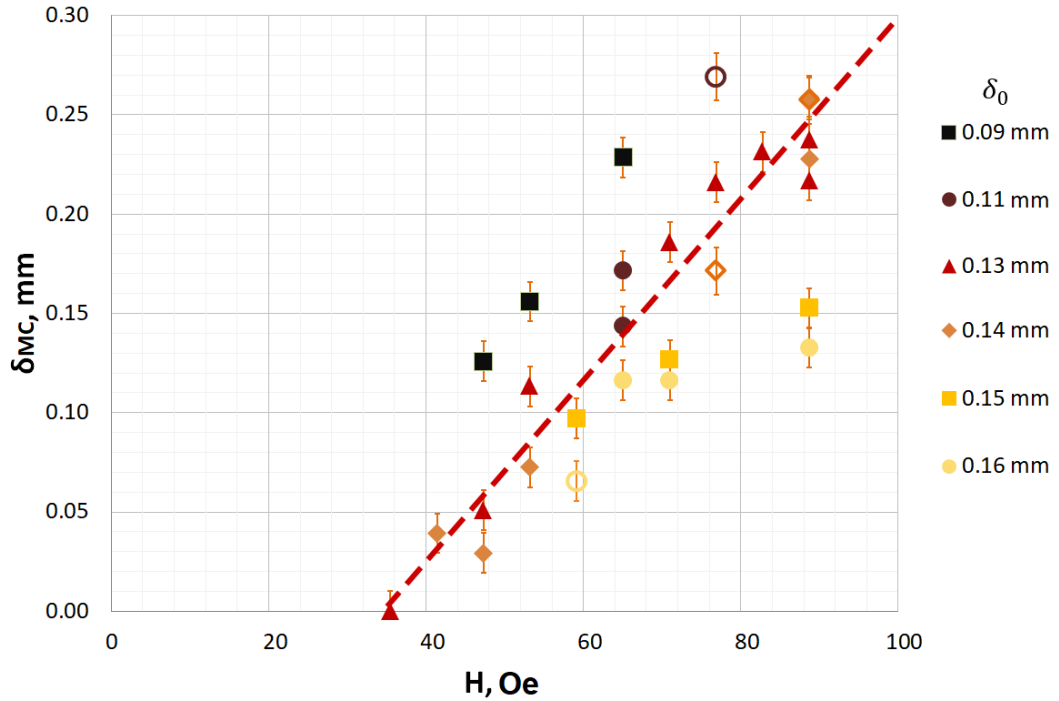
3.21. Figure: Mixing by magnetic micro-convection δ_{MC} with respect to the external magnetic field H for various δ_0 in micro-channel with thickness $h_1 = 0.135$ mm. Magnetic fluid: FF09-9$_{100\%}$. The empty markers represent the expected δ_{MC} obtained with attachment method.

The marker groups of various δ_0 seem parallel to each other for all experiments. This means that the rate at which the mixing δ_{MC} increases by increasing the external magnetic field is not affected by the initial smearing thickness.

By extrapolating the data points of a chosen δ_0 until they reach the horizontal axis an approximate critical value of magnetic field H_c for each smeared interface thickness can be obtained. This is the value before which no magnetic micro-convection can be observed for a given δ_0. For example, in fig. 3.21. markers representing experiments with initial smearing thickness $\delta_0 = 0.13$ mm are approximated with a straight line (the red dashed line in the graph). Using this approximation it can be estimated that the critical magnetic field in which the instability first emerges mixing water and the specific magnetic fluid FF09-9$_{100\%}$ if the initial smearing thickness is $\delta_0 = 0.13$ mm would be $H_c \approx 36$ Oe. As expected the likely values of H_c appear to be higher for larger δ_0. Visually during the experiments it is harder to notice H_c for experiments with larger δ_0, as the fingers in those experiments have a very low contrast, are short and have very blurred edges.

The estimated critical magnetic field values for various initial smearing thicknesses from the experiments within this chapter are collected. The example for magnetic fluid D107$_{50\%}$ is visible in table 3.3.. For other magnetic fluids the results are collected in Appendix §A.1.3. It is visible in the experimental data that the experiments with more diluted magnetic fluid have higher critical magnetic field values H_c to create an instability with the same initial smearing thickness δ_0 between the mixing fluids.

δ_0, mm	H_c, Oe
0.05	50
0.07	55
0.14	60
0.17	80
0.31	68
0.26	77
0.29	83
0.36	89

3.3. Table: Critical magnetic field for magnetic micro-convection to emerge for various initial smearing thicknesses δ_0, when mixing water and magnetic fluid D107$_{50\%}$ in micro-channel with thickness $h_1 = 0.135$ mm.

Due to data dispersion in it inconclusive whether H_c depends micro-channel thickness, although in it seems that the values of the critical magnetic field are slightly higher for experiments carried out in the thicker micro-channel (see fig. A.14a for $h_2 = 0.257$ mm). Within measured value range data series for estimated critical magnetic field with respect

to the initial smearing thickness appear linear. From this data the value of the critical magnetic field for mixing fluids with sharp initial interface can be estimated using linear approximation.

These estimated values of critical magnetic field for magnetic micro-convection to emerge if the mixing fluids have sharp initial interface are collected in tab. 3.4.. The critical magnetic field value $H_c = 49$ Oe here for the magnetic fluid D107$_{50\%}$ when mixing fluids with sharp initial interface is similar to the values of H_c for this magnetic fluid obtained in experiments reviewed in the previous two section: $H_c = 51$ Oe as estimated from the experiments with flowing fluids in section §3.1., and $H_c = 62$ Oe as obtained from the experiments with initially stagnant fluids and sharp initial interface in section §3.2..

MF	Dilution ratio	h, mm	H_c, Oe
D107	50%	0.135	49
FF09-9	100%	0.135	13
		0.257	23
	50%	0.135	30
		0.257	39
KTF11-1	100%	0.135	20
		0.257	18
	66%	0.135	40

3.4. Table: Estimated critical magnetic field for magnetic micro-convection to emerge when mixing fluids with sharp initial interface $\delta_0 = 0$ mm between the fluids.

Next the effect of other properties besides the initial smearing thickness and external magnetic field value of the experiments on magnetic micro-convection is inspected.

As it could be anticipated from the results in previous sections, micro-convection is oppressed by diluting the magnetic fluid. An example of this for Magnetic fluid FF09-9 is demonstrates in figure 3.22.. For other magnetic fluids explored the results are collected in Appendix §A.1.3. The same color tonality is chosen for the same dilution ratio of the magnetic fluid. The same shape of markers represent the same value of δ_0. The colors of the markers become lighter as the value δ_0 increases. The experiments represented here are carried out in different micro-channels: the thinner one ($h_1 = 0.135$ mm) in fig. 3.22.a and the thicker one ($h_2 = 0.257$ mm) in fig. 3.22.b respectively. In both graphs mixing due to magnetic micro-convection is greater for more concentrated magnetic fluids as the orange tonality markers are above the blue ones. δ_{MC} at the same initial smearing thickness is restricted by magnetic fluid dilution.

From these graphs it seems, that the value of δ_{MC} grows at a same rate by increasing external magnetic field for both dilution ratios of the magnetic fluid as the slope of the blue and orange markers seems the same for the measured values of the external magnetic

field. In other words, the dilution ratio (therefore also ϕ_{Vol} and $\Delta\rho$) does not affect the character of δ_{MC} with respect to the magnetic field.
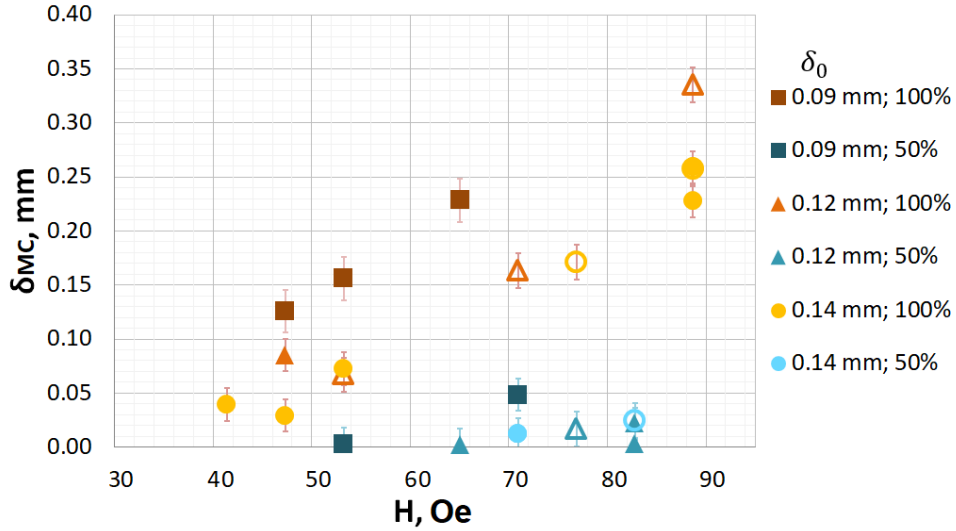

(a) $h_1 = 0.135$ mm
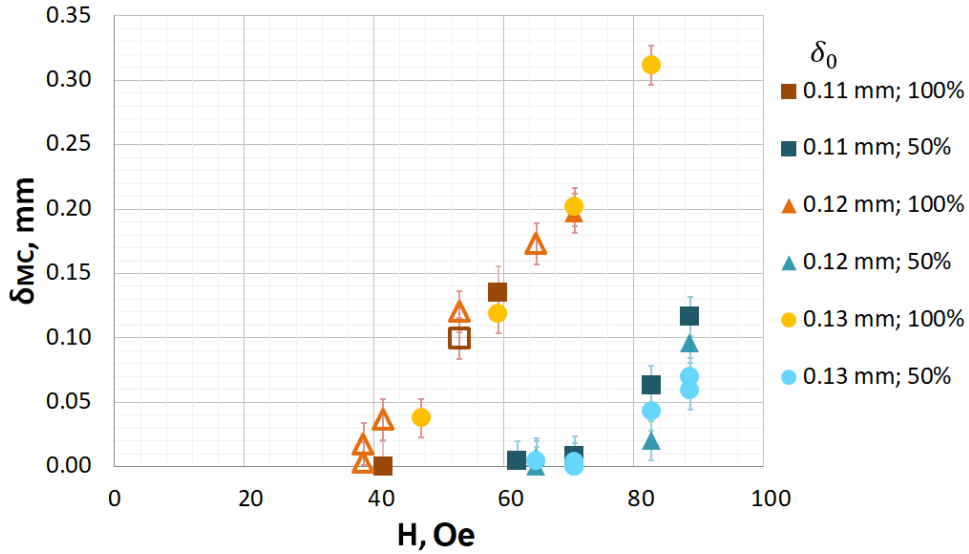
(b) $h_2 = 0.257$ mm

3.22. Figure: Dilution ratio effect of magnetic fluid FF09-9 on δ_{MC} for various δ_0. The same dilution ratio has the same color tonality of the markers. Empty markers represent δ_{MC} obtained with attachment method.

It seems that the initial smearing thickness does not affect the rate at which δ_{MC} changes with respect to a different dilution ratio. The difference between the markers of the same shape (in fig. 3.22.) in a vertical direction (the difference of δ_{MC} values between experiments in the same magnetic field with the same δ_0, but with different dilution ratios) is approximately the same for all marker shapes. This also means that within the measured range of values of the magnetic field the difference between the orange markers with respect to the vertical direction seems the same as in the blue markers (in fig. 3.22.).

Meaning that the dilution ratio has no effect on the rate at which the micro-convective mixing δ_{MC} decreases as the initial smearing thickness δ_0 is increased.

Although in the fig. 3.22. the behavior of δ_{MC} in aspect of the dilution ratio is similar-the value δ_{MC} is visibly larger in the experiments with more concentrated magnetic fluid for experiments in both microfluidics chips. The scene is different after the experimental units are made dimensionless.
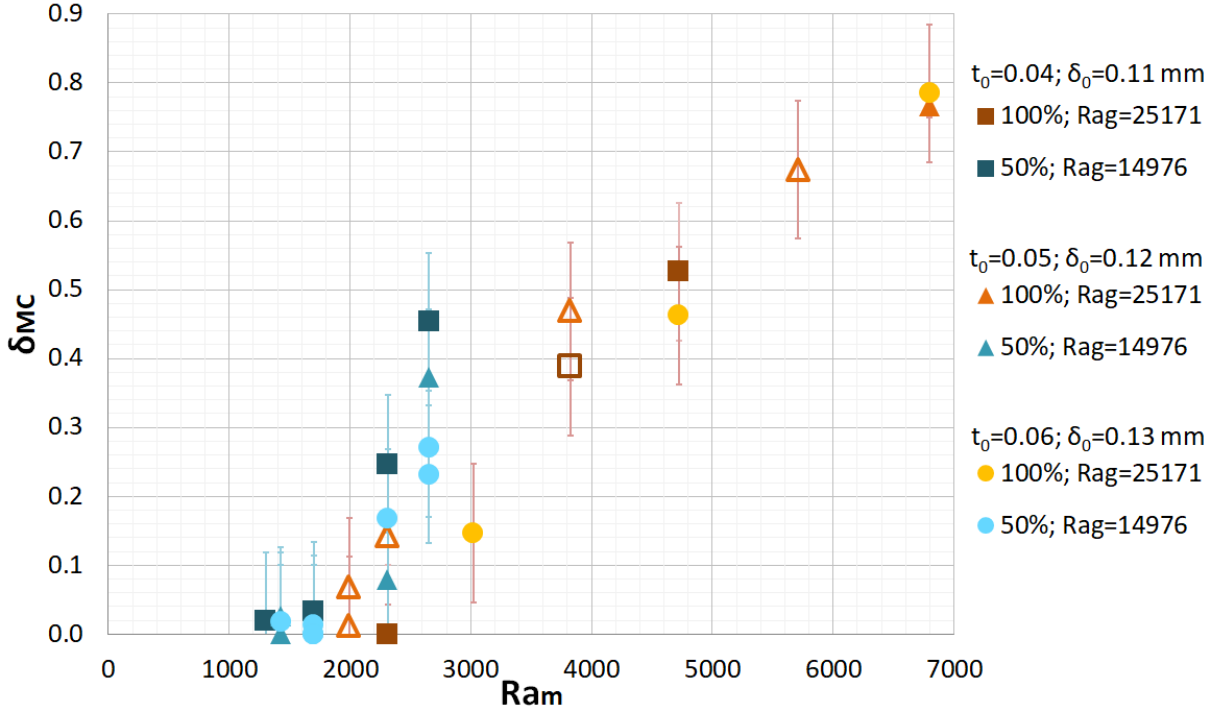
3.23. Figure: Dilution ratio effect on dimensionless δ_{MC} for various δ_0 in micro-channel with thickness $h_2 = 0.257$ mm. Magnetic fluid: FF09-9. Empty markers represent δ_{MC} from attachment method.

The value range of $\mathrm{Ra_m}$ for both fluids does not overlap much. The behavior of the magnetic micro-convection for larger values of $\mathrm{Ra_m}$ for the 50% diluted magnetic fluid are unknown as the magnetic field limit of the experimental system was reached. In the fig. 3.23. it is visible that for the same values of $\mathrm{Ra_m}$ the blue markers which represent experiments with magnetic fluid of dilution ratio 50% are above the orange markers for 100% concentrated magnetic fluid. Meaning that as expected magnetic micro-convection with respect to $\mathrm{Ra_m}$ is greater for more diluted fluid, as the gravitational effects are decreased from the gravity characterizing $\mathrm{Ra_g} \approx 25200$ for the FF09-9$_{100\%}$ to $\mathrm{Ra_g} \approx 15000$ for the FF09-9$_{50\%}$.

Visually the effect of different dilution ratios on the magnetic micro-convection for magnetic fluid KTF11-1 is presented in fig. 3.24.. The columns of image series should be inspected in pairs as the experiments of two different dilution ratios (100% and 66%) of the magnetic fluid, but with the same values of H and δ_0 are placed next to each other

It seems that the instability appears earlier in time for more concentrated magnetic fluid. The fingers are already visible at $t = 5$ s at $H = 71$ Oe and $\delta_0 = 0.13$ mm for KTF11-1$_{100\%}$, but not for KTF11-1$_{66\%}$.
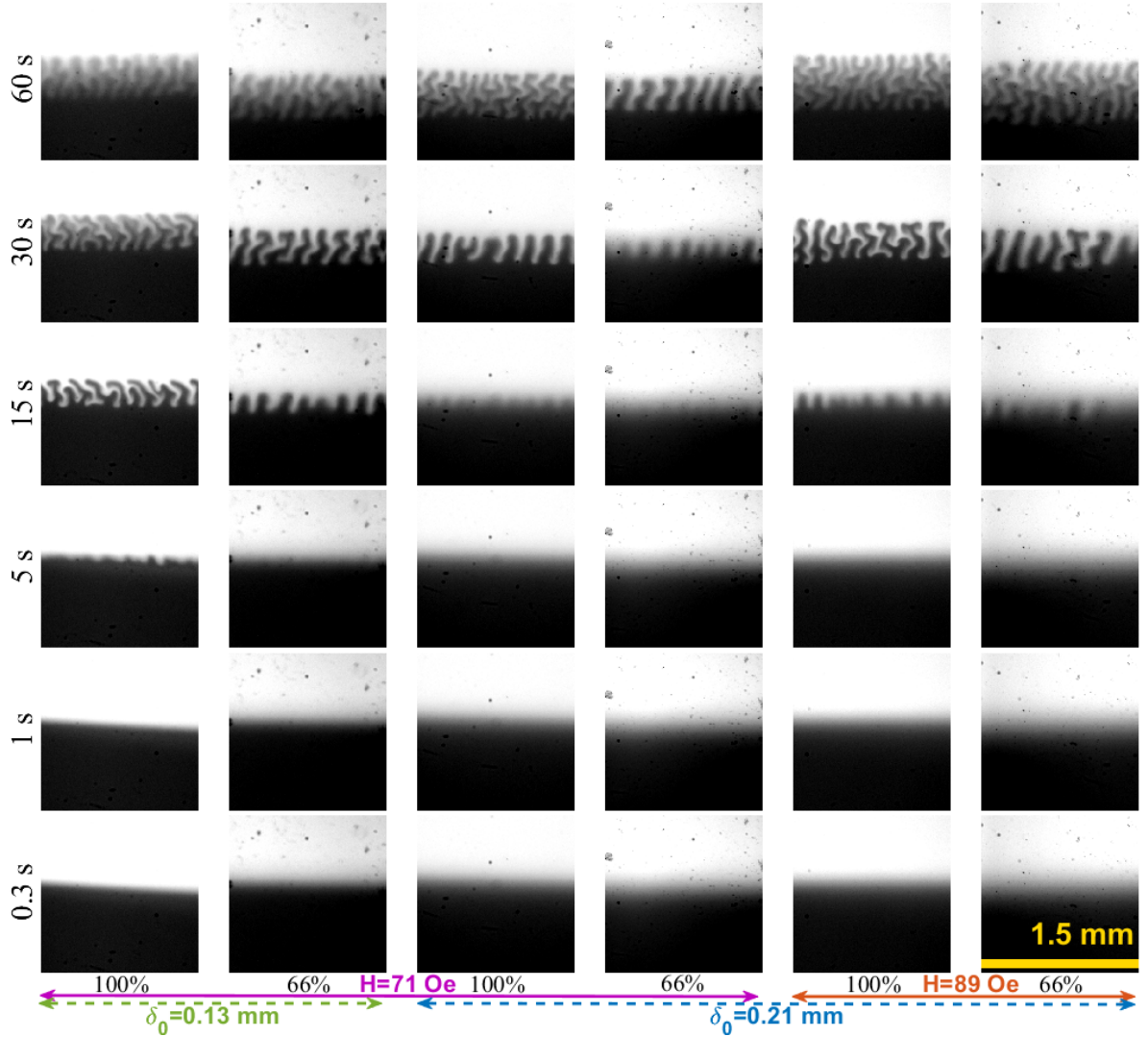
3.24. Figure: Image series of magnetic micro-convection dynamics for various dilution ratios of magnetic fluid KTF11-1 in micro-channel with thickness $h_1 = 0.135$ mm. A single image represents 1.5×1.5 mm large area.

The dilution ratio does not affect the characteristic wavelength of the magnetic micro-convection as there is the same amount of fingers visible in a region of the same size in each of these experiments once the instability emerges. However the dilution ratio of the magnetic fluid affects the nature of the fingers. The threshold value for fingers to become wavy or branched is higher for more diluted magnetic fluids. For example, in the third column in the fig. 3.24. it is visible that at 1 minute the fingers have started to branch in experiment with KTF11-1$_{100\%}$ at $H = 71$ Oe and $\delta_0 = 0.21$ mm. But for the experiment on the right for KTF11-1$_{66\%}$ with the same values of H and δ_0 the fingers are just slightly

wavy and they stay that way until they have reached their maximal height. This is also consistent with the data collected earlier, as $H = 71$ Oe is the threshold value of magnetic field for fingers to start branching for the 100% dilution; but for 66% dilution the threshold value is higher $H \approx 83$ Oe. And indeed in the last column of the fig. 3.24. with $H = 89$ Oe it is visible that fingers of the instability are branching at $t = 60$ s even for the experiment with 66% dilution ratio.

Another parameter whose effect on magnetic micro-convection was measured is the thickness of the micro-channel. The quantitative influence of the micro-channel thickness h on the mixing by magnetic micro-convection δ_{MC} for the magnetic fluid FF09-9 is presented in figures 3.25. and 3.26. for magnetic fluid dilution ratios 100% and 50% accordingly. Experiments in the same micro-channel are demonstrated in the same color tonality of the markers, but experiments with the same δ_0 has the same marker shape per graph. The experiments with the magnetic fluid FF09-9$_{100\%}$ were carried out in two different microfluidics chips ($h_1 = 0.135$ mm and $h_2 = 0.257$ mm), whereas the experiments with diluted FF09-9$_{50\%}$ magnetic fluid were carried out and compared between three different microfluidics chips ($h_1 = 0.135$ mm, $h_2 = 0.257$ mm and $h_3 = 0.399$ mm).

As it can be seen in the graph of fig. 3.26. the highest mixing due to magnetic micro-convection in the same magnetic field with the same initial smearing thickness can be achieved by the thickest ($h_3 = 0.399$ mm) micro-channel as the green markers that represent the experimental results in the thickest micro-channel are above all other markers. However the mixing difference between the two thinner micro-channels ($h_1 = 0.135$ mm and $h_2 = 0.257$ mm) is statistically insignificant for both dilution ratios as the blue and and orange markers are aligned within errors in both graphs (fig. 3.25. and 3.26.).

The micro-channel thickness effect on the micro-convection can not be expressed comparing only just the mixing in the two thinner micro-channels. In fig. 3.26. slightly larger values of δ_{MC} for the same values of magnetic field and initial smearing thickness seem to be achieved in the thinnest $h_1 = 0.135$ mm micro-channel, but in the fig. 3.25. this relationship seems to be the opposite. This difference also seems to increase as the magnetic field increases. For example, in fig. 3.25. the difference between the round markers in vertical direction ($\delta_{MC(h_2=0.257mm;\delta_0=0.13mm)}$ and $\delta_{MC(h_1=0.135mm;\delta_0=0.13mm)}$) is greater in the magnetic field $H = 85$ Oe that it is in the magnetic field $H = 71$ Oe.

The changes of δ_{MC} with respect to δ_0 does not seem to be affected by the thickness micro-channel. Although the difference between green markers with respect to vertical axis in absolute units seems to be bigger than the difference between the blue or orange markers in the fig. 3.26. the variations in change of δ_{MC} with respect to δ_0 due to the thickness micro-channel are statistically insignificant considering the experimental error.
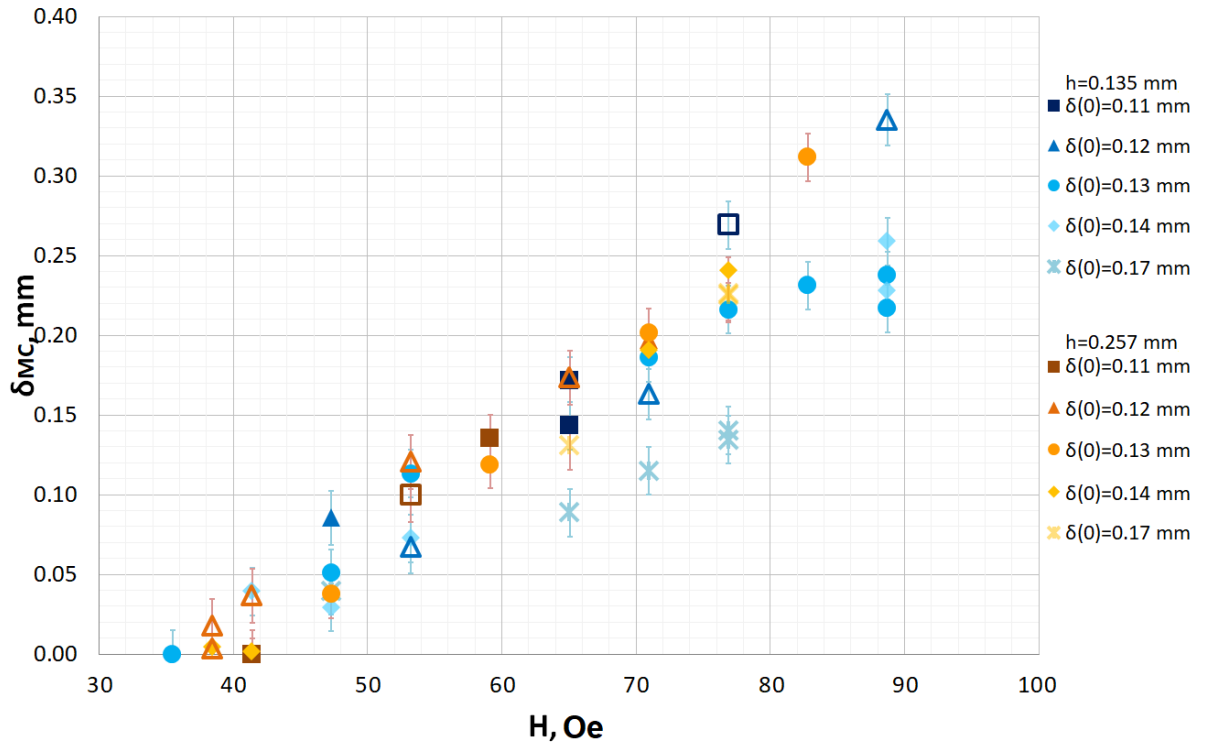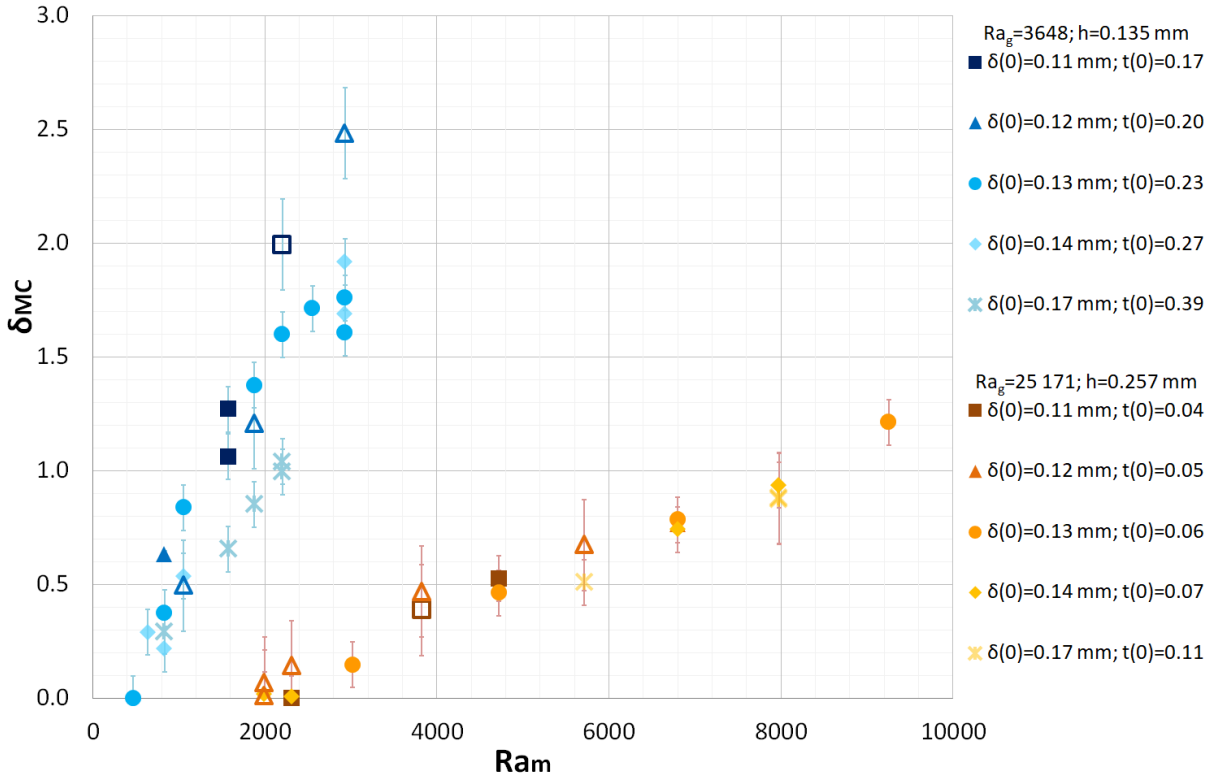
3.25. Figure: The effect of micro-channel thickness on δ_{MC} for various δ_0. Magnetic fluid: FF09-9$_{100\%}$ Empty markers represent δ_{MC} obtained with attachment method.
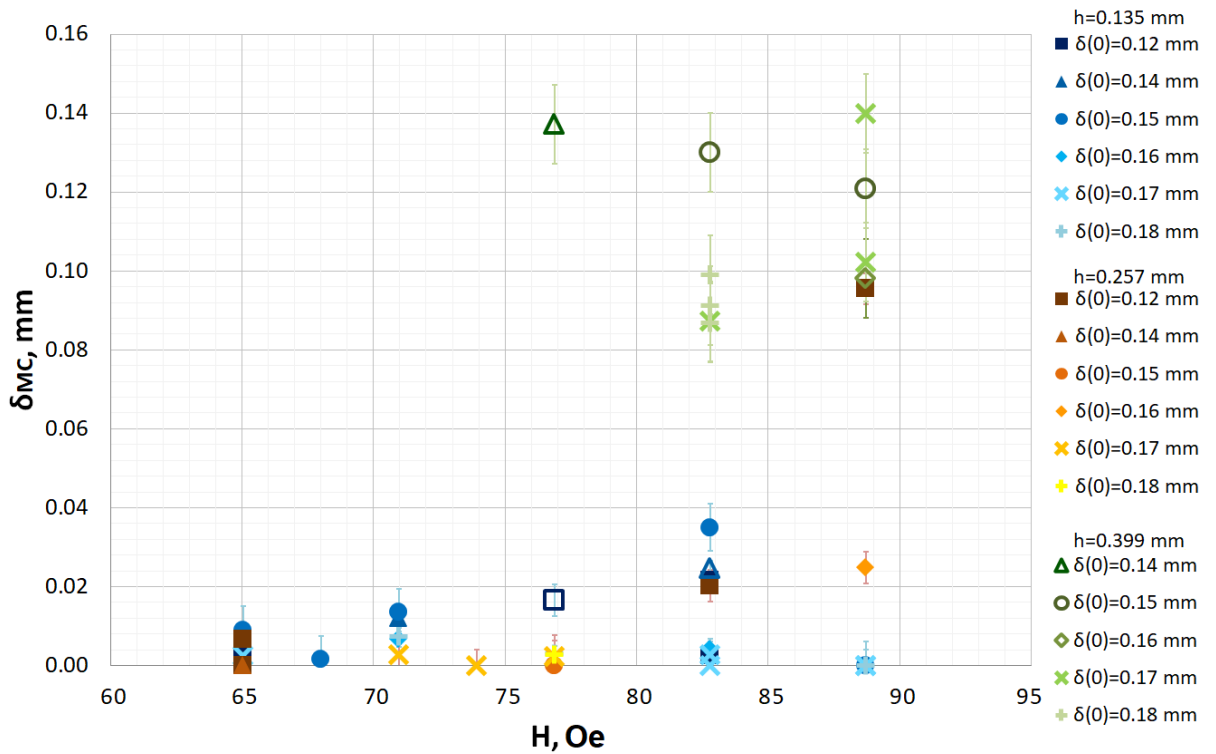
3.26. Figure: The effect of micro-channel thickness on δ_{MC} for various δ_0. Magnetic fluid: FF09-9$_{50\%}$. Empty markers represent δ_{MC} obtained with attachment method.

Also comparing the results with other magnetic fluids (see Appendix §A.1.3) it is inconclusive whether the initial smearing thickness has greater effect on magnetic micro-convection in the thickest micro-channel.

As mentioned earlier the changes of micro-channel thickness change the values of the dimensionless parameters $\mathrm{Ra_g} \sim h^3$ and $\mathrm{Ra_m} \sim h^2$ accordingly. The dimensionless time parameter t_0 for the same δ_0 also varies between different micro-channels, as the thickness value is used to express $t_0 = \frac{\delta_0^2}{4h^2}$. In figure 3.27. the effect of the micro-channel thickness on the dimensionless magnetic micro-convection mixing δ_{MC} is collected with aspect to the same physical $\delta_0(\mathrm{mm})$. The mixing due to magnetic micro-convection is greater for the thinnest micro-channel and therefore the smallest value of $\mathrm{Ra_g}$.

3.27. Figure: The effect of micro-channel thickness on dimensionless δ_{MC} for various δ_0. Magnetic fluid: FF09-9$_{100\%}$. Empty markers represent δ_{MC} obtained with attachment method.

Not only the absolute values of dimensionless δ_{MC} are greater for the same values of $\mathrm{Ra_m}$ for the smallest $\mathrm{Ra_g}= 3648$, but also the gain rate of δ_{MC} by increasing $\mathrm{Ra_m}$ is greater for the smaller $\mathrm{Ra_g}$ than it is for the bigger one $\mathrm{Ra_g} \approx 25200$. The value of δ_{MC} has increased by approximately 1.25 dimensionless units for the experiments with the smallest $\mathrm{Ra_g}= 3648$, while it has increased only by approximately 0.25 dimensionless units for the experiments with the bigger $\mathrm{Ra_g} \approx 25200$ within $\mathrm{Ra_m}$ region from 2000 to 3000 in the fig. 3.27.. As all of the blue marker sets seem parallel to each other just like the orange marker sets seem parallel to each other, the dimensionless t_0 does not affect the

growth rate of δ_{MC} with respect to $\mathrm{Ra_m}$. Therefore the fact that the dimensionless initial smearing parameter t_0 is not the same for the experimental series with both demonstrated $\mathrm{Ra_g}$ values does not affect the observation about different growth rates of δ_{MC} with respect to $\mathrm{Ra_m}$.

Visually the effect of different micro-channel thicknesses on the magnetic micro-convection for the magnetic fluid KTF11-1$_{66\%}$ is demonstrated in fig. 3.28.. One column represents one experiment in time. The columns are grouped in pairs, so that adjacent columns have the same values of the external magnetic field and initial smearing thickness, but different thicknesses of the used micro-channel.
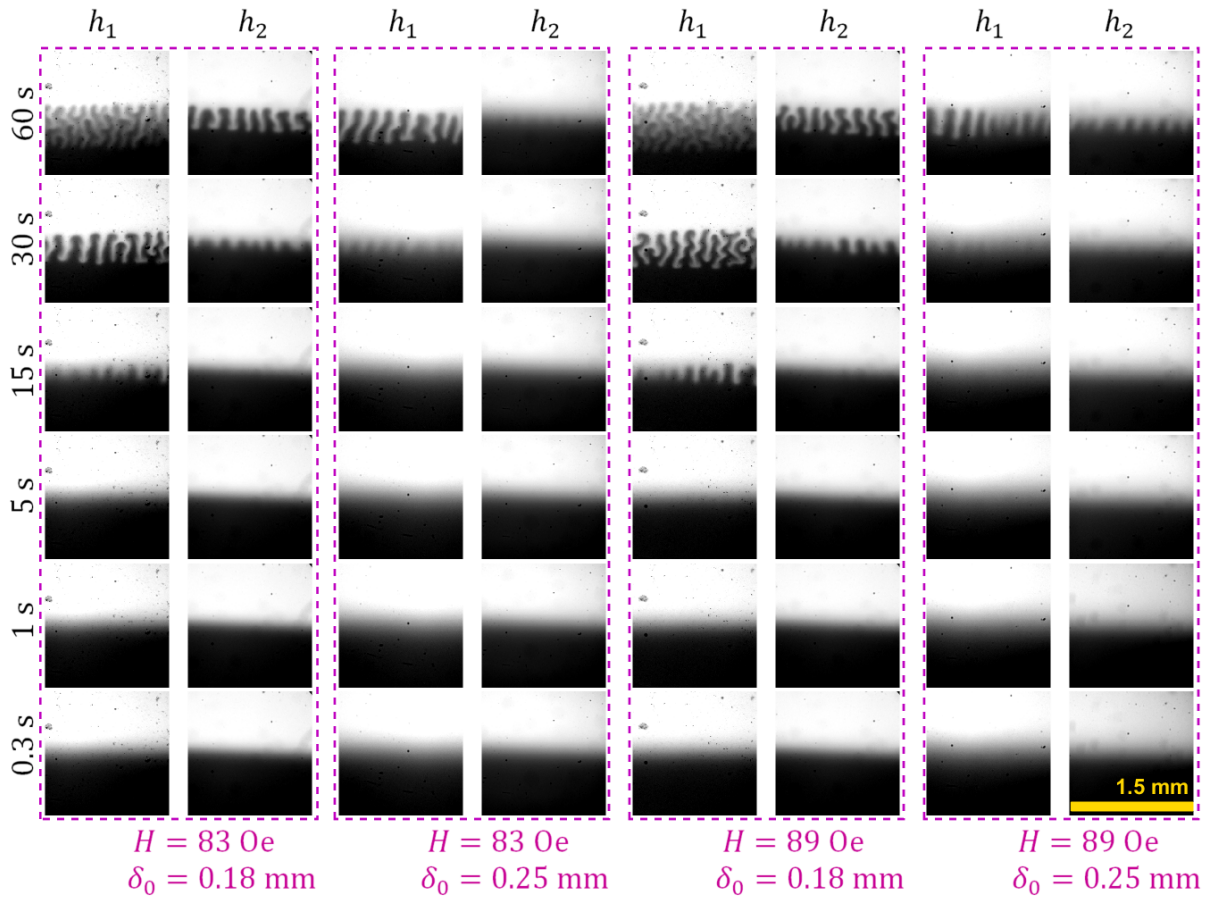
3.28. Figure: Image series of magnetic micro-convection dynamics for two micro-channel thicknesses: $h_1 = 0.135$ mm, $h_2 = 0.257$ mm. Magnetic fluid: KTF11-1$_{66\%}$. A single image represents 1.5 mm×1.5 mm region.

The results differ for different magnetic fluids. For the magnetic fluid KTF11-1$_{66\%}$ in fig. 3.28. it is apparent that the fingers of the instability emerge earlier in time in the thinner micro-channel ($h_1 = 0.135$ mm). This observation agrees with the quantitative results for this magnetic fluid. But for magnetic fluid FF09-9$_{50\%}$ the fingers of the instability appear earlier in the thicker ($h_2 = 0.257$ mm) micro-channel.

As discussed earlier (see tab. 3.2. and A1.) micro-channel thickness also has an effect

on the characteristic size of the instability and the fingers tend to become thicker in thicker micro-channels.

The development of the magnetic micro-convection in the thickest used micro-channel ($h_3 = 0.399$ mm) is visually demonstrated in fig. 3.29. for magnetic fluid FF09-9$_{50\%}$ (the same fluid as in figures 3.26. and A.20). In experiments carried out in the thickest micro-channel the interface between the fluids tended to slide down after switching off the syringe pumps as the denser magnetic fluid flowed underneath the water in the tubing and flowed out of the micro-channel. This is demonstrated in the fig. 3.29. as it is visible that the intercept between the mixing fluids is lower in each of the images next in time. Such experimental artifact was not observed in the thinner micro-channels. Due to this effect an extra periodic mixing layer was observed in addition to the usual fingers of the instability. This extra periodic pattern appeared as the concentration distribution of the magnetic fluid in the premixed layer is not the same as it would have been just due to the diffusion before the experiment, as in the experiments in thinner micro-channels. The premixed layer is more step-like here as the upper border of this extra periodic pattern is where initially the interface between the fluids were before switching of syringe pumps.
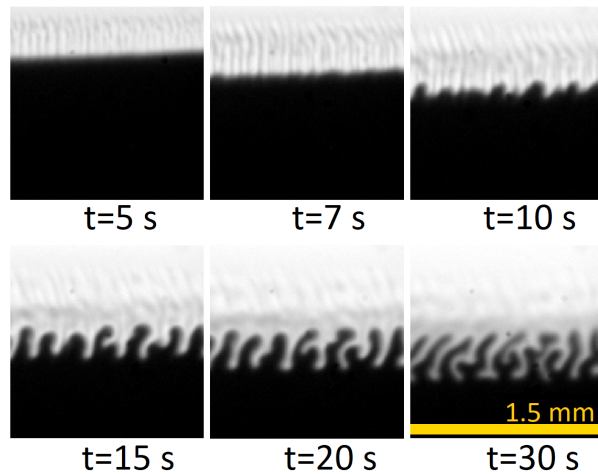
3.29. Figure: Image series of magnetic micro-convection dynamics in time for magnetic fluid FF09-9$_{50\%}$ in micro-channel with thickness $h_3 = 0.399$ mm in magnetic field $H = 88.7$ Oe with $\delta_0 = 0.07$ mm. A single image represents 1.5×1.5 mm region.

3.3.2. Mixing with magnetic micro-convection with respect to the initial smearing thickness

In this section the results of magnetic micro-convection dynamics with respect to the initial smearing thickness grouped by the external magnetic field are collected. Here it is demonstrated how the initial smearing thickness affects the mixing due magnetic micro-convection.

The quantitative influence of the initial smearing thickness δ_0 of the interface between

the magnetic fluid and water on the mixing by magnetic micro-convection δ_{MC} for various magnetic fields was explored. An example for magnetic fluid KTF11-$1_{100\%}$ is presented in figure 3.30.. For other magnetic fluids the results are collected in Appendix §A.1.3.

One data point in the graph represents one experiment with a specific initial smearing thickness δ_0 in a certain external magnetic field as shown in the legend. The results are grouped by magnetic field. The colors of markers become lighter as the value H of external magnetic field increases. The data series of different magnetic field values seem all parallel to each other in all three graphs, so the rate at which δ_{MC} decreases as the δ_0 increases is the same for all magnetic fields for the same magnetic fluid.

As expected δ_{MC} is higher for experiments in stronger magnetic fields at the same δ_0 as the lighter markers are above the darker ones.

By extrapolating all the data points of the same magnetic field H until they reach the vertical axis at $\delta_0 = 0$ the maximum value of δ_{MC} for this particular magnetic field can be expressed. For example, the mixing of water and magnetic fluid KTF11-$1_{100\%}$ in magnetic field $H = 82.8$ Oe is approximated by a straight, blue, dashed line in fig. 3.30.. This line meets the vertical axis at $\delta_{MC} \approx 0.21$ mm. So if the interface between the mixing fluids would be perfectly sharp it is expected that in the magnetic field $H = 82.8$ Oe the mixing due to magnetic micro-convection between these fluids could reach approximately $\delta_{MC:max} \approx 0.21$ mm. Coherently this estimated maximal value $\delta_{MC:max}$ of magnetic micro-convective mixing is expected to be higher for experiments in stronger magnetic fields.
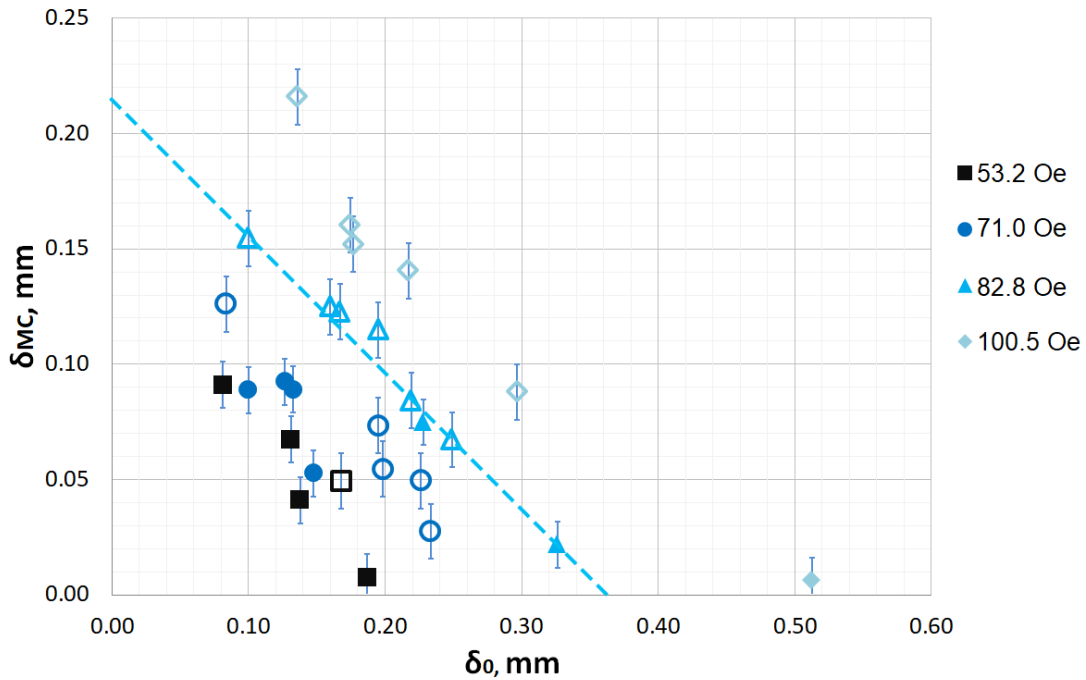
3.30. Figure: Mixing by magnetic micro-convection δ_{MC} with respect to δ_0 in various magnetic fields in micro-channel with thickness $h_1 = 0.135$ mm. Magnetic fluid: KTF11-$1_{100\%}$

The estimated maximal values of δ_{MC} are collected for all experiments. An example of the results for magnetic fluid D107$_{50\%}$ are visible in table 3.5.. Estimated $\delta_{\mathrm{MC:max}}$ values here agree with the ones represented in figure 3.16. obtained in experiments with initially stagnant fluids (§3.2.). Results for other magnetic fluids are collected in the Appendix §A.1.3. The results whether greater $\delta_{\mathrm{MC:max}}$ can be achieved in thinner microchip are contrasting for different magnetic fluids. More effective mixing due to magnetic micro-convection (higher values of δ_{MC}) was achieved in experiments with more concentrated magnetic fluids.

The thickness of the micro-channel as well as the dilution ratio of the magnetic fluid does not affect the rate at which $\delta_{\mathrm{MC:max}}$ increases with respect to the external magnetic field.

H, Oe	$\delta_{MC:max}$, mm
68.0	0.14
76.9	0.21
82.8	0.23
88.7	0.23

3.5. Table: Maximal value of δ_{MC} with respect to external magnetic field for sharp initial interface $\delta_0 = 0$ mm for magnetic fluid D107$_{50\%}$.

The effect of dilution ratio and thickness of the micro-channel on the mixing by magnetic micro-convection also was explored for all magnetic fluids. Here the examples of these experiments are reviewd in figures 3.31. and 3.32. accordingly. The results are grouped by the value of the external magnetic field. There is no dimensionless representation of these exact graphs as the value of $\mathrm{Ra_m}$ changes if dilution ratio or the thickness of the micro-channel is altered. Whereas dimensionless initial smearing parameter t_0 is affected by the micro-channel thickness as well, so the same δ_0 does not translate to the same t_0 if the experiments are carried out in micro-channels with different thicknesses. The dimensionless mixing due to magnetic micro-convection with respect to the initial smearing t_0 is reviewed in the next paragraph §3.3.3..

Markers describing experiments with the same dilution ratio of the magnetic fluid have the same color tonality in fig. 3.31.: violet markers represent the experiments with concentrated magnetic fluid FF09-9$_{100\%}$, whereas the green ones represent the experiments with diluted magnetic fluid FF09-9$_{50\%}$. Experiments carried out in the same external magnetic field have the same marker shape. The color of the markers becomes lighter as the value of the external magnetic field increases.

Mixing is more effective with more concentrated magnetic fluid. For example, micro-convective mixing for experiments in magnetic field $H = 76.7$ Oe and with initial smearing

thickness $\delta_0 = 0.11$ mm is $\delta_{\mathrm{MC}} = 0.05$ mm for magnetic fluid FF09-9$_{50\%}$, while for FF09-9$_{100\%}$ the mixing is more than five times greater as $\delta_{\mathrm{MC}} = 0.26$ mm.
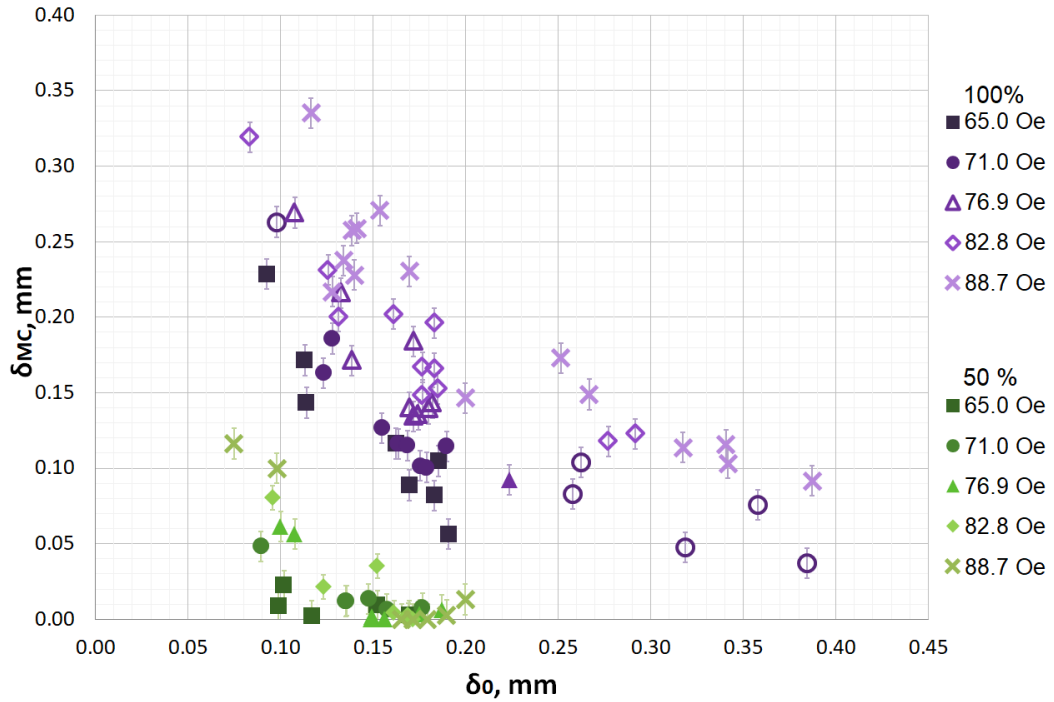
3.31. Figure: Dilution ratio effect on δ_{MC} in various magnetic fields in micro-channel with thickness $h_1 = 0.135$ mm. Magnetic fluid: FF09-9. Empty markers represent δ_{MC} obtained with attachment method.
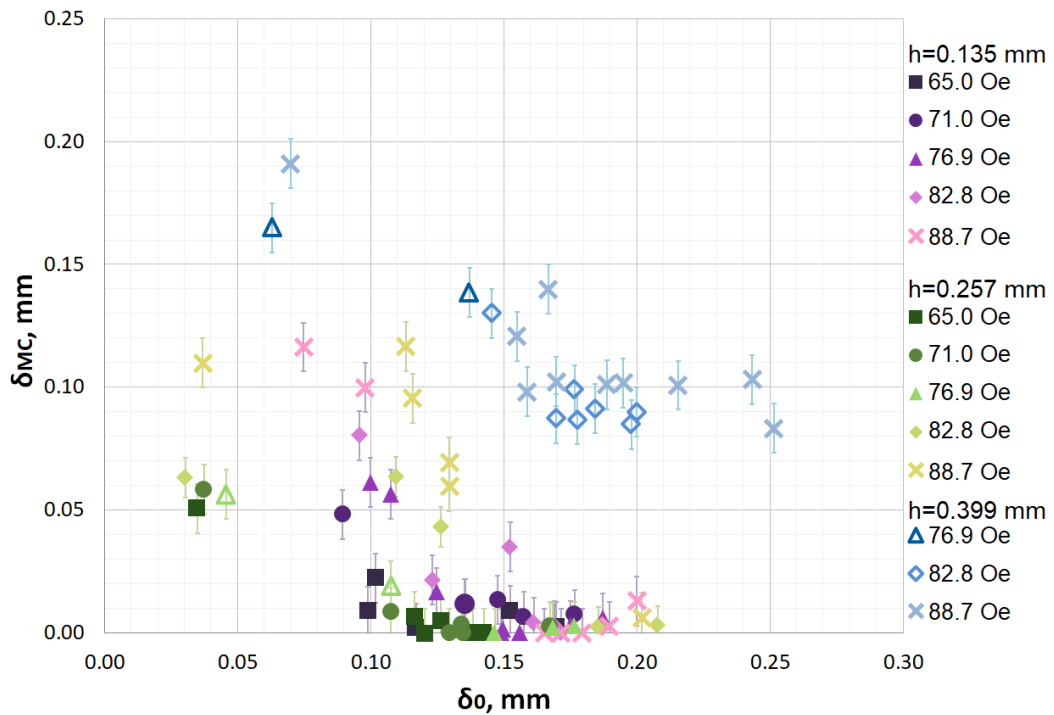
3.32. Figure: The effect of micro-channel thickness on δ_{MC}. Magnetic fluid: FF09-9$_{50\%}$. Empty markers represent δ_{MC} obtained with attachment method.

Comparing the experimental data series of different dilution ratios it appears that for the same values of δ_0 in the absolute units the violet markers are more dispersed than the green ones. Thus it is possible that the changes in magnetic field affect the change in δ_{MC} more if the magnetic fluid is more concentrated. To illustrate this, the difference in micro-convective mixing between experiments carried out in magnetic fields $H = 65$ Oe and $H = 76.9$ Oe if the initial smearing thickness is $\delta_0 = 0.11$ mm for more concentrated magnetic fluid (FF09-9$_{100\%}$) is $\Delta\delta_{MC} = \delta_{MC(H=76.9Oe)} - \delta_{MC(H=65Oe)} \approx 0.27 - 0.15 = 0.12$ mm, while for more diluted magnetic fluid it is three times smaller $\Delta\delta_{MC} \approx 0.05 - 0.01 = 0.04$ mm.

Also, the difference in mixing between experiments with magnetic fluids with different ratios increases if the external magnetic field is stronger. Meaning, in fig. 3.31. the difference of δ_{MC} in absolute values between "x" markers is bigger than between the square shaped markers for the same values of δ_0. For example, for experiments carried out in the magnetic field $H = 88.7$ Oe mixing difference between different dilution ratios is $\Delta\delta_{MC} = \delta_{MC(100\%)} - \delta_{MC(50\%)} \approx 0.37 - 0.07 = 0.27$ mm, while in magnetic field $H = 65.0$ Oe it is almost two times smaller $\Delta\delta_{MC} = \approx 0.15$ mm. So, the differences of micro-convective mixing for magnetic fluids with different dilution ratios are more pronounced in stronger magnetic fields.

As demonstrated previously in this chapter in figures 3.25., 3.26. and A.12 the thickness of the micro-channel differently affects the results of experiments with different magnetic fluids. Here as demonstrated in fig. 3.32., greater values of δ_{MC} when mixing water and magnetic fluid FF09-9$_{66\%}$ were achieved in the thickest micro-channel ($h_3 = 0.399$ mm). For example, micro-convective mixing parameter for experiments in the magnetic field $H = 88.7$ Oe and with initial smearing thickness $\delta_0 = 0.11$ mm is $\delta_{MC} \approx 0.16$ mm for experiments in the thickest micro-channel ($h_3 = 0.399$ mm), $\delta_{MC} \approx 0.11$ mm for experiments in medium micro-channel ($h_2 = 0.257$ mm) and $\delta_{MC} \approx 0.09$ mm for experiments in the thinnest micro-channel ($h_1 = 0.135$ mm).

The difference in magnetic micro-convective mixing due to micro-channel thickness is not linear. The medium micro-channel with $h_2 = 0.257$ mm is approximately 2 times thicker than the thinnest micro-channel with $h_1 = 0.135$ mm; and the thickest micro-channel with $h_3 = 0.399$ mm is approximately 3 times thicker than the thinnest micro-channel. But the difference of δ_{MC} visually is much greater between the two larger chips than it is between the two thinner ones where the difference due to experimental errors is statistically insignificant.

3.3.3. Mixing with magnetic micro-convection with constant $\mathbf{Ra_m}$ with respect to the initial smearing thickness

In order to quantify the gravitational and magnetic effects of various experiments collected in this chapter, the dimensionless results of magnetic micro-convection dynamics with

respect to the initial smearing thickness and grouped by $\mathrm{Ra_m}$ are reviewed in this section.

The initial smearing thickness δ_0 is expressed using a dimensionless time parameter $t_0 = \frac{\delta_0^2}{4h^2}$. t_0 represents dimensionless time for which the diffusion between the mixing fluids has been happening before the application of the external magnetic field (i.e. the beginning of the experiment). t_0 changes with respect to initial smearing thickness and thickness of the micro-channel. Therefore experiments with the same physical δ_0 that are carried out in different micro-channels do not have the same value of initial smearing parameter t_0. t_0 is smaller in thicker micrfluidics chips than in thinner ones for experiments that have the same physical δ_0. In this chapter the experiments are compared with respect to the dimensionless t_0 regardless of the micro-channel thickness.

The thickness of the micro-channel as well as the dilution ratio of the used magnetic fluid is expressed using gravitational Rayleigh number $\mathrm{Ra_g}$. As mentioned previously $\mathrm{Ra_g}$ is affected by micro-channel thickness and dilution ratio accordingly: $\mathrm{Ra_g} \sim h^3$ and $\mathrm{Ra_g} \sim \Delta\rho$ where $\Delta\rho$ is the density difference between the mixing fluids and of course is affected by the dilution ratio of the magnetic fluid. $\Delta\rho$ is higher in experiments with more concentrated magnetic fluids.

As mentioned the results in this chapter are grouped by the values of $\mathrm{Ra_m}$. $\mathrm{Ra_m}$ changes with respect to the thickness of the micro-channel less rapidly than $\mathrm{Ra_g}$ as $\mathrm{Ra_m} \sim h^2$. Also the fact that the dilution ratio affects the value of the $\mathrm{Ra_m}$ must be taken into account: $\mathrm{Ra_m} \sim M^2$, here magnetization M of the magnetic fluid is directly proportional to the concentration of the magnetic fluid. As it can be seen in fig. 3.33. the same $\mathrm{Ra_m}$ value for different dilution ratios means different value of the external magnetic field. For example $\mathrm{Ra_m} \approx 1940$ corresponds to the experiments with magnetic fluid KTF11-1$_{100\%}$ carried out in $H = 50$ Oe strong magnetic field, while for more diluted magnetic fluid KTF11-1$_{66\%}$ this same $\mathrm{Ra_m}$ describes experiments carried out in stronger $H = 77$ Oe magnetic field. So, in order to get approximately the same values of $\mathrm{Ra_m}$, stronger magnetic field must be applied to more diluted magnetic fluids. Also, due this fact, the values of $\mathrm{Ra_m}$ for different dilutions are not identical, but rounded within 5% of the exact value.

Finally, the mixing parameter due to magnetic micro-convection δ_{MC} is made dimensionless as well by dividing it with the thickness of a particular micro-channel the experiment was carried out in. Therefore again experiments carried out in different micro-channels, but with the same value of physical δ_{MC} do not have the same value of dimensionless δ_{MC}. Value of the dimensionless δ_{MC} for experiments with the same physical δ_{MC} is higher for experiments that are carried out in thinner micro-channels, for all other parameters unchanged.

In fig. 3.33. the effect of the dilution ratio of the magnetic fluid on the dynamics of the magnetic micro-convection for magnetic fluid KTF11-1 is demonstrated. One marker represents one experiment. Experiments with the same dilution ratio of the magnetic

fluid and the same value of Ra_g are colored in the same tonality: blue markers for more concentrated magnetic fluid KTF11-1$_{100\%}$ with higher Ra_g= 10744 and the brown markers for more diluted magnetic fluid KTF11-1$_{66\%}$ with smaller Ra_g= 4003. Results with the same value of Ra_m are represented by the same marker shape: squares for smaller Ra_m= 1940 and circles for larger Ra_m= 2640.

Consistent with the previous results gravity constricts the mixing of magnetic micro-convection as the values of δ_{MC} are smaller for the bigger Ra_g= 10744 than the smaller one Ra_g= 4003. To illustrate this, micro-convective mixing $\delta_{MC,Ra_g=4003} = 0.9$ and $\delta_{MC,Ra_g=10744} = 0.4$ for experiments with the same values of $t_0 = 0.2$ and Ra_m= 1940.
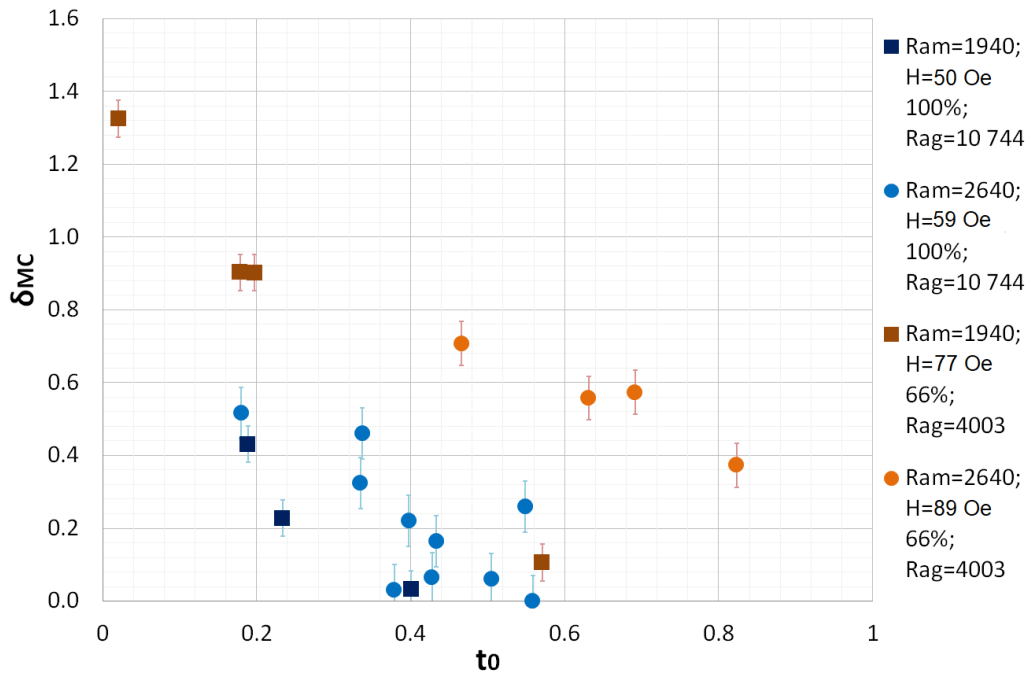
3.33. Figure: Dilution ratio effect on dimensionless δ_{MC} for various Ra_m in micro-channel with thickness $h_1 = 0.135$ mm. Magnetic fluid: KTF11-1.

The effect of the thickness of the micro-channel as well as the gravity is demonstrated in fig. 3.34. for magnetic fluid FF09-9$_{100\%}$. In this graph visually the effect of the Ra_g difference on the micro-convective mixing δ_{MC} is even more drastic than in a previous fig. 3.33.. Also the Ra_g difference between the experiments is greater here in fig. 3.34.. Experimental series with smaller Ra_g= 3648 are represented by purple markers and the green markers represent the experimental series with almost seven times larger gravitational Rayleigh number Ra_g= 25171. Experiments with approximately the same value of Ra_m are represented by the same shape of markers: squares for smaller $Ra_m \approx 2400$ and circles for larger $Ra_m \approx 3000$.

Although the measured t_0 value ranges do not overlap much, the effect of the gravity is undeniable here. The highest reached value of micro-convective mixing parameter for experiments with the largest gravitational Rayleigh number here is $\delta_{MC,Ra_g=25171} = 0.25$,

while for experiments with the smallest Ra_g this mixing parameter for the same initial smearing $t_0 = 0.1$ and $Ra_m \approx 3000$ is ten times greater $\delta_{MC,Ra_g=3648} = 2.5$.

So concluding from figures 3.33. and 3.34.: gravity restricts mixing due to the magnetic micro-convection between two fluids in a vertical micro-channel for various thicknesses of initially smeared initial interface.
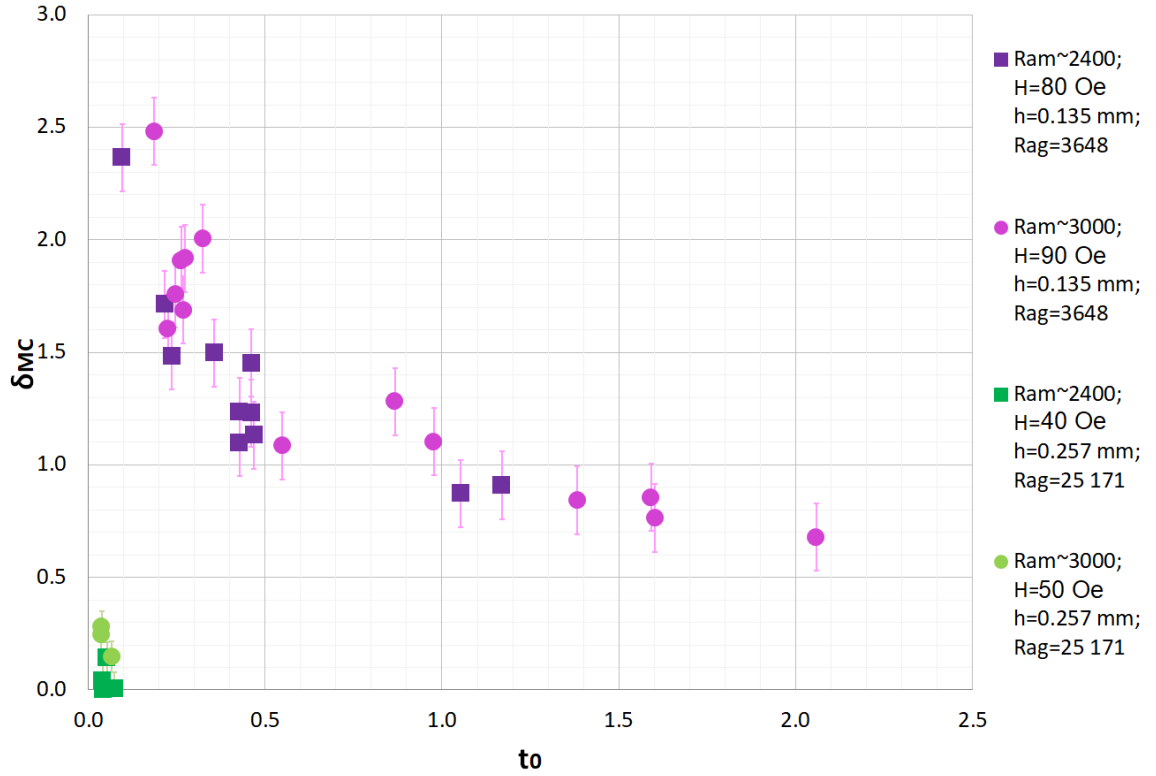
3.34. Figure: Dilution ratio effect on dimensionless δ_{MC} for various Ra_m in experiments with magnetic fluid FF09-9$_{100\%}$.

3.3.4. A specific amount of magnetic micro-convective mixing

In this section requirements to get a specific thickness of the mixed layer between two fluids due to magnetic micro-convection are explored.

An example of magnetic field that should be applied to get a specific δ_{MC} with respect to δ_0 is visible in figure 3.35. for experiments with magnetic fluid FF09-9$_{100\%}$. Additional experimental results are collected in Appendix §A.1.3. The results are grouped with the same marker color by the expected values of δ_{MC} as listed in the legend of the graph in mm. Markers become lighter in color as the value of desired δ_{MC} increases.

As expected, in order to achieve greater mixing due to magnetic micro-convection δ_{MC} experiments must be carried out in stronger external magnetic field. The black markers of $\delta_{MC} = 0$ mm represent the critical values of the external magnetic field H_c to create the instability in experiments with a set δ_0. The black markers are approximated with a straight, black, dashed line in fig. 3.35..
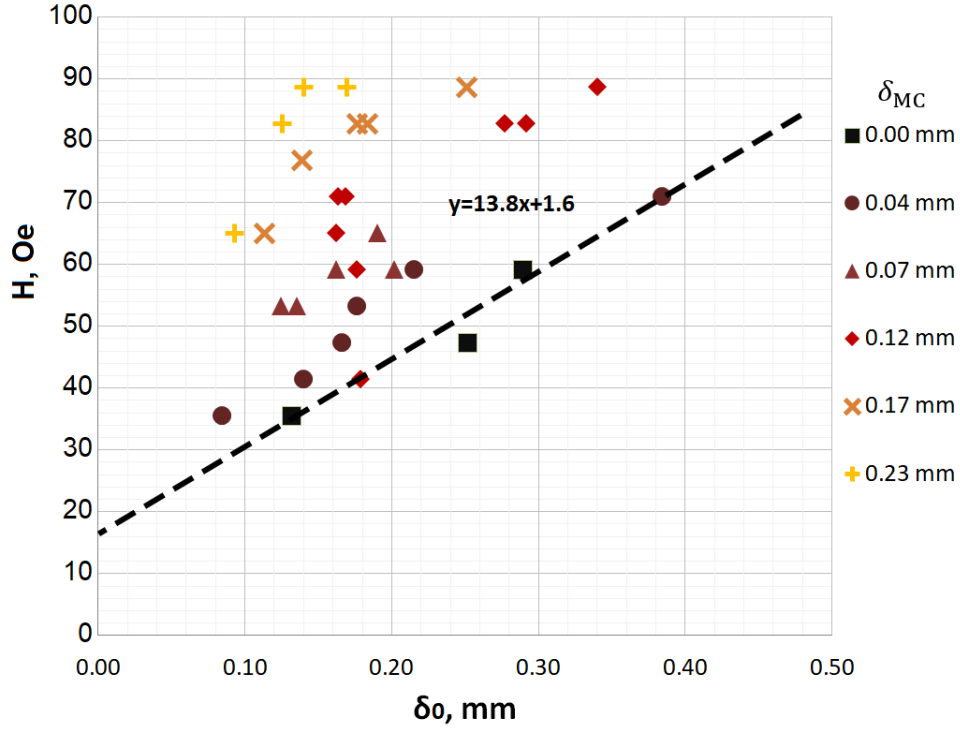
3.35. Figure: What magnetic field should be applied to get a specific δ_{MC} in micro-channel with thickness $h_1 = 0.135$ mm. Magnetic fluid: FF09-9$_{100\%}$.

For experiments with any value combination of initial smearing thickness δ_0 and magnetic field H with coordinates below this black line in the graph the magnetic micro-convection would not emerge. The intercept of the black line with the vertical axis at $\delta_0 = 0$ mm represents the critical value of magnetic field H_c for instability to emerge if the mixing fluids have sharp initial interface between them. The obtained value $H_c = 16$ Oe here is similar to the previously found $H_c = 13$ Oe for magnetic fluid FF09-9$_{100\%}$ in micro-channel with thickness $h_1 = 0.135$ mm. The data series in fig. 3.35. of a specific δ_{MC} appear parallel to each other, meaning that the rate at which the magnetic field should be increased as the δ_0 increases is the same for all desired values of δ_{MC}. However this rate (the slope of the approximated line) changes seem to be affected by the dilution ratio of the magnetic fluid. This slope is larger for experiments with more diluted magnetic fluids.

The values of the magnetic field H to be applied to obtain a particular δ_{MC} for initially sharp interface can be obtained by this linear approximation. If this value of the magnetic field is the same as H_c in experiment where δ_0 is the same as this desired particular δ_{MC}, then this would confirm the third hypothesis proposed for this work in Introduction. For results with magnetic fluid FF09-9$_{100\%}$ within error this hypothesis holds true. For example $H \approx 40$ Oe must be applied to obtain $\delta_{MC} \approx 0.10$ mm. And the $H_c \approx 40$ Oe if $\delta_0 \approx 0.10$ mm in micro-channel with thickness $h_1 = 0.135$ mm. For magnetic fluid KTF11-1 the critical magnetic field for particular δ_0 are bit smaller than the magnetic field that must be applied to obtain δ_{MC} with the same magnitude. For example, $H_c \approx 45$ Oe if

$\delta_0 \approx 0.10$ mm in micro-channel with thickness $h_1 = 0.135$ mm, while $H = 50$ Oe must be applied to obtain $\delta_{MC} = 0.10$ mm. So the hypothesis is confirmed qualitatively for experiments in horizontal magnetic field.

A slightly stronger magnetic field is necessary to induce the same amount of magnetic micro-convection in experiments with more diluted magnetic fluid. Also, results show that stronger magnetic fields are necessary to induce the same amount of magnetic micro-convection in experiments with thinner micro-channel for this magnetic fluid FF09-9.
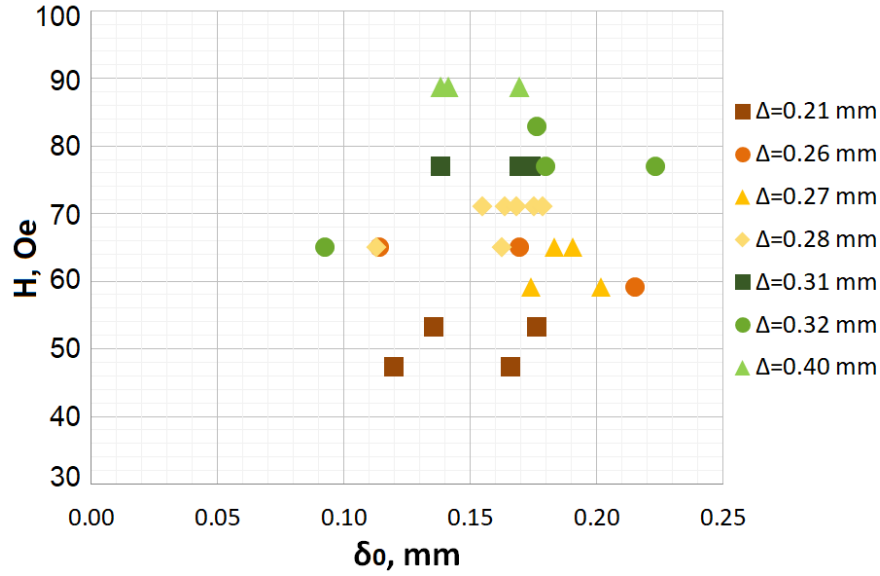
3.36. Figure: Magnetic field with respect to δ_0 for various values of total mixing length Δ in micro-channel with thickness $h_1 = 0.135$ mm. Magnetic fluid: FF09-$9_{100\%}$.

The total mixing length Δ consists of micro-convective mixing during the experiment and diffusive mixing before the experiment. In fig. 3.36. the necessary values of external magnetic field H with respect to initial smearing thickness δ_0 in order to obtain a specific total mixing length Δ when the motion due to magnetic micro-convection exhausts for experiments with magnetic fluid FF09-$9_{100\%}$ in micro-channel with thickness $h_1 = 0.135$ mm are collected. The data series for a specific total mixing length Δ appear all parallel to each other and horizontal within error. So it seems that the value of external magnetic field H in order to get a specific total mixing length does not depend on the initial smearing thickness, thus confirming the second hypothesis that was proposed at the beginning of this work.

3.3.5. Summary

Within this section it was demonstrated how the instability is affected by initial smearing between the fluids. The instability emerged later in time for experiments with larger δ_0. Only results with magnetic fluid KTF11-1 confirmed that δ_0 affects the characteristic size of the instability as proposed in [62]. Initial smearing affects the form of the fingers. Agreeing

with literature [17] it was showed that by increasing the thickness of the micro-channel, the characteristic λ of the instability increases as well.

The values of magnetic field that should be applied to get a specific δ_{MC} with respect to δ_0 are collected. Results showed that in the same magnetic field larger δ_{MC} can be achieved for smaller δ_0. Also it was found out that stronger magnetic field is necessary to induce the same amount of magnetic micro-convection in experiments with thinner micro-channel (for magnetic fluid FF09-9$_{50\%}$). Critical magnetic fields for various initial smearing thicknesses were found as well. And magnetic fluid dilution ratio did not affect the rate at which δ_{MC} decreases as δ_0 is increased.

Consistent with the previous results gravity constricts the mixing of magnetic micro-convection as the values of δ_{MC} are smaller for the bigger Ra_g.

The results showed that value of H in order to get a specific total mixing length Δ does not depend on δ_0, thus confirming the second hypothesis that was proposed at the beginning of this work. Also the third hypothesis was confirmed within error: H_c for a certain δ_0 is the same as the magnetic field H to induce δ_{MC} of the same magnitude if $\delta_0 = 0$.

3.4. Magnetic micro-convection in a vertical external magnetic field parallel to the microfluidics chip

In this section of the work the results of the dynamics of the magnetic micro-convection in experiments with the external magnetic field vertical and parallel to the chip as described in §2.4.3. are collected. In these experiments four different magnetic fluids were used: D107, KTF11-1, FF09-9 and FF21-5. Fluid FF09-9 was diluted by water to vary the experimental parameters similar as in previous sections. The experiments were carried out in micro-channels with two different thicknesses ($h_1 = 0.135$ mm and $h_2 = 0.257$ mm). In this section also, the experiments were carried out for several different initial smearing thicknesses.

Initial smearing effect on the magnetic micro-convection in a constant vertical external magnetic field in the thinnest micro-channel ($h_1 = 0.135$ mm) visually is demonstrated in figure 3.37. in $H = 41.4$ Oe with magnetic fluid FF21-5$_{100\%}$. Additional experimental examples are collected in Appendix §A.1.4. The vertical axis presents the time since the beginning of the experiment, while the horizontal axis contains information about the initial smearing thickness. One column of images represents a single experiment in time. The periodic pattern of this instability visually differs from the one in a horizontal magnetic field. The fingers are straight and pointy and there is no change in form to wavy and branched fingers unlike in the horizontal magnetic field. Just the same as in the horizontal magnetic field the fingers start to form only if a certain critical value H_c of magnetic field is applied. The fingers form relatively fast and after reaching their maximum height they stop growing. Then over the time the fingers fuse together due to diffusion. The instability appears earlier in experiments with smaller values of δ_0. For example, in the fig. 3.37. the instability is visible already at $t = 0.5$ s for the experiment with $\delta_0 = 0.13$ mm (first column), but in the experiment with just a bit larger initial smearing thickness $\delta_0 = 0.19$ mm (second column) the instability appears only around $t = 5$ s. The maximal height of the fingers is reached earlier in experiments with smaller values of δ_0. In fig. 3.37. in the experiment with $\delta_0 = 0.13$ mm the fingers already have started to diffuse after $t = 30$ s, but in the experiment with larger initial smearing thickness $\delta_0 = 0.35$ mm at this same time point, the fingers have just recently formed and they are still visible at $t = 60$ s unlike in the experiment with smaller $\delta_0 = 0.13$ mm.

Characterization of the wavelength of the instability in a vertical magnetic field is not as simple as in the horizontal magnetic field. To visualize this, figure 3.38. is used. The instability starts to form around $t = 3$ s. At $t = 5$ s and $t = 7$ s the fingers are normally visible and they appear thicker than in the later time points of this experiment. When watching the experiment in the video mode it is easier to perceive than from the image series. Nevertheless the fingers appear to form in more than one row along the thickness of the micro-channel. And as the needle-like fingers are searching a stable position the

rows of the fingers are sliding pass each other a bit and visually in the pictures it looks like the fingers are becoming thicker and then splitting up. At $t = 9$ s in the fig. 3.38. it is visible that the structures that looked like thicker fingers at $t = 7$ s are now split in two closely grouped fingers. As the time passes the distance between the "newly split" fingers increases.
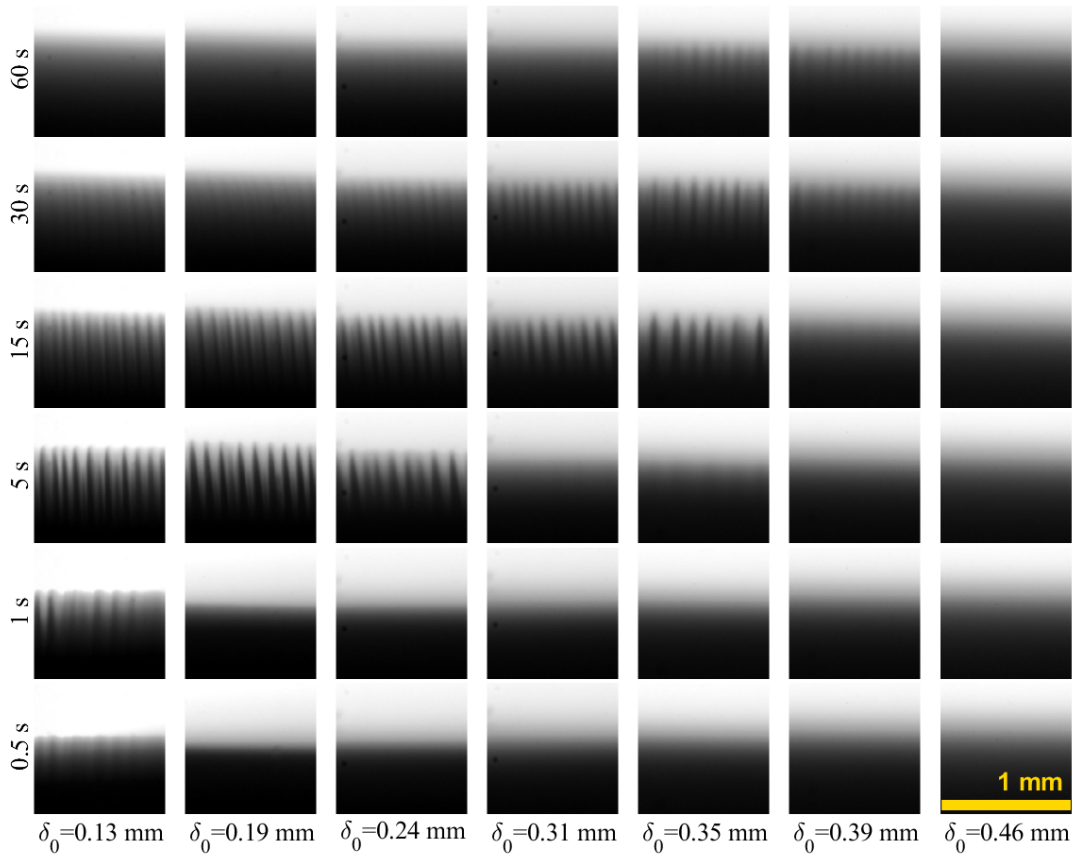
3.37. Figure: Image series of magnetic micro-convection dynamics with different δ_0 in a constant vertical magnetic field $H = 41.4$ Oe in micro-channel with thickness $h_1 = 0.135$ mm. Magnetic fluid: FF21-5$_{100\%}$. A single image represents 1.0×1.0 mm region.

Another effect that leads to assumption about fingers formed in several rows is the intensity of the pattern. The "thick fingers" are in darker color of black meaning, this formation is less transparent that makes one think, that it might be more than one finger right behind each other. Also at $t = 11$ s and $t = 13$ s very thin fingers become visible between the previously discussed finger pairs. These thinner fingers are also less vivid making one think, that they might be further away from camera. It seems that after some time the fingers have found their stable positions and the character of the picture does not change anymore (see fig. 3.38. at $t = 15$ s and $t = 17$ s) besides the diffusion due to which the fingers diffuse together after a longer period of time (see fig. A.23 column of $\delta_0 = 0.41$ mm at $t = 30$ s and $t = 60$ s). This probable finger forming in several rows makes it difficult to measure wavelength of the instability as it is not clear to which fingers

and at what time to count in. In [6] "finger splitting" was also observed in similar setup, but the probability of fingers forming in several rows was not assumed.
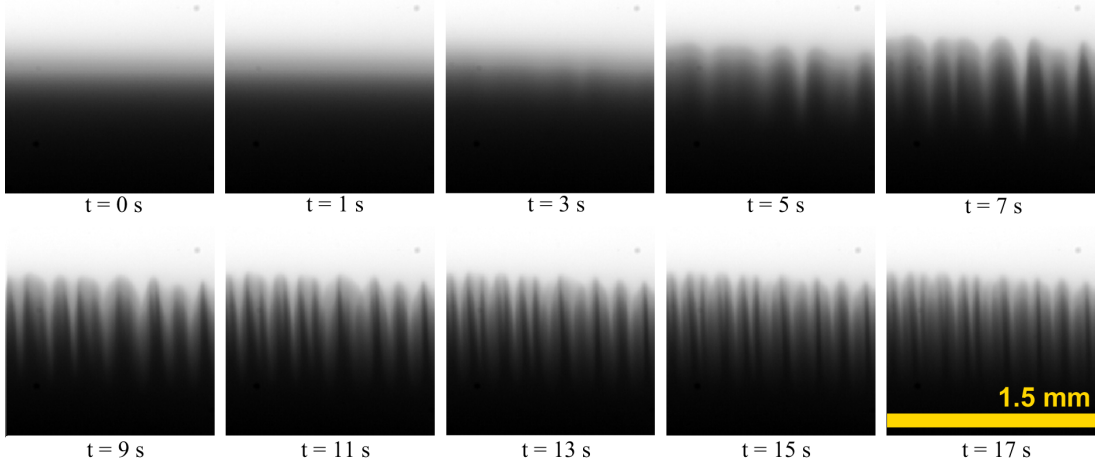
3.38. Figure: Image series of magnetic micro-convection dynamics in time for magnetic fluid FF21-5$_{100\%}$ in micro-channel with thickness $h_1 = 0.135$ mm in $H = 65.3$ Oe and with $\delta_0 = 0.41$ mm. A single image represents 1.5×1.5 mm region.

The information about the possible wavelength of the fingers for this type of instability is collected in the table 3.6.. The information was collected around 10 s after the beginning of the appearance of the instability, meaning "after the split (i.e. finger shifting) of the thicker fingers". The vivid, seemingly "front row" fingers were counted in, meaning in the fig. 3.38. at $t = 9$ s there are 14 fingers visible in the picture, making the estimated wavelength of the instability $\lambda \approx 0.11$ mm for this experiment. Unlike in the experiments with horizontal external magnetic field, here the initial smearing thickness did not seem to have any effect on the finger size.

h, mm	MF	λ, mm
0.135	FF09$_{100\%}$	0.10 ± 0.01
	D107$_{100\%}$	0.09 ± 0.01
	FF21-1$_{100\%}$	0.10 ± 0.03
0.257	FF09$_{100\%}$	0.10 ± 0.03
	FF09$_{66\%}$	0.14 ± 0.02
	FF09$_{50\%}$	0.12 ± 0.02
	D107$_{100\%}$	0.08 ± 0.01
	FF21-1$_{100\%}$	0.13 ± 0.04
	KTF11-1$_{100\%}$	0.11 ± 0.02

3.6. Table: Characteristic wavelength of the magnetic micro-convection in a vertical magnetic field. The error is one standart deviation.
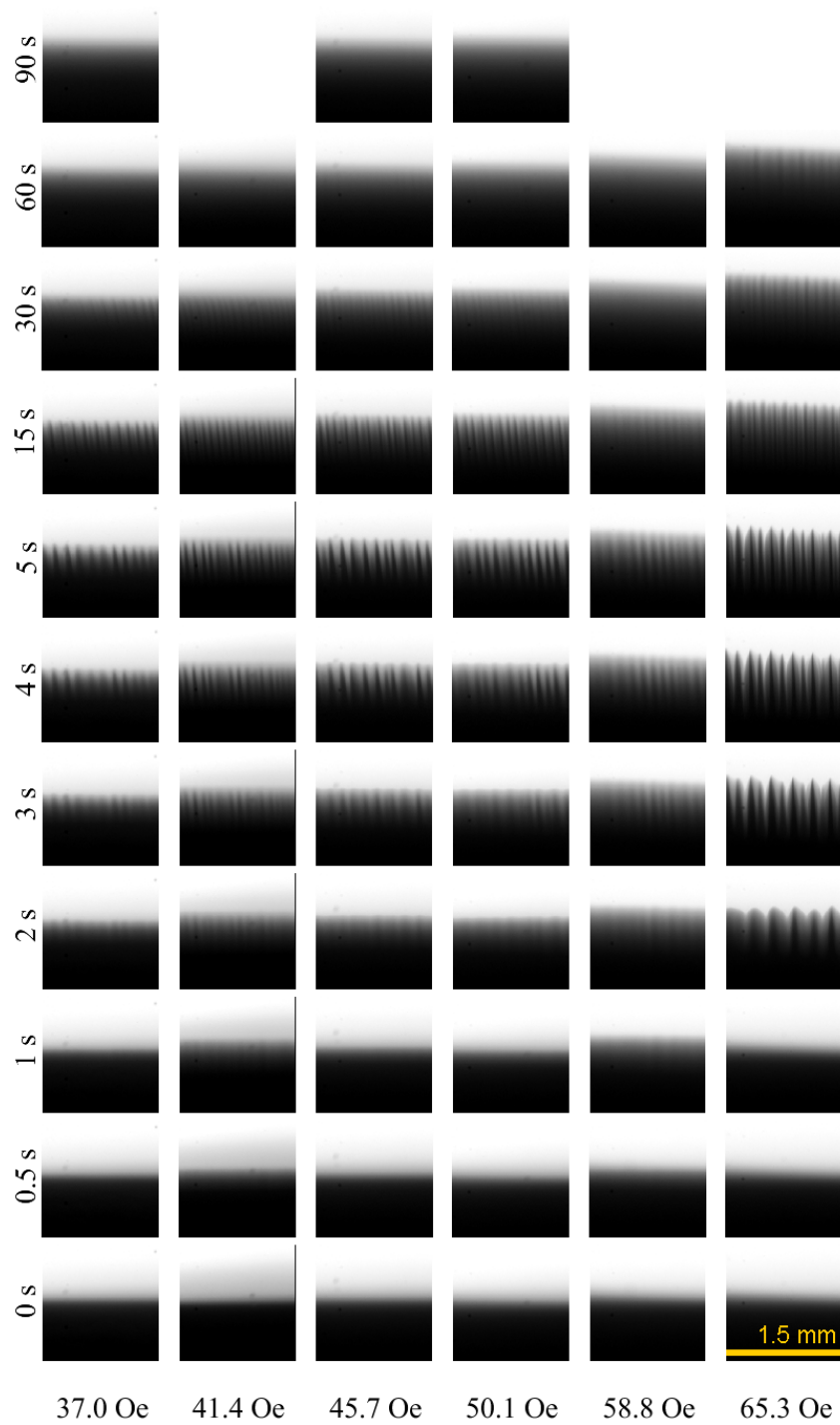
3.39. Figure: Image series of magnetic micro-convection dynamics in various vertical magnetic fields with $\delta_0 = 0.26$ mm in micro-channel with thickness $h_1 = 0.135$ mm for magnetic fluid FF21-5$_{100\%}$. A single image represents 1.5×1.5 mm region.

The effect of the strength of the vertical magnetic field on the magnetic micro-convection again for the experiments with magnetic fluid FF21-5$_{100\%}$ is demonstrated in fig. 3.39. for experiments with the same initial smearing thickness $\delta_0 = 0.26$ mm. It seems that the instability appears at the same time (somewhere between $t = 1$ s and $t = 2$ s), regardless

of the strength of the external magnetic field. But the fingers grow out taller in the experiments with stronger magnetic field. For example, at $t = 4$ s the fingers of the instability have grown 0.45 mm tall in magnetic field $H = 37$ Oe, while at the same time in stronger magnetic field $H = 63.5$ Oe the fingers have grown twice as tall and are 0.9 mm long at $t = 4$ s. Also it seems that as the fingers have reached their maximal height they have started to diffuse earlier in experiments with lower values of H, as it can be seen in the last column with $H = 65.3$ Oe in the fig.3.39. that there are still visible fingers at $t = 60$ s, but for all the other experiments demonstrated in this figure the fingers have already been diffused at this time point. In the last column of fig. 3.39. also the mentioned "finger shifting" is visible very good.

3.4.1. Magnetic micro-convective mixing with respect to the vertical external magnetic field

In this section the results of magnetic micro-convection dynamics with respect to vertical external magnetic field grouped by δ_0 are collected.

An example of the quantitative influence of the initial smearing thickness δ_0 of the interface between the magnetic fluid and water on the mixing by magnetic micro-convection δ_{MC} is presented in figure 3.40. for magnetic fluid FF09-9$_{100\%}$. Additional experiments are collected in Appendix §A.1.4. One data point in the graph represents one experiment in a constant vertical external magnetic field with the initial smearing thickness δ_0 as shown in the legend of graphs in mm. Similar as in the experiments with horizontal external magnetic field, it is confirmed that mixing by magnetic micro-convection is more effective for sharper interfaces (smaller values of δ_0) between the mixing fluids.

By extrapolating the data points of a chosen δ_0 until they reach the horizontal axis at $\delta_{MC} = 0$ an approximate critical value of magnetic field H_c at which the instability appears for each smeared interface thickness can be obtained. The same is in the experiment in the horizontal external magnetic field the likely values of H_c are higher for larger initial smearing thicknesses. The relationship between δ_{MC} and magnetic field is not perfectly linear, but for the collected magnetic field value range the linear fit was chosen. In fig. 3.40. markers representing experiments with initial smearing thickness $\delta_0 = 0.06$ mm are approximated with a straight line (light purple dashed line in the graph) and markers representing experiments with initial smearing thickness $\delta_0 = 0.13$ mm are approximated with a straight line (dark purple dotted line in the graph) as well. Using this approximation it can be estimated that the critical magnetic field in which the instability first emerges mixing water and the specific magnetic fluid (FF09-9$_{100\%}$) if the initial smearing thickness is $\delta_0 = 0.06$ mm would be $H_c \approx 20$ Oe and for initial smearing thickness $\delta_0 = 0.13$ mm this value would be $H_c \approx 39$ Oe.

H_c values are estimated for all the experiments carried out within the scope of this

chapter. The results are visualized and visible in Appendix §A.1.4. Results show that stronger magnetic field must be applied for experiments with the same initial smearing thickness carried out in the thinnest micro-channel ($h_1 = 0.135$ mm). In the horizontal magnetic field the opposite effect was observed. Also, for more diluted magnetic fluids the value of the critical magnetic field is higher for all other experimental parameters unchanged. The dilution ratio of the magnetic fluid does not affect the rate at which the critical magnetic field value changes with respect to the initial smearing thickness. However, this rate is different for different magnetic fluids.
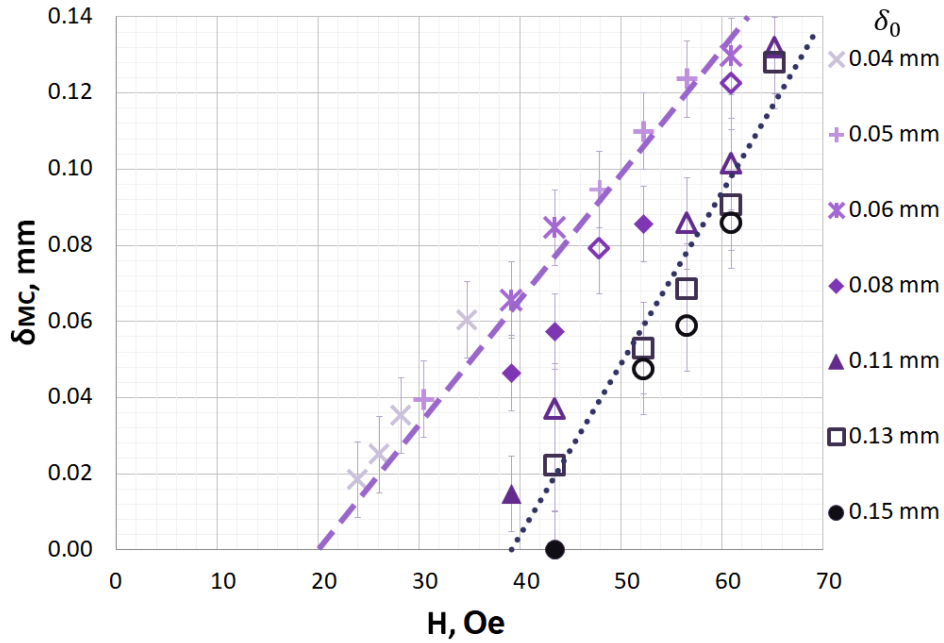
3.40. Figure: δ_{MC} with respect to H for various δ_0 in micro-channel with thickness $h_2 = 0.257$ mm. Magnetic fluid: FF09-9$_{100\%}$. Empty markers represent δ_{MC} obtained with attachment method.

MF	Dilution ratio	h, mm	Hc, Oe
D107	100%	0.135	1.1
		0.257	6.2
KTF11-1	100%	0.135	13.7
		0.257	5.4
FF21-5	100%	0.135	5.8
FF09-9	100%	0.257	5.1
	66%		13.3
	50%		20.0

3.7. Table: Critical vertical magnetic field for magnetic micro-convection to emerge when mixing fluids with sharp initial interface $\delta_0 = 0$ mm between the fluids

118

Estimated values of critical magnetic field for magnetic micro-convection to emerge if the mixing fluids have sharp initial interface are collected in tab. 3.7.. The values of the critical magnetic field were obtained using linear fit of the data collected in figures A.24 and A.25.
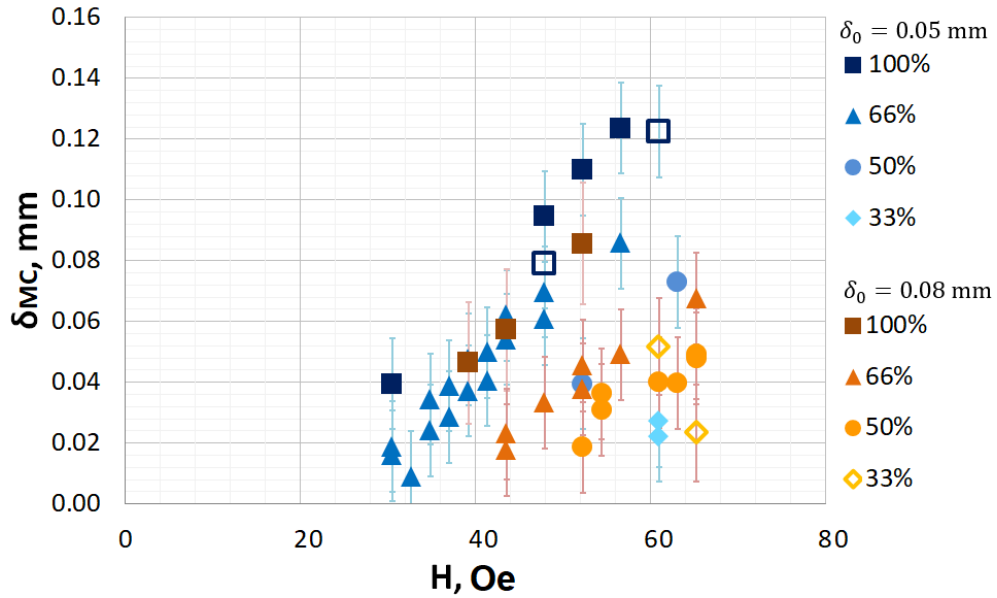
(a) Smaller values of δ_0
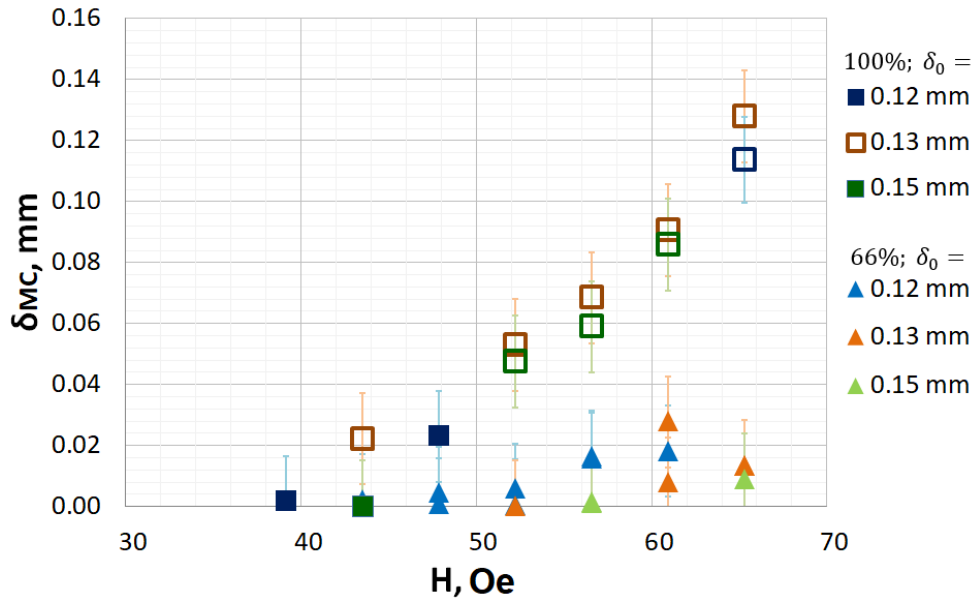
(b) Larger values of δ_0

3.41. Figure: Dilution ratio effect on δ_{MC} for various δ_0 in a vertical external magnetic field H for magnetic fluid FF09-9 in micro-channel with thickness $h_2 = 0.257$ mm. Empty markers represent δ_{MC} obtained with attachment method.

Next the effect of dilution ratio of the magnetic fluid (FF09-9) on magnetic micro-convection is reviewed in fig. 3.41.. One marker in the graph represents one experiment. The markers with the same color tonality are grouped by the same initial smearing thickness.

Experiments carried out with magnetic fluid of the same concentration are represented by the same marker shape. In the first graph (fig. 3.41.a) results for two different values of initial smearing thickness δ_0 for four different dilution ratios of the magnetic fluid are presented. Blue markers there represent experiments with smaller $\delta_0 = 0.05$ mm and orange markers are for larger $\delta_0 = 0.08$ mm. In the second graph (fig. 3.41.b) experiments with only two different dilution ratios of the magnetic fluid, but for three different initial smearing thicknesses are presented. In this graph the dynamics of magnetic micro-convection for larger values of initial smearing thicknesses is collected.

As already known the smaller initial smearing thickness results in greater mixing by the magnetic micro-convection as the blue markers are above the orange ones. Greater values of micro-convective mixing δ_{MC} for experiments with the same initial smearing thickness and external magnetic field can be achieved if the magnetic fluid is more concentrated. For example, for experiments with initial smearing thickness $\delta_0 = 0.05$ mm in fig. 3.41.a mixing for the most concentrated fluid is larger $\delta_{MC(100\%)} \approx 0.09$ mm than for a diluted fluid $\delta_{MC(66\%)} \approx 0.07$ mm in the same magnetic field $H = 48$ Oe. In fig. 3.41.b there are no experimental results for more diluted fluids (50% and 33%) as the critical magnetic field value H_c for these dilution ratios was not even reached and was out of the magnetic field value range of the experimental system.

Judging from fig. 3.41.b it seems that the dilution ratio of the magnetic fluid affects the rate at which the micro-convective mixing δ_{MC} changes with respect to the external magnetic field. As in this graph it appears that the slope of the marker series (squares in the graph) representing the most concentrated fluid (100%) is steeper than the slope of the marker series (triangles in the graph) representing experiments with a diluted (66%) magnetic fluid. So it seems, that changes in the value of the magnetic field causes greater changes in micro-convective mixing δ_{MC} if the magnetic fluid is more concentrated.

The gravity effects on the δ_{MC} with respect to Ra_m are reviewed in fig. 3.42., which represents the experimental results from the previous fig. 3.41. made dimensionless. As expected the data series that represent experiments with the most diluted magnetic fluid and therefore experiments with the smallest $Ra_g = 5931$ (rhombus markers) are above other data series with the same δ_0, meaning that in the dimensionless units the mixing enhancement due the magnetic micro-convection is greater for smaller values of Ra_g. The measured value range of Ra_m does not overlap much for experiments with different dilution ratios. However, within the measured region it seems that the rate of the changes of δ_{MC} with respect to Ra_m is not affected by the dilution ratio of the magnetic fluid as all data series seem parallel to each other.

An example of visual effects of different dilution ratios of magnetic fluid FF09-9 are presented in figure 3.43.. One column represents one experiment in time, the vertical axis show seconds since the beginning of the experiment. Additional experiments are reviewed

in Appendix §A.1.4. The instability not only emerges earlier in time in experiments with more concentrated magnetic fluids, but the rate at which the fingers of the instability grow is faster in more concentrated magnetic fluids as well. The initial smearing thickness is $\delta_0 = 0.08$ mm for all of the presented experiments in fig. 3.43.. The instability is undeniably visible at $t = 5$ s for all values of H for the experiments with most concentrated magnetic fluid FF09-9$_{100\%}$, on the other hand the at the same time point the instability is not visible in the experiments with magnetic fluid FF09-9$_{50\%}$.
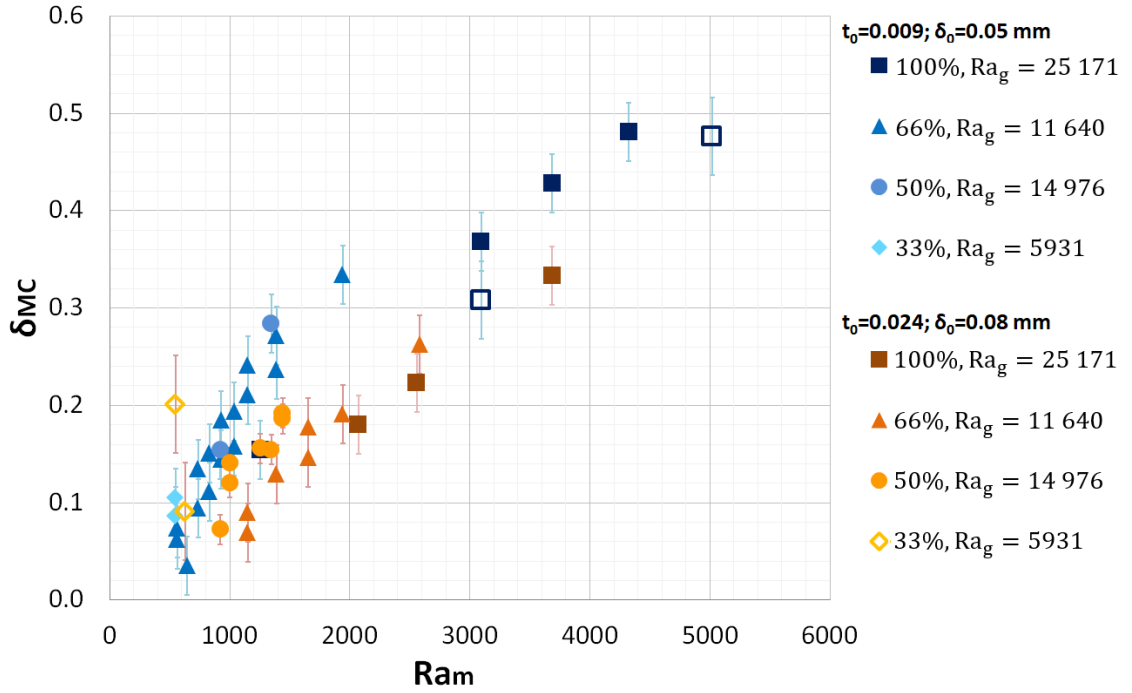
3.42. Figure: Dilution ratio effect on dimensionless δ_{MC} for various initial smearing thicknesses for magnetic fluid FF09-9 in micro-channel with thickness $h_2 = 0.257$ mm. Empty markers represent δ_{MC} obtained attachment method.

It is inconclusive whether the dilution ratio of the magnetic fluid affects the rate at which the maximal height of the fingers is reached. It must be taken into account that the mixing fluids are diffusing together all the time, also during the active phase of the magnetic micro-convection. Therefore, when the micro-convective motion ceases the fingers of the instability could be with a bit blurry edges due to the diffusion, and visually it is hard to distinguish when the active phase of the magnetic micro-convection have completely stopped, especially for slower experiments, like experiments with more diluted magnetic fluids.

Next, the role of the micro-channel thickness is investigated. An example of the quantitative effects of the thickness of the micro-channel on magnetic micro-convection for magnetic fluid D107$_{100\%}$ are presented in fig. 3.44.. Additional experimental results are collected in Appendix §A.1.4. One marker in the graph represents one experiment.

Markers of the same color tonality are grouped by the thickness of the micro-channel. The blue markers represent the experiments in thinner micro-channel with thickness $h_1 = 0.135$ mm, but the orange markers represent the experiments in thicker micro-channel with $h_2 = 0.257$ mm. The same initial smearing thickness is represented by the same marker shape. All marker series appear parallel to each other, so it seams that the micro-channel thickness here does not affect the rate at which δ_{MC} changes with respect to the external magnetic field.
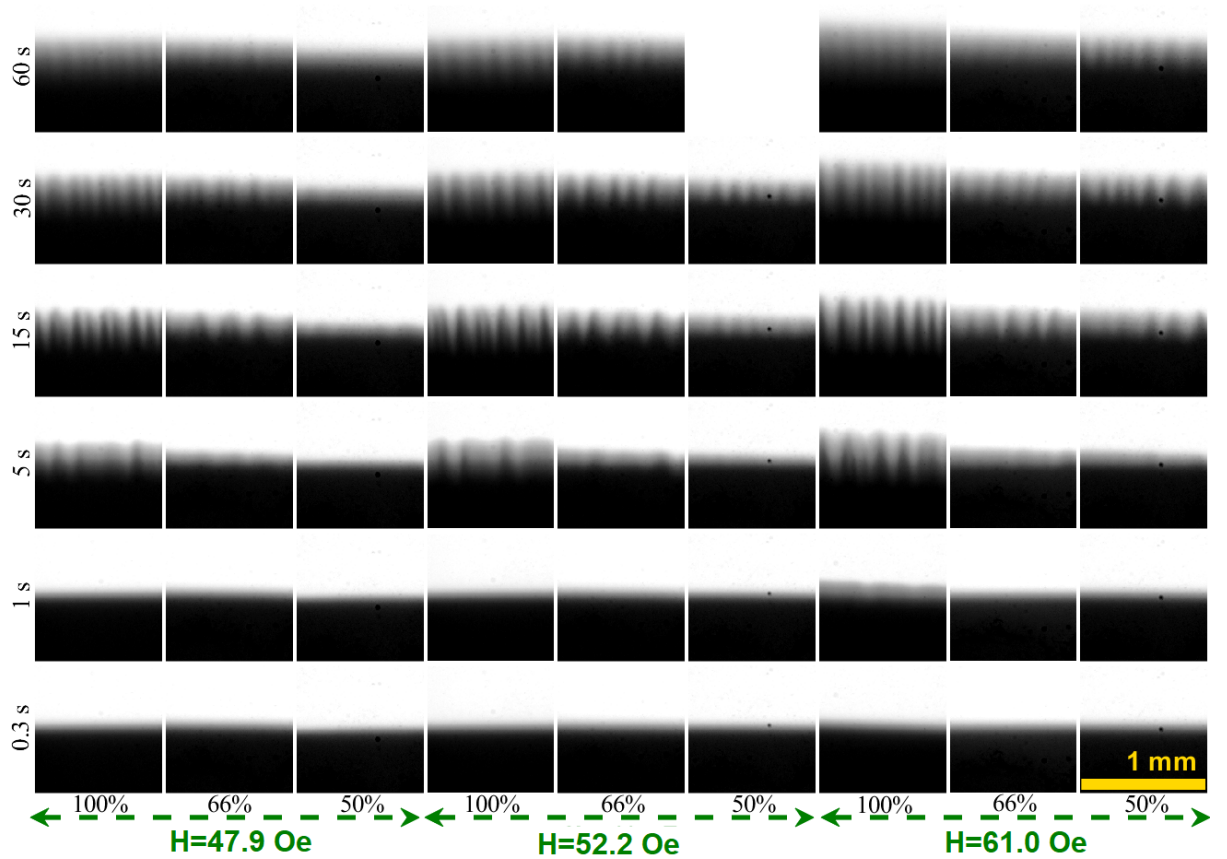
3.43. Figure: Image series of magnetic micro-convection dynamics for various dilution ratios of the same magnetic fluid FF09-9 in micro-channel with thickness $h_2 = 0.257$ mm with $\delta_0 = 0.08$ mm. A single image represents 1.0×1.0 mm region.

Greater mixing enhancement due to the magnetic micro-convection in the same magnetic field with the same initial smearing thickness can be achieved in experiments done in the thicker micro-channel with $h_2 = 0.257$ mm. For example, for magnetic fluid D107$_{100\%}$ in fig. 3.44. micro-convective mixing in the thickest micro-channel is $\delta_{MC(h_2=0.257mm)} \approx 0.05$ mm, while in the thinnest micro-channel it is two times smaller $\delta_{MC(h_1=0.135mm)} \approx 0.025$ mm for the same value of the external magnetic field $H = 41$ Oe. For magnetic fluid KTF11-1$_{100\%}$ this relationship in the horizontal magnetic field as presented in the previous chapter is opposite.
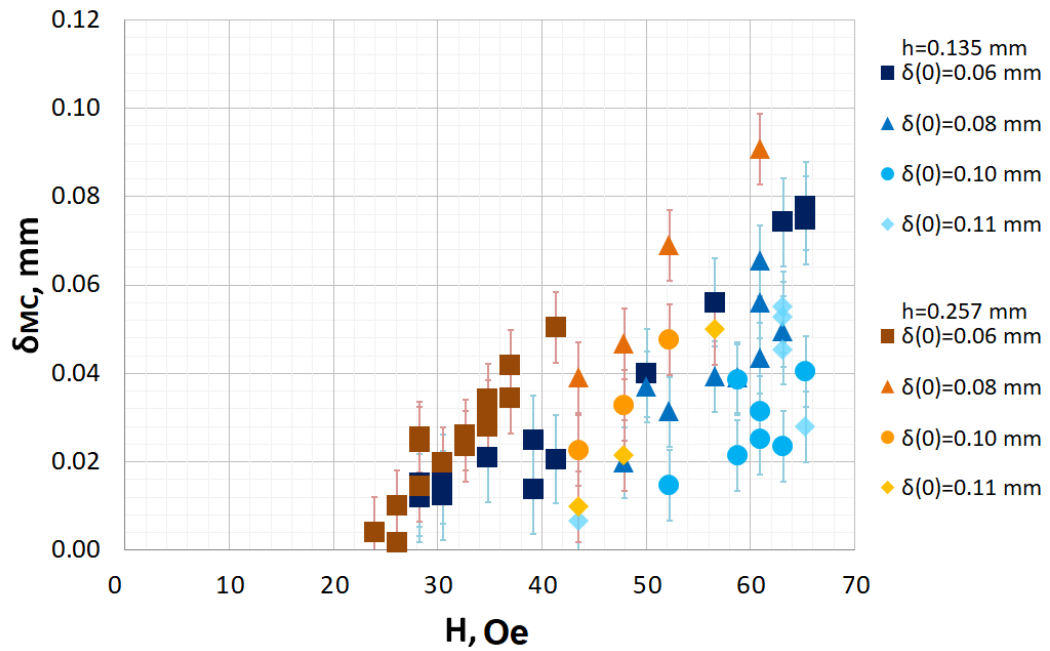
3.44. Figure: The effect of micro-channel thickness on δ_{MC} for various δ_0 for magnetic fluid D107$_{100\%}$.
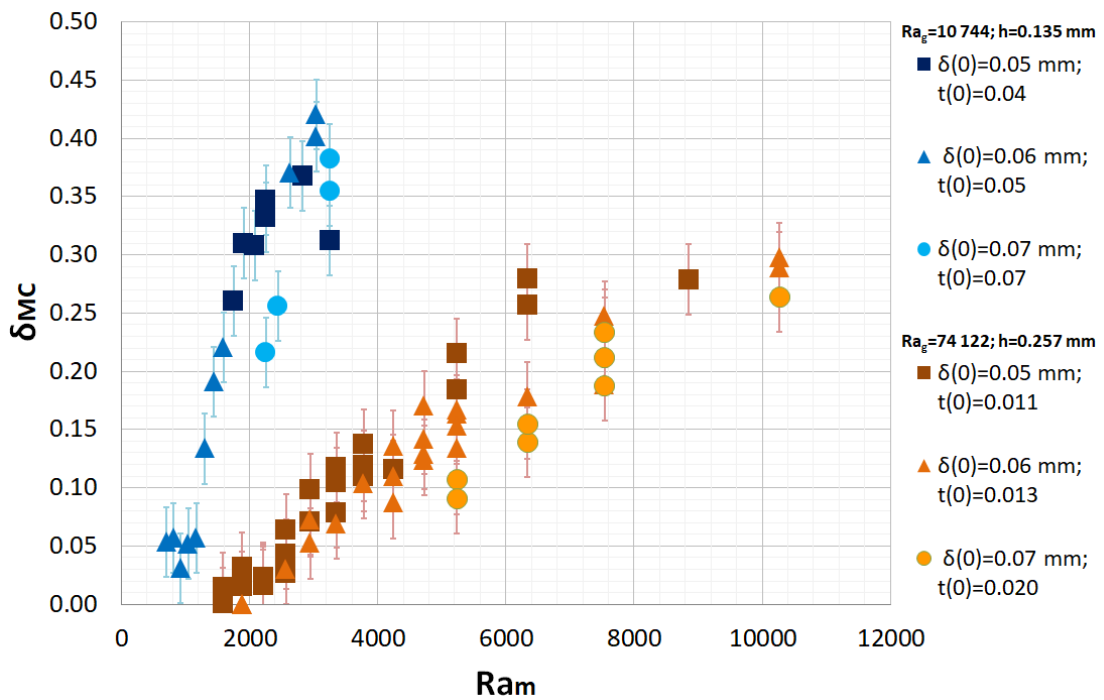
3.45. Figure: The effect of Ra$_g$ on dimensionless $\delta - \mathrm{MC}$ for various initial smearing thicknesses for magnetic fluid KTF11-1$_{100\%}$

Dimensionless perspective is presented in fig. 3.45. as micro-convective mixing δ_{MC} with respect to magnetic Rayleigh number Ra$_{\mathrm{m}}$. Markers of the same color tonality are grouped by the thickness of the micro-channel, or here the same gravitational Rayleigh

number Ra_g. The blue markers represent the experiments with smaller $Ra_g = 10744$, but the orange markers represent the experiments with larger $Ra_g = 74122$. The same initial smearing thickness is represented by the same marker shape by a graph. Although it must be noted that dimensionless time parameter t_0 for the same physical initial smearing thickness δ_0 varies between different micro-channels as the t_0 is inversely proportional to the micro-channel thickness squared. So in the thickest micro-channel ($h_2 = 0.257$ mm) the values of t_0 are smaller than those in the thinnest micro-channel ($h_1 = 0.135$ mm) for the same values of δ_0 (mm). Just like in experiments with magnetic micro-convection driven by horizontal external field, here as well the gravity suppresses the mixing.

(a) $h_1 = 0.135$ mm $\qquad$ (b) $h_2 = 0.257$ mm
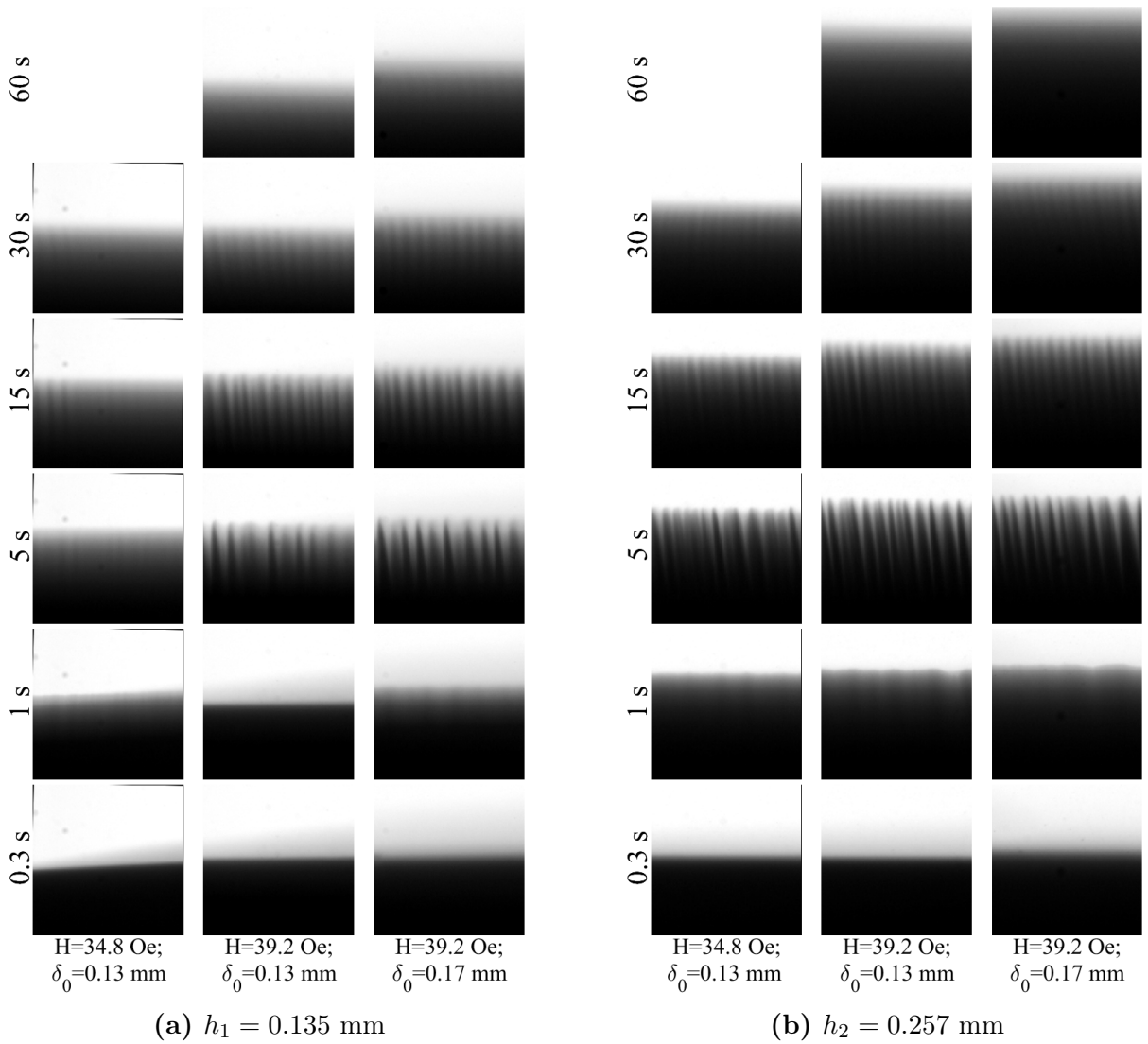
3.46. Figure: Image series of magnetic micro-convection dynamics for various micro-channel thicknesses for magnetic fluid FF09-9$_{100\%}$. A single image represents 1.0×1.0 mm region.

Visually the effect of different micro-channel thicknesses on the magnetic micro-convection in a vertical magnetic field is demonstrated in fig. 3.46. for magnetic fluid FF09-9$_{100\%}$.

There experiments with the same initial smearing thickness and in the same magnetic field but in two different micro-channels are compared. One column represents a single experiment in time. The fingers of the instability here have grown taller in the thickest micro-channel, when the same time since the beginning of the experiment has passed. For example, at $t = 5$ s for experiments carried out in magnetic field $H = 39.2$ Oe and with initial smearing thickness $\delta_0 = 0.17$ mm the fingers in the thinnest micro-channel have grown approximately 0.50 mm tall, while the fingers in the thickest micro-channel have grown larger: approximately 0.65 mm tall.

In the thickest micro-channel the previously mentioned "finger shifting" in the vertical magnetic field is even more noticeable. The behavior of the instability fingers is explored more in figures 3.47. and 3.48.. In fig. 3.47. image series of the development of the magnetic micro-convection in time for magnetic fluid FF21-5$_{100\%}$ in magnetic field $H = 43.5$ Oe is explored. The initial smearing thickness between the mixing fluids for this experiment is $\delta_0 = 0.7$ mm. An interesting phenomenon that characterizes many experiments in vertical magnetic field is visible here: the instability emerges, and fluids rapidly mix after the application of the magnetic field without visible fingers at the beginning. Here it is visible in picture $t = 1$ s, then already at $t = 1.5$ s outlines of the fingers become visible. At $t = 2$ s there are 6 well distinguishable finger shapes, but at $t = 3$ s it is already visible that the thicker of them are about to "split" in two. At $t = 5$ s there are many narrow individual fingers visible and in the video material it appears like more than one row of fingers is shifting pass each other. Starting from the time point $t = 10$ s the finger pattern ceases to change, the fingers still continue to grow in height a bit until just diffusion remains.
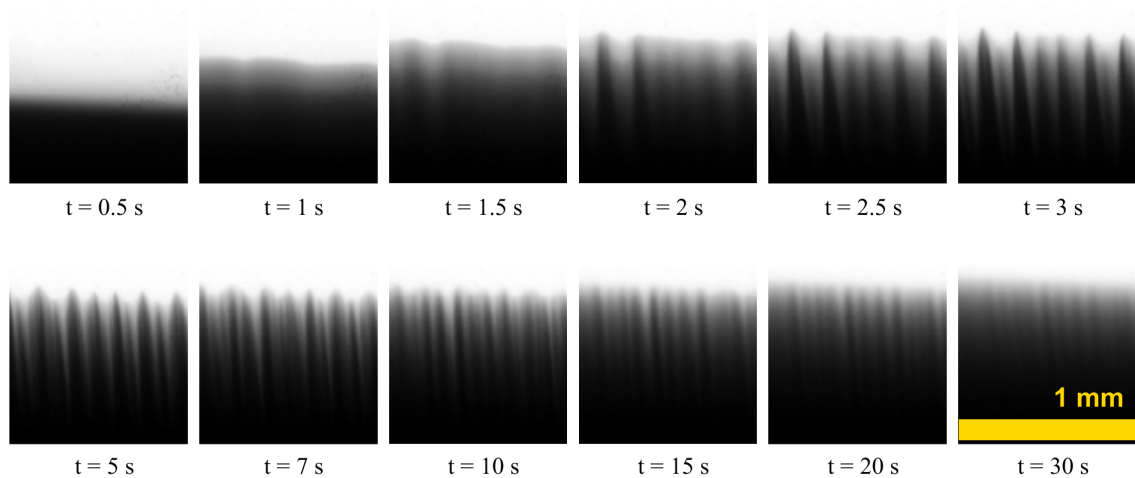
3.47. Figure: Image series of magnetic micro-convection dynamics in time for magnetic fluid FF21-5$_{100\%}$ in micro-channel with thickness $h_2 = 0.257$ mm. $H = 43.5$ Oe. $\delta_0 = 0.17$ mm. A single image represents 1.0×1.0 mm region.

(a) $t = 2$ s

(b) $t = 3$ s

(c) $t = 5$ s

(d) $t = 10$ s
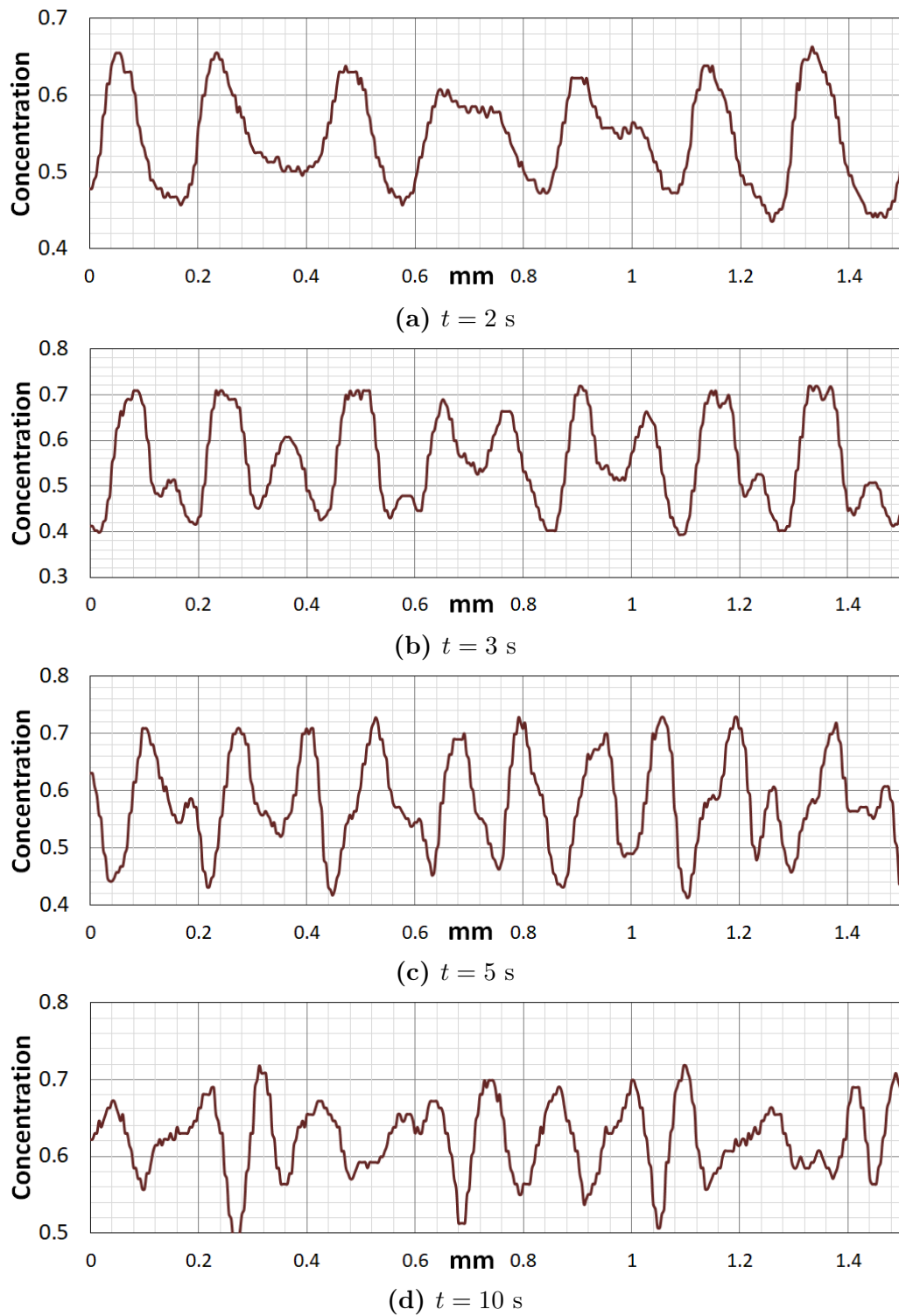
3.48. Figure: Finger distribution from intensity measurements for magnetic fluid FF21-$5_{100\%}$ in micro-channel with thickness $h_2 = 0.257$ mm in magnetic field $H = 43.5$ Oe. $\delta_0 = 0.17$ mm.

In fig. 3.48. the concentration distribution along the horizontal axis of the experiment presented in fig. 3.47. at four different times since the beginning of the experiment is explored. The concentration is measured at the same place along a horizontal line 0.5 mm

126

from the bottom of the fingers since they first appear. The concentration is normalized to relative units, where $c = 1$ corresponds to pure magnetic fluid and $c = 0$ represents clear water. It is visible that within the measured region (1.5 mm) there are seven wide peaks, meaning there are seven wide finger structures visible. Already at $t = 3$ s, just one second later, smaller secondary peaks have appeared and now together there are twice as many: 14 peaks.

3.4.2. Magnetic micro-convective mixing with respect to the initial smearing thickness

In this section the results of magnetic micro-convection dynamics in a vertical external magnetic field with respect to the initial smearing thickness grouped by the strength of the external magnetic field are collected. There is no dimensionless representation of the exact graphs collected in this section as the dimensionless initial smearing parameter t_0 is affected by the micro-channel thickness and the magnetic Rayleigh number $\mathrm{Ra_m}$ is affected by both: dilution ratio of the magnetic fluid and the thickness of the micro-channel. So the same δ_0 does not translate to the same t_0 and the same magnetic field does not translate to the same value of $\mathrm{Ra_m}$ if the experiments are carried out in micro-channels with different thicknesses and for magnetic fluids with various dilution ratios. The dimensionless mixing due to magnetic micro-convection with respect to the initial smearing t_0 is reviewed in the next paragraph §3.4.3..

The quantitative influence of the initial smearing thickness δ_0 on the mixing by magnetic micro-convection δ_{MC} for various magnetic fields is presented in fig. 3.49. for experiments carried out in the thinnest micro-channel ($h_1 = 0.135$ mm) with magnetic fluid FF21-5. Additional experimental data is collected in Appendix §A.1.4. One data point in the graph represents one experiment with a specific initial smearing thickness δ_0 in a certain external magnetic field as shown in the legend. The results are grouped by magnetic field and the colors of markers become lighter as the value H of external magnetic field increases. The same is in horizontal field micro-convective mixing is larger for experiments in stronger magnetic fields at the same δ_0 as the lighter markers are above the darker ones in all four graphs. For example, here the mixing due to magnetic micro-convection reaches up to $\delta_{\mathrm{MC}} = 0.064$ mm in the magnetic field $H = 52.2$ Oe, while it is more than three times smaller $\delta_{\mathrm{MC}} = 0.018$ mm in the magnetic field $H = 34.8$ Oe if the initial smearing thickness is $\delta_0 = 0.30$ mm.

Results show that the magnetic field affects mixing differently for different magnetic fluids. For magnetic fluid KTF11-1$_{100\%}$ the data series of different magnetic field values seem all parallel to each other over the measured range of δ_0 and magnetic field. So the rate at which δ_{MC} changes with respect to the initial smearing thickness δ_0 is the same for all magnetic fields. However in fig. 3.49. for magnetic fluid FF21-5$_{100\%}$ the data series of

different magnetic field values are not parallel to each other within measured value range for δ_0 and magnetic field. Data series describing experiments in a stronger magnetic field have steeper slope, meaning that for this magnetic fluid in stronger magnetic fields the rate at which δ_{MC} decreases by increasing the initial smearing thickness δ_0 is larger than in weaker magnetic fields.
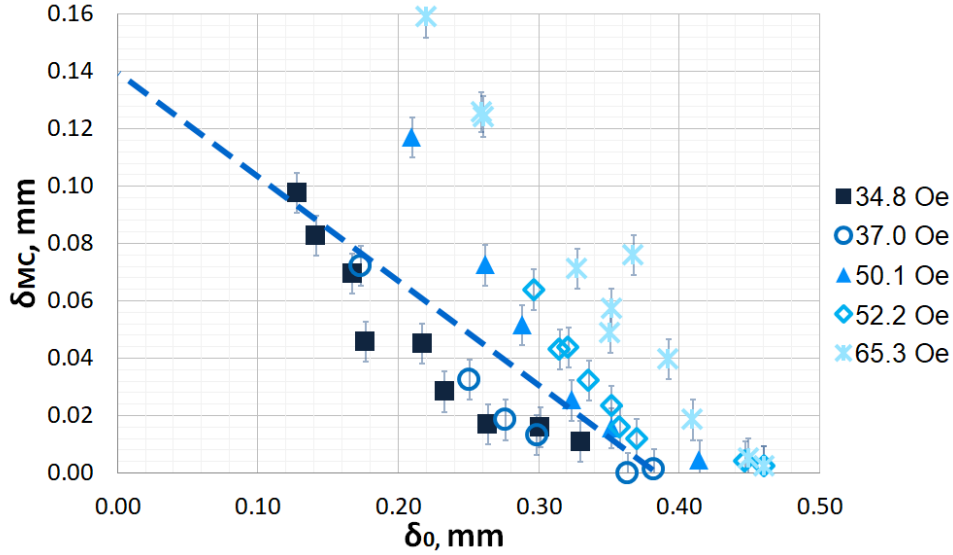
3.49. Figure: δ_{MC} with respect to δ_0 for various values of vertical external magnetic field in micro-channel with thickness $h_1 = 0.135$ mm. Magnetic fluid: FF21-5$_{100\%}$

By extrapolating all the data points of the same magnetic field H until they reach the vertical axis at $\delta_0 = 0$ mm the maximum value of δ_{MC} for this particular magnetic field can be expressed. The relationship is not strictly linear, but here miucroconvective mixing in a vertical magnetic field $H = 37$ Oe is approximated by a straight, blue, dashed line in fig. 3.49.. This line meets the vertical axis at $\delta_{MC} = 0.14$ mm. So mixing these fluids with perfectly sharp initial interface it is expected that in the magnetic field $H = 37$ Oe the mixing due to magnetic micro-convection between these fluids could reach approximately $\delta_{MC:max} \approx 0.14$ mm. Understandably this estimated maximal value $\delta_{MC:max}$ of micro-convective mixing is expected to be higher for experiments in stronger magnetic fields.

Also using this approximation until the linear line reaches the horizontal axis at $\delta_{MC} = 0$ mm the value of of initial smearing thickness δ_0 for which the particular magnetic field H_c is a critical one can be obtained. For example, in fig. 3.49. the blue, dashed line for experiments in $H = 37$ Oe crosses the horizontal axis at $\delta_0 = 0.38$ mm. So it is expected that $H_c = 37$ Oe would be a critical magnetic field in which the instability would first emerge in experiments with initial smearing thickness $\delta_0 = 0.38$ mm for magnetic fluid FF21-5$_{100\%}$. As expected for larger values of δ_0 the expected H_c values are higher as well. These values agrees with the ones demonstrated in figures A.24 and A.25. This approximation is carried out for all experiments and the visual results are collected

in Appendix §A.1.4. Micro-convective mixing is more effective for more concentrated magnetic fluids. Results show that experiments carried out in the thickest micro-channel have larger values of $\delta_{\text{MC:max}}$ for the same values of external magnetic field. So, when mixing water and magnetic fluid in a vertical external magnetic field greater mixing thickness can be achieved in a thicker micro-channel.

The effect of dilution ratio on the mixing by magnetic micro-convection in a vertical external magnetic field with respect to initial smearing thickness is reviewed in fig. 3.50. for magnetic fluid FF09-9 in a micro-channel with thickness $h_2 = 0.257$ mm. Markers describing experiments with the same dilution ratio of the magnetic fluid have the same color tonality. Purple markers represent the experiments with more concentrated magnetic fluid FF09-9$_{100\%}$, the green markers represent the experiments with diluted magnetic fluid FF09-9$_{66\%}$ and the orange markers represent the experiments with even more diluted magnetic fluid FF09-9$_{66\%}$. Experiments carried out in the same magnetic field have the same marker shape. The color of the markers becomes lighter as the value of the magnetic field increases.

The most effective mixing due to magnetic micro-convection can be achieved with the most concentrated magnetic fluid FF09-9$_{100\%}$ as the purple markers are above all others for the same values of the initial smearing thickness δ_0. For example, micro-convective mixing for experiments in magnetic field $H = 47.9$ Oe (squared markers) and with initial smearing thickness $\delta_0 = 0.08$ mm is $\delta_{\text{MC;100\%}} = 0.08$ mm for FF09-9$_{100\%}$, while for magnetic fluid FF09-9$_{66\%}$ it is $\delta_{\text{MC;66\%}} = 0.03$ mm and for even more diluted FF09-9$_{50\%}$ it is just $\delta_{\text{MC;50\%}} = 0.01$ mm.

Similar as with experiments in the horizontal magnetic field it appears that for the same values of δ_0 are more dispersed for the purple markers when comparing the experimental data series of different dilution ratios. Therefore it is possible that the changes in magnetic field affect the change in micro-convective mixing more if the magnetic fluid is more concentrated. To illustrate this, the difference in micro-convective mixing between experiments carried out in magnetic fields $H = 65.3$ Oe ("x" marker shape) and $H = 56.6$ Oe (triangle marker shape) for experiments with the initial smearing thickness $\delta_0 = 0.11$ mm is compared. This difference for the most concentrated magnetic fluid (purple markers) is $\Delta\delta_{\text{MC}} = \delta_{MC(H=65.3Oe)} - \delta_{MC(H=56.6Oe)} = 0.135 - 0.085 = 0.05$ mm, while for magnetic fluid with dilution ratio FF09-9$_{66\%}$ (green markers) this difference is five times smaller $\Delta\delta_{\text{MC}} \approx 0.01$ mm.

Due to this effect the difference in mixing between experiments with magnetic fluids with different ratios increases if the external magnetic field is stronger. Meaning that the difference of δ_{MC} in absolute values between "x" markers (the strongest magnetic field $H = 65.3$ Oe) is bigger than between the square shaped markers (the weakest magnetic field $H = 47.9$ Oe) for the same values of initial smearing thickness δ_0. So the differences

of micro-convective mixing in a vertical external magnetic field between the magnetic fluids with different dilution ratios are more pronounced in stronger magnetic fields.
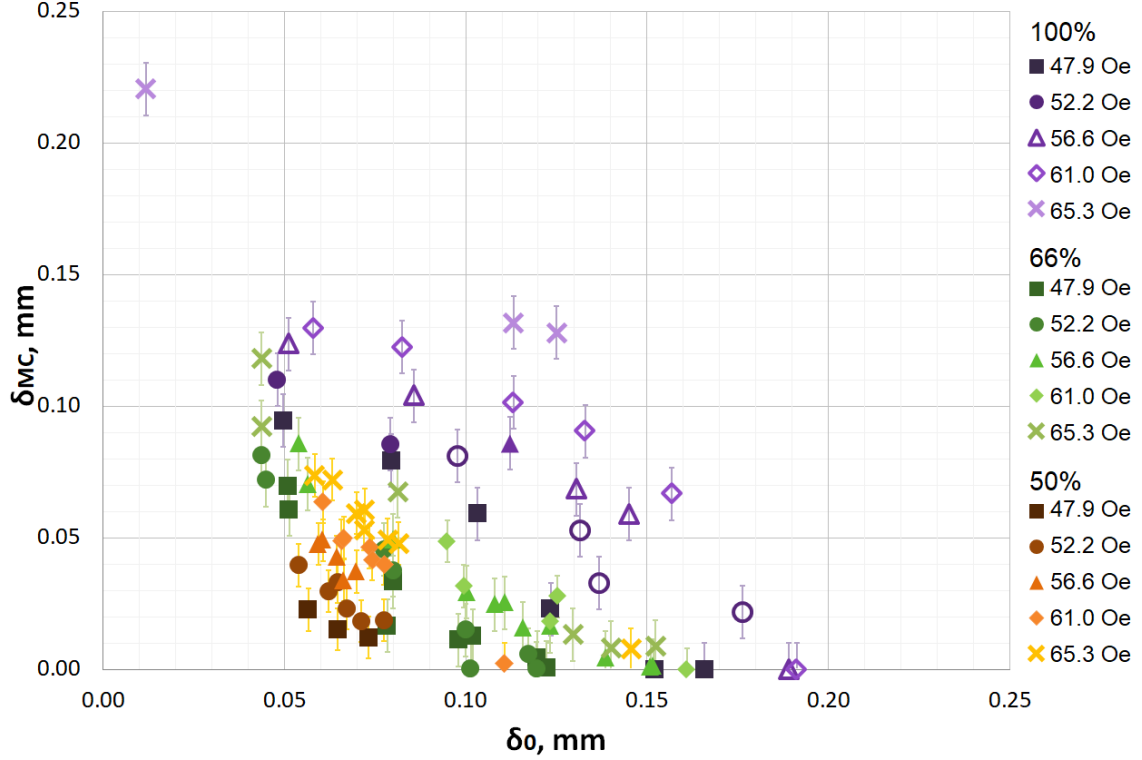

3.50. Figure: Dilution ratio effect on δ_{MC} with respect to δ_0 in a vertical magnetic field for magnetic fluid FF09-9 in micro-channel with thickness $h_2 = 0.257$ mm. Empty markers represent δ_{MC} obtained with attachment method.

The effect of the micro-channel thickness on the mixing by magnetic micro-convection in a vertical external magnetic field with respect to initial smearing thickness is reviewed in figure 3.51. for magnetic fluid $D107_{100\%}$. The experiments carried out in the thinnest micro-channel ($h_1 = 0.135$ mm) are represented by purple markers and the experiments carried out in the thickest micro-channel ($h_2 = 0.257$ mm) are represented by green markers. The color of the markers becomes lighter as the value of the external magnetic field increases. Experiments carried out in the same magnetic field are represented by the same marker shape by a figure.

The micro-convective mixing is more effective in the thickest micro-channel. For example, micro-convective mixing in the magnetic field $H = 65.3$ Oe ("x" shaped markers) and with initial smearing thickness $\delta_0 = 0.135$ mm is $\delta_{MC} \approx 0.045$ mm in the thickest micro-channel, while it is approximately four times smaller in the thinnest micro-channel $\delta_{MC} \approx 0.012$ mm.

The difference in micro-convective mixing between experiments carried out in two different magnetic fields but with the same initial smearing thickness δ_0 from fig. 3.51. is compared for both micro-channel thicknesses. For example, difference in micro-convective

mixing between experiments carried out in magnetic fields $H = 65.3$ Oe ("x" shaped markers) and $H = 43.5$ Oe (square shaped markers) for experiments with the initial smearing thickness $\delta_0 = 0.125$ mm for experiments carried out in the thickest micro-channel (green markers) is $\Delta\delta_{\mathrm{MC};h_2=0.257\mathrm{mm}} = \delta_{\mathrm{MC};H=65.3\mathrm{Oe}} - \delta_{\mathrm{MC};H=43.5\mathrm{Oe}} \approx 0.044 - 0.004 = 0.04$ mm, while for experiments carried out in the thinnest micro-channel (purple markers) it is four times smaller $\Delta\delta_{\mathrm{MC};h_1=0.135\mathrm{mm}} \approx 0.012 - 0.002 = 0.01$ mm. So by changing the strength of the vertical magnetic field the micro-convective mixing is more affected in the thickest micro-channel.
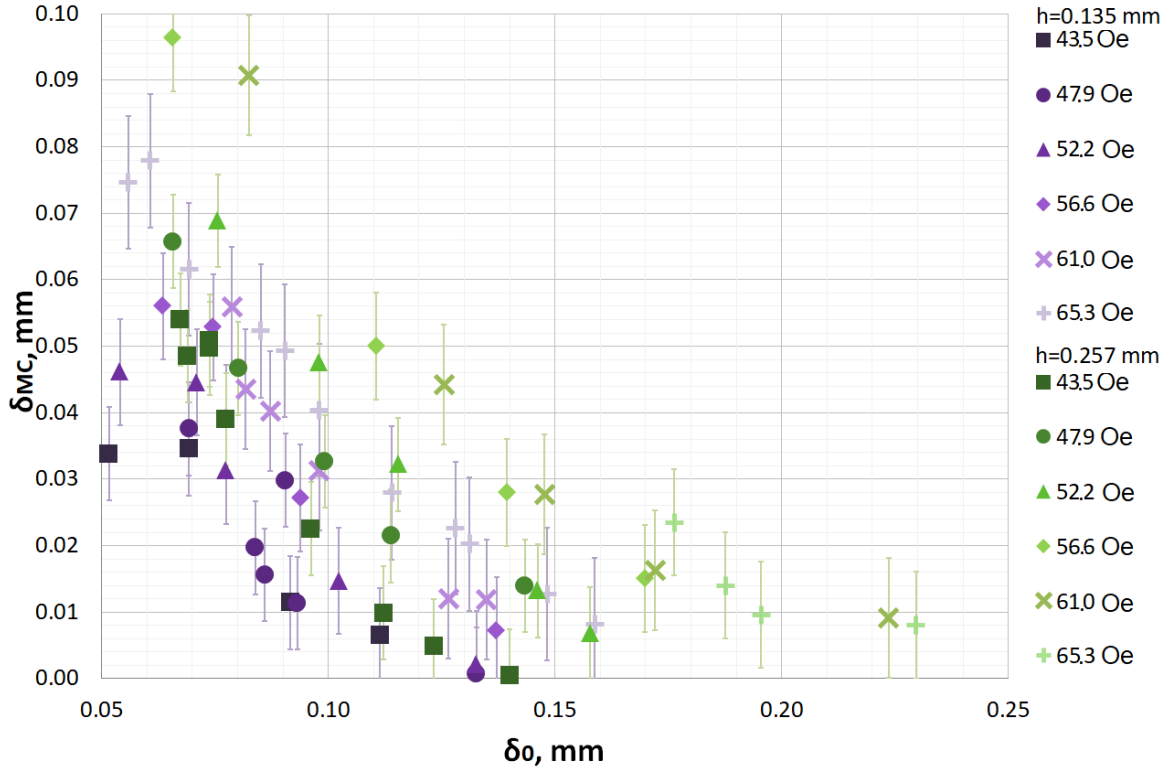
3.51. Figure: The effect of micro-channel thickness on δ_{MC} with respect to δ_0 in a vertical external magnetic field for magnetic fluid D107$_{100\%}$.

This effect also means that the difference in micro-convective mixing parameter δ_{MC} between the experiments in different micro-channels is more pronounced if the value of the vertical external magnetic field is higher. In the fig. 3.51. it is visible as for the same initial smearing thickness δ_0 the difference between "x" shaped markers that represent experiments in $H = 65.3$ Oe strong magnetic field is greater than the difference between square shaped markers that represent experiments in weaker $H = 43.5$ Oe magnetic field. For example, for experiments with initial smearing thickness $\delta_0 = 0.08$ mm difference in micro-convective mixing between experiments carried out in different micro-channels is $\Delta\delta_{\mathrm{MC};H=65.3\mathrm{Oe}} = \delta_{\mathrm{MC};h_2=0.257\mathrm{mm}} - \delta_{\mathrm{MC};h_1=0.135\mathrm{mm}} \approx 0.09 - 0.042 = 0.048$ mm for experiments carried out in stronger magnetic field $H = 65.3$ Oe, while it is more than two times smaller $\Delta\delta_{\mathrm{MC};H=43.5\mathrm{Oe}} \approx 0.038 - 0.018 = 0.02$ mm for experiments carried out in weaker

magnetic field $H = 43.5$ Oe.

3.4.3. Magnetic micro-convective mixing in a vertical magnetic field with constant Ra_m with respect to the initial smearing thickness

In this chapter dimensionless results are reviewed to quantify the gravitational and magnetic effects on the magnetic micro-convection in a vertical external magnetic field. The initial smearing thickness δ_0 is expressed using the dimensionless time parameter t_0 that represents dimensionless time for which the diffusion between the mixing fluids has been happening before the application of the external magnetic field. The results are grouped by magnetic Rayleigh number Ra_m.

First the effect of the dilution ratio of the magnetic fluid is explored. As mentioned already before, changing dilution ratio of the magnetic fluid both dimensionless Rayleigh numbers are affected. The density of the magnetic fluid decreases as it is diluted with distilled water and $\text{Ra}_\text{g} \sim \Delta\rho$. Also the volume fraction of the magnetic particles decreases and is directly proportional to the dilution ratio. Therefore magnetization of the fluid changes and $\text{Ra}_\text{m} \sim M^2$.

The effect of dilution ratio on the dimensionless mixing by magnetic micro-convection δ_MC in a vertical external magnetic field with respect to dimensionless initial smearing time parameter t_0 for magnetic fluid FF09-9 in micro-channel with thickness $h_2 = 0.257$ mm is reviewed in fig. 3.52.. One marker there represents one experiment. The same dilution ratio (the same value of Ra_g) has the same color tonality of the markers. Experiments carried out with concentrated magnetic fluid FF09-9$_{100\%}$ with $\text{Ra}_\text{g} = 25171$ are represented by purple markers and experiments carried out with diluted magnetic fluid FF09-9$_{50\%}$ with $\text{Ra}_\text{g} = 14976$ are represented by orange markers. Experiments with the same value of Ra_m are represented by the same marker shape: circles for larger value of $\text{Ra}_\text{m} = 2570$ and squares for approximately two times smaller $\text{Ra}_\text{m} = 1160$. As expected the greater micro-convective mixing δ_MC values can be achieved for experiments with larger values of Ra_m. So mixing by magnetic micro-convection in a vertical external magnetic field can be enhanced by increasing magnetic Rayleigh number. Judging by fig. 3.52. it is hard to evaluate gravitational effects on the magnetic micro-convection in a vertical magnetic field as the orange and purple markers for the same value of Ra_m and t_0 are aligned within margin of error.

The effect of the thickness of the micro-channel as well as the gravity is demonstrated in fig. 3.53. for magnetic fluid KTF11-1 Due to the fact that $\text{Ra}_\text{m} \sim h^2$ and there were no recorded experiments with identical values of Ra_m between different micro-channels, the values of Ra_m are rounded within 5% of the exact value. Here the gravity effects are undeniable.
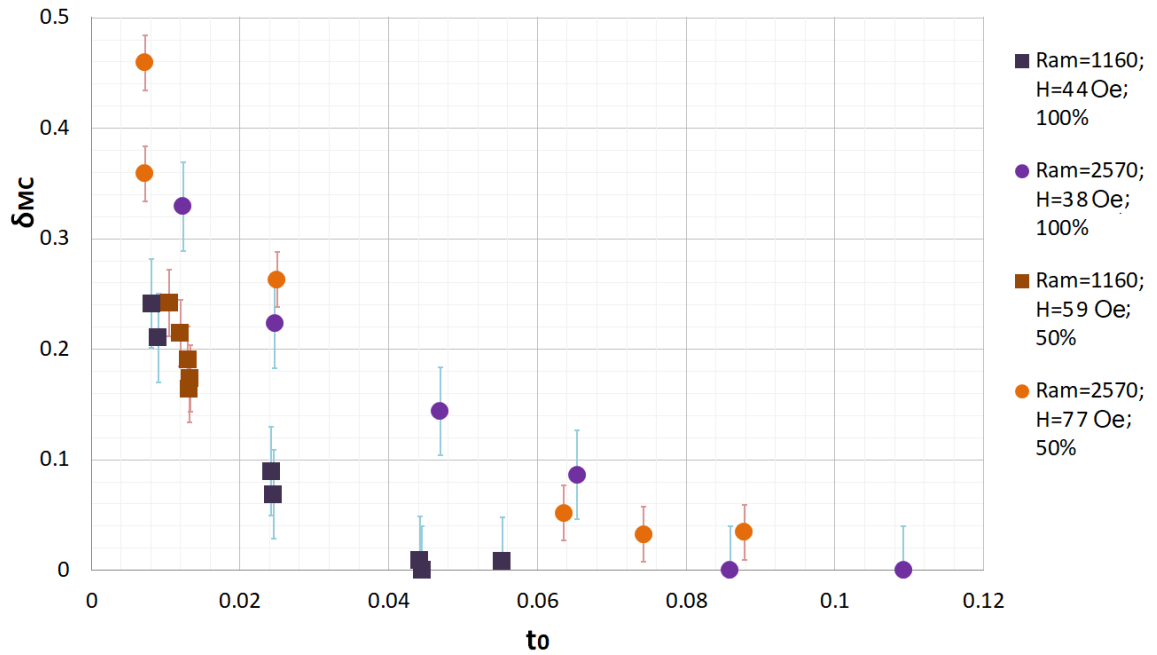
3.52. Figure: Dilution ratio effect on dimensionless δ_{MC} in a vertical magnetic field with respect to initial smearing t_0 for various $\mathrm{Ra_m}$. Magnetic fluid FF09-9 in micro-channel with thickness $h_2 = 0.257$ mm is explored here.
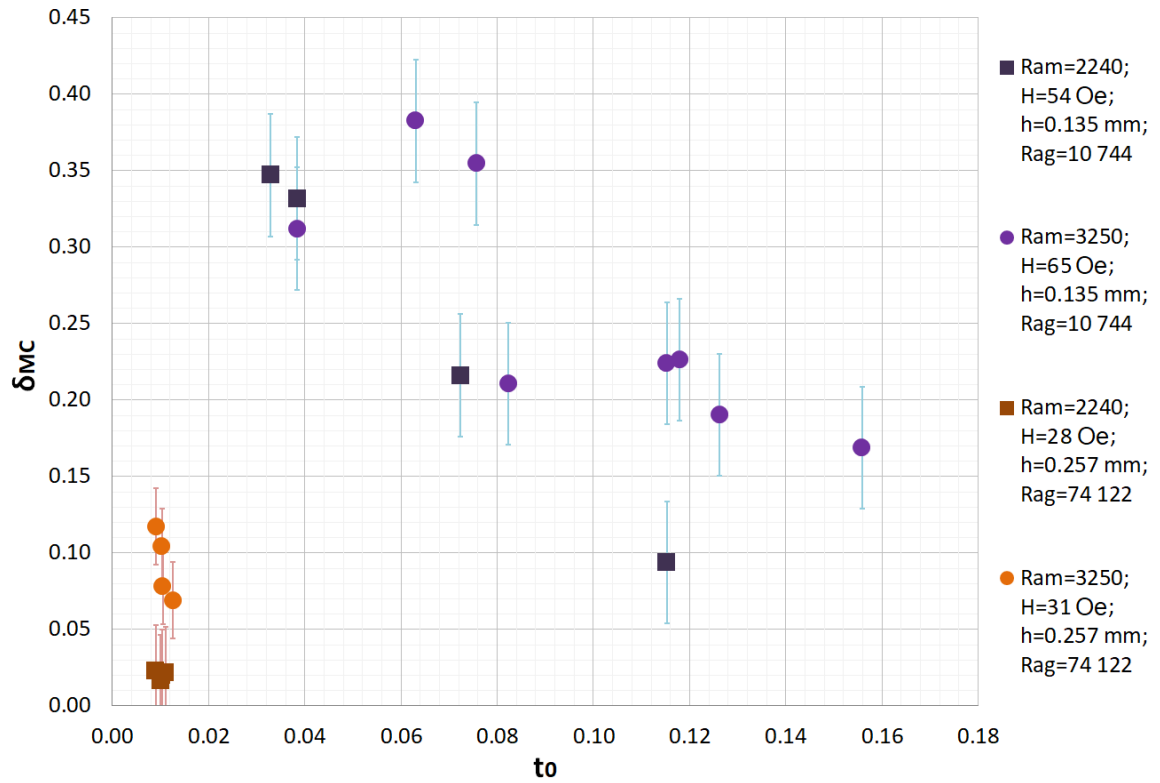
3.53. Figure: The effect of the micro-channel thickness on dimensionless δ_{MC} in a vertical magnetic field with respect to initial smearing t_0 for various values of $\mathrm{Ra_m}$ for magnetic fluid: KTF11-1$_{100\%}$.

In fig. 3.53. for magnetic fluid KTF11-1 there are two values of Ra_g explored for two different values of Ra_m. Experiments carried out in the thinnest micro-channel ($h_1 =$ 0.135 mm) have Ra_g= 10744 and are represented by purple markers. However experiments carried out in the thickest micro-channel ($h_2 = 0.257$ mm) have approximately seven times larger Ra_g= 74122 and are represented by orange markers. For both series of Ra_g larger values of micro-convective mixing δ_{MC} are achieved in experiments with also larger values of Ra_m= 3250 as the round markers representing those experiments are above the square ones for smaller values of Ra_m= 2240. For example, for experiments with smaller Ra_g= 10744 with initial smearing time $t_0 = 0.075$ dimensionless micro-convective mixing is $\delta_{MC;Ra_m=3250} \approx 0.36$ for experiment with larger magnetic Rayleigh number, while $\delta_{MC;Ra_m=2240} \approx 0.22$ for experiment with smaller magnetic Rayleigh number. So the gain of mixing by magnetic micro-convection here by increasing Ra_m is $\Delta\delta_{MC} \approx 0.14$. It is not conclusive as the regions of measured t_0 do not overlap for experiments with various values of Ra_g here as well as the margin of error is relatively large, but it appears in fig. 3.53. that there is bigger dispersion of δ_{MC} between different values of Ra_m for experiments with smaller Ra_g (purple markers).

3.4.4. Quantitative characterization of magnetic micro-convective mixing in a vertical external magnetic field

In this section requirements to get a specific thickness of the mixed layer between two fluids due to magnetic micro-convection in a vertical external magnetic field are explored.

The values of magnetic field that should be applied to get a specific δ_{MC} with respect to initial smearing thickness δ_0 are collected. In fig. 3.54. mixing for magnetic fluid FF09-9 with three different dilution ratios (100%, 66% and 50%) is explored. The results are grouped with the same marker shape by the expected values of δ_{MC}. Experiments carried out with magnetic fluid with the same dilution ratio are represented by markers with the same color tonality. Orange markers describe show results with the most concentrated magnetic fluid FF09-9$_{100\%}$, green markers represent FF09-9$_{66\%}$ and purple markers ore for FF09-9$_{50\%}$. In order to achieve greater mixing by magnetic micro-convection δ_{MC} the value of the vertical external magnetic field H must be increased. In this figure the best it can be seen for the most diluted magnetic fluid (purple markers) as the value range of δ_0 overlap nicely for these experiments. For example, if the initial smearing thickness is $\delta_0 = 0.06$ mm the value of the external magnetic field should be $H \approx 65$ Oe in order to induce magnetic micro-convection with $\delta_{MC} = 0.07$ mm ("x" shaped markers), $H \approx 55$ Oe to induce magnetic micro-convection with $\delta_{MC} = 0.04$ mm (triangle shaped markers) and $H \approx 45$ Oe to induce magnetic micro-convection with $\delta_{MC} = 0.02$ mm (circle shaped markers).

The square shaped markers in fig. 3.54. for $\delta_{MC} = 0$ mm represent the critical values

of the magnetic field to first induce the magnetic micro-convection for experiments with set corresponding initial smearing thickness δ_0. It is visible that the same value of the magnetic field that is a critical one for the most diluted magnetic fluid for a certain initial smearing thickness δ_0, for experiments with more concentrated magnetic fluids is a critical magnetic field for experiments with higher values of δ_0. For example, magnetic field $H_c \approx 42$ Oe is a critical one for experiments with FF09-9$_{50\%}$ if the initial smearing thickness is $\delta_0 \approx 0.07$ mm, for experiments with a bit more concentrated FF09-9$_{66\%}$ it is the critical magnetic field if the initial smearing thickness for the experiment is $\delta_0 \approx 0.11$ mm, and for FF09-9$_{100\%}$ it is the critical magnetic field if the initial smearing thickness for the experiment is even bigger $\delta_0 \approx 0.13$ mm.

For experiments with the same initial smearing thicknesses δ_0 stronger magnetic fields are necessary to achieve the same values of micro-convective mixing δ_{MC} if the experiment is carried out with more diluted magnetic fluid.
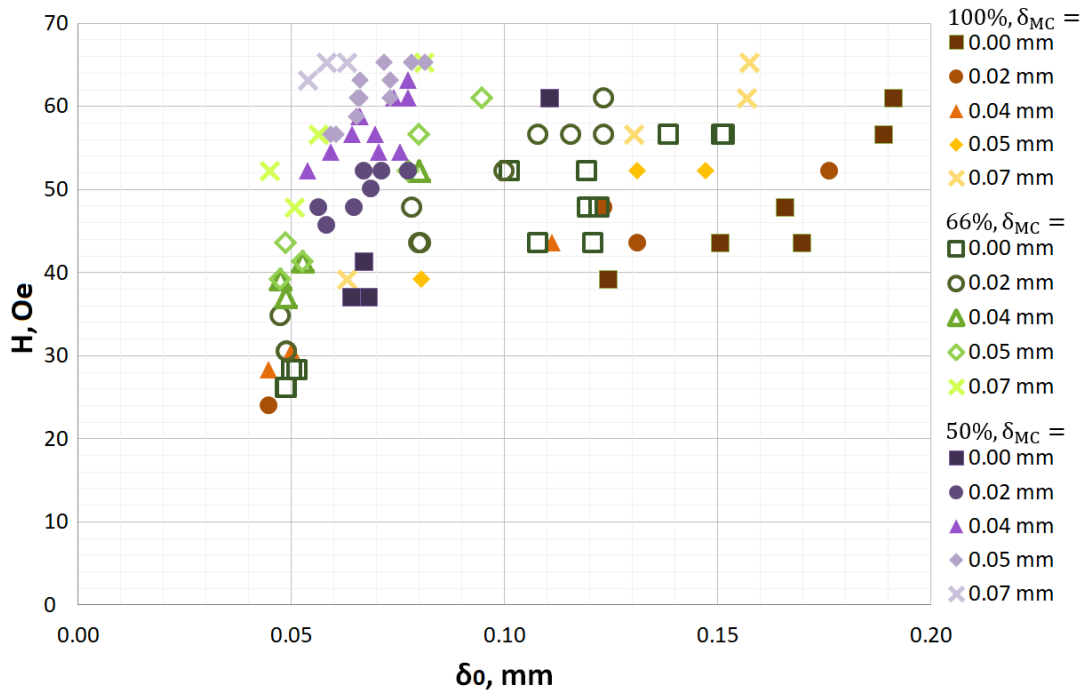
3.54. Figure: What magnetic field H should be applied to get a specific δ_{MC} with respect to δ_0 for various dilution ratios of the magnetic fluid FF09-9 in micro-channel with thickness $h_2 = 0.257$ mm.

The micro-channel thickness effects are demonstrated in figure 3.55. for magnetic fluid KTF11-1$_{100\%}$. Experiments carried out in the thinnest micro-channel ($h_1 = 0.135$ mm) are represented by orange markers and experiments carried out in the thickest micro-channel are represented by the green ones. The results are grouped with the same marker shape by the obtained values of δ_{MC}.
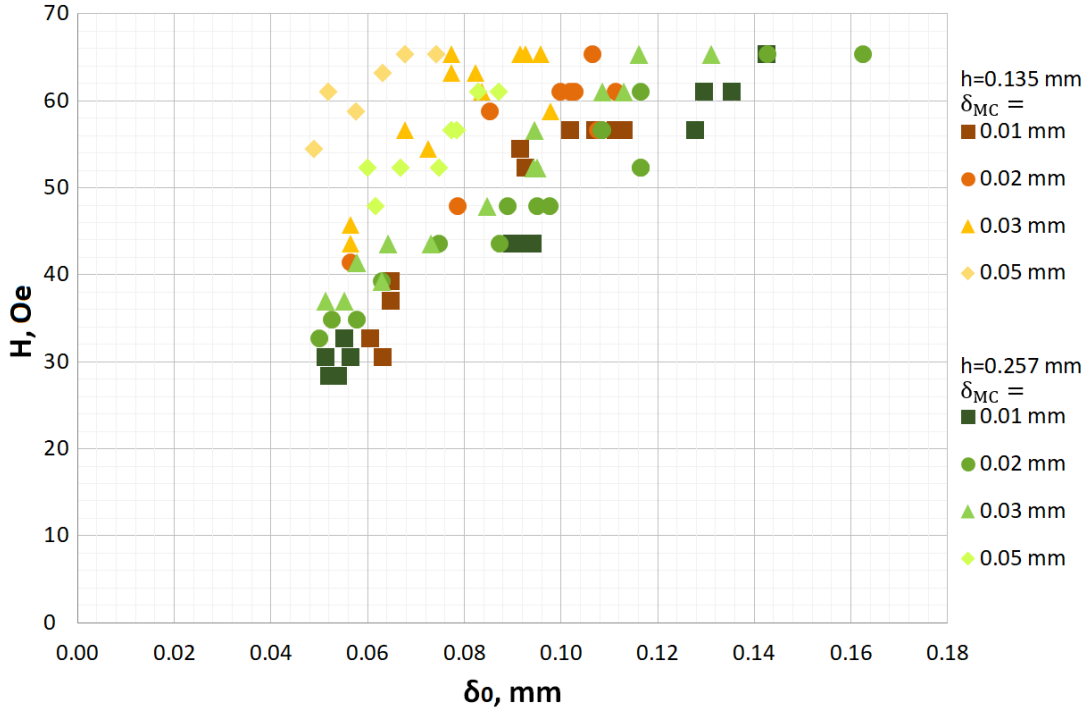
3.55. Figure: What magnetic field H should be applied to get a specific δ_{MC} with respect to δ_0 for experiments in different micro-channels. Magnetic fluid: KTF11-1$_{100\%}$.

Stronger vertical magnetic field must be applied to the experiments in the thinnest micro-channel in order to create the same amount of mixing δ_{MC} as in thicker micro-channel. For the same values of the initial smearing thickness δ_0 the difference of magnetic field between experiments carried out in different micro-channels is less pronounced for the squared markers that represent the smallest δ_{MC} than for the rhombus markers that represent the largest δ_{MC}. Meaning that the magnetic field H to achieve a certain micro-convective mixing δ_{MC} must be changed more between the experiments in various micro-channels if the desired values of δ_{MC} are higher. For example, $H \approx 60$ Oe must be applied in order to create $\delta_{\mathrm{MC}} = 0.05$ mm large micro-convective mixing in the thinnest micro-channel. To achieve the same amount of micro-convective mixing in the thickest micro-channel weaker $H \approx 50$ Oe magnetic field must be applied, thus making the difference in magnetic field values between the experiments carried out in different micro-channels to be $\Delta H_{\delta_{\mathrm{MC}}=0.05mm} = 10$ Oe. However to achieve smaller mixing by magnetic micro-convection $\delta_{\mathrm{MC}} = 0.01$ mm values of the external magnetic field that must be applied agree within the margin of the error for experiments carried out in different micro-channels. Therefore making the difference in magnetic field values between the experiments carried out in different micro-channels almost non-existent $\Delta H_{\delta_{\mathrm{MC}}=0.01mm} \approx 0$ Oe.

The total mixing length Δ that consists both of micro-convective mixing during the experiment and diffusive mixing before the experiment is explored in fig. 3.56. for magnetic fluid KTF11-1$_{100\%}$ in the thickest micro-channel ($h_2 = 0.257$ mm). One marker describes

one experiments and the color of the markers become lighter as the value of the total mixing length Δ increases.

In order to achieve greater total mixing values for experiments with the same initial smearing thickness stronger magnetic field must be applied.

Results presented here appear similar to the experiments in horizontal magnetic field. The data series for a specific total mixing length Δ appear all parallel to each other and horizontal within error. Thus it seems that the value of external magnetic field H is not dependent on the initial smearing thickness δ_0 in order to achieve a specific total mixing length Δ confirming the second hypothesis presented in Introduction also for experiments in vertical magnetic field. So for these particular experimental series the maximal total mixing of the fluids when magnetic micro-convection has exhausted itself is set by external magnetic field.

For experiments carried out in the thinnest micro-channel ($h_1 = 0.135$ mm) the data dispersion was larger.
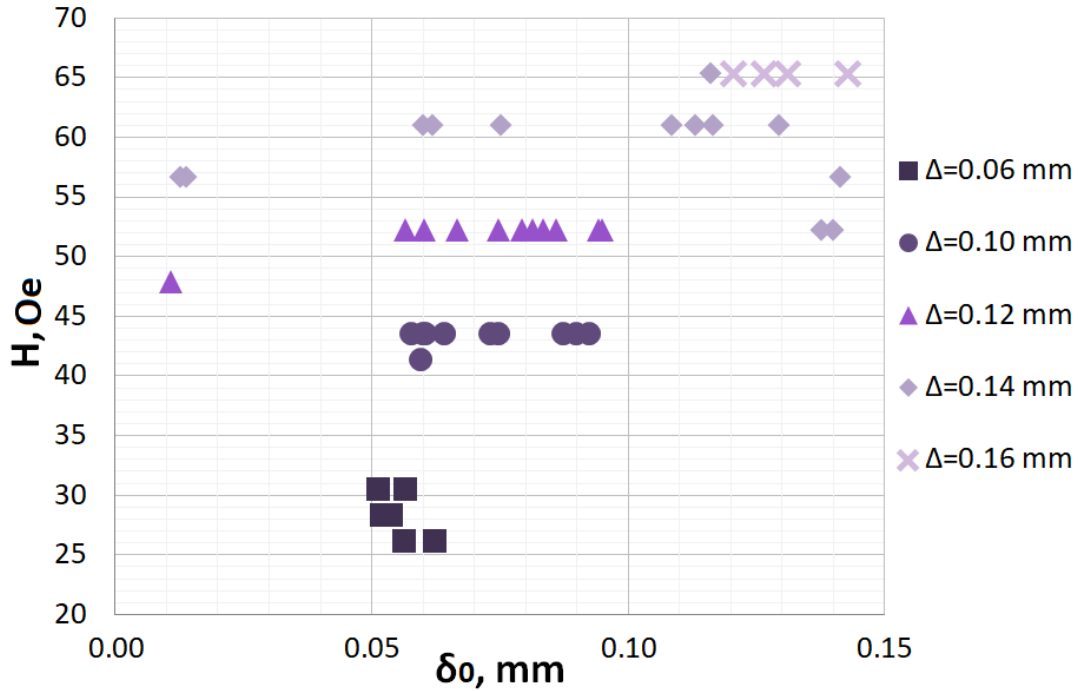
3.56. Figure: Magnetic field with respect to δ_0 for various values of total mixing length Δ for magnetic fluid KTF11-1$_{100\%}$ in micro-channel with thickness $h_2 = 0.257$ mm.

3.4.5. Summary

The periodic pattern of magnetic instability in a vertical magnetic field visually differs from the one in a horizontal magnetic field. Fingers grow out straight and after some time they might split, which has also been observed in literature [6]. Just the same fingers form only if a certain critical magnetic field H_c is applied. Within this section values of H_c are determined for various magnetic fields and various initial smearing thicknesses

δ_0. Values of H_c are larger for experiments with larger initial smearing thicknesses δ_0. Mixing of the fluids in a vertical magnetic field is limited by initial smearing as smaller δ_{MC} are achieved for experiments with larger δ_0. Unlike in experiments in a horizontal magnetic field, here the instability appears at the same time, regardless of the strength of the external magnetic field applied.

The effects of micro-channel thickness are also explored within this section. It appears that the micro-convective mixing is more effective in the thickest micro- channel. Also micro-convective mixing is more effective for more concentrated magnetic fluids, and this difference of δ_{MC} between various dilution ratios is more pronounced in stronger magnetic fields.

Wavelength characterization of the instability in a vertical magnetic field is more complicated than in a horizontal magnetic field due to the splitting of the fingers. Characteristic λ of the instability is not affected by δ_0.

Dimensionless analysis shows that same gain of Ra_m causes greater gain of micro-convective mixing in thinner micro-channel, where gravitational effects Ra_g are smaller. Just like in experiments with magnetic micro-convection driven by horizontal external field, here as well the gravity suppresses the mixing.

3.5. Measurements with stero micro-PIV

In this section the experimental results of stereo-μPIV measurements are collected.

The experiments were carried out with magnetic fluid KTF09-9$_{33\%}$. As it is visible in the table 2.1. the density difference between this magnetic fluid and distilled water is very small: $\Delta\rho = 0.008$ g/cm^3. In comparison, the experiments described in [53] were carried out with magnetic fluid D107, with $\Delta\rho = 0.148$ g/cm^3. Microfluidics chip with long Y-shaped micro-channel (as presented in figure 2.15..c) with thickness $h_1 = 0.135$ mm and channel width $d \approx 1.62$ mm was used for the measurements. The chip was placed horizontally so that the direction of gravity field is perpendicular to the plane of the micro-channel. The plane of the microfluidics chip is described using x and y axes, but the direction of the gravity is along z-axis.
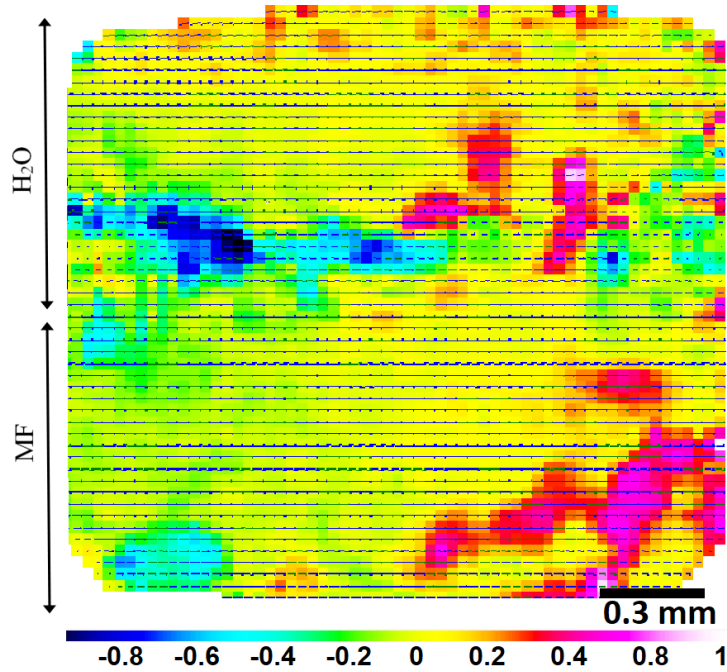
3.57. Figure: Normalized velocity field along z-axis. $t = 6$ s, $u_{z,min} = -8.58 \cdot 10^{-4}$ m/s, $u_{z,max} = 7.40 \cdot 10^{-4}$ m/s. Position of xy-plane 0.022 mm from top wall of the micro-channel. The image represents 1.6×1.6 mm region.

An example of a velocity field measurement near the top of the micro-channel is shown in figure 3.57.. The captured plane is approximately 0.022 mm away from top wall of the micro-channel. A normalized velocity field in a z-direction, along the gravity field is represented by a color gradient. Positive velocities represent movement towards top glass and the negative velocities represent sinking. Magnetic fluid occupies the lower half and water the upper one of the xy-plane of the microfluidics chip at the beginning of the experiment as denoted by the arrows in the figure. The measurement is made $t = 6$ s after the flow has been stopped. A blue, horizontally stretched region representing fluid movement in downwards direction is visible in the middle of the micro-channel near the

initial interface between the fluids, indicating of some kind of convective motion. Given the time since the start of the experiment and the location of this sinking region both in xy-plane and z-direction, it is possible that the motion of the magnetic fluid is captured.
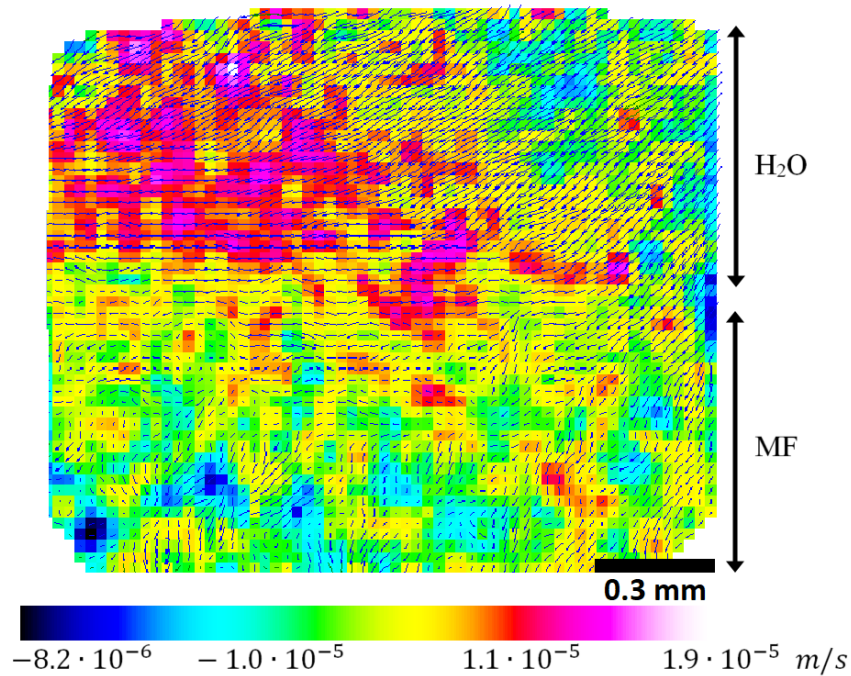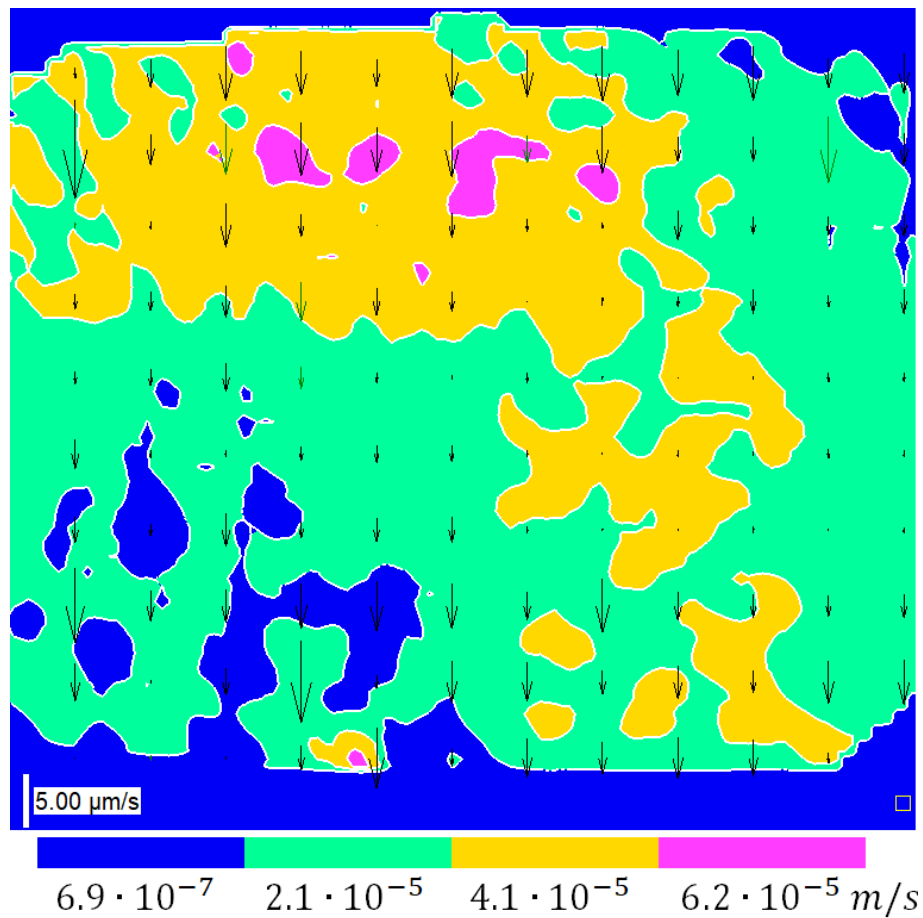

(a) $t = 10$ s
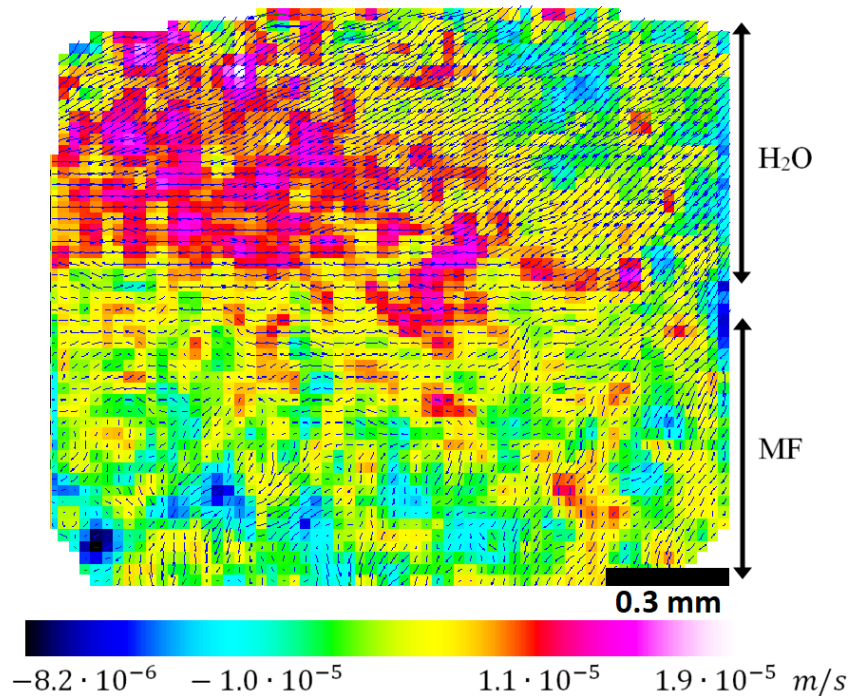
(b) $t = 40$ s

3.58. Figure: A velocity field along z-axis for various time moments t since the syringe pump has been switched off. Position of xy-plane: 0.045 mm from top wall of the microchannel. Images represents 1.6×1.6 mm region.

Series of velocity field over time since the flow has been stopped for the same experiment is demonstrated in figures 3.58. and 3.59.. Here the xy-plane is a bit lower than in previous example: 0.045 mm away from the top wall of the micro-channel. But this region still represents upper half of the micro-channel, but relatively close to the mid-layer of the micro-channel. The velocity field in z-direction is represented by color gradient. At the beginning of the experiment the magnetic fluid occupies the lower half and water the upper one of the xy-plane of the microfluidics chip as denoted with arrows in the figures. 3.58. for both time moments a horizontal velocity field distribution is visible. Fluid is moving towards the top glass in the water region. This might be caused by magnetic fluid that is creeping below the water layer and causing upwards movement of water. Also close the region of the initial interface between the fluids, a sinking movement of the fluids in the region that initially corresponded to magnetic fluid is visible.

It is expected that after some time the magnetic fluid will flow underneath, therefore the water will be on the surface in the initial interface region. When that happens it is impossible to say which vectors represent magnetic fluid, which water in this region with the current experimental setup. Also it is expected that over time the convective motion will start to decay as the diffusion will start to dominate.
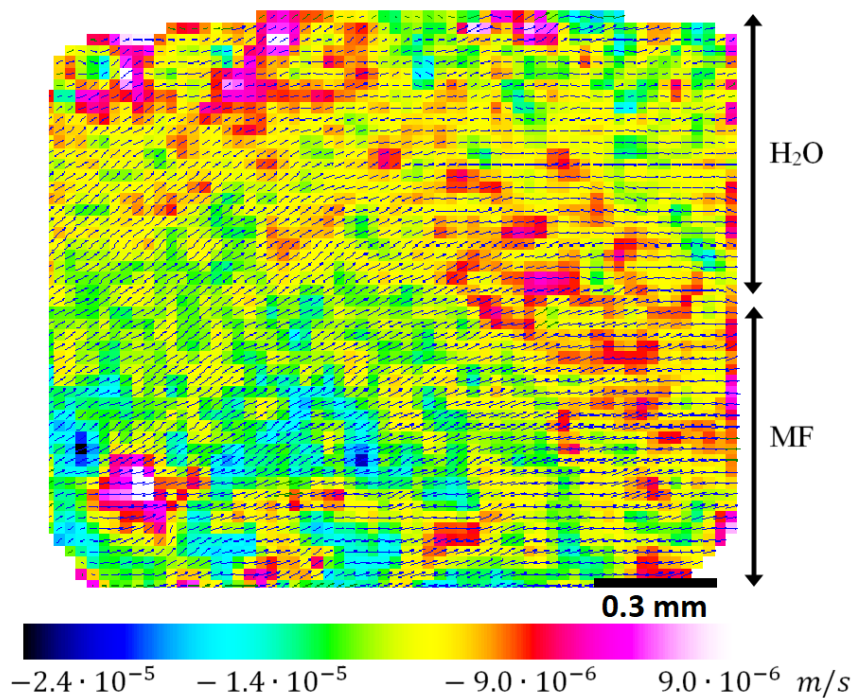
3.59. Figure: A velocity field along z-axis at $t = 60$ s since the syringe pump has been switched off. Position of xy-plane: 0.045 mm from top wall of the micro-channel. The image represents 1.6×1.6 mm region.

In fig. 3.59. that demonstrates the same experiment, but later when already 1 minute since switching of the syringe pump has passed, the horizontal disparity of the vector field

has become a bit ambiguous. Still in the lower part of the xy-plane that most likely still represents magnetic fluid, sinking motion is detected and in the upper part of xy-plane that still most likely represent water upwards motion is detected. This agrees with the intuition of how the fluids should move if the magnetic fluid is slipping under water.

A different experiment is demonstrated in figures 3.60. and 3.61.. In these figures xy-plane 0.069 mm from the top wall of the micro-channel is captured, meaning these figures represent the situation in the mid-layer of the micro-channel. Here $t = 52$ s since switching off syringe pump has passed. Just like in figures before the upper part of the region represented at the beginning of the experiment is filled with water and the lower part with magnetic fluid. In fig. 3.60. the velocity field along z-axis is visualized by color, and along x-axis by vector-arrows. The y-direction (direction of the flow created by syringe pump, when pumping in fresh fluids) is neglected here. In z-direction the vector field has horizontal distribution. The upper part that initially represents water is moving towards the top wall of the micro-channel. It is plausible that by yellow and pink regions there the motion of water is captured.

3.60. Figure: A velocity field at $t = 52$ s since the syringe pump has been switched off. Position of xy-plane: 0.069 mm from top wall of the micro-channel. Z-direction is represented by colors and x-direction by vector-arrows. The image represents 1.6×1.4 mm region.

Also it is visible that in xy-plane all of the vector-arrows are pointing downwards, but in the region of the initial interface this movement is not so distinguished any more. This might be due to the fact that in the mid-layer of the micro-channel this long since the beginning of the experiment definitely some mixing between the fluids has happened and it is impossible to separately represent the movements of two fluids here.

The same experiment, but visualized as a 3D vector field is demonstrated in figure 3.61.. The top of the micro-channel is faced towards the viewer here.
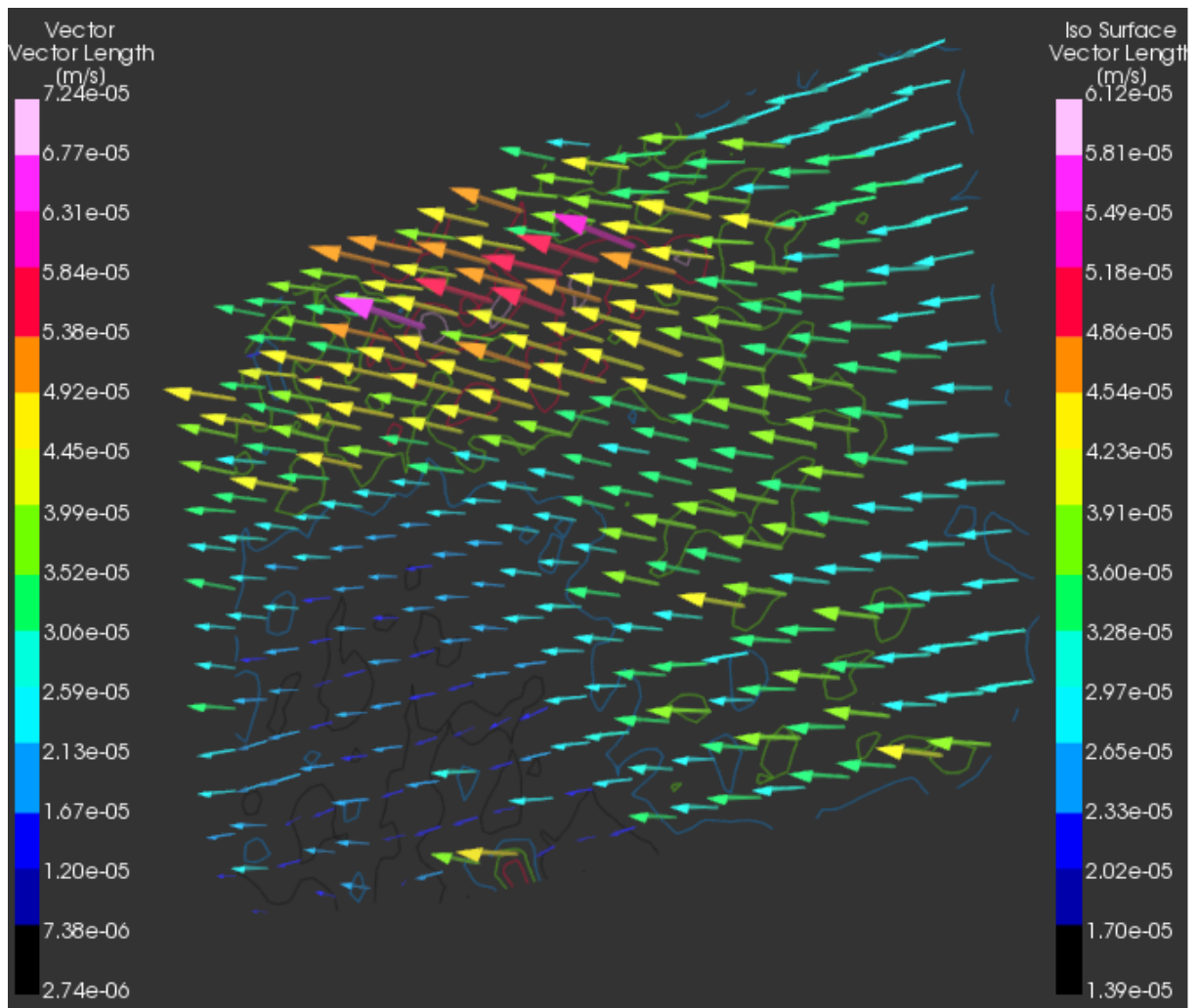
3.61. Figure: A velocity field at $t = 52$ s since the syringe pump has been switched off. Position of xy-plane: 0.069 mm from top wall of the micro-channel.

Further two experiments that are not analyzable are demonstrated, to highlight some hardships that must be accounted when carrying out similar experiments. In figure 3.62. a measurement is made $t = 20$ s after switching of the syringe pump. Position of the xy-plane represented here is 0.049 mm from top wall of the micro-channel, that represents a layer close to the middle of the micro-channel. Z-direction of the fluid movement is represented by colors, but x-direction by vector-arrows. A movement in the longitudinal y-direction is

omitted here. A vertical distribution of the fluid in z-direction is detected here. Intuitively such movement should not bee here, so it is suspected tha the microfluidics chip here could be a little bit tilted during the experiment.
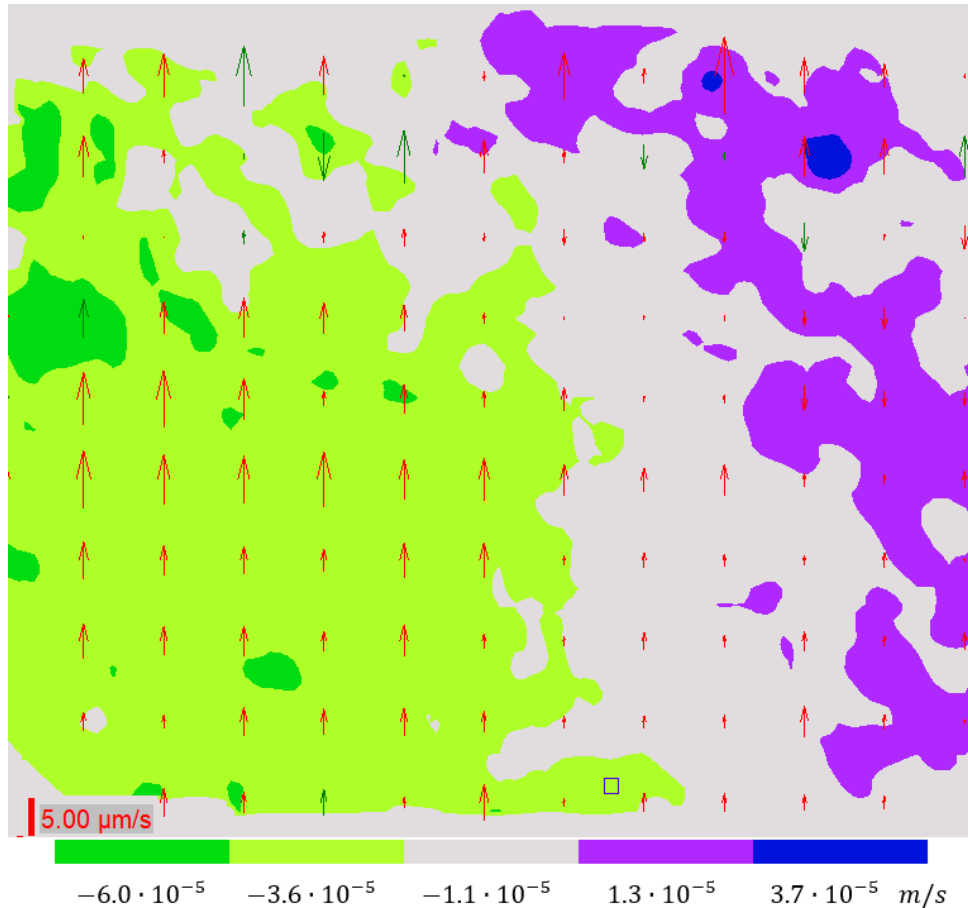
3.62. Figure: A velocity field at $t = 20$ s since the syringe pump has been switched off. Position of xy-plane: 0.049 mm from top wall of the micro-channel. Z-direction is represented by colors and x-direction by vector-arrows. The image represents 1.6×1.4 mm region.

In figure 3.63. a measurement is made right after switching of the syringe pump. Position of the xy-plane represented here is 0.087 mm from top wall of the micro-channel, that represents a layer close to the bottom of the micro-channel. Z-direction of the fluid movement is represented by colors, but x-direction by vector-arrows. A movement in the longitudinal y-direction is omitted here. A vector field demonstrated here is chaotic. It might be due to the fact, that the flow created by syringe pump has just been stopped abruptly.
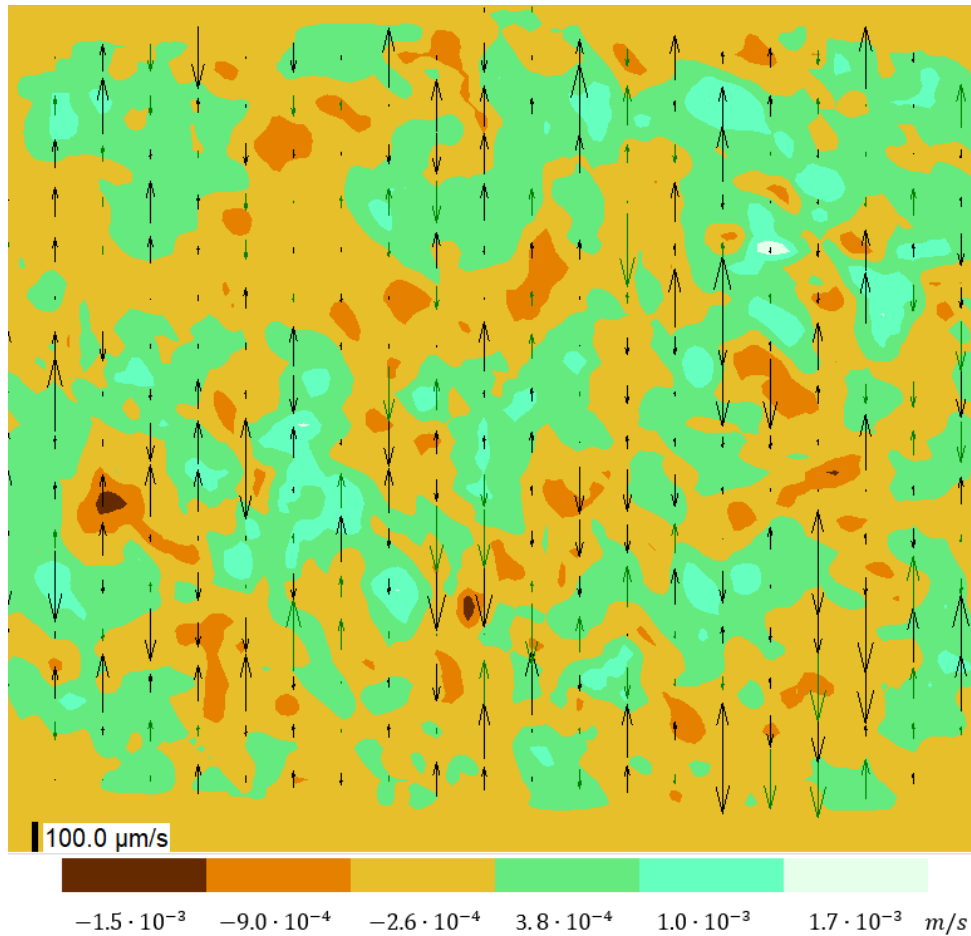
3.63. Figure: A velocity field right after the syringe pump has been switched off. Position of xy-plane: 0.087 mm from top wall of the micro-channel. Z-direction is represented by colors and x-direction by vector-arrows. The image represents 1.6×1.4 mm region.

3.5.1. Summary

Vector field has been measured in different horizontal layers of the horizontally placed microfluidics chip at various times since the beginning of the experiment. It is harder to analyze experiments that are captured right after or too long after the syringe pump has been switched off. A part of the results agree with intuitively expected motion where the magnetic fluid slips under the water.

4. Chapter

Discussion

In this chapter the results of this thesis are compared with each other. Also numerical simulations and theoretical predictions that were carried out by colleagues are considered.

In order to to compare the experimental results with theoretical ones dimensionless quantities already introduced earlier are used. For convenience the experimental quantities and the conversion to the corresponding dimensionless quantities are collected in table 4.1.. h here represents the thickness of a micro-channel. For the diffusion coefficient D the values from table 2.1. are used.

Experimental quantity	Dimensionless complement
δ_{MC}, mm	$\delta_{\mathrm{MC:ND}} = \frac{\delta_{\mathrm{MC}}}{h}$
δ_0, mm	$\delta_{0:ND} = \frac{\delta_0}{h}$
	$t_0 = \frac{\delta_0^2}{4h^2}$
H, Oe	$\mathrm{Ra_m} = \frac{M_0^2 h^2}{12\eta D}$
$\Delta\rho$, g/cm^3 and dilution ratio	$\mathrm{Ra_g} = \frac{\Delta\rho g h^3}{12\eta D}$

4.1. Table: Conversion from experimental to dimensionless quantities.

The experimental quantities here are demonstrated with their usual units, the dimensions of a corresponding quantity, of course must be accounted for when expressing dimensionless quantities. Initial smearing thickness δ_0 can be expressed by either dimensionless thickness δ_0 or dimensionless time t_0 for which the diffusion has been happening to obtain the particular smearing δ_0. As it is visible all dimensionless parameters are affected by micro-channel thickness. For example, $t_0 \sim h^{-2}$, which means that for the same physical δ_0 (mm) in two different micro-channels the value of t_0 differs. Also it must be noted as magnetic properties are reduced by diluting magnetic fluids, $\mathrm{Ra_m}$ will be affected as well. It means, that in this study, where various dilutions of a particular

magnetic fluid are used to get magnetic fluids with various densities, at the same magnetic field H the magnetic Rayleigh number $\mathrm{Ra_m}$ is higher for more dense fluid.

4.1. Comparison between experimental results with flowing fluids and theoretical predictions

Here the predictions about the micro-convection with initially stagnant fluids (longitudinal flow-rate $Q = 0$ $\mu l/min$) derived from the experiments with flowing fluids described in §3.1. are compared with theoretical predictions from linear stability analysis carried out by colleagues.

For theoretical considerations the evolution magnetic micro-convection between two miscible, initially stagnant fluids in a Hele-Shaw cell was described by equations 1.26, 1.27 and 1.28 described in §1.4. [25]. The value of the magnetostatic potential ϕ_m on the boundary of the Hele-Shaw cell is given by [64, 65]. The boundary conditions for the velocity v components in two dimensions (x- vertical direction, along the growth of the fingers; y- longitudinal direction, along the interface between the fluids) and concentration c as well as conditions of the periodicity across, which require that the fluids are motionless at both ends of the Hele-Shaw cell are given by [25] and reads:

$$
\begin{aligned}
v_x(0,y) = v_y(0,y) = 0, & \quad c(0,y) = 1, \\
v_x(L_x,y) = v_y(L_x,y) = 0, & \quad c(L_x,y) = 0, \\
\overline{v}(x,0,t) = \overline{v}(x,L_y,t), & \quad c(x,0,t) = c(x,L_y,t).
\end{aligned}
\tag{4.1}
$$

The linear stability analysis for a step-like concentration distribution on the boundary between the two fluids was carried out in [25]. The theoretical model considered in the article confirmed that the gravitational force stabilizes the magnetic micro-convection, which agrees to the experimental results.

The critical field values H_c estimated for the case with initially stagnant fluids from table 3.1. were used to calculate the critical magnetic Rayleigh number Ra_{mc} via eq. 1.24. As the critical field values H_c used here have a notable uncertainty, the estimated error is chosen to be 3σ large. The values of the calculated Ra_{mc} are collected in table 4.2.

Magnetic fluid	$\mathrm{Ra_g}$	$Ra_{mc} \pm \Delta Ra_{mc}$
$D107_{100\%}$	4657	775 ± 199
$D107_{66\%}$	3031	564 ± 77
$D107_{50\%}$	2225	395 ± 85
$D107_{33\%}$	1412	323 ± 68

4.2. Table: Experimentally estimated values of the critical magnetic Rayleigh number for the instability in a horizontal magnetic field with initially stagnant fluids

These experimental points are compared with values obtained from the linear stability analysis in figure 4.1.. As it can be seen the experimental results agree with the theoretical ones within the margin of error. Also this graph confirms the gravitational influence of the instability. It is visible that for experiments with higher gravitational Rayleigh numbers (when the density difference between the mixing fluids is higher) the critical magnetic Rayleigh number for the instability to first emerge also must be higher.
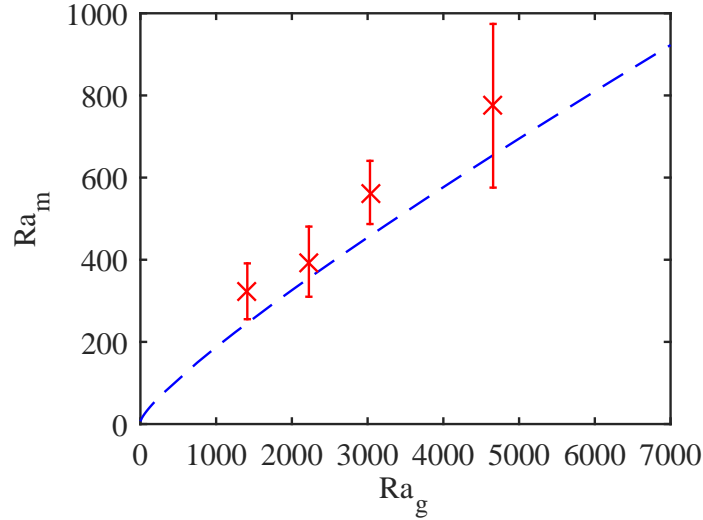
4.1. Figure: Comparison of the critical Rayleigh numbers Ra_g and Ra_m between experimental and theoretical results for the instability in a horizontal magnetic field. Data from linear analysis are given by a blue dashed line, while experimental points by red crosses and error bars. *Fig.18. from [25]*.

The comparison between the experimental and theoretical results of the characteristic finger size of the instability was done as well. Dimensionless wave-numbers k were calculated from the wavelength λ values collected in 3.1.. Theoretical results are obtained from the growth increment data, where the fastest growing mode is chosen [25]. The experimental data is averaged for similar magnetic field values for the same dilution of the magnetic fluid. The comparison is demonstrated in figure 4.2.. The value range of Ra_m is experimentally restricted as the maximal value of the magnetic field generated by the coil system is restricted as well. Also magnetic susceptibility decreases by diluting magnetic fluid. As magnetic Rayleigh number is affected by this change ($Ra_m \sim \chi^2$) the value of Ra_m is even more experimentally limited for diluted magnetic fluids. Therefore Ra_m value range for the experimental data is smaller than for the theoretical results.

The experimental results here have the same order of magnitude as well the sequence of the data are similar to the theoretical results. The values of the wave-number are close to constant and experimentally they overlap within the margin of the error. However in absolute values there are some differences.
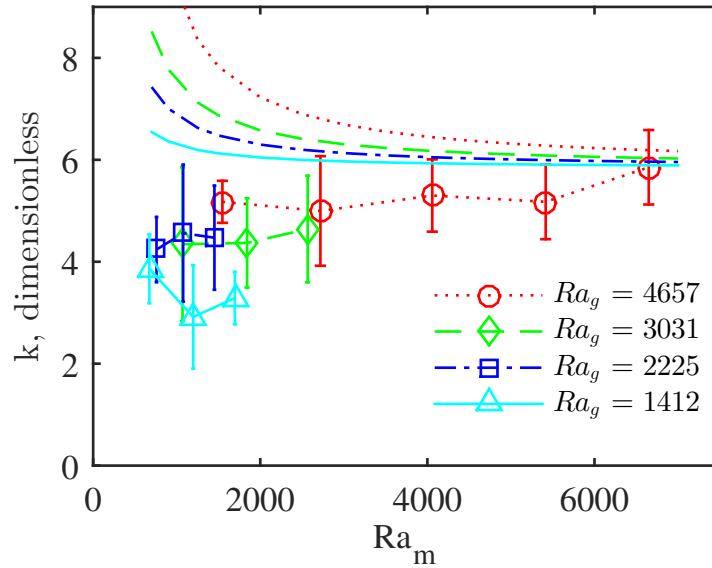
4.2. Figure: Comparison of the characteristic wave-number k between experimental and theoretical results as a function of the magnetic Rayleigh number Ra_m for several gravitational Rayleigh numbers Ra_g in a horizontal magnetic field. The experimental data is represented by markers with tracer lines and the theoretical data with smooth lines. The same value of Ra_g is represented by the same color. Red dotted lines correspond to magnetic fluid $D107_{100\%}$ (Ra_g= 4657), green dashed lines to $D107_{66\%}$ (Ra_g= 3031), blue dash-dotted lines to $D107_{50\%}$ (Ra_g= 2225) and cyan lines to the most diluted magnetic fluid $D107_{33\%}$ (Ra_g= 1412). *Fig.18. from [25]*.

All the results from the theoretical model are given considering perfectly sharp interface between the mixing fluids before the application of the magnetic field. Experimentally with the current setup it is impossible to create interface that is perfectly sharp, where the mixing before an experiment would be $\delta_0 = 0$. Experimentally the smearing time along the interface is different after Y junction in the micro-channel as the diffusion takes place. For example, for the slowest flow-rate $Q = 1 \ \mu l/min$ investigated in §3.1. average velocity in y-direction is $\overline{v} \approx 0.25$ mm/s if the width of the micro-channel is $w = 1$ mm. So, to cross the field of view that is $\Delta y = 2$ mm long $t \approx 8$ s long time period is necessary. In dimensionless units it is $t_0 = t \cdot D/h^2 \approx 0.03$. Therefore the smearing time ranges from 0 to this value in this microfluidics chip.

A study in a similar system of magnetic micro-convection [62] has showed analytically that the wave-number k describing the instability decreases if the initial smearing parameter t_0 is increased. This could be one aspect that explains the differences between the theoretical and experimental results in fig. 4.2.. However experimental results in §3.3., where δ_0 effects on the instability were investigated, were inconclusive whether λ is affected by initial smearing. due to high data dispersion. The experiments carried out with magnetic fluid KTF11-1 (see tab. 3.2.) confirmed that λ increases if δ_0 increases. For other magnetic fluids (see tab. A1.) the data dispersion was too big for conclusions.

4.2. Comparison between experimental results with initially stagnant fluids and theoretical predictions

Here the results of the experiments with initially stagnant fluids described in §3.2. are compared with theoretical predictions from linear stability analysis and numerical simulations carried out by colleagues. Here the theoretical model (carried out by colleagues) was improved as a system of three liquid layers with isotropic initial magnetic particle concentration was investigated by the linear analysis. This system matches the experimental reality better than the step-like situation with two layers described in previous section §4.1., as experimentally in the experimental setup used here, there always is a premixed layer of both fluids when starting an experiment. The development of the micro-convection was calculated using Brinkman model and investigating the stability on both borders between two phases of liquids.

The nature of the micro-convection qualitatively agrees between experiments and numerical simulations as can be noted from figure 4.3. where the magnetic micro-convection is explored numerically for several values of Ra_g and Ra_m at a certain moment in the experiment.
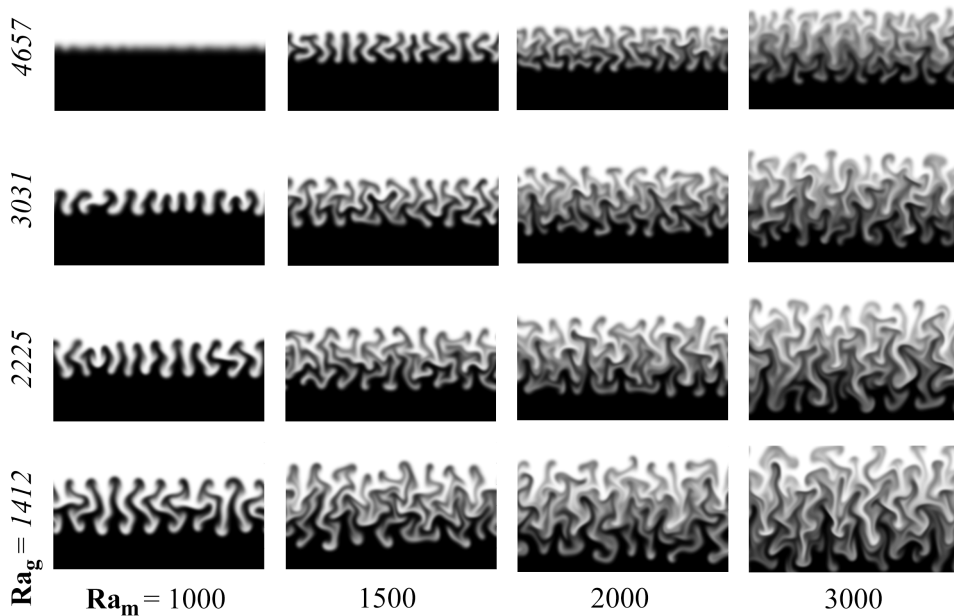
4.3. Figure: The concentration images of the numerical simulations (carried ut by A. Tatuļčenkovs) of the magnetic micro-convection for experiments with initially stagnant fluids for various gravitational Ra_g and magnetic Rayleigh Ra_m numbers for a dimensionless time $t = 0.015$, the geometric and initial time parameters: $L_x = 10$, $L_y = 20$, $t_0 = 0.0033$.

Both in numerical simulations and experiments the fingers of the instability appear after applying magnetic field stronger than the critical one H_c. They grow until they reach some maximal height. After emerging, fingers have uniform height and they tend to bend

and branch if the magnetic field is strong enough until the mixing has reached a stage when they remain stationary and only diffusion takes place.

The mixing length due to the micro-convection δ_{MC} is obtained similarly from both experimental data and simulations. The comparison of mixing enhancement by the magnetic micro-convection of experimental and numerical data is shown in figure 4.4.. Here the experimental results are converted to dimensionless quantities and expressed using markers. The lines correspond to the results from numerical simulations. The same color is used to describe the experiments with the same gravitational Rayleigh number. For example the red circles describing experimental results with magnetic fluid $D107_{100\%}$ correspond to the red dotted line that describes the numerical simulation results for $Ra_g = 4657$.
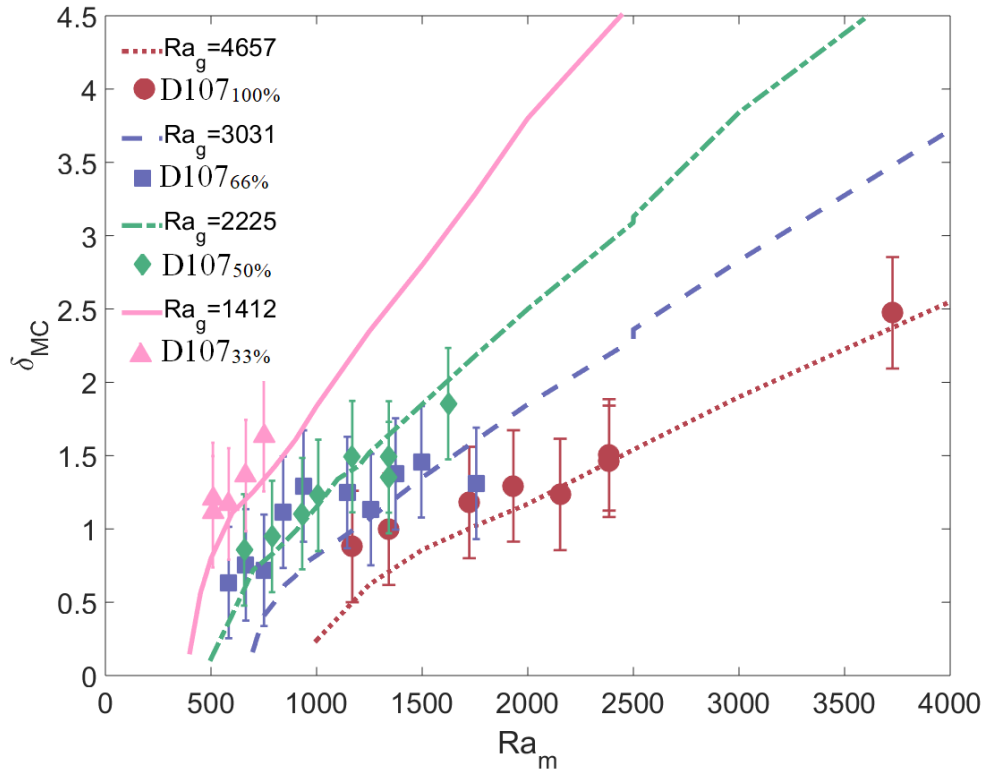
4.4. Figure: Comparison for experimental data with numerical simulation for δ_{MC} as a function of Ra_m. The numerical simulations are shown as lines, with the same color of the corresponding experiment. The error-bars characterize the precision of the experimental setup, as well as initial smearing of the interface.

The nature of the numerical and experimental results qualitatively seem the same. The results agree especially well for magnetic fluids $D107_{100\%}$, $D107_{50\%}$ and $D107_{33\%}$ within the margin of the error. As the $Ra_m \sim \chi^2$ experimentally the values of Ra_m are more restricted for diluted fluids, as by diluting the magnetic fluids its magnetic susceptibility decreases as well. The more diluted the original magnetic fluid, the smaller the value of Ra_m for the same external magnetic field H. Gravity plays a larger role for the denser

(higher Ra_g) fluids, by restricting δ_{MC}.

As described earlier due to the initial interface fluctuation after turning off the syringe pumps an average initial smearing $\overline{\delta_{t=0s}} = 0.08 \pm 0.02$ mm is created. The initial smearing might be considered as a diffusion happening for some time. That way calculating to time $\delta_{t=0s}$, using equation 1.19 the value $t_0 = 29 \pm 14$ s is found. By converting the result to a dimensionless quantity the value $t_0 = 0.10 \pm 0.05$ is obtained.

A numerical simulation for mixing with magnetic micro-convection with various initial smearing parameters are visually demonstrated in figure 4.5.. Here the instability is simulated with different values of initial smearing (from $t_0 = 0.075$ till $t_0 = 0.135$) and an image of an experiment with $\delta_0 = 0.094$ mm (which corresponds to the dimensionless initial smearing time parameter $t_0 = 0.073$) is added in the bottom right corner for comparison. Experimentally the fingers appear at $t = 2.1$ s. In the numerical simulation the fingers become visible at $t = 4.7$ s (dimensionless time $t = 0.016$) for the sharpest initial interface with initial smearing parameter $t_0 = 0.075$. But in the simulation with the largest initial smearing $t_0 = 0.145$ the fingers start to form only at $t = 9$ s (dimensionless time $t = 0.029$) as it is visible in fig. 4.5.b.

The instability emerges earlier if the premixed layer of both fluids is thinner. The initial smearing between the fluids affects not only the rate of the instability but also the form of the fingers. This observation agrees with the experimental results in §3.3. where δ_0 effects on magnetic micro-convection are explored.

For example, in fig. 4.5.c it is demonstrated that the fingers grow out straight and stay that way till the end of the experiment if the initial smearing value is larger ($t_0 = 0.145$, second image from the right on the second row). But if the interface between the fluids is sharper ($t - 0 = 0.075$), then with the same magnetic fluid and in the same magnetic field the fingers may even branch (first image from the left on the first row). In the numerical simulations the height of the fingers seems visually the same at the end of the experiments (see fig. 4.5.c). Results in §3.3. also show that initial smearing restricts the evolution of different (straight $\to$ wavy $\to$ branched) forms of micro-convective fingers.

The average wavelength of the instability experimentally was found $\overline{\lambda} = 0.12 \pm 0.02$ mm. This value agrees with the experimentally found wavelength in the experiments with flowing fluids, where $\overline{\lambda_{\text{flow}}} = 0.15 \pm 0.05$ mm was found for concentrated magnetic fluid D107$_{100\%}$ and slightly larger values for other dilutions. In experiments with horizontal magnetic chip described in [53] for the same magnetic fluid also $\lambda_{\text{hor}} = 0.15$ mm was found. Results from §3.3. with initially smeared interface for magnetic fluid D107$_{66\%}$ also agree within error with value: $\lambda_{\text{smeared}} = 0.16 \pm 0.04$ mm. Recalculating λ obtained from the experiments with initially stagnant fluids to dimensionless wave-number value $\overline{k_{\text{exp}}} = 7.3 \pm 1.0$ is obtained, which agrees with theoretical predictions. As it does not seem to be dependent on the dilution ratio of the magnetic fluid it also does not seem to be dependent on Ra_g.
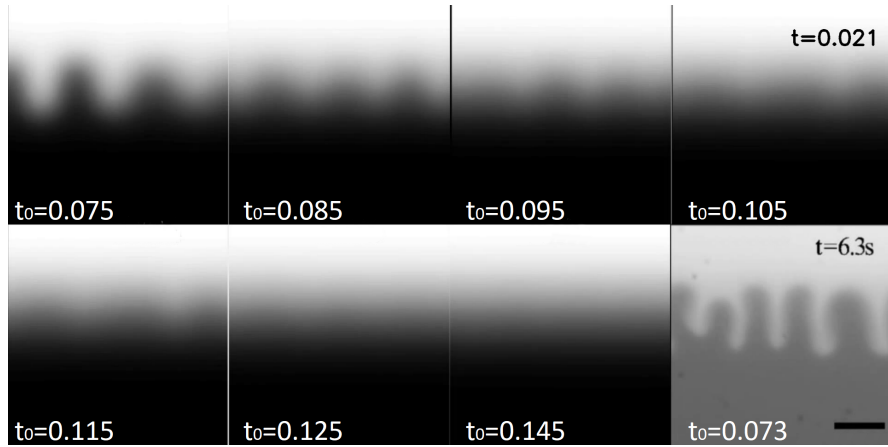
(a) $t = 6.3$ s or dimensionless $t = 0.021$
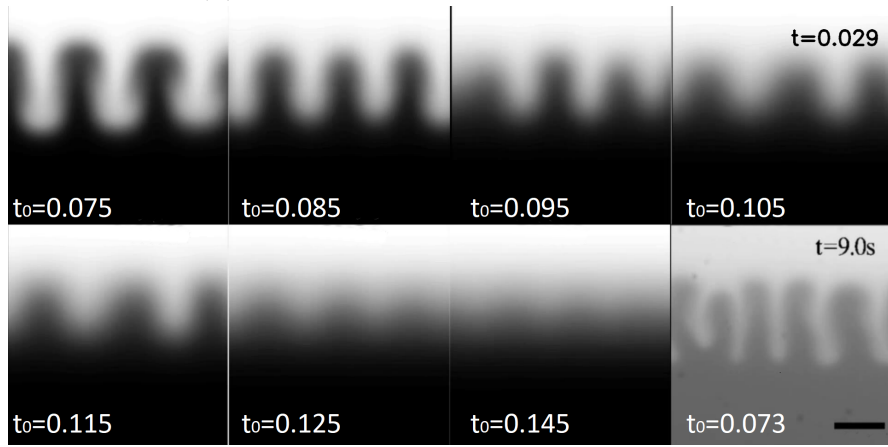
(b) $t = 9.0$ s or dimensionless $t = 0.029$
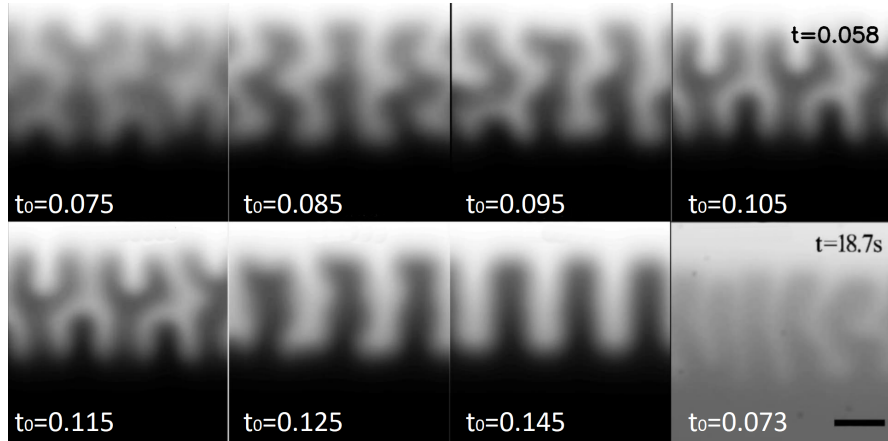
(c) $t = 18.7$ s or dimensionless $t = 0.058$

4.5. Figure: Magnetic micro-convection development for various initial smearing parameters t_0. Compariosn between numerical simulations and experiment (lower right frame). Magnetic fluid: D107$_{100\%}$, Ra$_g$= 4657, $H = 50$ Oe, Ra$_m$= 1705. The scale bar is 0.1 mm long.

Critical values of the magnetic field are compared between experiments from §3.1. and §3.2. and numerical simulations. Experimental values of the critical magnetic field H_c ore converted to magnetic Rayleigh numbers Ra$_m$. As it is impossible to carry out an

experiment without an initial smearing with the current experimental system, the critical Ra_m values for the instability to emerge from numerical simulations for various initial smearing parameters t_0 are included. If the initial smearing is bigger, the critical value of Ra_m increases. The comparison is collected in table 4.3.. There is a good agreement of the critical Ra_m values between the experimental data and the simulations within this study as the average initial smearing $\overline{\delta_{t=0s}} = 0.08$ mm experimentally converts to the $t_0 = 0.1$ in the simulations. The critical values of Ra_m and H_c are affected by the gravity effects (Ra_g). The magnetic Rayleigh number Ra_m must be higher in order to start the fingering instability for the experiments with higher Ra_g.

Source	$D107_{100\%}$ $Ra_g= 4657$	$D107_{66\%}$ $Ra_g= 3031$	$D107_{50\%}$ $Ra_g= 2225$	$D107_{33\%}$ $Ra_g= 1412$
Numerical simulation $t_0 = 0.001$	662	477	360	250
Numerical simulation $t_0 = 0.0033$	687	487	364	255
Numerical simulation $t_0 = 0.01$	725	499	382	263
Numerical simulation $t_0 = 0.1$	1085	733	554	374
Analytically [25]	655	458	355	246
Estimated experimentally in §3.1.	775 (35 ± 2 Oe)	473 (41 ± 1 Oe)	395 (50 ± 2 Oe)	328 (69 ± 2 Oe)
Experiments in §3.2.	1170 ± 170 (41.4 ± 1.5 Oe)	598 ± 85 (44.4 ± 1.5 Oe)	596 ± 80 (59.1 ± 1.5 Oe)	473 ± 55 (79.8 ± 1.5 Oe)

4.3. Table: The critical values of Ra_m (and H_c for experiments) for the magnetic micro-convection to emerge.

Values of the critical magnetic field for initially stagnant fluids H_c obtained in §3.2. are slightly higher than the ones estimated in §3.1. where H_c was considered as a function of the velocity of the flow rate of the fluids and H_c for the situation of $Q = 0$ µl/min was found by a linear fit. The differences between the results may raise due to the present initial smearing in experiments collected in §3.2.. Also the fingers at H_c might be too small to notice by the current experimental setup. The interface between the fluids is much sharper if the fluids are being pumped as in §3.1., especially for stronger flow-rates. Thus even small fingers are contrasted and can be noticed easily with flowing fluids.

In §3.3. for experiments with initially smeared interface the critical magnetic field for magnetic fluid $D107_{50\%}$ if the initial interface between the fluids is sharp was estimated $H_c = 49$ Oe (see tab. 3.4.. This result is close with estimation from flowing fluid experiments. An interesting development of micro-convective mixing parameter δ_{MC} can

be observed if magnetic Rayleigh number Ra_m is divided with the critical value $\text{Ra}_{m,c}$ for numerical simulations and the magnetic field H divided with critical magnetic field H_c for experiments. As it is demonstrated in figure 4.6.. this relationship seems to be coinciding for all values of the used Ra_g. $\text{Ra}_{m,c}$ is proportional to H_c^2. Therefore the ratio H/H_c of the experimental results is squared. The experimental results arrange themselves around the results from the numerical simulations. The experiments are described using markers and lines are used for the numerical simulations. The same color is used to describe results with the same magnetic fluid. The vertical axis of the graph corresponds to the dimensionless mixing parameter due to magnetic micro-convection δ_{MC}. But the horizontal axis describes the ratios $\text{Ra}_m/\text{Ra}_{mc}$ for numerical simulations and $(H/H_c)^2$ for experimental results, and both of these axis coincide.

It is suspected that the critical values of the magnetic field and Ra_m include a significant information about the gravity effects on the development of the micro-convection. Therefore the gravity effect on δ_{MC} is excluded by these divisions.
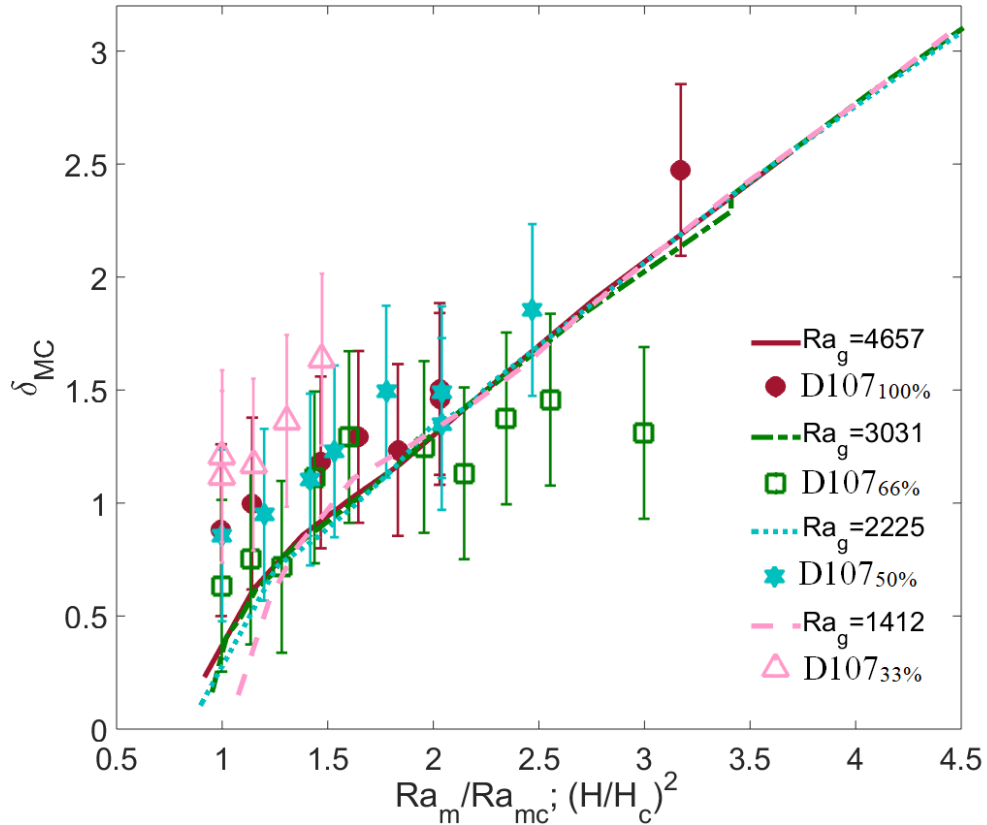
4.6. Figure: The development of dimensionless δ_{MC}. The numerical results are described with $\text{Ra}_m/\text{Ra}_{mc}$, but the experiments with $(H/H_c)^2$ - both of these axis coincide. The numerical simulations are shown as lines, with the same color as the corresponding experimental markers.

4.3. Comparison of the experimental results of the magnetic instabilities in horizontal and vertical magnetic field

Here the results with initially smeared interfaced from §3.3. for experiments carried out in horizontal magnetic field are compared to experiments from §3.4. carried out in vertical magnetic field. The visual comparison between these instabilities is demonstrated in figures 4.7. and 4.8.. One column there represents a particular experiment in time.

(a) Horizontal magnetic field

H=65 Oe; δ_0=0.09 mm

(b) Vertical magnetic field.

H=65 Oe; δ_0=0.06 mm   H=65 Oe; δ_0=0.07 mm   H=65 Oe; δ_0=0.09 mm
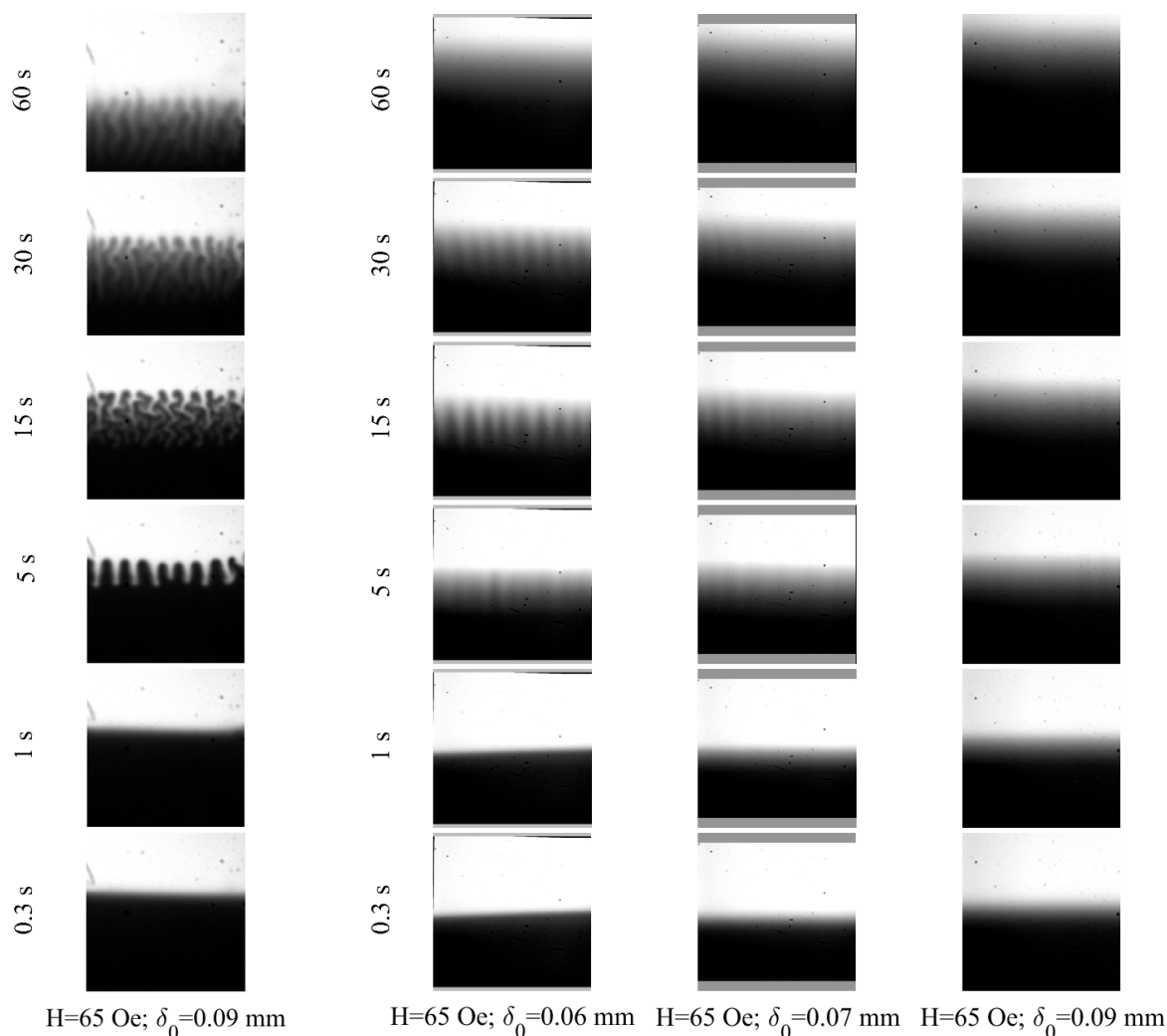
4.7. Figure: Comparison between horizontal and vertical magnetic field's $H = 65$ Oe effect on magnetic micro-convection in micro-channel with thickness $h_1 = 0.135$ mm. Magnetic fluid FF09-9$_{100\%}$. A single image represents 1×1 region.

In both magnetic field directions instability emerges only if a certain critical value of magnetic field H_c has been met. Fingers grow taller in stronger magnetic fields. And the instability is restricted by the initial smearing between the mixing fluids. For both directions of the magnetic field H_c values are greater for larger δ_0. H_c values are larger

for experiments in a vertical magnetic field for other experimental parameters matching. The shape of the instability fingers is affected by the direction of the external magnetic field. Fingers in horizontal magnetic field in high enough fields are wavy and even branch. Their tips have rounded shape. However, in a vertical magnetic field, the fingers of the instability grow out perfectly straight and their tips are sharp and pointy. In horizontal magnetic field the characteristic width of one finger is the same for all of the fingers during the experiment. In contrast, in vertical magnetic field, the fingers may split after some time, or tiny and thin fingers appear between the primary ones. Both in horizontal and vertical magnetic field the fingers stop growing, when they reach some maximal value. Though the mixing still happens as diffusion prevails.

H=48 Oe; δ_0=0.10 mm   H=65 Oe; δ_0=0.11 mm

(a) Horizontal magnetic field

H=48 Oe; δ_0=0.10 mm   H=65 Oe; δ_0=0.11 mm

(b) Vertical magnetic field.
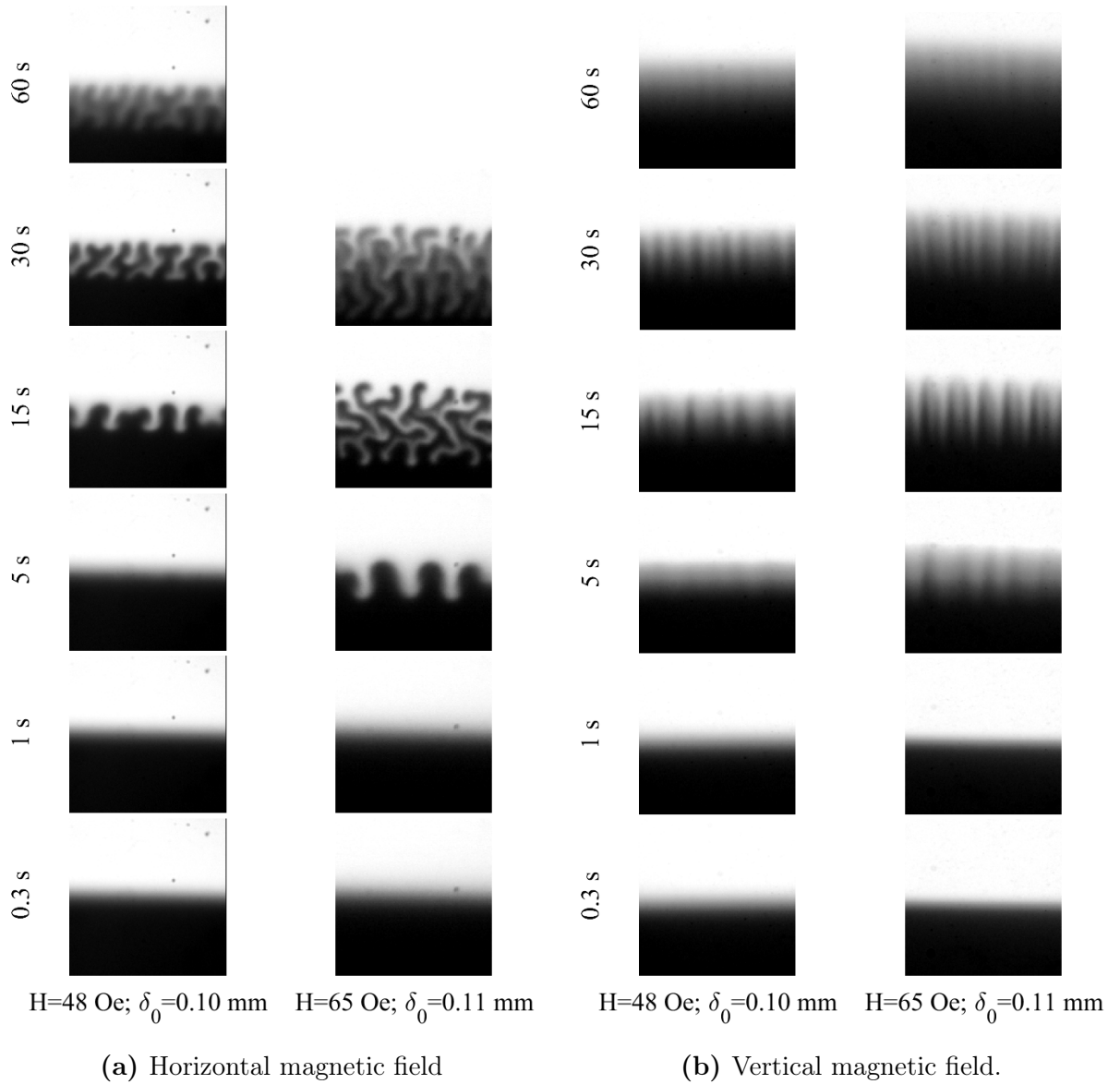
4.8. Figure: Comparison between horizontal and vertical magnetic field's effect on magnetic micro-convection in micro-channel with thickness $h_2 = 0.257$ mm. Magnetic fluid FF09-9$_{100\%}$. A single image represents mm1 × 1 region.

In figure 4.7. experiments with magnetic fluid FF09-9$_{100\%}$ in micro-channel with thickness $h_1 = 0.135$ mm are carried out in magnetic field $H = 65$ Oe. In a horizontal magnetic field (fig. 4.7.a) at $t = 5$ s in experiment prominent fingers are visible that later become wavy. In an experiment with the same $\delta_0 = 0.09$ mm in a vertical magnetic field (fig. 4.7.b) fingers are almost indistinguishable. After applying the magnetic field, the mixing length increased rapidly, but the finger structures are seldom and vague. Distinguishable fingers are visible only if $\delta_0 \leq 0.07$ mm.

In figure 4.8. experiments carried out in thicker micro-channel $h_2 = 0.257$ mm are presented. Here, in a horizontal magnetic field (fig. 4.8.a) the instability emerges earlier if the external magnetic field is stronger. At $t = 5$ s already prominent fingers have formed for stronger magnetic field $H = 65$ Oe, while in weaker magnetic field $H = 48$ Oe the instability has not yet emerged. While in a vertical magnetic field (fig. 4.8.b) at $t = 5$ s the instability has emerged in both magnetic fields.

4.3.1. Mixing due to magnetic micro-convection with respect to magnetic field

Here micro-convective mixing δ_{MC} with respect to magnetic field value is explored. An example of results is demonstrated in figure 4.9. for magnetic fluid KTF11-1$_{100\%}$ in micro-channel with thickness $h_1 = 0.135$ mm. Additional results are collected in Appendix §A.1.5. The results are grouped by initial smearing δ_0. The same δ_0 is represented by the same marker shape. The color of the markers becomes lighter as the value of δ_0 increases. Experiments carried out in a horizontal magnetic field are represented by red markers, while green ones are for experiments carried out in a vertical magnetic field.
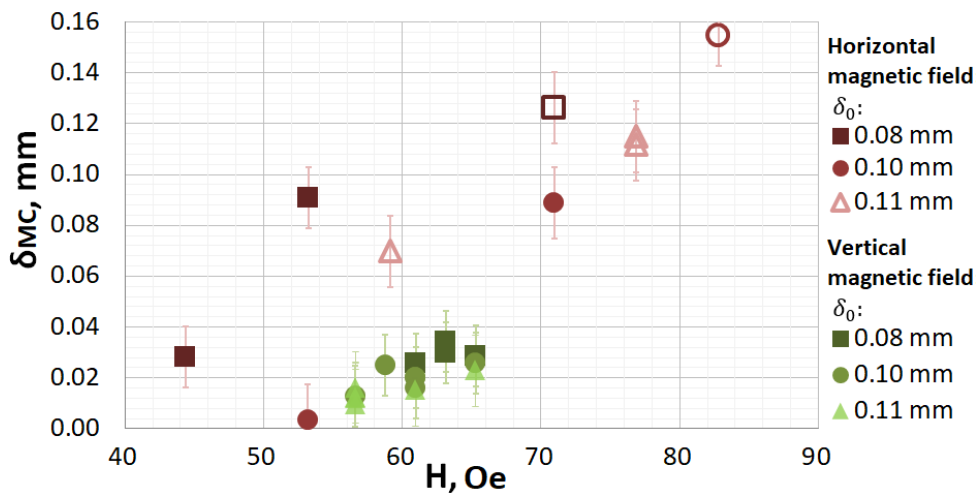
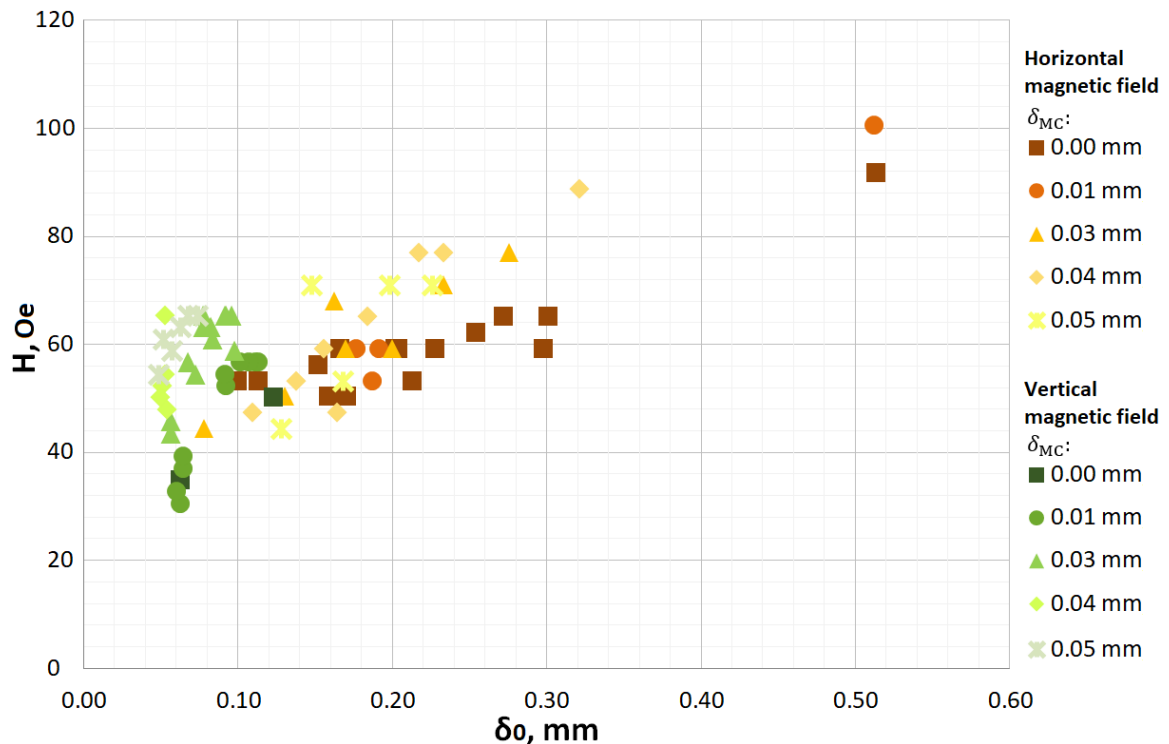**4.9. Figure:** Comparison between horizontal and vertical magnetic field's effect on magnetic micro-convection δ_{MC} with respect to magnetic field for various δ_0 in a micro-channel with thickness $h_1 = 0.135$ mm. Magnetic fluid: KTF11-1$_{100\%}$. Empty markers represent δ_{MC} obtained with attachment method.

Greater δ_{MC} values are achieved in horizontal magnetic field. This is true for both explored micro-channel thicknesses ($h_1 = 0.135$ mm, $h_2 = 0.257$ mm) for all investigated magnetic fluids. Differences in obtainable δ_{MC} for the same magnetic field intensity between horizontal and vertical magnetic field direction are larger if the initial smearing between the mixing fluids is smaller. A factor that might enhance the mixing in a horizontal magnetic field, is that fingers are not stationary— they tend to branch and mix. And if the δ_0 is smaller the finger character in the horizontal magnetic field is more active. The rate at which δ_{MC} increases as the value of magnetic field is increased is the same for both directions of magnetic field. The difference between the direction of the magnetic field with respect to δ_{MC} is smaller in thickest micro-channel ($h_2 = 0.257$ mm).

4.3.2. Mixing due to magnetic micro-convection with respect to initial smearing thickness

Here δ_{MC} with respect to initial smearing thickness is explored. An example of graphical results is demonstrated in figure 4.10. for magnetic fluid FF09-9$_{100\%}$ in micro-channel with thickness $h_1 = 0.135$ mm. Additional results are collected in Appendix §A.1.5. The results are grouped by the value of the external magnetic field. The same value of magnetic field is represented by the same marker shape. The color of the markers becomes lighter as the value of H increases. The experiments in horizontal magnetic field are represented by blue markers, while orange markers are for the experiments in a vertical magnetic field.
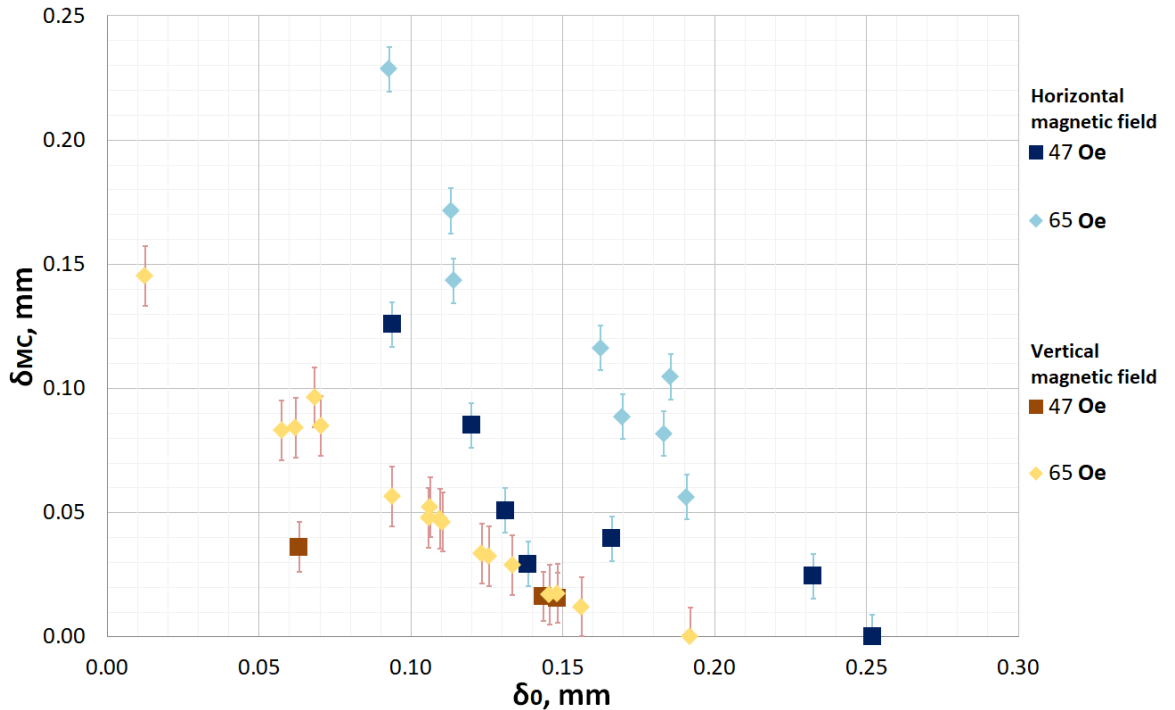
4.10. Figure: Comparison between horizontal and vertical magnetic field's effect on magnetic micro-convection. δ_{MC} with respect to δ_0 for various magnetic fields for magnetic fluid FF09-9$_{100\%}$ in micro-channel with thickness $h_1 = 0.135$ mm.

All experimental results agree, that greater values of δ_{MC} can be obtained if mixing is carried out in a horizontal magnetic field. Due to data dispersion it is not possible to conclude whether the difference in δ_{MC} between horizontal and vertical magnetic fields for the same values of δ_0 is affected by magnetic field intensity.

4.3.3. Magnetic field intensity to obtain a specific micro-convective mixing

Here the magnetic field values in order to obtain a specific micro-convective mixing length δ_{MC} are explored. The results between horizontal and vertical magnetic field are compared. An example of results is demonstrated in figure 4.11. for magnetic fluid KTF11-1$_{100\%}$ in micro-channel with thickness $h_1 = 0.135$ mm. Additional results are collected in Appendix §A.1.5. Results of magnetic field with respect to initial smearing δ_0 arranged by δ_{MC} values are reviewed. The results with the same δ_{MC} are represented by the same marker shape per graph. The color of the markers becomes lighter as the values of δ_{MC}increase. Experiments carried out in a horizontal magnetic field are represented by orange markers, while experiments carried out in a vertical magnetic field are represented by green ones.

The results show, that for the same values of δ_0 stronger magnetic field must be applied to create the same amount of δ_{MC} if the applied magnetic field is vertical.

4.11. Figure: Comparison between horizontal and vertical magnetic field's effect on magnetic micro-convection. What value of H must be applied to obtain certain δ_{MC} (denoted in legend) with respect to δ_0 for magnetic fluid KTF11-1$_{100\%}$ in micro-channel with thickness $h_1 = 0.135$ mm.

4.4. Comparison of the results in a vertical magnetic field with data from literature

Here the comparison between experimental results of this thesis reviewed in §3.4. and a studies [6, 39] are carried out.

The study [39] carried out by K. Ērglis and his colleagues investigates magnetic instability in a horizontally placed microfluidics chip, where external magnetic field is vertical, perpendicular to the microfluidics chip. Experimentally grainy structure was observed there that was caused by a normal field instability as the denser magnetic fluid was slipping underneath water. A theoretical model for the case of a normal-field instability between miscible fluids for a case with infinite vertical direction is investigated there. In the experiments carried out there the wavelength of the normal-field instability caused structure is 20 μm. For all experiments in vertical magnetic field carried out within this thesis the scale of wavelength is $\lambda \approx 0.1$ mm as collected in table 3.6.. In [39] characteristic scale of the wave-number is set as $(\Delta\rho/(D\eta))^{1/3}$, where D is a diffusion coefficient, $\Delta\rho$ is a density difference between the mixing fluids, η is the viscosity of the mixing fluids and g is standard gravity. The characteristic wave-number (dimensionless) in [39] is estimated to be $k = (3/32)^{1/3}$. Using these relations the wavelength values λ^* according to the theory carried out in [39] are compared with the experimental ones λ obtained within this thesis in table 4.4.. It must be noted, that the theory in [39] was carried out for infinite layer, while in this thesis the experimental system is confined. Experimental λ values are approximately two times larger, than the ones theoretically estimated. Also, it must be noted, that experimentally, the primary vivid fingers were counted as described in §3.4.. If the secondary narrow fingers would be included in λ expression, the experimental values of would be even closer to the theoretically estimated λ^*.

| | $h_1 = 0.135$ mm | | $h_1 = 0.257$ mm | | | | |
	$D107_{100\%}$	FF21-5	$D107_{100\%}$	KTF11-1$_{100\%}$	FF09-9$_{100\%}$	FF09-9$_{66\%}$	FF09-9$_{50\%}$
λ, mm	0.09	0.10	0.08	0.11	0.10	0.14	0.12
λ^*, mm	0.05	0.02	0.05	0.04	0.05	0.06	0.06

4.4. Table: Comparison of the wavelength values obtained experimentally and using theory from [39].

The study [6] carried out by M. S. Krakov and his colleagues investigates magnetic instability in a vertical magnetic field. There kerosene based miscible fluids were investigated. The magnetic fluid contained magnetite nano-particles stabilized with oleic acid. The thickness of the microfluidcs chip used in [6] 0.19 mm is comparable with the ones used for experiments in vertical field within the study. Also similar as in the study of this thesis, in the study by Krakov *et al.* it was discovered that after the primary peaks have

formed, smaller satellites appear between them. The numerical simulations reveal that an upward flow forms in the centre of the main peaks, and a downward one forms along the diffusion front on the outer side of the peaks. This downward flow creates numerous secondary vortexes as it breaks up into secondary flows when reaching the bottom of the container. One to three secondary peaks might appear between two primary ones and over time they would disappear due to diffusion. The similar effect was observed in experiments within this thesis, however the visual splitting of the fingers might also appear if the fingers are emerging in several rows as it is explained in §3.4.. The finger formation in several rows, although not proposed in [6], seems plausible also due to the size of the characteristic $\lambda \approx 0.1$ mm, as micro-channels with thicknesses $h_1 = 0.135$ mm and $h_2 = 0.257$ mm were used here. Also the study by Krakov *et al.* showed that wavelength of the instability decreases with increasing magnetic field and magnetic Rayleigh number $\mathrm{Ra_m}$. The wavelength determination within this thesis was inconvenient as the fingers were "shifting", but qualitatively such relationship was not observed here.

Similar as in the study of this work, the study by Krakov *et al.* also investigated the effect of the initial smearing thickness between the mixing fluids on the instability. The simulations also revealed that with an increase in the initial width of the diffusion layer, the wavelength of unstable perturbations increases almost linearly. Therefore it was concluded in the study that the investigated instability is different from the Rosensweig's normal-field instability as then the wavelength of the instability should decrease. However, within this thesis the results show that characteristic λ of the instability is not affected by δ_0.

Unlike in the experiments in the study of this thesis where both mixing fluids occupied approximately equal parts of the micro-channel, within the study by Krakov *et al.* the thickness of the kerosene (non-magnetic upper fluid) layer was always much greater than the thickness of the magnetic fluid layer in the microfluidics chip. The experimental study by Krakov *et al.* reveals that this ratio of layer thicknesses have effect on the wavelength of the instability. It was found that λ decreases if the layer of the magnetic fluid is smaller.

4.5.   Possible future directions

Here the possible experiments that might compliment this thesis are listed.

Magnetic field effect on magnetic micro-convection could be explored in experiment where the interface smearing between the fluids gradually increases within the same micro-channel. This could be achieved by tilting the microfluidics chip after it has been filled with fluids for experiments with initially stagnant fluids. Or this could be achieved with experimental system with long Y-shaped channels, small fluid flow and large ROI. Therefore the interface would start to diffuse once the fluids meet in the micro-channel and the interface smearing would be smaller near the Y-junction but larger near the outlet

of the channel. This way it would be visible within one experiment whether the total mixing length is the same all over the interface once the fingers of the instability have reached their maximal length.

The instability in vertical magnetic field could be explored more, to determine whether the fingers are appearing in several rows. And if it is so, how the thickness of the micro-channel limits this.

4.6. Summary

Within the Discussion experimental data conversion to dimensionless quantities were carried out. The experiments were compared with the results of linear stability analysis and numerical simulations carried out by colleagues and literature.

The theoretical model considered in [25] confirmed experimental observations that the gravitational force stabilizes the magnetic micro-convection. The critical values of Ra_m and H_c are affected by the gravity effects (Ra_g). The magnetic Rayleigh number Ra_m must be higher in order to start the fingering instability for the experiments with higher Ra_g. Both in numerical simulations and experiments the fingers of the instability appear after applying magnetic field stronger than the critical one. H_c for initially stagnant fluids with sharp interface was estimated with various methods within this thesis and they all qualitatively agree with each other and numerical simulations. It is suspected that the critical values of the magnetic field and Ra_m include a significant information about the gravity effects on the development of the micro-convection.

Also numerical simulations agree with the experimental ones that initial smearing restricts the evolution of different forms of micro-convective fingers.

The characteristic λ of the instability in a horizontal magnetic field was broadly explored. The results of λ value obtained within this thesis from several types of experiments (with either flowing, initially stagnant or initially smeared fluids) are consistent with numerical simulations and literature [53]. Experimental results of this thesis results agree with [62] theoretical predictions that characteristic λ of the instability in a horizontal magnetic field increases if initial smearing thickness δ_0 is increased.

Greater mixing due to magnetic micro-convection can be achieved in horizontal magnetic field than in vertical one. One factor that might enhance the mixing in a horizontal magnetic field, is that fingers in a horizontal magnetic field have more active character.

Both in a horizontal magnetic field and in a vertical magnetic field the instability emerges in magnetic field larger than some critical one and the fingers reach some maximal height and then stop growing.

CONCLUSIONS

Here the conclusions from the experimental results if this Thesis together with corresponding theoretical predictions are arranged in four groups according to the four main experimental sections (§3.1., §3.2., §3.3. and §3.4.) of this work.

Generally, the results show that gravity limits the mixing of both fluids and the effect of magnetic micro-convection is restricted by the thickness of pre-mixed layer of fluids. Initial parameters of the experiment can be manipulated by geometry of the micro-channel. The experimental results of the characteristic size of the instability and critical magnetic fields showed good agreement with the theoretical predictions carried out by colleagues and literature review. The dynamics of the magnetic micro-convection over various experimental parameters was explored. The properties of magnetic fluids significantly affect the mixing dynamic: if susceptibility and nano-particle concentration of the magnetic fluid decreases, the mixing due to micro-convection also decreases. All three hypothesis proposed at the beginning of this work are qualitatively confirmed.

Flowing fluids in Y-shaped micro-channel

During this part of the study it was showed that gravitational effects can be important even for microscopic systems with small density differences. Especially for this experimental system where gravitational Rayleigh numbers Ra_g were quite large due to the size of the microfluidics chip used ($h_1 = 0.135$ mm) and notable density difference between the used magnetic fluids and water. It was demonstrated experimentally how gravity and fluid flow stabilize the fingering instability of magnetic-microconvection in a vertical channel. The maximal height of the fingers decreased if the flow-rate of the fluids was increased and higher values of critical magnetic Rayleigh number Ra_m are necessary in order to induce the instability for higher values of gravitational Rayleigh numbers Ra_g.

The experimental results of the critical magnetic field and the characteristic size of the instability were in good agreement with theoretical model of magnetic micro-convection, based on the Brinkman equation.

Initially stagnant fluids

Within this part of the study the magnetic micro-convection was successfully observed experimentally for initially stagnant mixing fluids. It was showed experimentally that gravity limits the micro-convection, by restricting the mixing length due to the micro-convection δ_{MC}. This agrees with the numerical simulations and linear stability analysis results. The experiments and numerical simulations agreed both qualitatively and quantitatively.

The experimental results of micro-convective mixing as a relationship of δ_{MC} with respect to Ra_m show a good quantitative and qualitative agreement both with the numerical

simulations and with the linear analysis for all values of Ra_g in this study. δ_{MC} is smaller for higher values of Ra_g for the same values of Ra_m. Thus demonstrating that gravity limits the magnetic micro-convection.

The results of the critical magnetic fields show good agreement between the experiments carried out by flowing and initially stagnant fluids. The experimental results show good agreement with numerical simulations as well. Smaller Ra_m values are necessary in order to induce the magnetic micro-convection in the experiments with smaller values of Ra_g.

Initially smeared interface between the fluids

Magnetic micro-convective mixing is restricted by the amount of initial smearing. The experimental results and numerical simulations showed that critical values of Ra_m and magnetic fields accordingly are higher if the thickness of the premixed layer is greater. Initial smearing restricts the evolution of different forms of micro-convective fingers. Also initial smearing affects the characteristic size of the instability. The characteristic wavelength of the instability increases if the initial smearing is increased. The characteristic wavelength of the instability is also affected by the thickness of the micro-channel— the wavelength increases in thicker micro-channels.

The total mixing length that consists of micro-convective mixing and diffusive mixing can be achieved by a specific value of external magnetic field and does not depend on the thickness of the pre-mixed layer between the fluids if the mixing is carried out in a horizontal magnetic field. Also, there is an agreement between the magnetic field value to create a certain micro-convective mixing length and the critical magnetic field for a the initial smearing thickness, which is the same as desired convective mixing length with initially sharp interface.

Instability in a vertical magnetic field

Instability appears at the same time, regardless of the strength of the external magnetic field applied that is higher than the critical magnetic field for the instability to emerge.

Dimensionless analysis shows that the instability is restricted by gravity as the same gain of Ra_m causes grater gain of micro-convective mixing in thinner micro-channel, where Ra_g is smaller. Dimensionally larger amount of micro-convective mixing was archived in thicker micro-channel.

Greater mixing due to magnetic micro-convection in the same magnetic field intensity can be achieved in horizontal magnetic field than in vertical one for the same amount of initial smearing between the fluids.

The characteristic wavelength of the instability explored within this experimental setup is not affected by initial smearing. The fingers tend to spit and shift during the experiment in a way that suggests the finger forming in several rows.

BIBLIOGRAPHY

[1] R. E. Rosensweig, *Ferrohydrodynamics*, Dover Publications, **2018**.

[2] E. Blums, A. Cebers, M. M. Maiorov, *Magnetic Fluids*, De Gruyter, **1997**.

[3] J.-C. Bacri, R. Perzynski, D. Salin, *Endeavour* **1988**, *12*, 76–83.

[4] C. Flament, G. Pacitto, J.-C. Bacri, I. Drikis, A. Cebers, *Physics of Fluids* **1998**, *10*, 2464–2472.

[5] I. M. Coutinho, J. A. Miranda, *Physics of Fluids* **2020**, *32*.

[6] M. S. Krakov, A. R. Zakinyan, A. A. Zakinyan, *Journal of Fluid Mechanics* **2021**, *913*.

[7] M. Maiorov, A. Cēbers, *Magnetohydrodynamics* **1983**, *19*, 376–380.

[8] M. Maiorov, A. Cēbers, *Magnetohydrodynamics* **1980**, *16*, 21–27.

[9] B. Delmotte, M. Youssef, S. Sacanna, A. Donev, P. Chaikin, *Nature Physics* **2017**, *13*, 375–379.

[10] M. Shliomis, *Soviet Physics - Uspekhi* **1974**, *17*, 153–169.

[11] N. Convery, N. Gadegaard, *Micro and Nano Engineering* **2019**, *2*, 76–91.

[12] K. Oh, *Micromachines* **2017**, *8*, 343.

[13] N.-T. Nguyen, Z. Wu, *Journal of Micromechanics and Microengineering* **01/2005**, *15*, 1.

[14] X. Chen, L. Zhang, *Microchim Acta* **2017**, *184*, 3639–3649.

[15] C.-Y. Lee, C.-L. Chang, Y.-N. Wang, L.-M. Fu, *International journal of molecular sciences* **2011**, *12*, 3263–87.

[16] C.-Y. Chen, *Physics of Fluids* **2003**, *15*, 1086–1089.

[17] C. Derec, P. Boltenhagen, S. Neveu, J.-C. Bacri, *Magnetohydrodynamics* **2008**, 135–142.

[18] H. Li, C.-Y. Kao, C.-Y. Wen, *Journal of Fluid Mechanics* **2018**, *836*, 374–396.

[19] V. F. M. B. M. Berkovsky, M. S. Krakov, **1993**, *337*, 243.

[20] Q. A. Pankhurst, J. Connolly, S. K. Jones, J. Dobson, *Journal of Physics D: Applied Physics* **2003**, *36*, R167.

[21] J. P. Bullivant, S. Zhao, B. J. Willenberg, B. Kozissnik, C. D. Batich, J. Dobson, *International Journal of Molecular Sciences* **2013**, *14*, 17501–17510.

[22] T. E. Videbæk, S. R. Nagel, *Physical Review Fluids* **2019**, *4*, 033902.

[23] I. M. Coutinho, J. A. Miranda, *Physical Review Fluids* **2020**, *5*.

[24] Y. Z. Sinzato, F. R. Cunha, *Applied Mathematical Modelling* **2019**, *75*, 572–588.

[25] G. Kitenbergs, A. Tatuļčenkovs, L. Puķina, A. Cēbers, *The European Physical Journal E.* **2018**, *41*, 138.

[26] L. Puķina-Slava, A. Tatuļčenkovs, A. Cēbers, G. Kitenbergs, *arXiv:2310.15323* **2023**.

[27] R. T. Birge, *American Journal of Physics* **1934**, *2*, 41–48.

[28] N. Carron, *arxiv.org/abs/1506.01951* **2015**.

[29] G.-R. F. José, *Complex fluid-flows in microfluidics*, Springer, **2018**.

[30] S. Grebenyuk, A. R. Abdel Fattah, M. Kumar, B. Toprakhisar, G. Rustandi, A. Vananroye, I. Salmon, C. Verfaillie, M. Grillo, A. Ranga, *Nature Communications* **2023**, *14*.

[31] C. Hou, Y. Gu, W. Yuan, W. Zhang, X. Xiu, J. Lin, Y. Gao, P. Liu, X. Chen, L. Song, *Materials Today Bio* **2023**, *19*.

[32] P. Lakhera, V. Chaudhary, B. Bhardwaj, P. Kumar, S. Kumar, *Biosensors and Bioelectronics: X* **2022**, *11*.

[33] C. D. Chin, V. Linder, S. K. Sia, *Lab on a Chip* **2007**, *7*, 41–57.

[34] X. Zhang, Y. Zhang, W. Guo, S. Jiao, X. Liu, *Chemosensors* **2023**, *11*.

[35] D. S. Dkhar, R. Kumari, S. J. Malode, N. P. Shetti, P. Chandra, *Journal of Pharmaceutical and Biomedical Analysis* **2023**, *223*.

[36] G. M. Whitesides, *Nature* **2006**, *442*, 368–373.

[37] T. M. Squires, S. R. Quake, *Reviews of Modern Physics* **2005**, *77*, 977–1026.

[38] W. Raza, S. Hossain, K.-Y. Kim, *Micromachines* **2020**, *11*.

[39] K. Erglis, A. Tatulcenkov, G. Kitenbergs, O. Petrichenko, F. Ergin, B. Watz, A. Cebers, *Journal of Fluid Mechanics* **2013**, *714*, 612–633.

[40] G. Kitenbergs, A. Tatulcenkovs, K. Erglis, O. Petrichenko, R. Perzynski, A. Cebers, *Journal of Fluid Mechanics* **2015**, *774*, 170–191.

[41] W. Yang, Y. Zhang, X. Yang, C. Sun, Y. Chen, *Journal of Nanoparticle Research* **2022**, *24*.

[42] R. Bailey, *Journal of Magnetism and Magnetic Materials* **1983**, *39*, 178–182.

[43] J. Philip, *Advances in Colloid and Interface Science* **2023**, *311*.

[44] M. Akimoto, Y. Morimoto, *Journal of Pharmacobio-Dynamics* **1982**, *5*, S–15.

[45] R. S. Newbower, *IEEE Transactions on Magnetics* **1973**, *9*, 447–450.

[46]   J. De Vicente, D. J. Klingenberg, R. Hidalgo-Alvarez, *Soft Matter* **2011**, *7*, 3701–3710.

[47]   P. Allia, G. Barrera, P. Tiberto, *Physical Review Applied* **2019**, *12*.

[48]   A. Wu, P. Ou, L. Zeng, *Nano* **2010**, *5*, 245–270.

[49]   R. Massart, *IEEE Transactions on Magnetics* **1981**, *17*, 1247–1248.

[50]   O. Petrichenko, PhD thesis, University of Latvia, **2014**.

[51]   E. Dubois, V. Cabuil, F. Boué, R. Perzynski, *Journal of Chemical Physics* **1999**, *111*, 7147–7160.

[52]   J. C. Thomas, *Journal of Colloid and Interface Science* **1987**, *117*, 187–192.

[53]   G. Kitenbergs, PhD thesis, University of Pierre and Marie Curie, University of Latvia, **2015**.

[54]   N. Farkas, J. A. Kramar, *Journal of Nanoparticle Research* **2021**, *23*.

[55]   P. Pusey, *Neutrons X-rays and Light: Scattering Methods Applied to Soft Condensed Matter* **2002**, 3–21.

[56]   P. A. Hassan, S. Rana, G. Verma, *Langmuir* **2015**, *31*, 3–12.

[57]   A. Einstein, *Investigations on the theory of the Brownian movement*, Dover Publications, Mineola, NY, **1956**.

[58]   J.-C. Bacri, R. Perzynski, D. Salin, V. Cabuil, R. Massart, *Journal of Magnetism and Magnetic Materials* **1986**, *62*, 36–46.

[59]   J.-C. Baci, R. Perzynski, D. Salin, J. Servais, *Journal de physique Paris* **1987**, *48*, 1385–1391.

[60]   E. L. Cussler, *Cambridge Series in Chemical Engineering: Diffusion: Mass Transfer in Fluid Systems*, 3rd ed., Cambridge University Press, **2009**.

[61]   B. S. Bokstein, M. I. Mendelev, D. J. Srolovitz, *Thermodynamics and kinetics in materials science*, Oxford University Press, **2005**.

[62]   M. Igonin, A. Cebers, *Physics of Fluids* **2003**, *15*, 1734–1744.

[63]   A. Cebers, *Magnetohydrodynamics* **1997**, *33*, 48–55.

[64]   A. Cēbers, *Magnetohydrodynamics* **1981**, *17*, 113–121.

[65]   D. P. Jackson, R. E. Goldstein, A. O. Cebers, *Physical Review E* **1994**, *50*, 298–307.

[66]   Y. A. Hassan, T. K. Blanchat, C. H. Seeley Jr, *Measurement Science and Technology* **1992**, *3*, 633–642.

[67]   R. Lindken, J. Westerweel, B. Wieneke, *Experiments in Fluids* **2006**, *41*, 161–171.

[68]   A. Prasad, *Experiments in Fluids* **2000**, *29*, 103–116.

[69] S. T. Wereley, C. D. Meinhart, *Annual Review of Fluid Mechanics* **2010**, *42*, 557–576.

[70] F. G. Ergin, B. B. Watz, N. F. Gade-Nielsen, *Sensors (Switzerland)* **2018**, *18*.

[71] T. T. Al-Housseiny, P. A. Tsai, H. A. Stone, *Nature Physics* **2012**, *8*, 747–750.

[72] E. O. Dias, J. A. Miranda, *Physical Review E - Statistical Nonlinear and Soft Matter Physics* **2013**, *87*.

[73] I. Bischofberger, R. Ramachandran, S. R. Nagel, *Soft Matter* **2015**, *11*, 7428–7432.

[74] L. Dos Reis, J. A. Miranda, *Physical Review E - Statistical Nonlinear and Soft Matter Physics* **2011**, *84*.

[75] S. Jackson, H. Power, D. Giddings, D. Stevens, *Computer Methods in Applied Mechanics and Engineering* **2017**, *320*, 606–632.

[76] I. Bischofberger, R. Ramachandran, S. R. Nagel, *Nature Communications* **2014**, *5*.

[77] B. An, D. Solorzano, Q. Yuan, *Energies* **2022**, *15*.

[78] J. S. Hong, M. C. Kim, *International Journal of Heat and Mass Transfer* **2023**, *201*.

[79] C.-Y. Wen, C.-Y. Chen, D.-C. Kuan, S.-Y. Wu, *Journal of Magnetism and Magnetic Materials* **2007**, *310*, Proceedings of the 17th International Conference on Magnetism, e1017–e1019.

[80] C.-Y. Wen, C.-Y. Chen, D.-C. Kuan, *Physics of Fluids - PHYS FLUIDS* **2007**, *19*.

[81] M. Igonin, A. Cebers, *Journal of Magnetism and Magnetic Materials* **2002**, *252*, 293–295.

[82] M. Igonin, PhD thesis, Universite Paris 7 - Denis Diderot, **2004**.

[83] C.-Y. Chen, C.-Y. Wen, *Journal of Magnetism and Magnetic Materials* **2002**, *252*, 296–298.

[84] C.-Y. Chen, H.-J. Wu, L. Hsu, *Journal of Magnetism and Magnetic Materials* **2005**, *289*, 364–366.

[85] C.-Y. Chen, H.-J. Wu, *Physics of Fluids* **2005**, *17*, 042101–1–042101–8.

[86] C.-Y. Chen, W.-K. Tsai, J. A. Miranda, *Physical Review E - Statistical Nonlinear and Soft Matter Physics* **2008**, *77*.

[87] G. Kitenbergs, K. Ērglis, R. Perzynski, A. Cēbers, *Journal of Magnetism and Magnetic Materials* **2015**, *380*, 227–230.

[88] G. Kitenbergs, A. Cēbers, *Journal of Magnetism and Magnetic Materials* **2020**, *498*, 166247.

[89] C. Flament, S. Lacis, J.-C. Bacri, A. Cebers, S. Neveu, R. Perzynski, *Physical Review E - Statistical Physics Plasmas Fluids and Related Interdisciplinary Topics* **1996**, *53*, 4801–4806.

[90] A. Engel, H. Langer, V. Chetverikov, *Journal of Magnetism and Magnetic Materials* **1999**, *195*, 212–219.

[91] S. A. Lira, J. A. Miranda, *Physical Review E - Statistical Nonlinear and Soft Matter Physics* **2011**, *84*.

[92] M. S. Krakov, *Journal of Magnetism and Magnetic Materials* **2020**, *498*, 166186.

[93] F. G. Ergin, S. Tomas, C. Patrascu, *E3S Web of Conferences* **2019**, *85*.

[94] F. G. Ergin, B. B. Watz, K. Erglis, A. Cebers, *ASME 2010 10th Biennial Conference on Engineering Systems Design and Analysis* **2010**, *5*, 649–653.

[95] T. G. Mayerhöfer, S. Pahlow, J. Popp, *Chemphyschem : a European journal of chemical physics and physical chemistry* **2020**, *21*, 2029–2046.

[96] B. C. Smith, *Fundamentals of Fourier transform infrared spectroscopy, second edition*, 2nd ed., CRC Press, **2009**.

Appendix A

Additional Information

A.1 Additional Figures of the Experimental Results

Here additional experimental results that compliment the main text of this thesis are collected.

A.1.1 Magnetic micro-convection experiments with flowing fluids

Here additional experimental results that compliment §3.1. are reviewed.

Micro-convection dynamics while both fluids are being pumped for diluted magnetic fluid $D107_{66\%}$ is showed in the fig. A.1. At $t = 0.0$ s the magnetic field ($H = 75$ Oe) is turned on. The same as in the experiments with the concentrated magnetic fluid the instability emerges after short time ($t = 1.3$ s) and then, it slowly smears with the flow that is going from left to right. After some time (in this case $t \approx 10$ s) an equilibrium state for the dynamics of the instability is reached. Though it must be noted that the instability is still continuously forming on the fresh interface on the left side as the flow is going from left to right. And these freshly grown fingers quickly smears on the way to the right side.

| 0.0 s | 0.7 s | 1.3 s | 2.0 s | 2.6 s |
| 3.3 s | 4.6 s | 6.3 s | 7.9 s | 9.9 s |
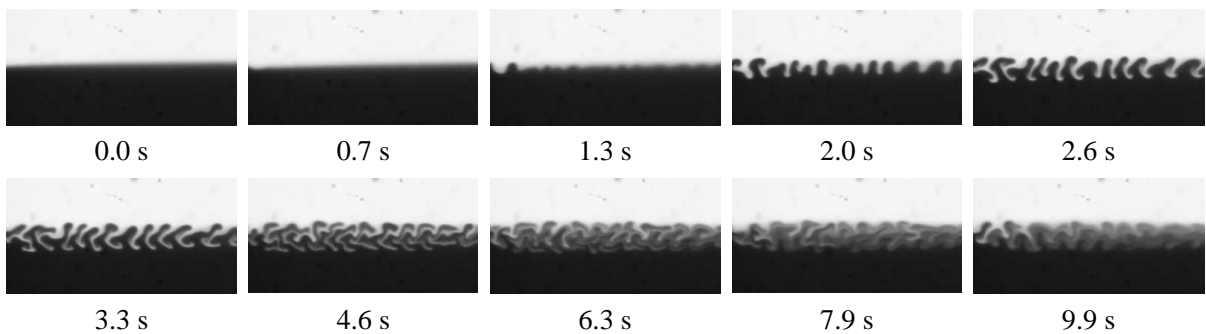
A.1 Figure: Image series of magnetic micro-convection dynamics in time in Y-shaped microfluidics chip. Magnetic fluid: $D107_{66\%}$, Magnetic field: $H = 75$ Oe. Flow rate of the syringe pump for each fluid: $Q = 1$ µl/min. Width of the micro-channel: $w = 1$ mm. Each image is 1.0×2.0 mm large. The contrast of the images is changed, for displaying purpose. *Fig.5. from [25]*

An example of experiments with switched of syringe pump, but apparent parasitic longitudinal flow is demonstrated in figure A.2. The contrast of the images is increased for easier perception. Fluid inlets are on the left side of the images and outlet is on the

right side. In a short moment ($t = 2$ s) after the application of the magnetic field the fingers of the instability have emerged (see fig. A.2b). After a second (see fig. A.2c) all of the fingers have tilted to the same side, indicating the presence of longitudinal flow although the syringe pump has been switched off few moments before the experiment. As the experiment proceeds, the flow is undeniably obvious, the fingers are moving to the right side at their base (to the outlet direction). Also the interface level between the fluids drops over time as the magnetic fluid flows out of the open outlet due to gravity and the parasitic motion caused by external magnetic field.

(a) t=0 s   **(b)** t=2 s   **(c)** t=3 s   **(d)** t=5 s

(e) t=10 s   **(f)** t=15 s   **(g)** t=25 s   **(h)** t=60 s
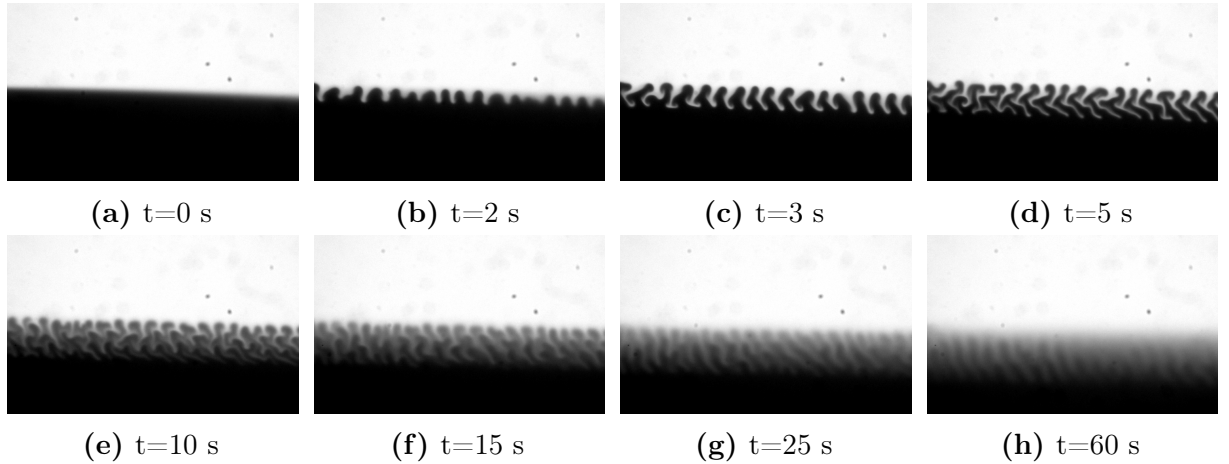
A.2 Figure: Image series of magnetic micro-convection dynamics in time in Y-shaped micro-channel with syringe pump turned off. Magnetic fluid: D107$_{100\%}$, Magnetic field: $H = 59$ Oe. Size of a region represented by a single image is 2.3×1.4 mm.

A.1.2   Magnetic micro-convection experiments with initially stagnant fluids

Here additional experimental results that compliment §3.2. are reviewed.

In the main text the results with the most concentrated magnetic fluid D107$_{100\%}$ are reviewed. The experiments with diluted magnetic fluids are collected in figures A.3 for magnetic fluid D107$_{66\%}$, A.4 for magnetic fluid D107$_{50\%}$, and in A.5 for the most diluted magnetic fluid D107$_{33\%}$. The vertical axis of the figures represent the time since the beginning of the experiment, when magnetic field is turned on. The horizontal axis describe the value of the horizontal, external magnetic field. One column represents a single experiment in time. The contrast of the images is changed for displaying purposes so that at the beginning of the experiment the clear water is white and clear magnetic fluid appears black. All of the experiments are carried out in a rectangular pool-shaped micro-channel with thickness $h_1 = 0.135$ mm. The fluid pumping here, has been stopped few moments before the experiment.
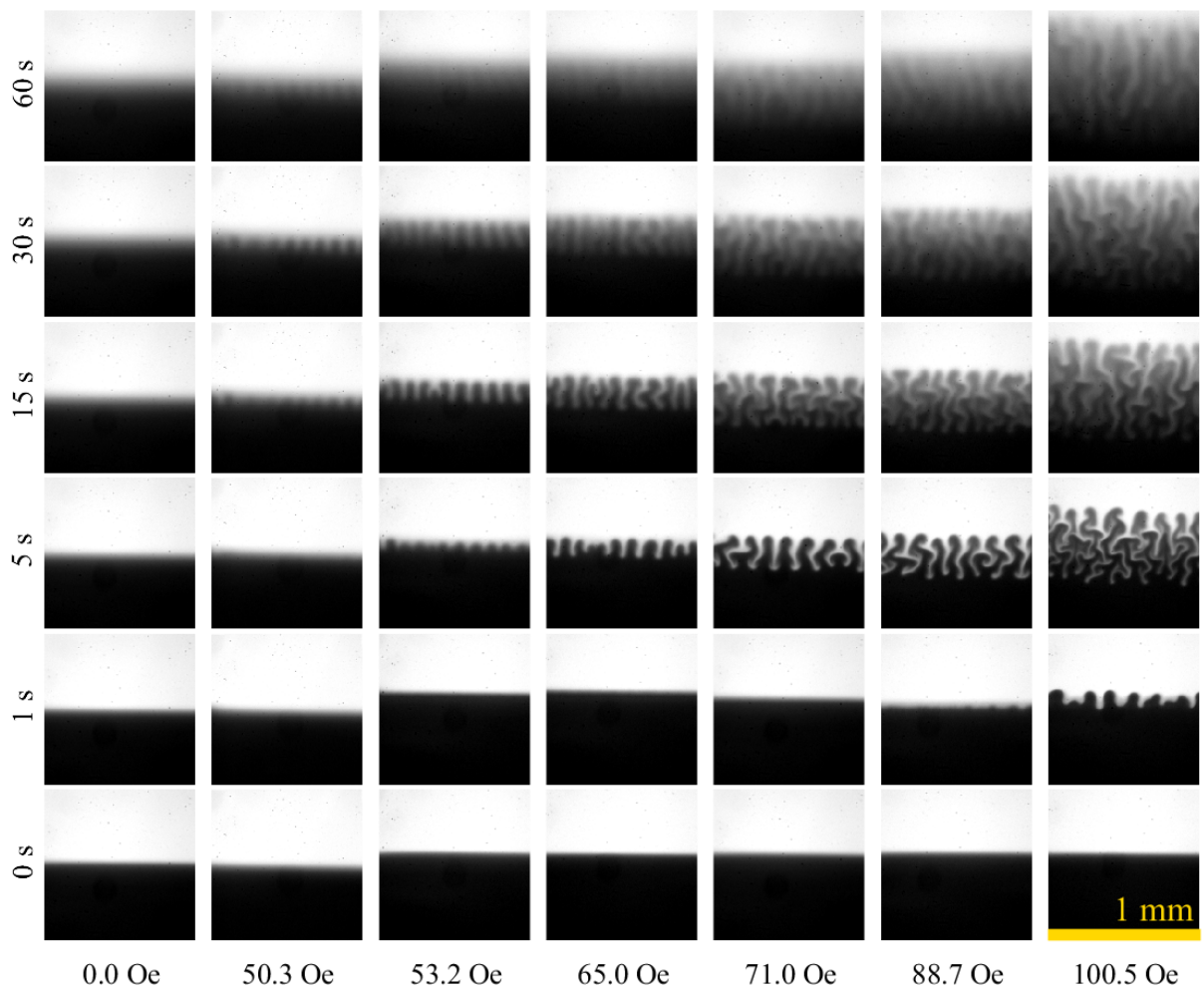
A.3 Figure: Image series of magnetic micro-convection dynamics with magnetic fluid with D107$_{66\%}$ in various magnetic fields in micro-channel with thickness $h_1 = 0.135$ mm.
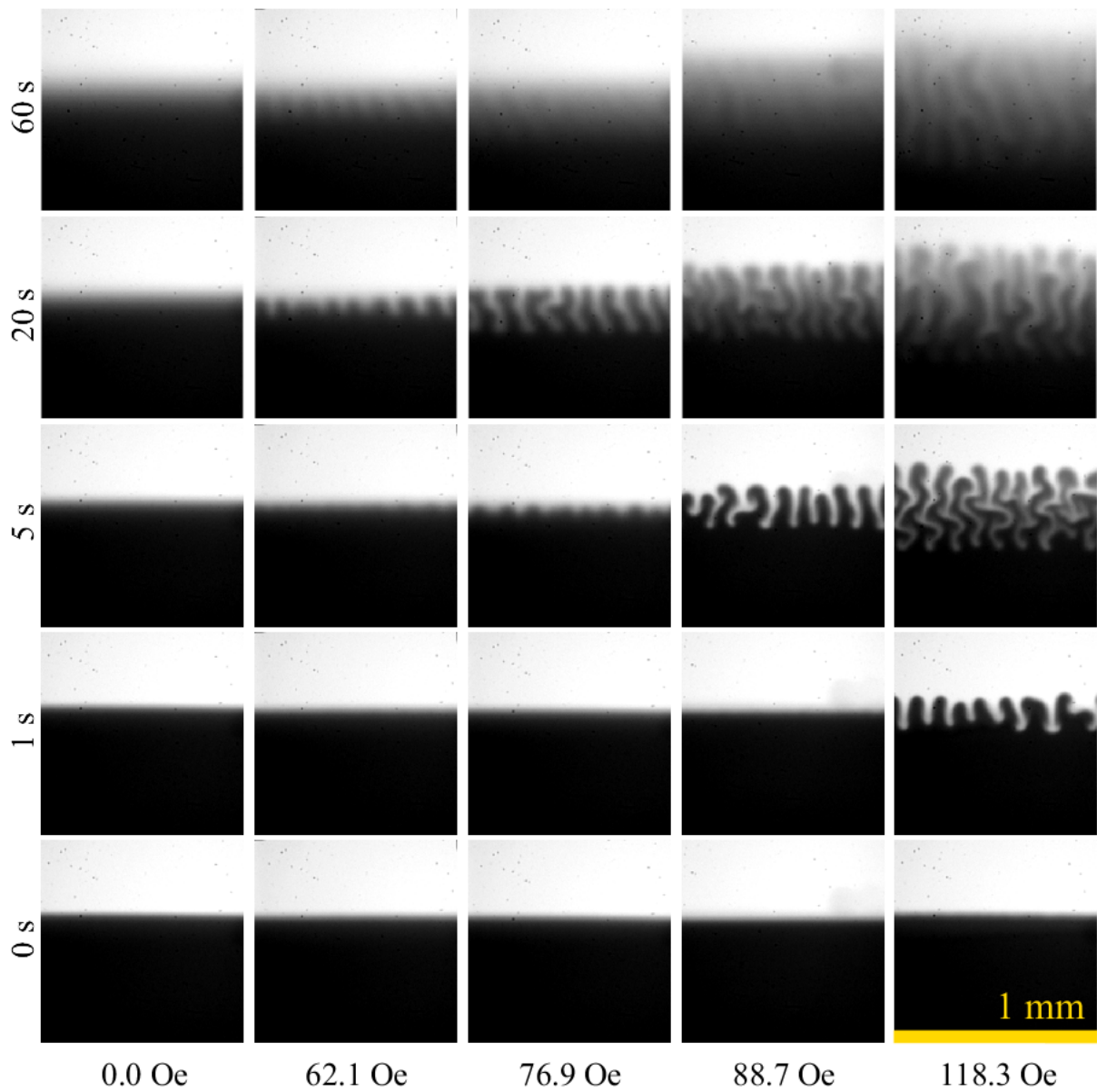
A.4 Figure: Image series of magnetic micro-convection dynamics with magnetic fluid with D107$_{50\%}$ in various magnetic fields in micro-channel with thickness $h_1 = 0.135$ mm.
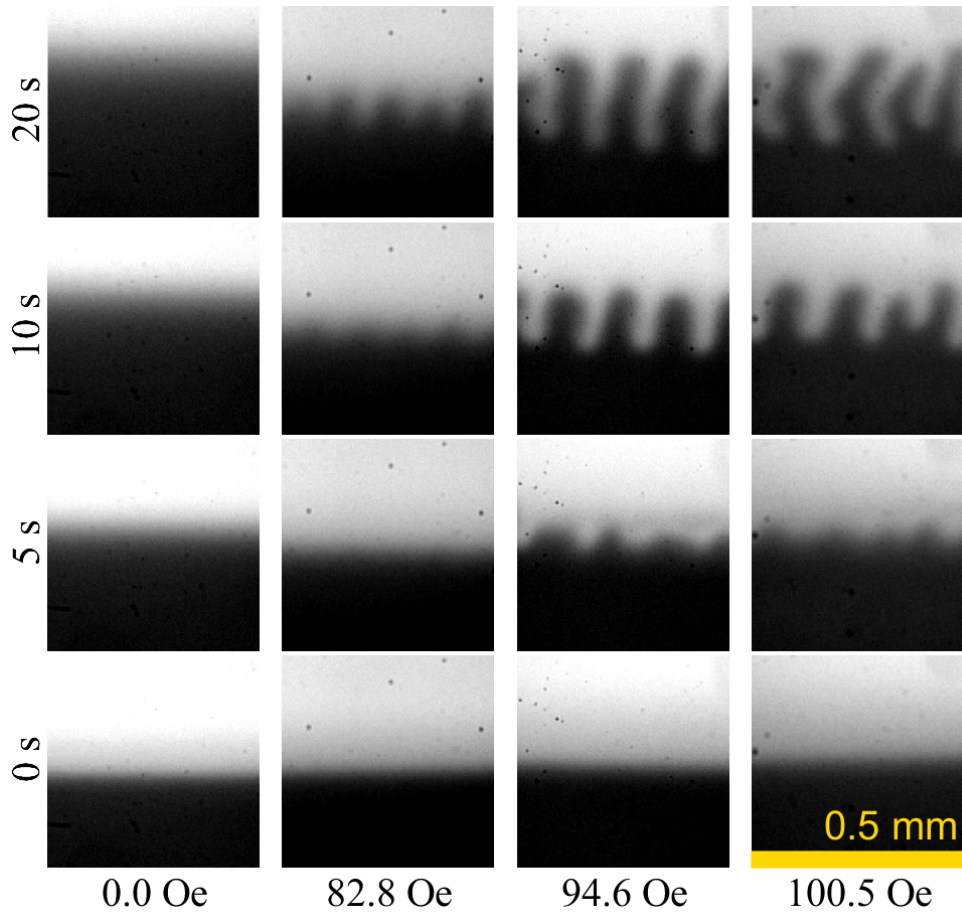
A.5 Figure: An image series of magnetic micro-convection dynamics with magnetic fluid D107$_{33\%}$ in various magnetic fields in micro-channel with thickness $h_1 = 0.135$ mm.

A.1.3   Magnetic micro-convection experiments with initially smeared fluids

Here additional experimental results that compliment §3.3. are reviewed.

In the table A1. the dependence of characteristic wavelength λ with respect to the initial smearing thickness δ_0 for the magnetic fluids not reviewed in the main text is collected. There, experiments of the same magnetic fluid in the same magnetic field and with the same initial smearing thickness are colored blue; from these experiments the value of the experimental inaccuracy can be obtained. It is visible from these experiments that the value of λ varies within ± 0.05 mm for experiments with the same parameters. Therefore some of the changes of λ are not statistically significant. Although it seems, that the overall tendency is that for the experiments with sharper initial interfaces between the mixing fluids the characteristic wavelength of the magnetic micro-convection is smaller.

h, mm	MF	H, Oe	δ_0, mm	λ, mm	observation
0.135	FF09-9$_{100\%}$	59.1	0.15	0.20	no statistically significant correlation
			0.17	0.18	
			0.20	0.20	
			0.22	0.18	
		82.8	0.08	0.17	no statistically significant correlation
			0.13	0.20	
			0.16	0.17	
			0.18	*0.17*	
			0.18	*0.18*	
			0.18	*0.20*	
			0.28	0.20	
	D107$_{66\%}$	82.8	0.13	0.10	λ is not affected by change of δ_0
			0.15	0.15	
			0.14	0.16	
			0.14	0.17	
			0.14	0.19	
			0.14	0.21	
0.257	FF09-9$_{100\%}$	76.9	0.14	0.22	no statistically significant correlation
			0.15	0.20	
			0.17	0.29	
			0.21	0.29	
			0.27	0.25	
	FF09-9$_{66\%}$	88.7	0.04	0.14	λ increases as δ_0 increases
			0.12	0.20	
			0.13	*0.20*	
			0.13	*0.25*	
0.399	FF09-9$_{66\%}$	88.7	0.07	0.17	
			0.16	0.20	

A1. Table: Characteristic wavelength of the magnetic micro-convection in experiments with magnetic fluids FF09-9 and D107

Effects of the magnetic field intensity

Next, here the additional figures representing experiments of the magnetic micro-convection dynamics with respect to external magnetic field are collected.

The results for the magnetic fluid KTF11-1 are collected in figures A.6, A.7, A.8 for different magnetic fluid dilution ratios and micro-channel thicknesses.
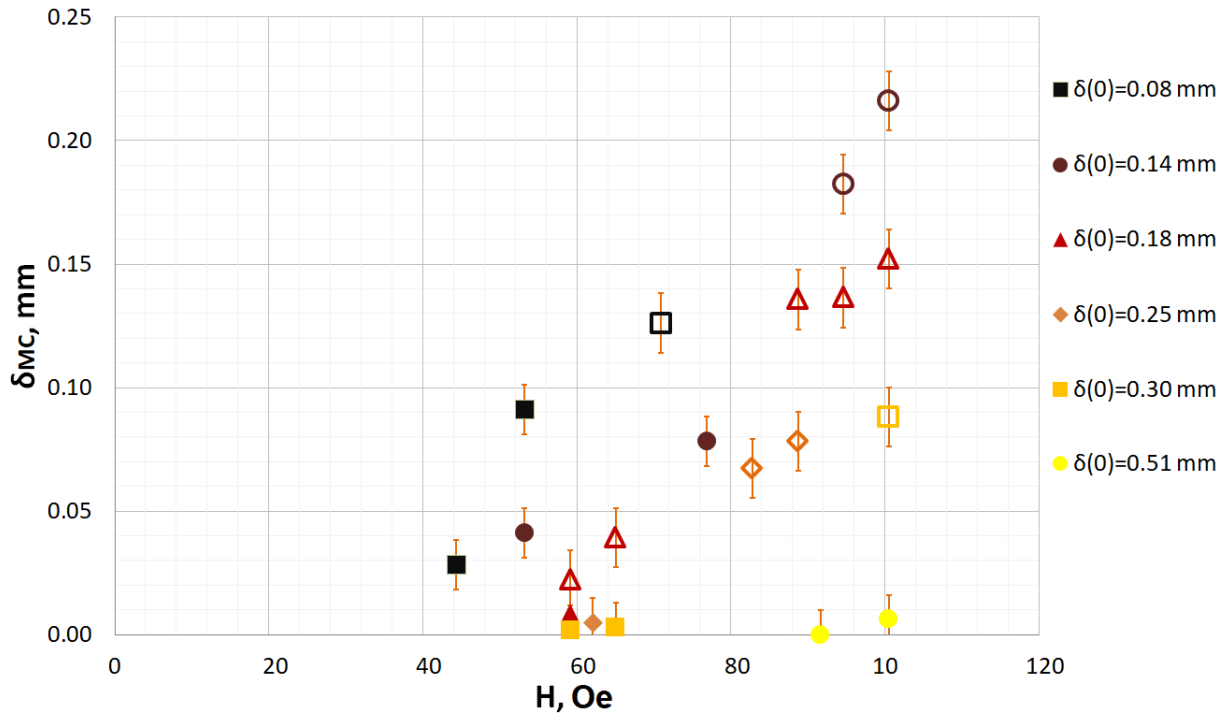
A.6 Figure: Mixing by magnetic micro-convection δ_{MC} with respect to the external magnetic field H for various initial smearing thicknesses δ_0 in micro-channel with thickness $h_1 = 0.135$ mm. Magnetic fluid: KTF11-1$_{100\%}$. The empty markers represent the expected values of the δ_{MC} obtained with attachment method.
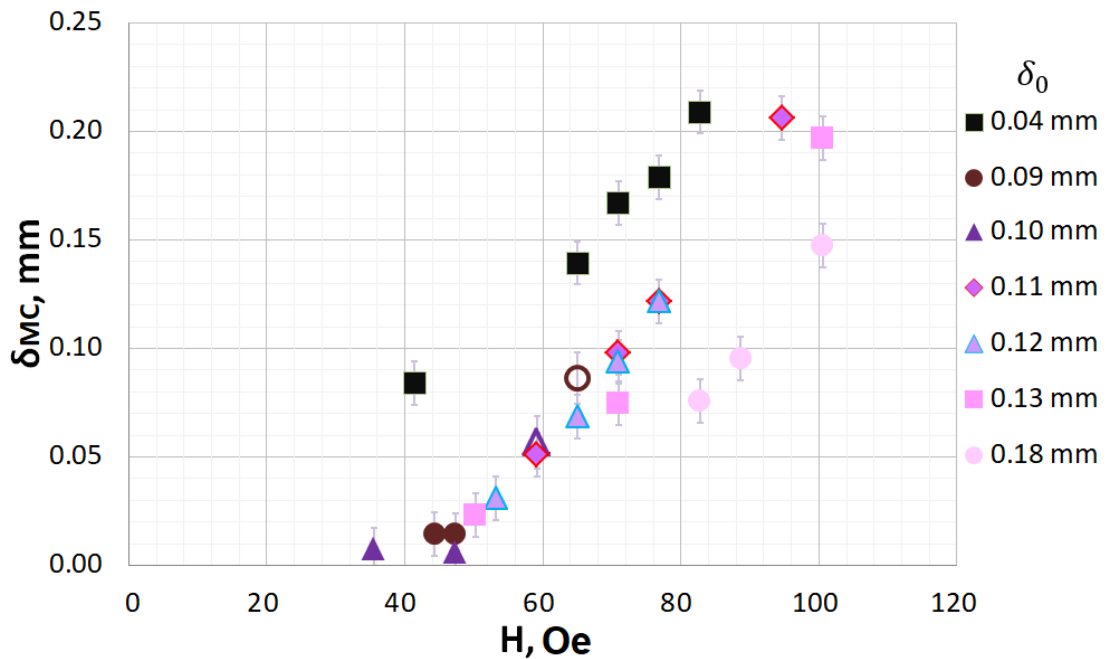
A.7 Figure: Mixing by magnetic micro-convection δ_{MC} with respect to the external magnetic field H for various initial smearing thicknesses δ_0 in micro-channel with thickness $h_1 = 0.135$ mm. Magnetic fluid: KTF11-1$_{66\%}$. The empty markers represent the expected values of the δ_{MC} obtained with attachment method.
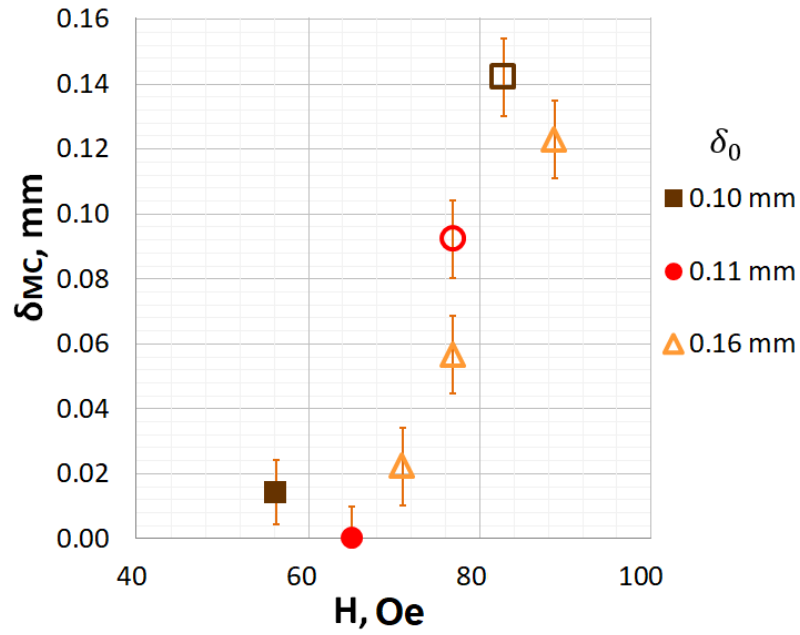
A.8 Figure: Mixing by magnetic micro-convection δ_{MC} with respect to the external magnetic field H for various δ_0 in micro-channel with thickness $h_2 = 0.257$ mm. Magnetic fluid: KTF11-1$_{100\%}$. The empty markers represent the expected values of the δ_{MC} obtained with attachment method.

The results for the magnetic fluid FF09-9$_{50\%}$ are collected in figures A.9, A.10, and A.11 for experiments in three different micro-channel thicknesses.
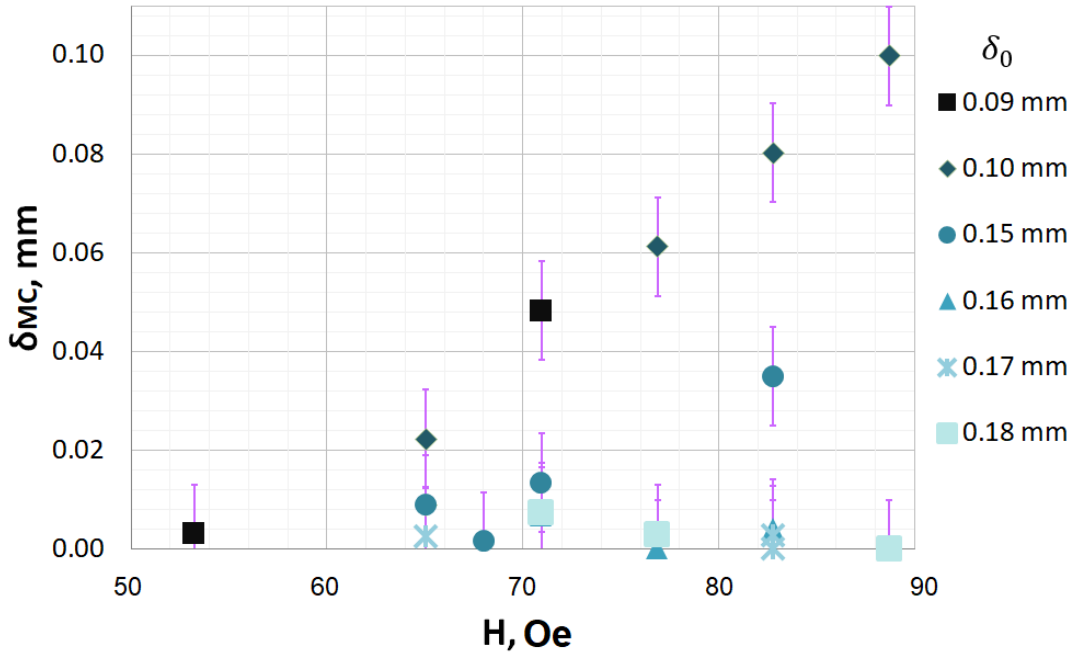
A.9 Figure: Mixing by magnetic micro-convection δ_{MC} with respect to the external magnetic field H for various initial smearing thicknesses δ_0 of the interface between both fluids in micro-channel with thickness $h_1 = 0.135$ mm. Magnetic fluid: FF09-9$_{50\%}$.
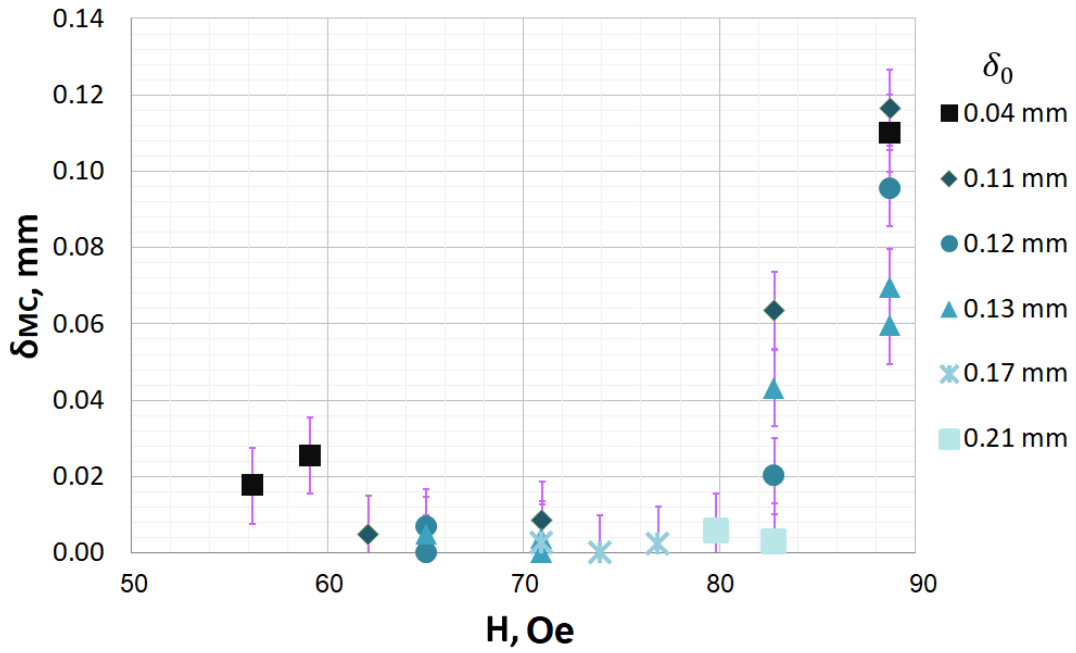
A.10 Figure: Mixing by magnetic micro-convection δ_{MC} with respect to the external magnetic field H for various initial smearing thicknesses δ_0 of the interface between both fluids in micro-channel with thickness $h_2 = 0.257$ mm. Magnetic fluid: FF09-9$_{50\%}$.
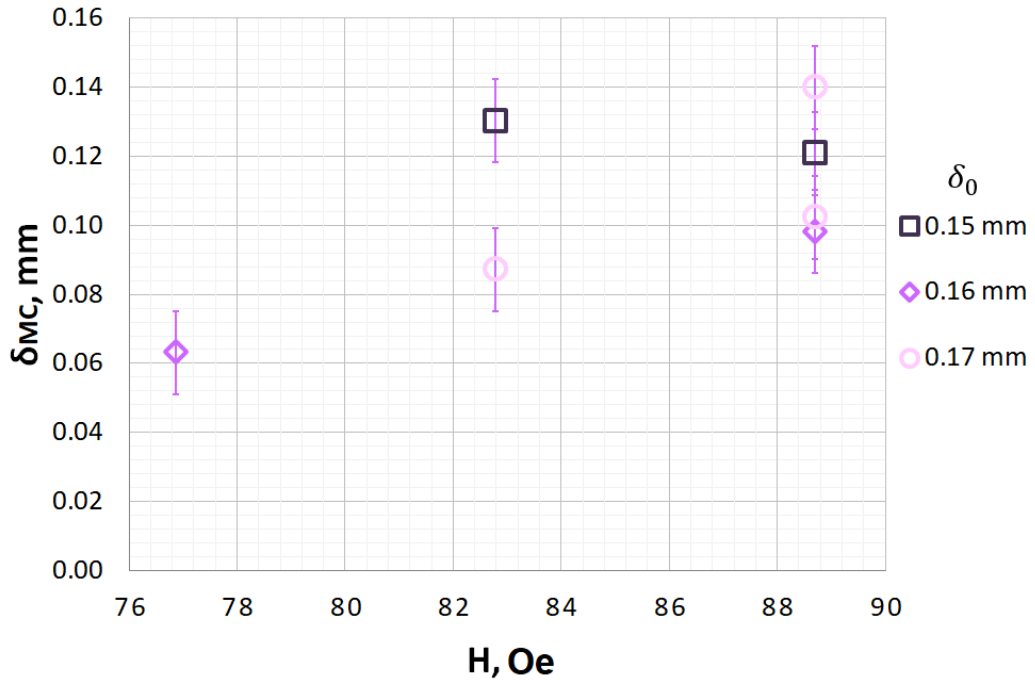
A.11 Figure: Mixing by magnetic micro-convection δ_{MC} with respect to the external magnetic field H for various initial smearing thicknesses δ_0 of the interface between both fluids in micro-channel with thickness $h_3 = 0.399$ mm. Magnetic fluid: FF09-9$_{50\%}$. All of the data are obtained with attachment method.

The effect of the thickness of the micro-channel on the magnetic micro-convection for

the magnetic fluid KTF11-1$_{100\%}$ is reviewed in fig. A.12 . Experiments with this magnetic fluid were carried out in three different microfluidic chips: $h = 0.050$ mm, $h_1 = 0.135$ mm and $h_2 = 0.257$ mm.
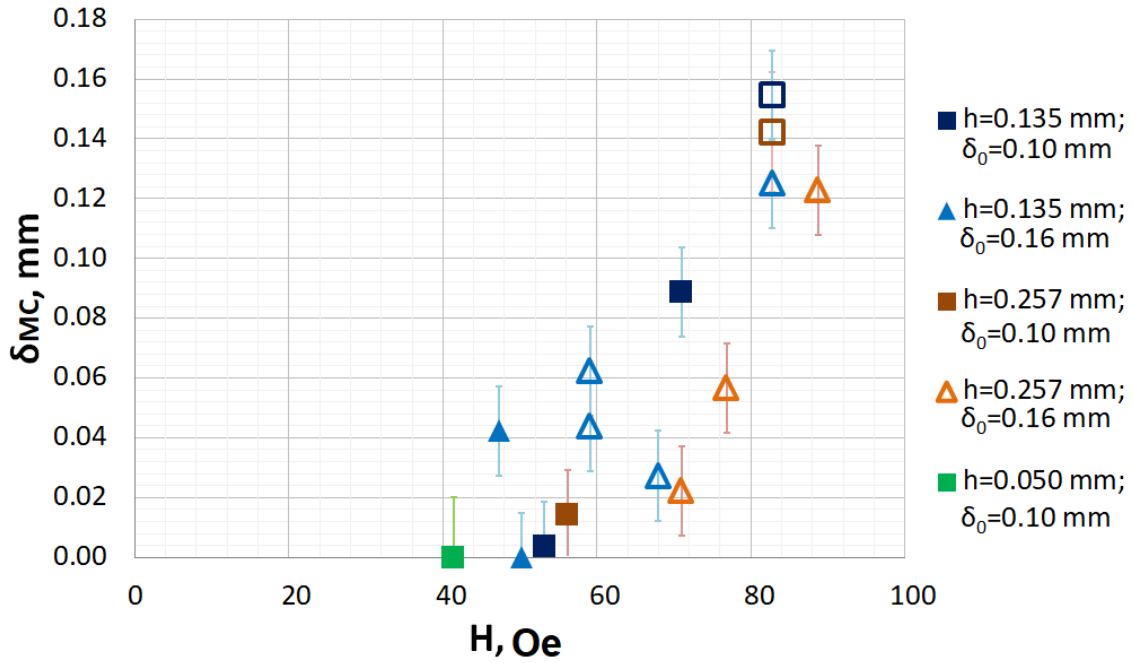
A.12 Figure: The effect of micro-channel thickness on δ_{MC} for various δ_0. Magnetic fluid: KTF11-1$_{100\%}$. Empty markers represent δ_{MC} obtained with attachment method.
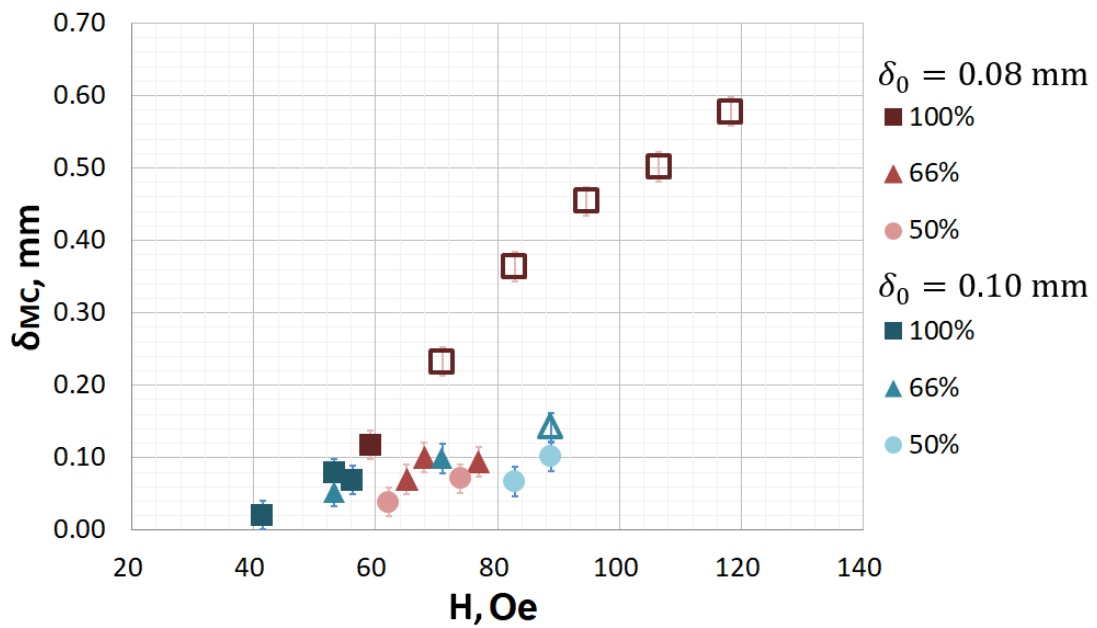
A.13 Figure: Dilution ratio effect of the magnetic fluid D107 on δ_{MC} for two different δ_0 (denoted in the legend) in micro-channel with thickness $h_1 = 0.135$ mm. Empty markers represent the expected δ_{MC} from the attachment method.
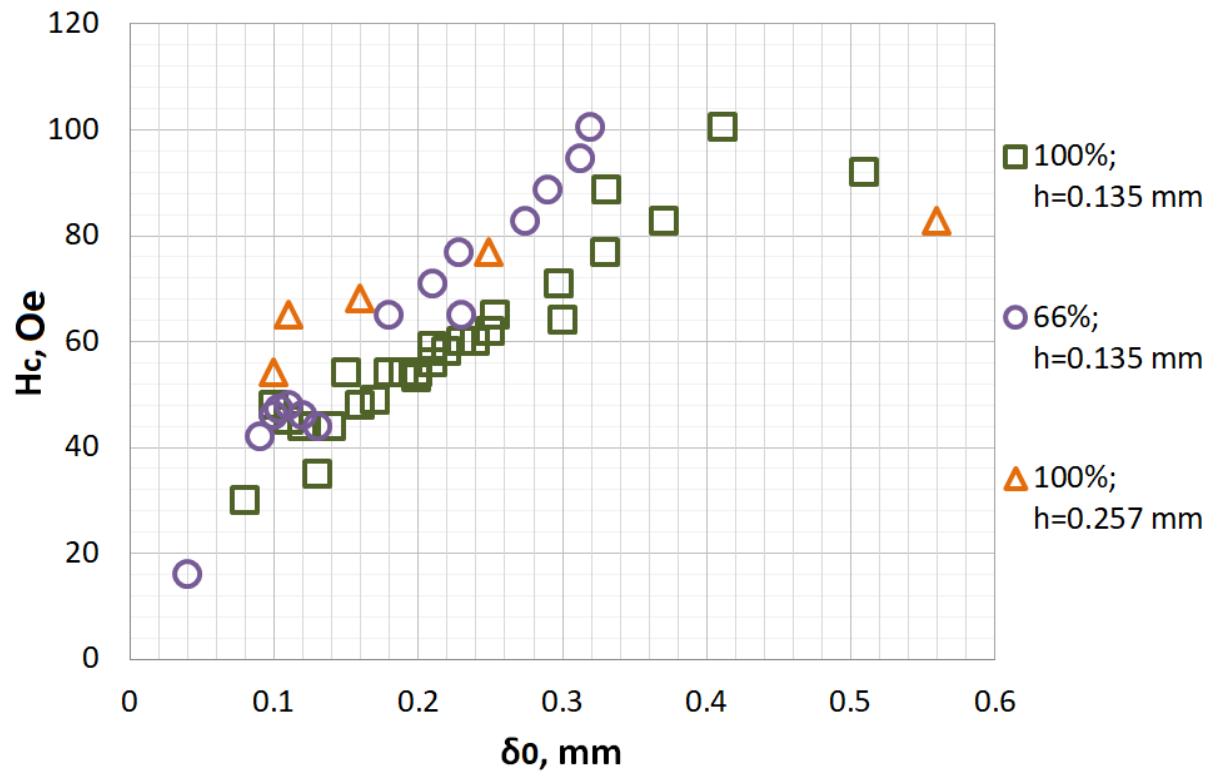
(a) Magnetic fluid: KTF11-1 with dilution ratios 100% and 66%
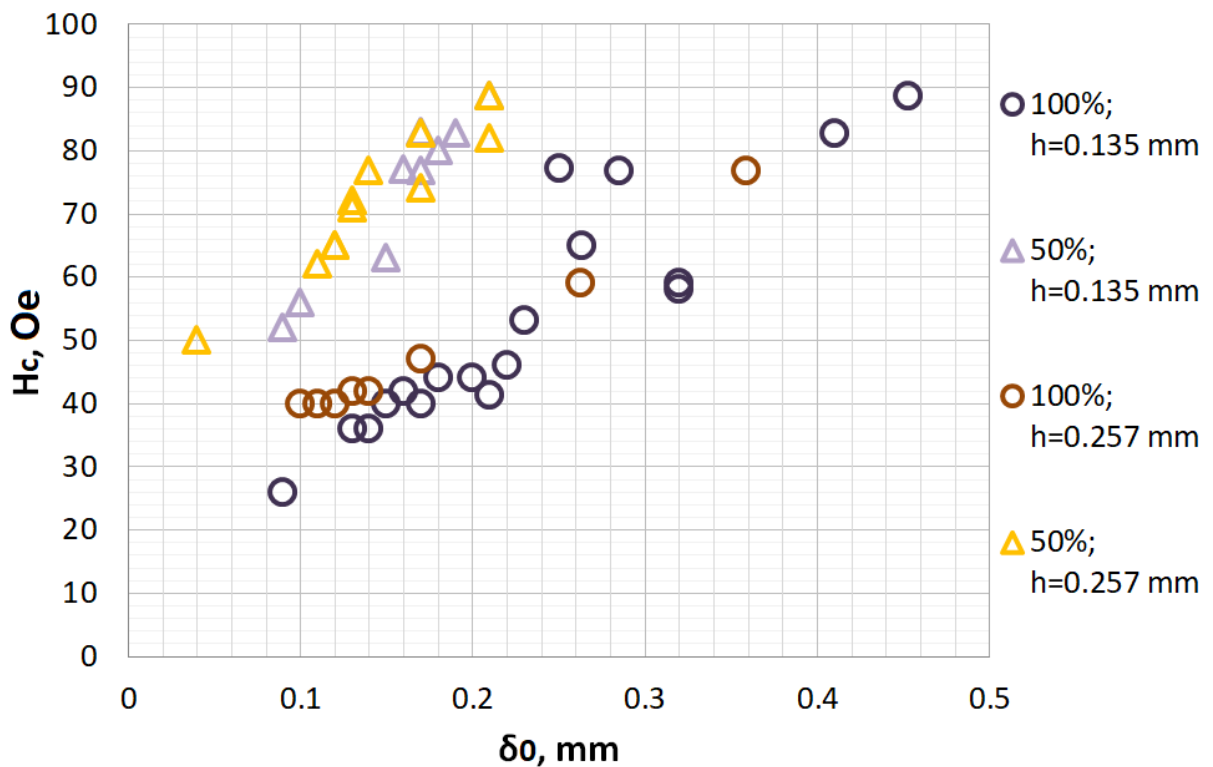
(b) Magnetic fluid: FF09-9 with dilution ratios 100% and 50%

A.14 Figure: Critical magnetic field for magnetic micro-convection to emerge with respect to initial smearing thickness δ_0.

The effects of magnetic fluid dilution ratio are reviewed in figure A.13 . In the fig. A.13

results of experiments of the magnetic fluid D107 for two different initial smearing values $\delta_0 = 0.08$ mm and $\delta_0 = 0.10$ mm are collected. Experiments with the same δ_0 are colored in the same tonality, but experiments with the same magnetic fluid dilution ratio have the same marker shape. Although the differences are relatively small and the magnetic field value range does not overlap too mach for the experiments with the same dilution ratio, the magnetic micro-convection effect is greater in experiments with more concentrated magnetic fluids.

Next the values of the critical magnetic field H_c for the instability to emerge with respect to the initial smearing thickness δ_0 are collected in figure A.14 for magnetic fluids KTF11-1 and FF09-9 for various dilution ratios in two different micro-channels: $h_1 = 0.135$ mm and $h_2 = 0.257$ mm. In these graphs the effect of the magnetic fluid dilution can be observed. For example, for fluid FF09-9$_{100\%}$ the critical magnetic field is $H_c \approx 81$ Oe,while it is almost two times smaller $H_c \approx 45$ Oe for magnetic fluid FF09-9$_{50\%}$ for experiments with the same initial smearing thickness $\delta_0 = 0.2$ mm. Also, by extrapolating the data to the vertical axis where $\delta_0 = 0$ the value of the critical magnetic field for mixing fluids with sharp initial interface can be estimated.

Effects of the initial smearing

Here the additional figures representing experiments of the magnetic micro-convection dynamics with respect to the initial smearing thickness δ_0 are collected.
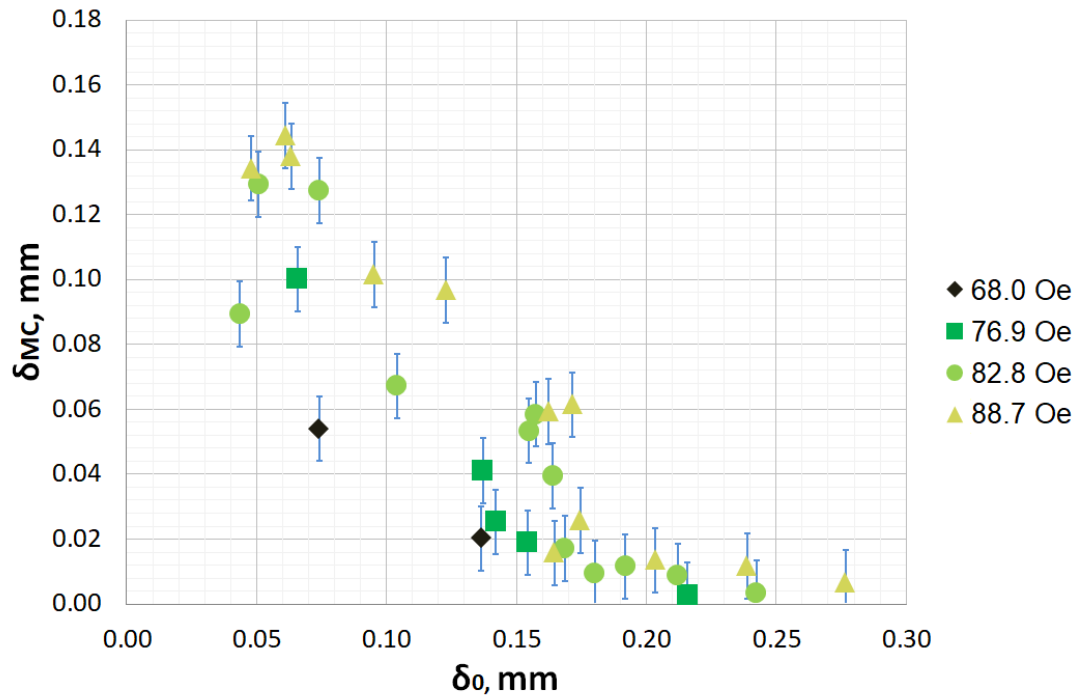
A.15 Figure: Mixing by magnetic micro-convection δ_{MC} with respect to δ_0 in micro-channel with thickness $h_1 = 0.135$ mm. Magnetic fluid: D107$_{50\%}$.
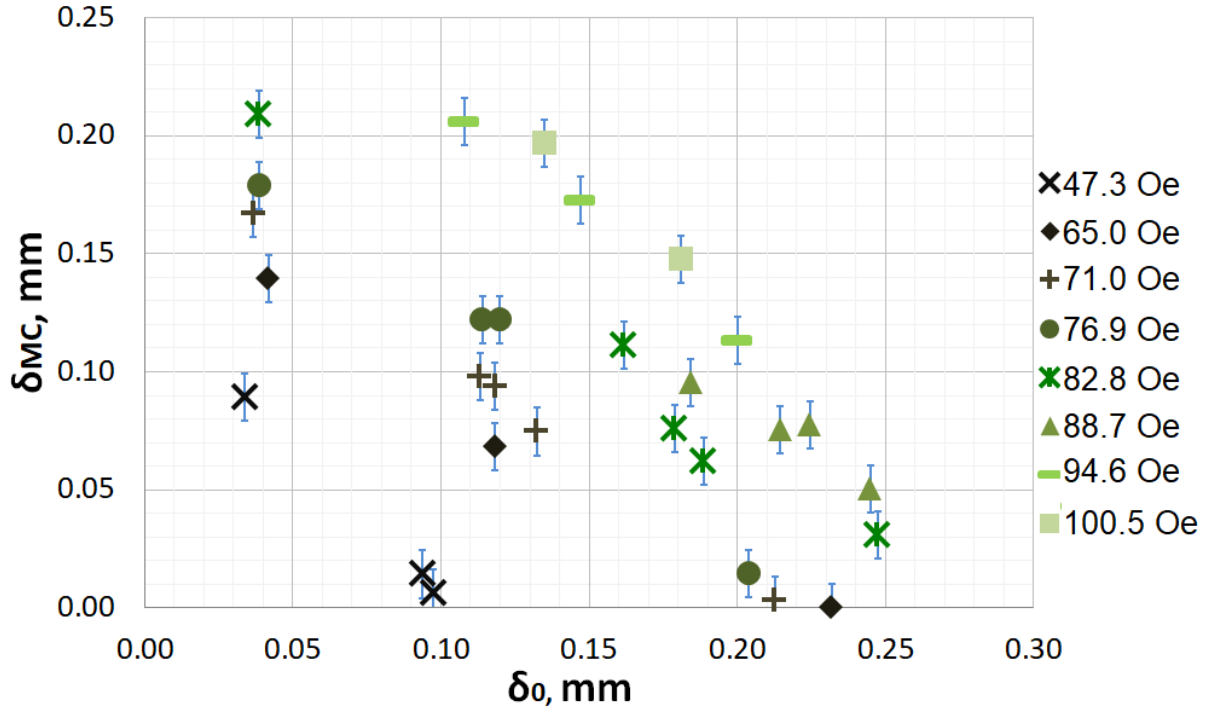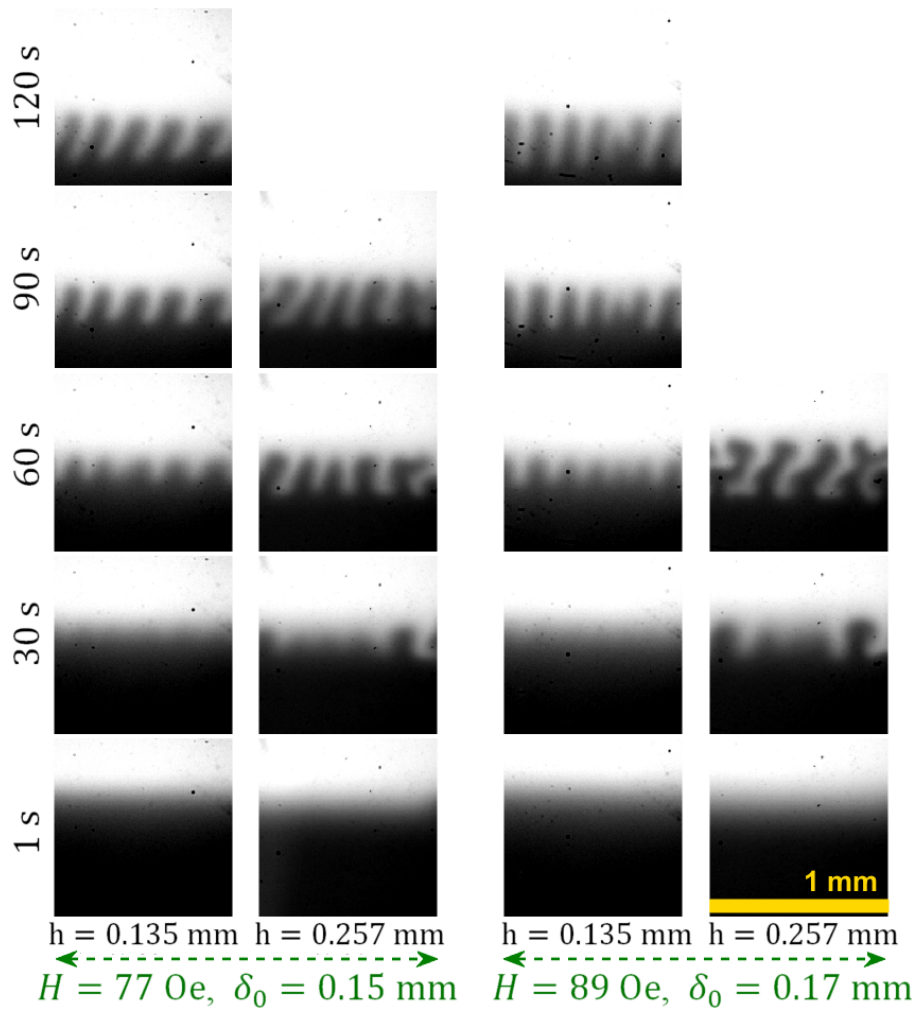
A.16 Figure: Mixing by magnetic micro-convection δ_{MC} with respect to δ_0 in various magnetic fields in micro-channel with thickness $h_1 = 0.135$ mm. Magnetic fluid: KTF11-$1_{66\%}$.

In figures A.15 and A.16 results for magnetic fluids D107$_{50\%}$ and KTF11-$1_{66\%}$ are collected accordingly.

In fig. A.17 values of $\delta_{MC:max}$ for magnetic fluids KTF11-1 and FF09-9 are collected for various dilution ratios and micro-channel thicknesses. As explained in the main text of this thesis $\delta_{MC:max}$ is the maximal value of micro-convective mixing, which can be achieved in a specific magnetic field if the interface between the mixing fluids is perfectly sharp. The markers in fig. A.17 have the same color tonality for experiments carried out in the same micro-channel: purple markers for thinner micro-channel $h_1 = 0.135$ mm and orange markers for the thicker micro-channel $h_2 = 0.257$ mm. The same dilution ratio of the magnetic fluid is represented by the same marker shape per graph.

A relationship between $\delta_{MC:max}$ and the external magnetic field with respect to the micro-channel thickness is contrasting for magnetic fluids KTF11-1 and FF09-9. In fig. A.17a the purple markers representing thinnest micro-channel are above the orange ones, while in fig. A.17b the orange markers are above the purple ones.

So in experiments with magnetic fluid KTF11-1 more effective mixing due to magnetic micro-convection (higher values of δ_{MC}) can be achieved in a thinner micro-channel ($h_1 = 0.135$ mm), whereas for experiments with magnetic fluid FF09-9 the opposite is true. In experiments with magnetic fluid FF09-9 more effective mixing due to magnetic micro-convection was achieved in the thicker ($h_2 = 0.257$ mm) micro-channel.
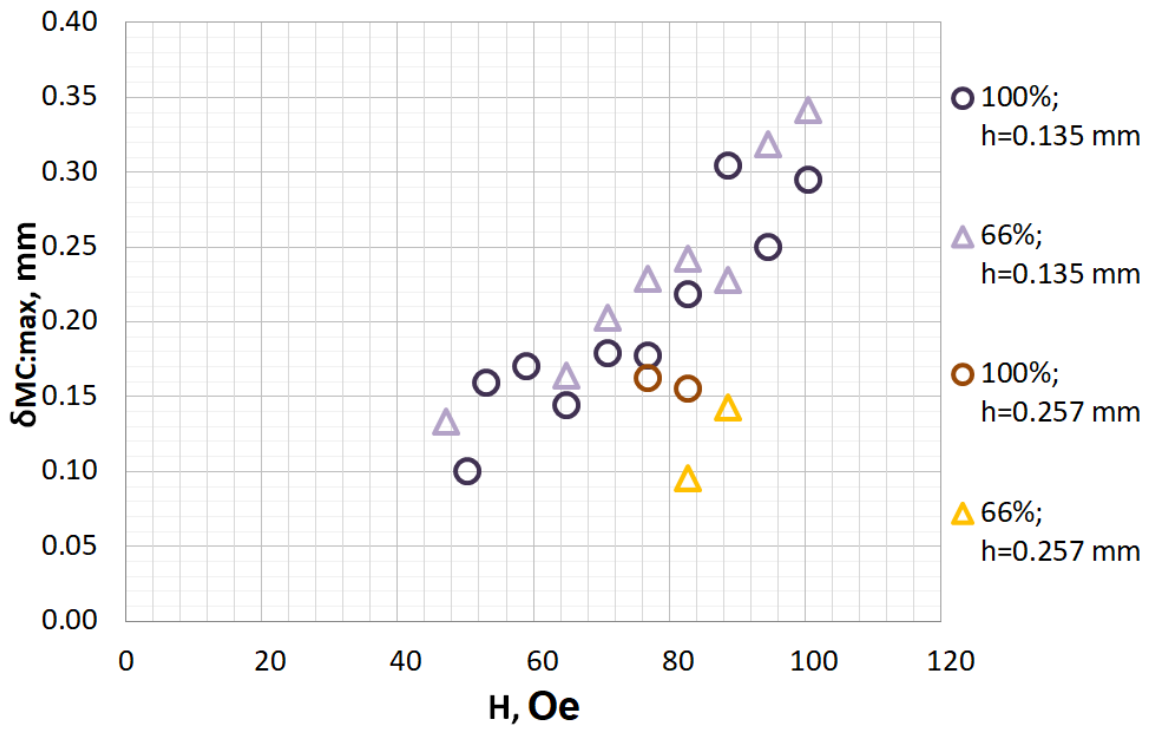
(a) Magnetic fluid: KTF11-1
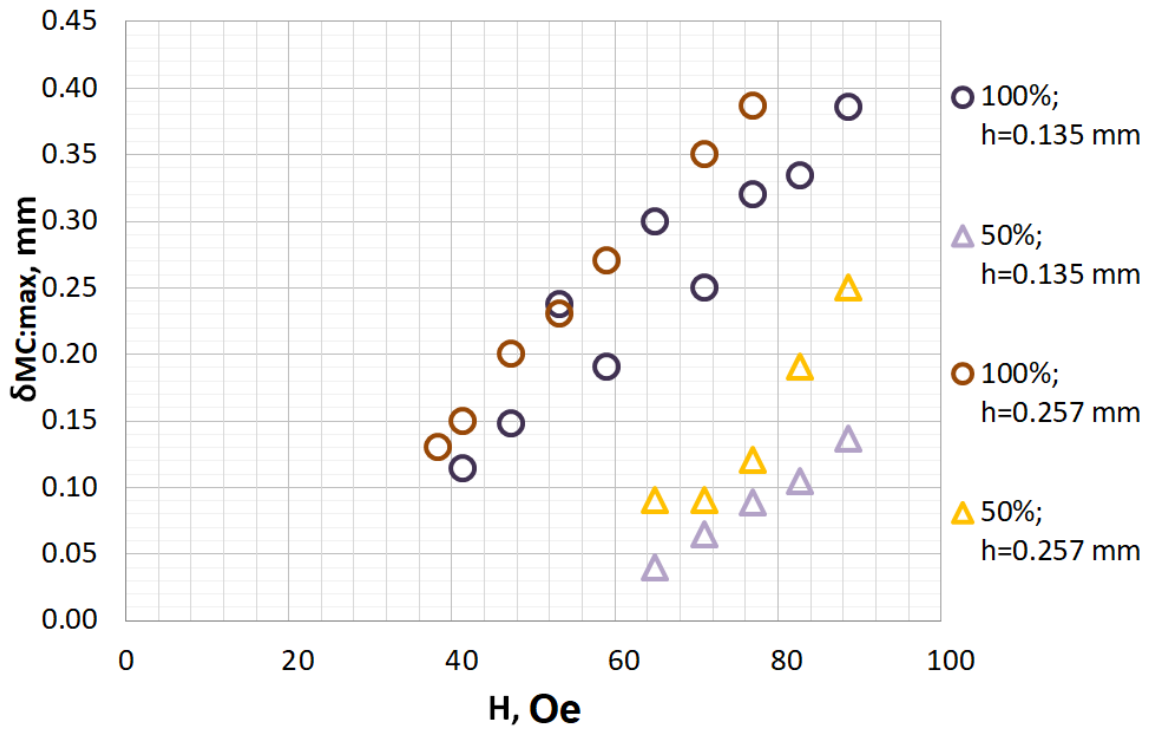
(b) Magnetic fluid: FF09-9

A.17 Figure: Maximal value of δ_{MC} with respect to external magnetic field for sharp initial interface $\delta_0 = 0$ mm between the mixing fluids.

In figure A.19 the effect of the dilution ratio is explored for magnetic fluid KTF11-1 in micro-channel with thickness $h_1 = 0.135$ mm.
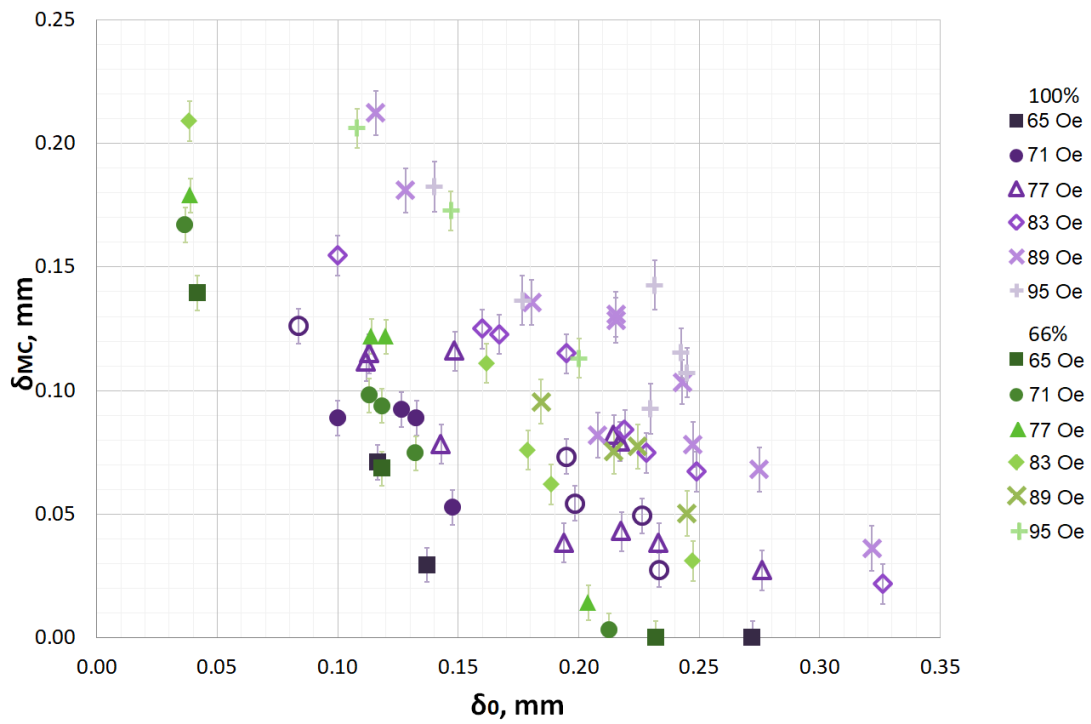
A.18 Figure: Dilution ratio effect on δ_{MC} with respect to δ_0 in various magnetic fields in micro-channel with thickness $h_1 = 0.135$ mm. Magnetic fluid: KTF11-1.

In figure A.19 the effect of the micro-channel thickness is explored for magnetic fluid FF09-9$_{100\%}$.
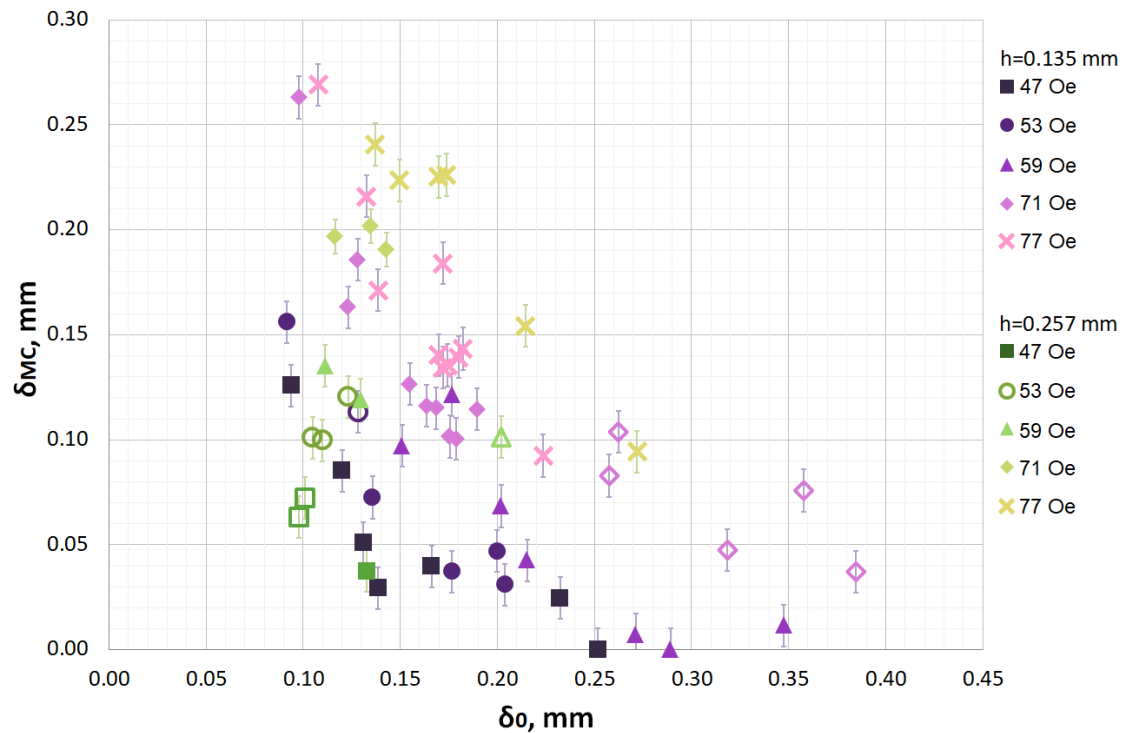
A.19 Figure: Micro-channel thickness effect on δ_{MC} with respect to δ_0 in various magnetic fields in micro-channel with thickness $h_1 = 0.135$ mm. Magnetic fluid: FF09-9$_{100\%}$.

Visually the effect of the micro-channel thickness for magnetic fluid FF09-9$_{50\%}$ are reviewed in figure A.20. Here in experiments with magnetic fluid FF09-9$_{50\%}$ the fingers of the instability appear earlier in the thicker ($h_2 = 0.257$ mm) micro-channel. For both values of H and δ_0 there are visible fingers already at $t = 30$ s in the experiments in the thicker micro-channel, whereas the fingers of same height are visible more than $30s$ later in the thinner micro-channel.

In fig. 3.26. in the last pair of columns as there are 6 fingers characterizing the instability in the thinner micro-channel, while in the thicker micro-channel with all other parameters unchanged there are only 4 fingers.

A.20 Figure: Image series of magnetic micro-convection dynamics for various micro-channel thicknesses. Magnetic fluid: FF09-9$_{50\%}$. A single image represents 1.0 mm×1.0 mm region.

A specific amount of micro-convective mixing

Here the additional figures for magnetic field with respect to the initial smearing thickness δ_0 in order to obtain a specific micro-convective mixing length δ_{MC} are collected.
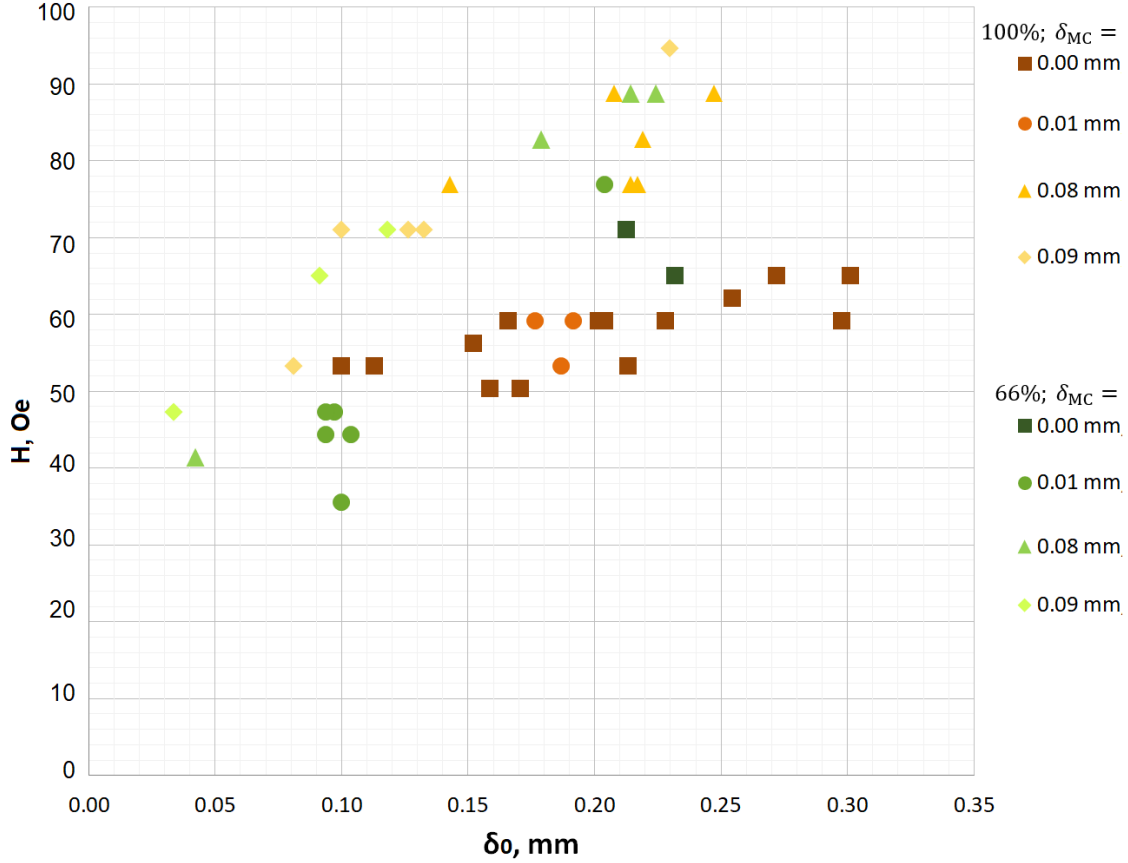
A.21 Figure: What magnetic field should be applied to get a specific δ_{MC} with respect to the dilution ratio in micro-channel with thickness $h_1 = 0.135$ mm for magnetic fluid KTF11-1 .

In figure A.21 dilution ratio effects of the magnetic fluid KTF11-1 in micro-channel with thickness $h_1 = 0.135$ mm are explored. Orange markers represent experiments with concentrated magnetic fluid KTF11-1$_{100\%}$ and green markers represent experiments with diluted KTF11-1$_{50\%}$. It appears that green markers are slightly above the brown ones, meaning that a slightly stronger magnetic field is necessary to induce the same amount of magnetic micro-convection in experiments with more diluted magnetic fluid.

In fig. A.22 effect of the micro-channel thickness on magnetic field H with respect to initial smearing thickness δ_0 in order to obtain a specific δ_{MC} is demonstrated for magnetic fluid FF09-9$_{100\%}$. Orange markers represent the experiments carried out in the micro-channel with thickness $h_1 = 0.135$ mm, but the green ones represent the experiments carried out in two times thicker micro-channel $h_2 = 0.257$ mm. It appears that the orange markers are slightly above the green ones, meaning that a stronger magnetic field

is necessary to induce the same amount of magnetic micro-convection in experiments with thinner micro-channel for this magnetic fluid. This difference is best visible with triangle shaped markers representing the results with largest demonstrated $\delta_{\mathrm{MC}} = 0.23$ mm.
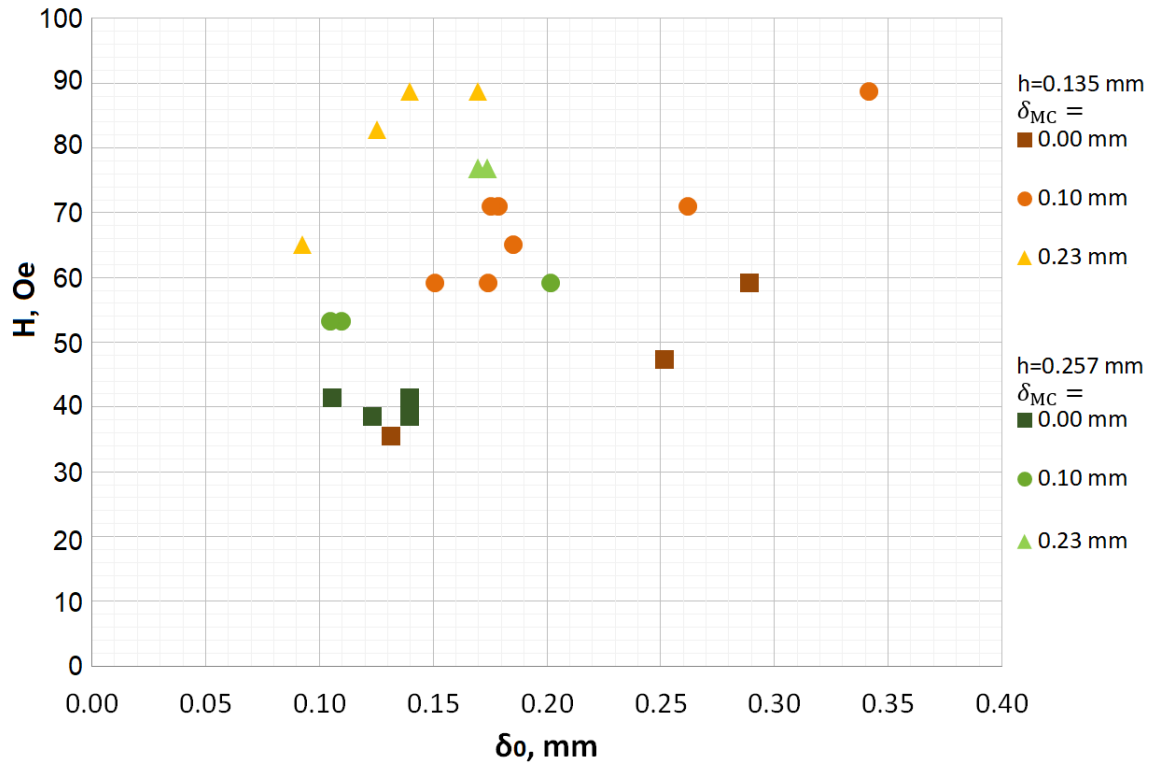
A.22 Figure: What magnetic field should be applied to get a specific δ_{MC} with respect to the micro-channel thickness. Magnetic fluid: FF09-9$_{100\%}$.

A.1.4 Magnetic micro-convection experiments in vertical magnetic field

Here the additional experimental data are collected that compliments the results reviewed in §3.4..

Effects of the initial smearing

Here, the additional experimental results of how the initial smearing affects the magnetic instability in a vertical magnetic field are collected.

In figure A.23 the dynamics of the instability in vertical field $H = 65.3$ Oe for magnetic fluid FF21-5$_{100\%}$ in micro-channel with thickness $h_1 = 0.135$ mm is explored. The vertical axis represents the time since the beginning of the experiment, when the magnetic field was applied. The horizontal axis represent the information about the initial smearing thickness δ_0 before the experiment. Each column represents single experiment in time. The contrast of the images is changed for displaying purpose so that at the beginning of the experiment clear water is represented by white color, but clear magnetic fluid by black color.
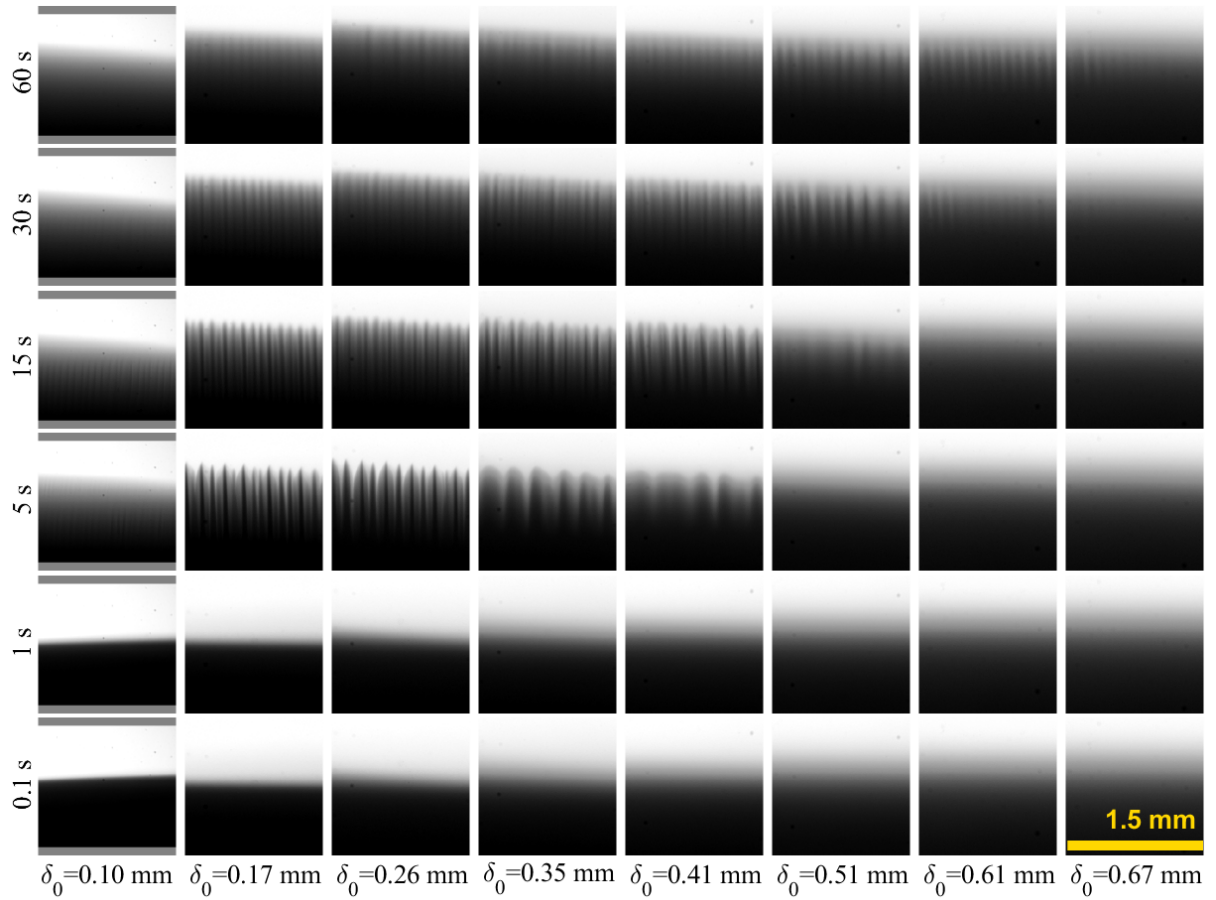
A.23 Figure: Image series of magnetic micro-convection dynamics with different δ_0 in a constant vertical magnetic field $H = 65.3$ Oe in micro-channel with thickness $h_1 = 0.135$ mm. Magnetic fluid: FF21-5$_{100\%}$. micro-channel: $h_1 = 0.135$ mm. A single image represents 1.5×1.5 mm region.

The critical magnetic field values for the instability to emerge with respect to the initial smearing thickness δ_0 are collected in figures A.24 and A.25. The results are collected for the experiments carried out in both used micro-channel thicknesses: $h_1 = 0.135$ mm and $h_2 = 0.257$ mm. In all of the figures the data representing the experiments carried out in the thinnest micro-channel ($h_1 = 0.135$ mm) is above. So to mix fluids in vertical magnetic fields, stronger magnetic field must be applied to create the instability in the thinnest macro-channel. Magnetic fluid FF09-9 (see fig. A.25b) is explored for four different dilution ratios. The more diluted the magnetic fluid, the stronger field must be applied to create the instability. The color of the markers, there becomes lighter for experiments carried out with more diluted magnetic fluid.
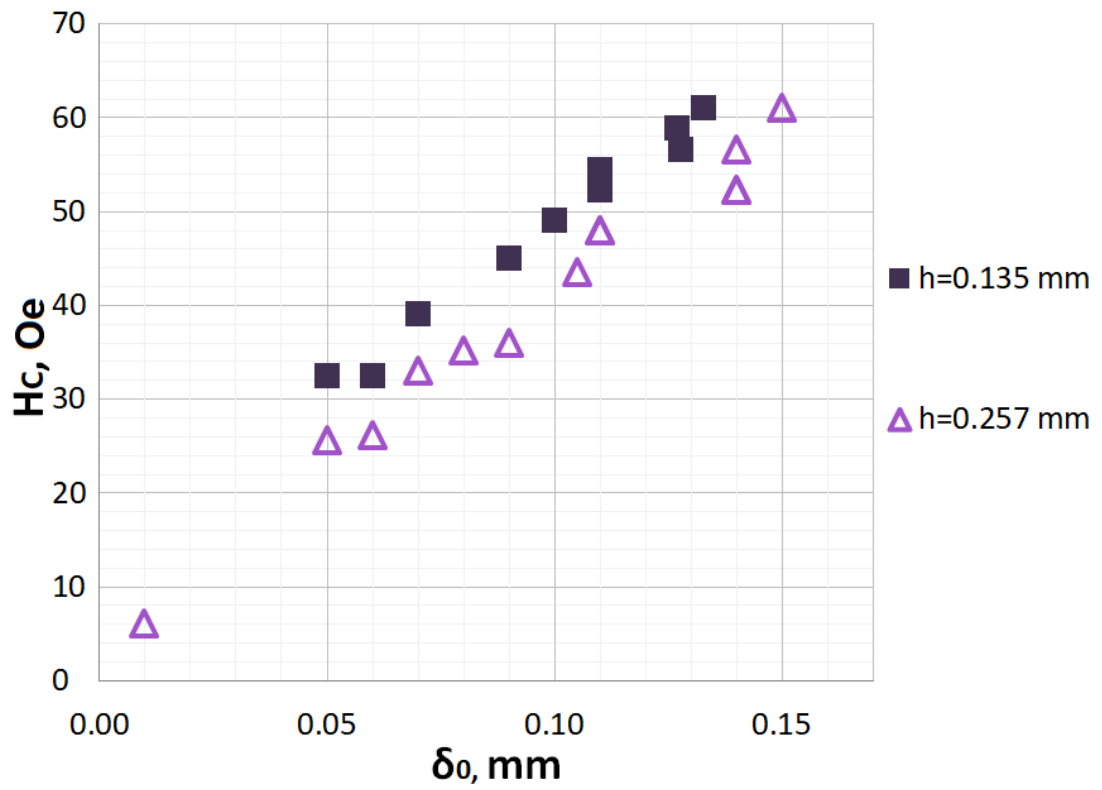
(a) KTF11-1$_{100\%}$
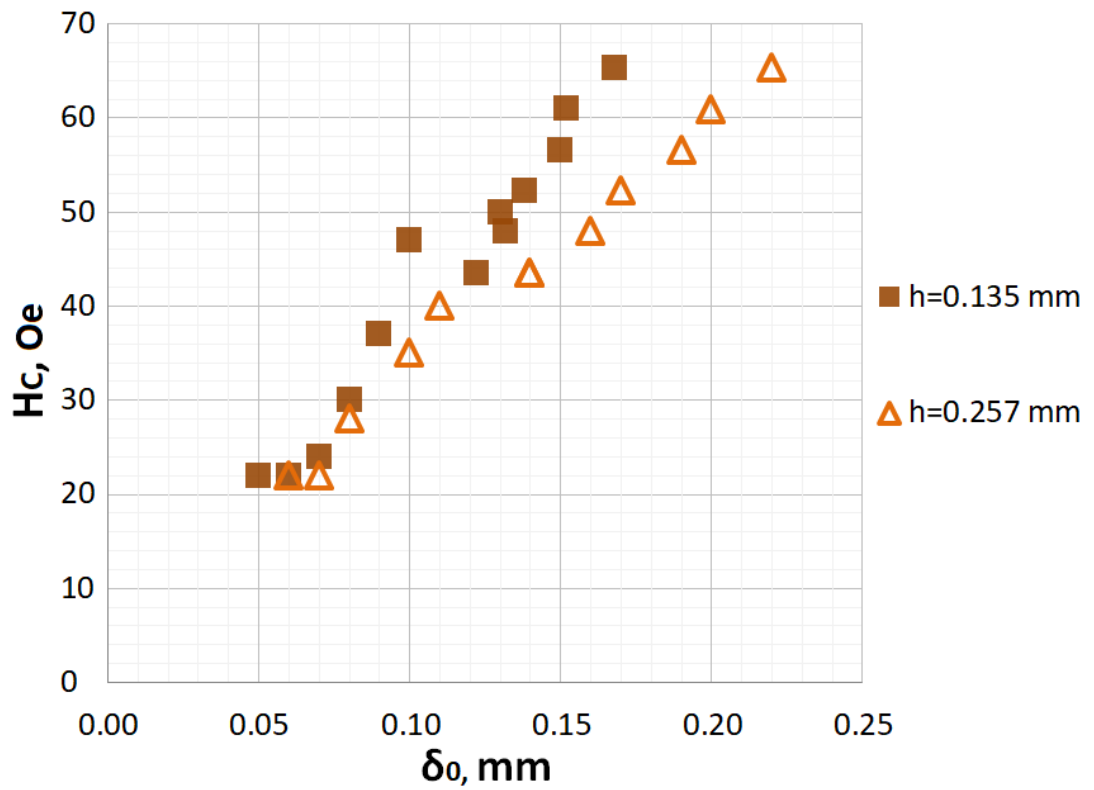
(b) D107$_{100\%}$

A.24 Figure: Critical magnetic field H_c for magnetic micro-convection to emerge with respect to δ_0 for experiments in different micro-channels.
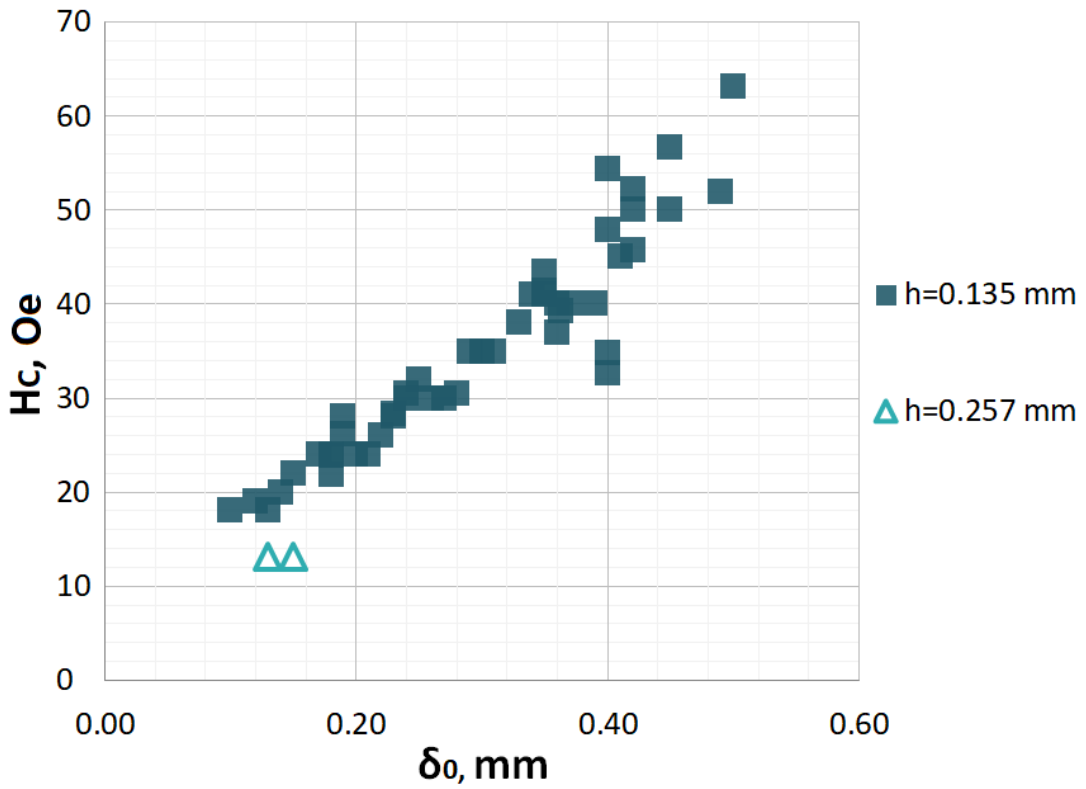
(a) FF21-5$_{100\%}$
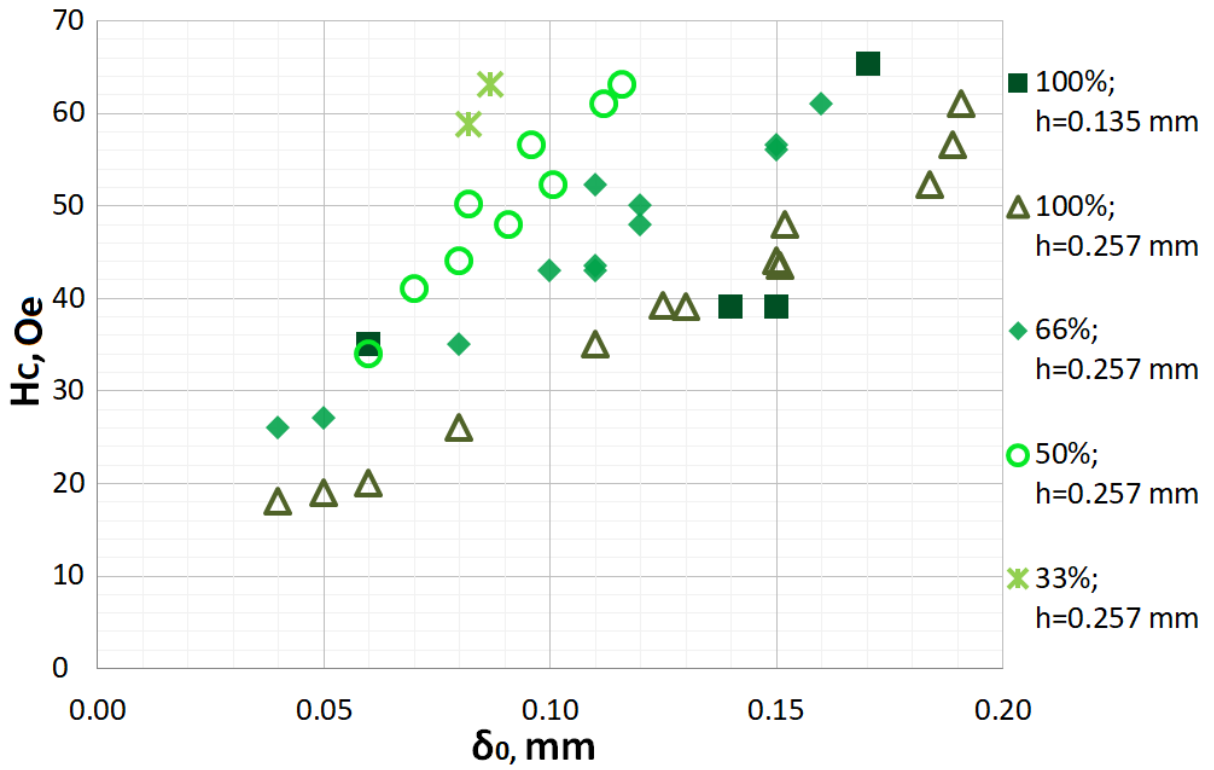
(b) FF09-9

A.25 Figure: Critical magnetic field H_c for magnetic micro-convection to emerge with respect to δ_0 in different micro-channels.

In figure A.26 micro-convective mixing δ_{MC} with respect to δ_0 for magnetic fluid KTF11-$1_{100\%}$ is explored. The results are grouped by magnetic field. The color of the markers becomes lighter as the magnetic field increases. The experiment here are carried out in the thinnest micro-channel: $h_1 = 0.135$ mm.
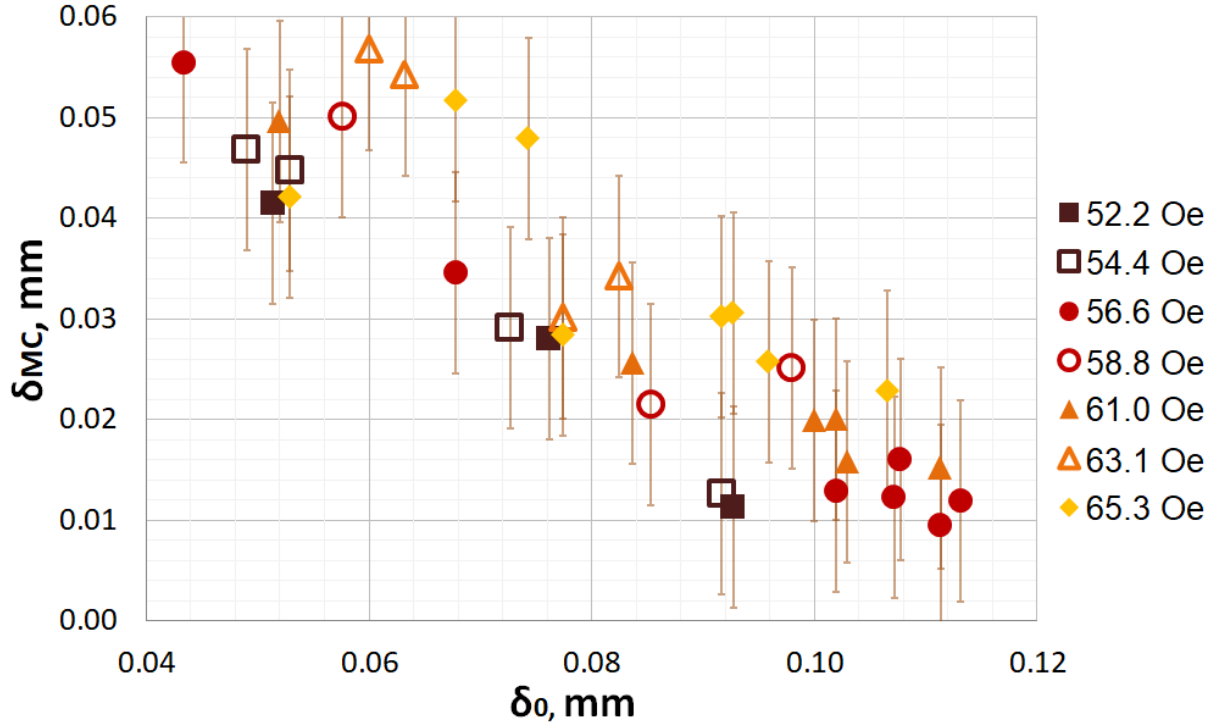
A.26 Figure: δ_{MC} with respect to δ_0 for various values of vertical external magnetic field in micro-channel with thickness $h_1 = 0.135$ mm for magnetic fluid KTF11-$1_{100\%}$.

Experiments carried out in the thickest micro-channel for magnetic fluids D107$_{100\%}$ and KTF11-$1_{100\%}$ are presented in figure A.27. The results are grouped by magnetic field and the color of the markers becomes lighter as the magnetic field increases. The data series of different magnetic field values here appear parallel to each other, so there the rate at which δ_{MC} decreases as the δ_0 increases is the same for all magnetic fields for the same magnetic fluid.

As expected higher values of δ_{MC} for the same initial smearing thickness δ_0 can be achieved in stronger magnetic fields in both exploed micro-channel thicknesses.
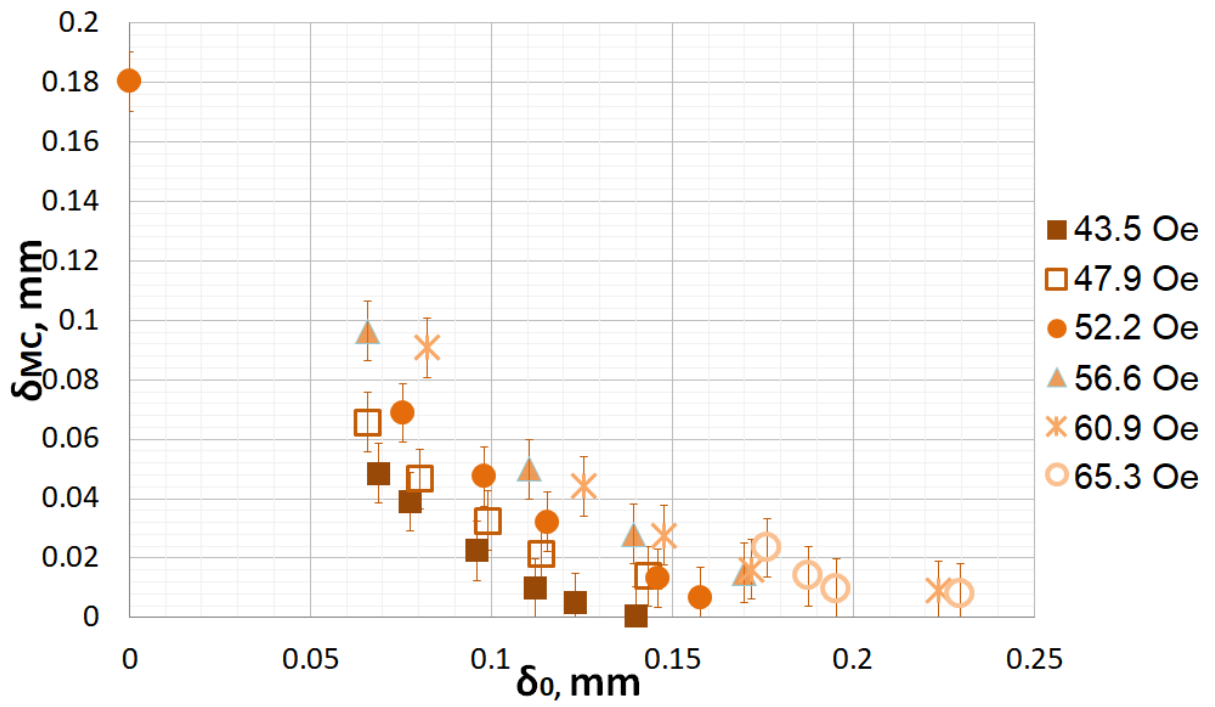
(a) D107$_{100\%}$
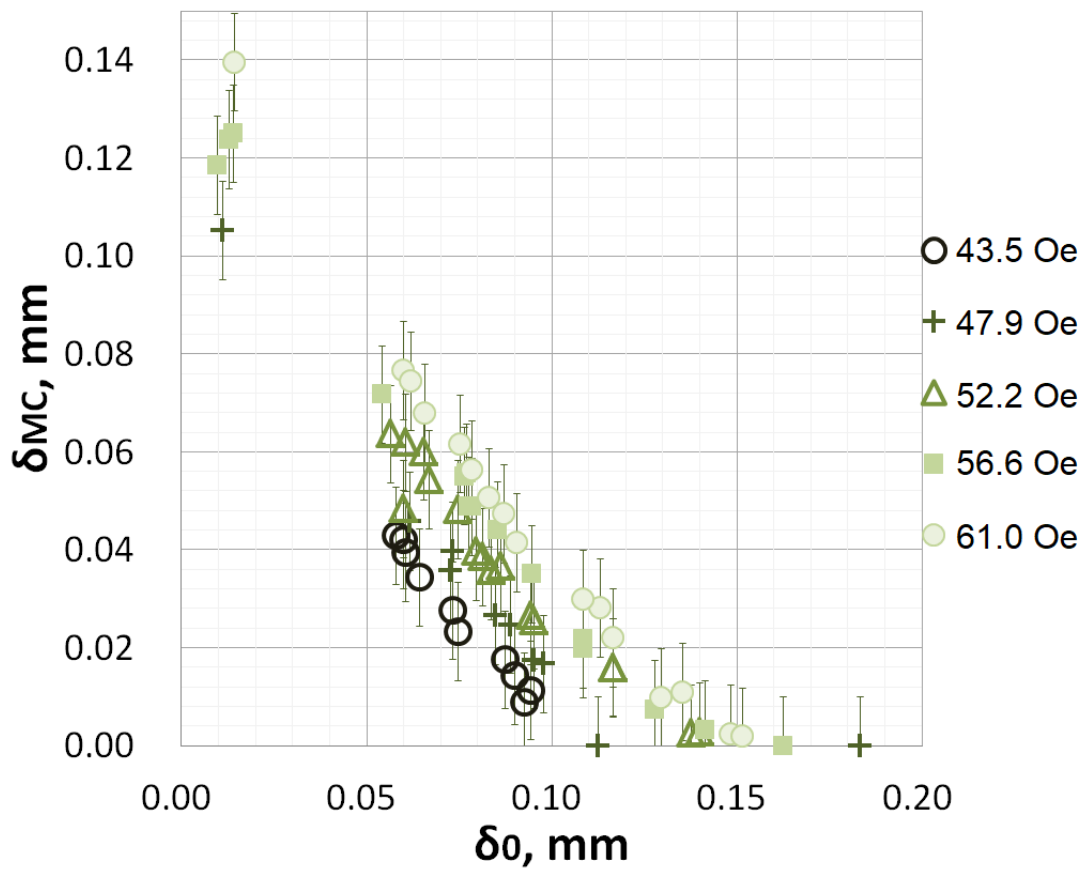
(b) KTF11-1$_{100\%}$

A.27 Figure: δ_{MC} with respect to δ_0 for various values of vertical external magnetic field in micro-channel with thickness $h_2 = 0.257$ mm.

The effect of micro-channel thickness on δ_{MC} with respect to δ_0 for magnetic fluid KTF11-1$_{100\%}$ is reviewed in figure A.28. The results are grouped by magnetic field. The same magnetic field value is represented with the same marker shape. Experiments carried out in the thinnest micro-channel ($h_1 = 0.135$ mm) are represented with purple markers, and experiments carried out in the thickest micro-channel ($h_2 = 0.257$ mm) are represented with green markers. The color of the markers becomes lighter as the magnetic field value increases. Here greater mixing due to magnetic micro-convection is achieved in the thickest micro-channel.
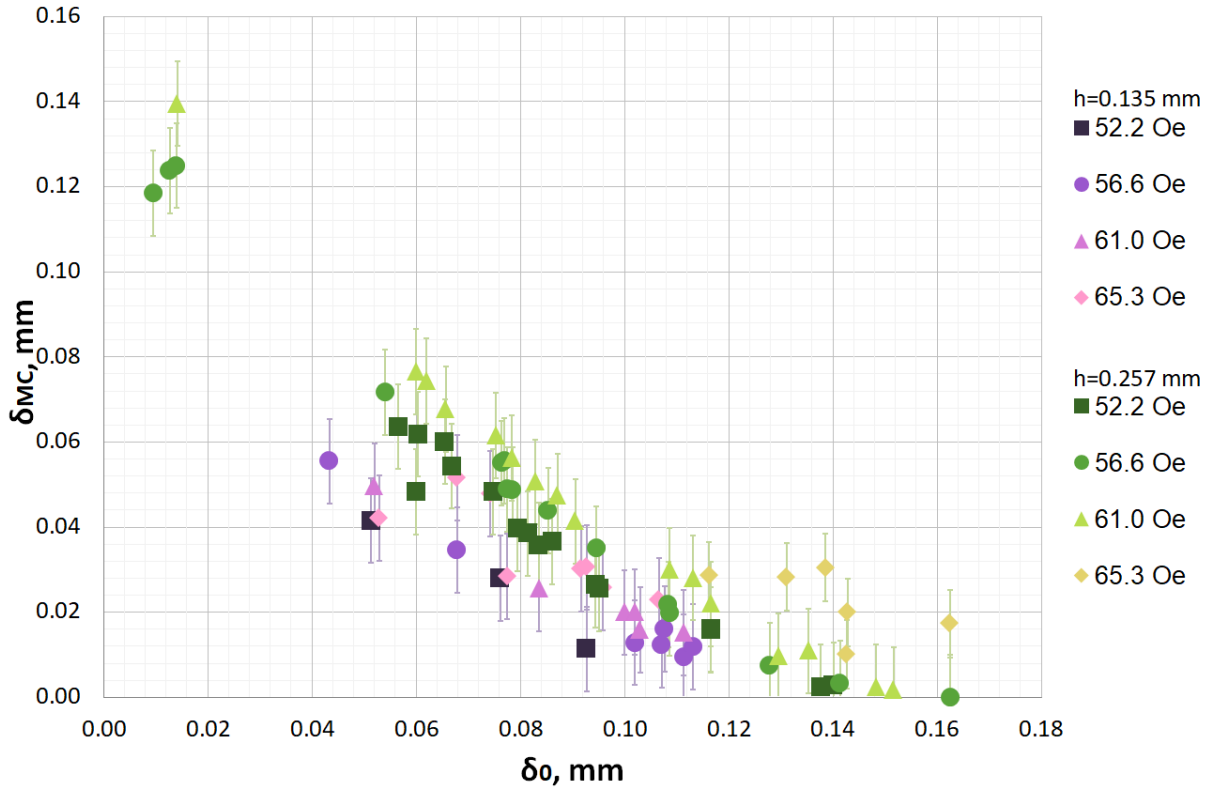
A.28 Figure: The effect of micro-channel thickness on δ_{MC} with respect to δ_0 in a vertical external magnetic field for magnetic fluid KTF11-1$_{100\%}$.

Dimensionless relationship of micro-convective mixing with respect the initial smearing is demonstrated in figure A.29. The vertical axis here represents the dimensionless δ_{MC} and the horizontal axis represents dimensionless time parameter t_0 for which both fluids have been diffusing before the experiment. Experiments are carried out with magnetic fluid FF21-5 in two different micro-channels. Micro-channel thickess affects the gravitational Rayleigh number. Both experimental series are for a quite large value of Ra$_m$~ 700000. The green markers representing experiments carried out in the thinnest micro-channel ($h_1 = 0.135$ mm) with smaller Ra$_g$= 80052 are above the red markers representing experiments carried out in the thickest micro-channel ($h_2 = 0.257$ mm) with larger Ra$_g$= 552294 for the same values of initial smearing time t_0. For example for experiments with with initial smearing time $t = 0.01$ dimensionless micro-convective mixing is $\delta_{MC;Ra_g=80052} \approx 1.75$ for

experiment with the smallest gravitational Rayleigh number, while $\delta_{\mathrm{MC,Ra_g}=552294} \approx 0.42$ for experiment with the largest gravitational Rayleigh number. So here it is visible how gravity restricts the magnetic micro-convection.
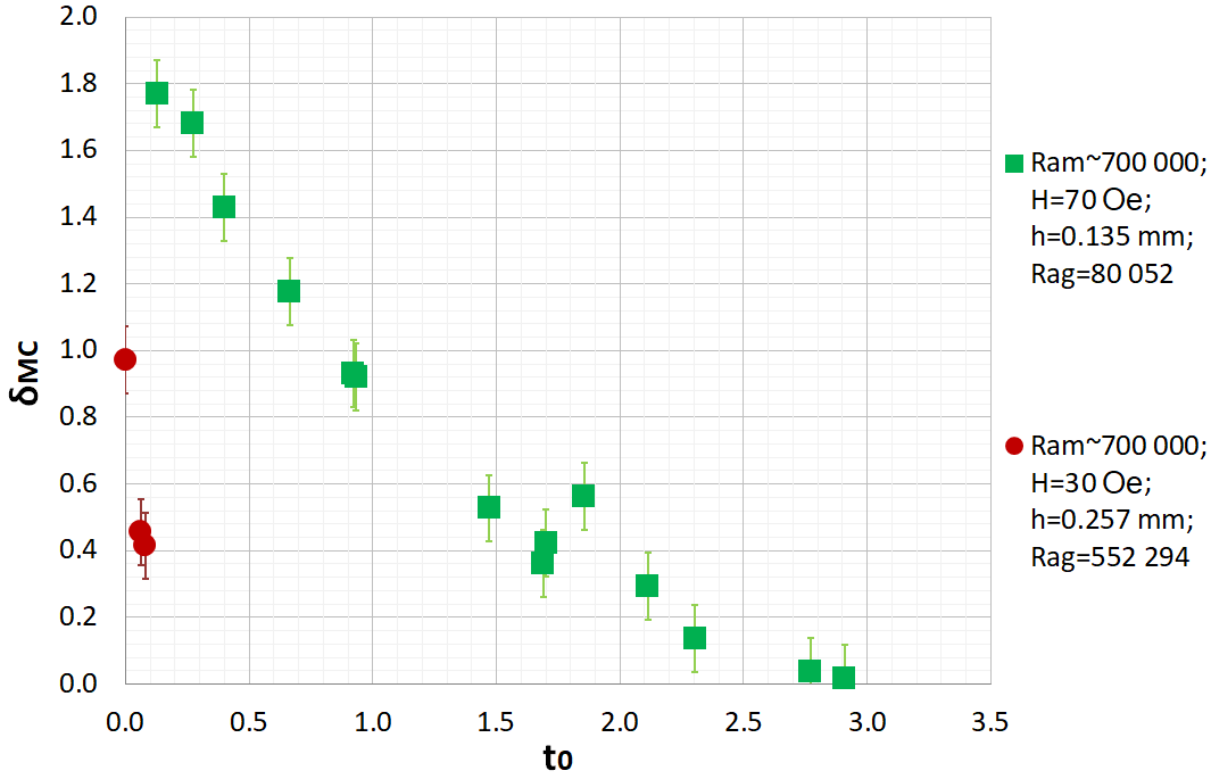

A.29 Figure: The effect of the micro-channel thickness on dimensionless δ_{MC} in a vertical magnetic field with respect to initial smearing t_0 for Magnetic fluid: FF21-5$_{100\%}$.

In figure A.30 magnetic field values to obtain a specific micro-convective mixing length δ_{MC} with respect to initial smearing thickness δ_0 for magnetic fluid FF09-9$_{100\%}$ in two different micro-channels ($h_1 = 0.135$ mm and $h_2 = 0.257$ mm) are explored. It is visible that in the thinnest micro-channel stronger magnetic fields must be applied to achieve the same micro-convective mixing length for experiments with the same initial smearing.

Next in figureA.31 magnetic field values to obtain a specific total mixing length Δ with respect to initial smearing thickness δ_0 for magnetic fluid KTF11-1$_{100\%}$ in thinnest micro-channel ($h_1 = 0.135$ mm) is explored. There is bigger dispersion of magnetic field values H in order to achieve the same total mixing length Δ than in experiments carried out in the thickest micro-channel ($h_2 = 0.257$ mm). For example, to achieve the total mixing $\Delta = 0.07$ mm the magnetic field varies from $H = 31$ Oe to $H = 42$ Oe.
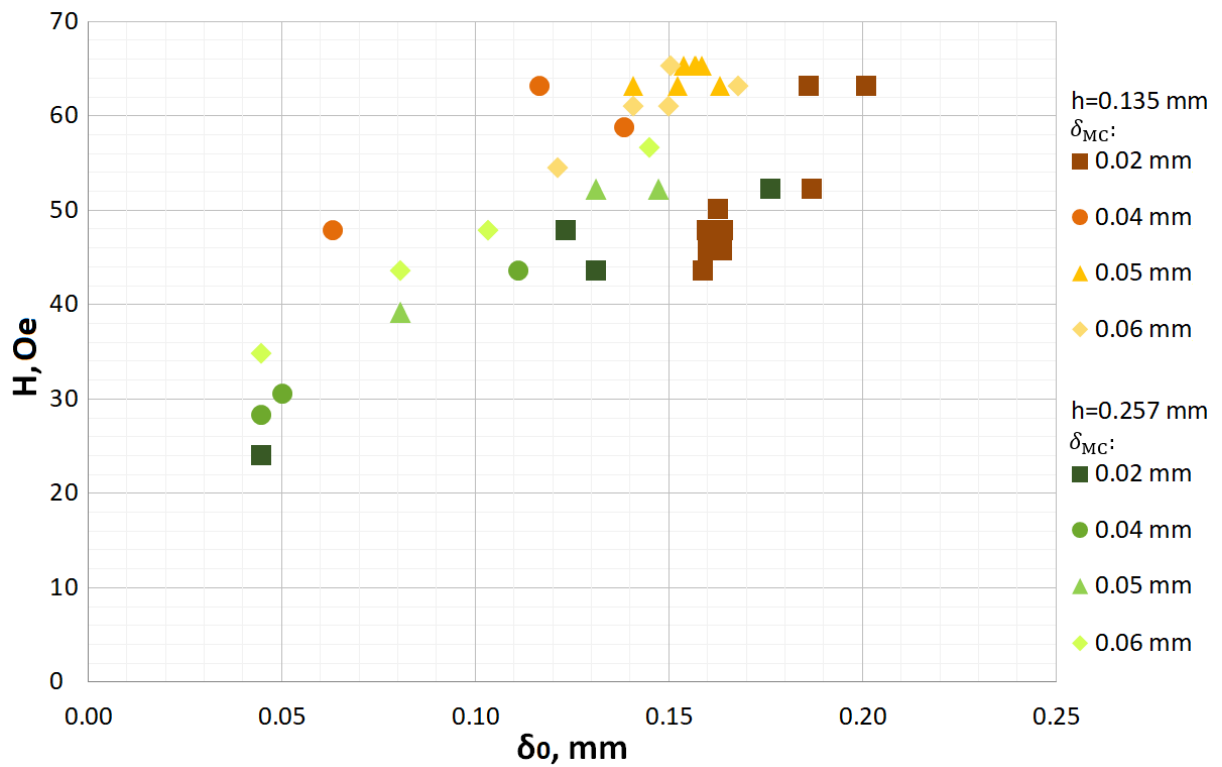
A.30 Figure: What magnetic field H should be applied to get a specific δ_{MC} with respect to δ_0 for experiments in different micro-channels. Magnetic fluid: FF09-9$_{100\%}$.
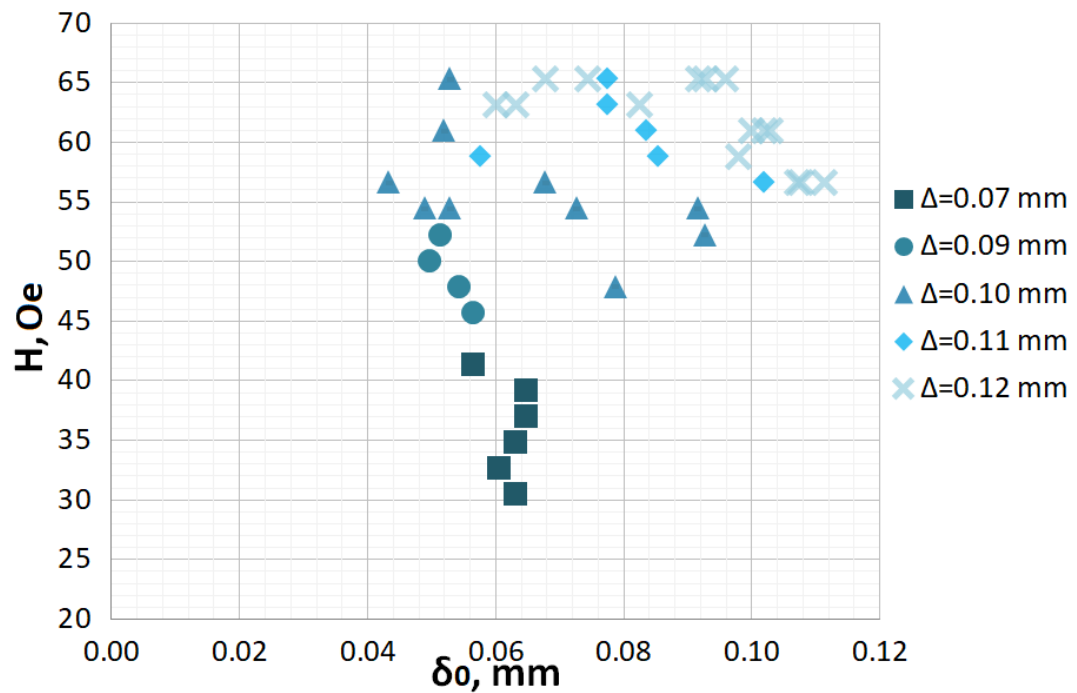
A.31 Figure: Magnetic field with respect to δ_0 for various values of total mixing length Δ for magnetic fluid KTF11-1$_{100\%}$ in micro-channel with thickness $h_1 = 0.135$ mm.

Effects of the magnetic field

Here, the additional experimental results of how the value of the vertical, external magnetic field affects the magnetic instability are collected.

In figure A.32 micro-convective mixing length δ_{MC} with respect to the magnetic field for magnetic fluid FF09-9$_{66\%}$ is explored. The experiments here are carried out in the micro-channel with thickness $h_2 = 0.257$ mm. The results are grouped by initial smearing thickness δ_0./ The color of the markers becomes darker as the values of δ_0 increase. As expected greater micro-convective mixing between the fluids can be achieved if the initial smearing thickness δ_0 is smaller.
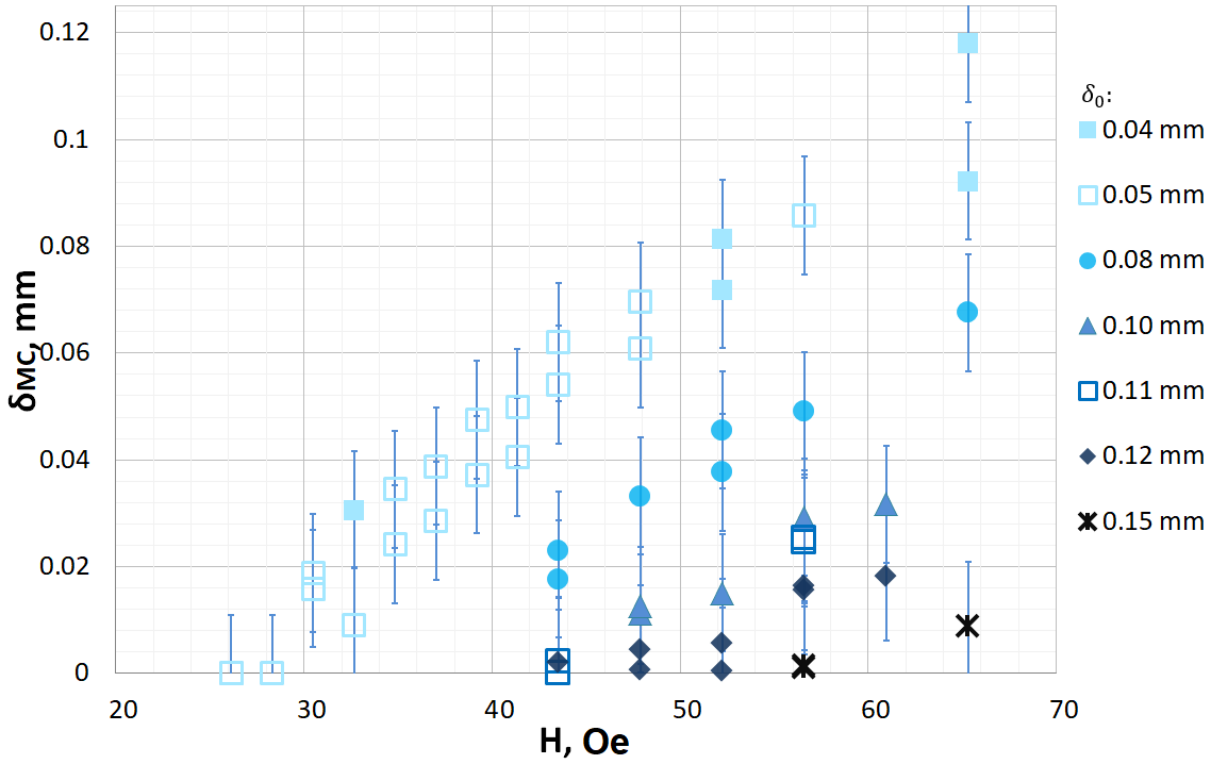
A.32 Figure: δ_{MC} with respect to H for various δ_0 in micro-channel with thickness $h_2 = 0.257$ mm. Magnetic fluid: FF09-9$_{66\%}$.

In figure A.33 the δ_{MC} of the same magnetic fluid is explored but in micro-channels with different thicknesses. The experiments are carried out with magnetic fluid KTF11-1$_{100\%}$. The results are grouped by initial smearing thickness δ_0./ The color of the markers becomes darker as the values of δ_0 increase. The change of δ_{MC} due to δ_0 at the same values of H is greater in the thicker micro-channel with $h_2 = 0.257$ mm. For example, the difference between the values of δ_{MC} when the $\delta_0 = 0.05$ mm and $\delta_0 = 0.09$ mm while magnetic field is $H = 60$ Oe is approximately $\Delta\delta_{\text{MC}} \approx 0.05 - 0.02 = 0.03$ mm in micro-channel with $h_1 = 0.135$ mm, whereas in the thicker micro-channel with $h_2 = 0.257$ mm this difference is $\Delta\delta_{\text{MC}} \approx 0.07 - 0.03 = 0.04$ mm. This will be explored further later in this chapter, as

by judging from these two graphs it seems that the thickness of the micro-channel affects the δ_0 effect on the δ_{MC}.
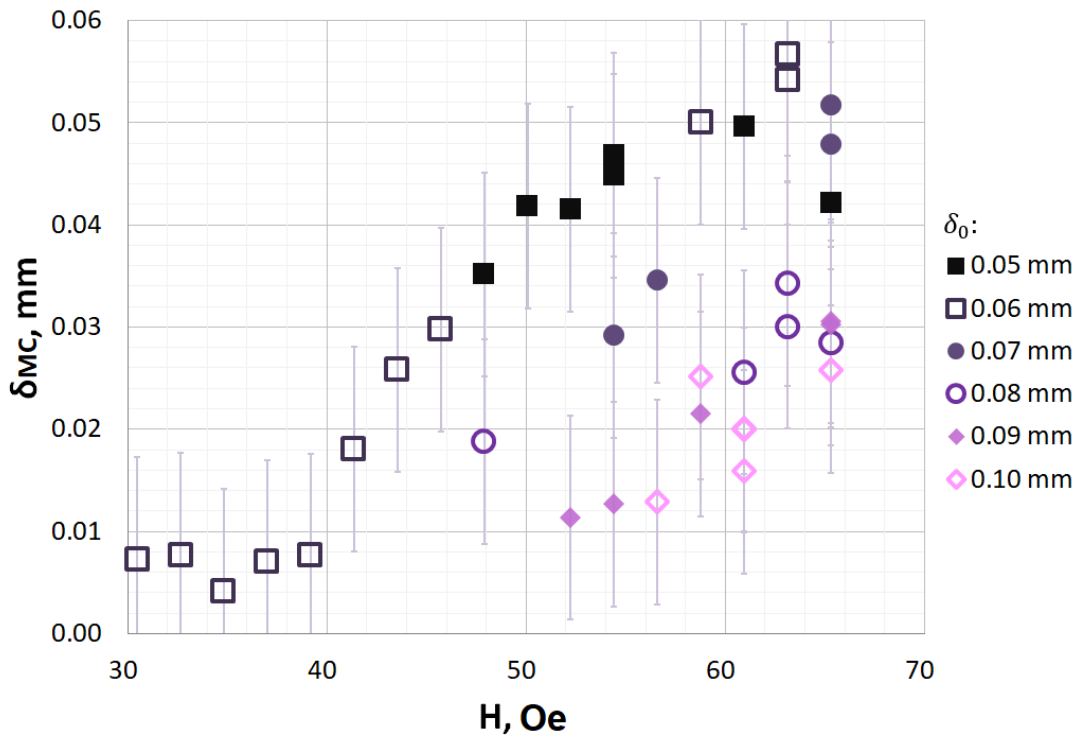

**(a)** $h_1 = 0.135$ mm
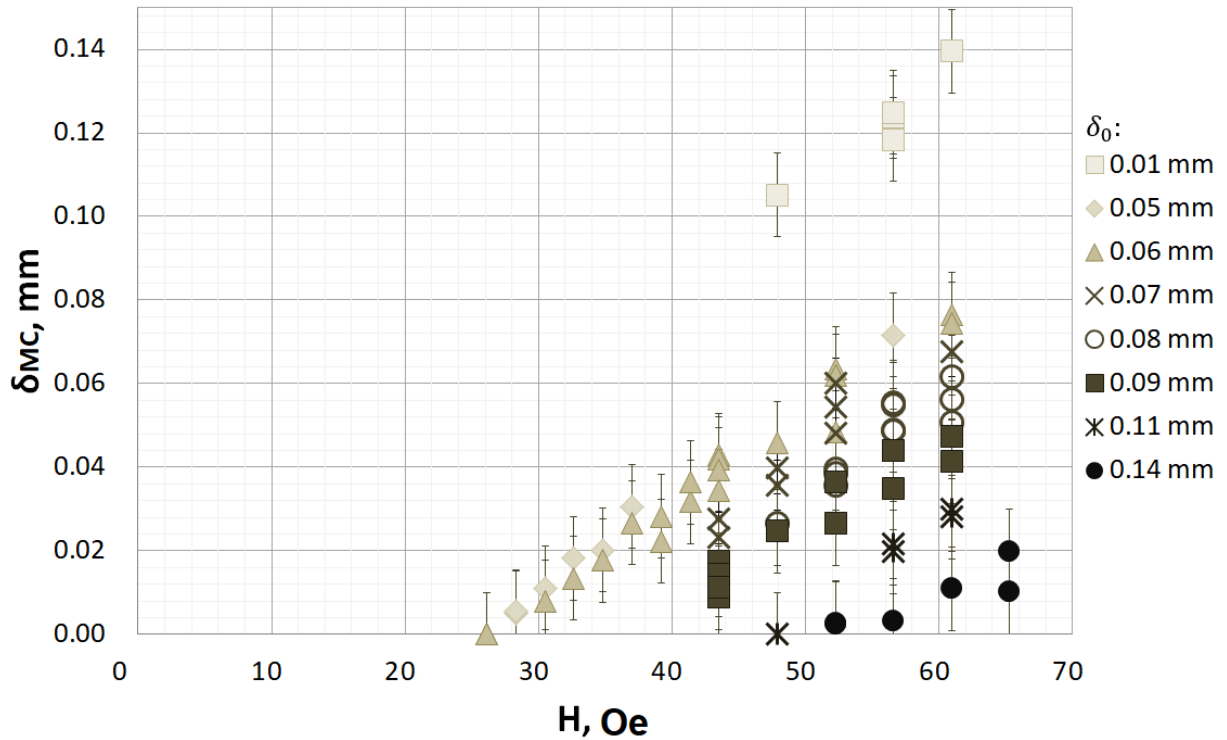
(b) $h_2 = 0.257$ mm

A.33 Figure: δ_{MC} with respect to H for various δ_0 in two different micro-channels. Magnetic fluid: KTF11-1$_{100\%}$.

In the experiments with external magnetic field positioned vertically there are two possible directions of the magnetic field. The magnetic field can be directed upwards (opposite to the gravity $\vec{g}$) or downwards (the same direction as the gravity $\vec{g}$).The effect of this direction of the vertical magnetic field is reviewed in fig. A.34. It is visible from this fig. that the differences in the values of δ_{MC} between upwards ("up"- blue markers in the graph) or downwards ("down"- red markers in the graph) are statistically insignificant as the deviation between the values is smaller than the errors of the measured data. All other graphs and pictures in this chapter represent the data measured in an upwards directed vertical external magnetic field.
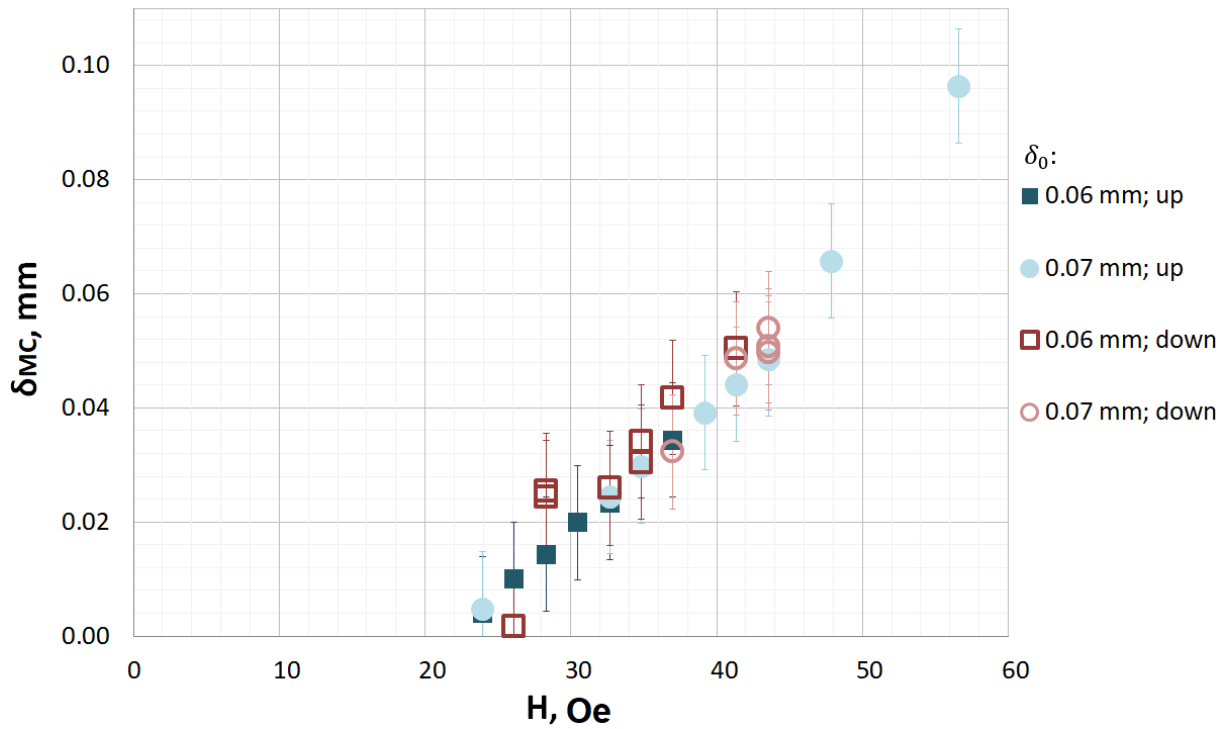
A.34 Figure: Effect of magnetic field's direction (up or down) on δ_{MC} for various δ_0 in micro-channel with thickness $h_2 = 0.257$ mm for magnetic fluid D107$_{100\%}$.

Next the effect of the micro-channel thickness is explored in figure A.35 for magnetic fluid KTF11-1$_{100\%}$. The experiments are grouped by initial smearing thickness δ_0. The same marker shape corresponds to the same δ_0 per graph. Experiments carried out in the thinnest micro-channel ($h_1 = 0.135$ mm) are represented with blue markers and the experiments carried out in the thickest micro-channel ($h_2 = 0.257$ mm) are represented with orange markers. The color of the markers becomes lighter as the value of δ_0 increases. Greater mixing due to magnetic micro-convection here is achieved in the thickest micro-channel for the same values of δ_0 in the same magnetic field.
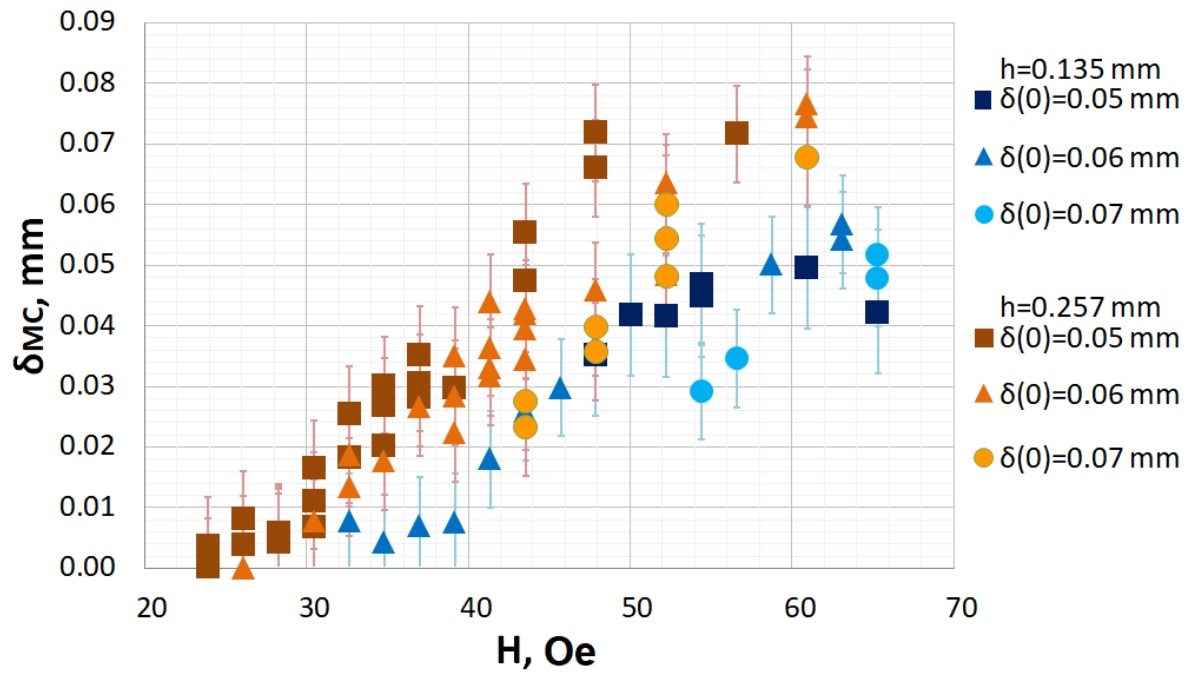
(a) Smaller values of δ_0
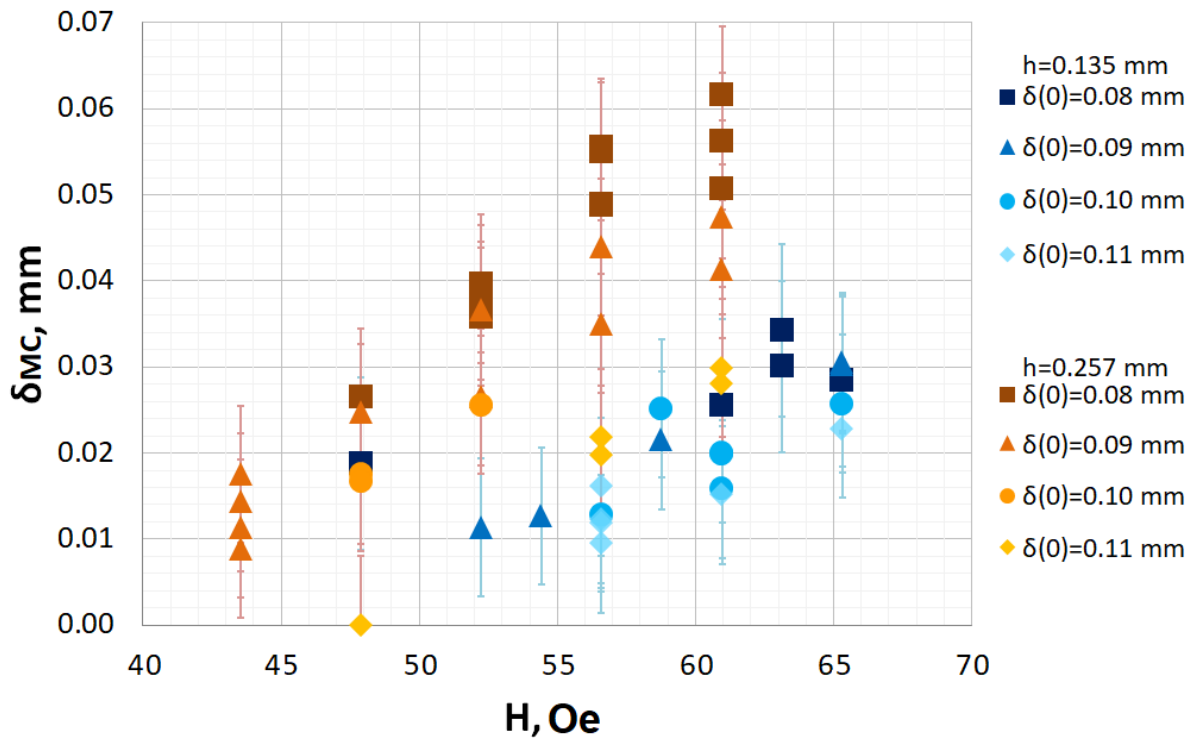

(b) Bigger values of δ_0

A.35 Figure: The effect of micro-channel thickness on δ_{MC} for various δ_0 for magnetic fluid KTF11-1$_{100\%}$.

In figure A.36 maximal achievable micro-convective length $\delta_{MC,max}$ is explored in two graphs for all the investigated magnetic fluids. $\delta_{MC,max}$ is the value of the micro-convective mixing length that can be achieved in a certain magnetic field if the interface between the

mixing fluids is perfectly sharp at the beginning of the experiment. $\delta_{MC,max}$ values are estimated as explained more in the main text of this thesis.
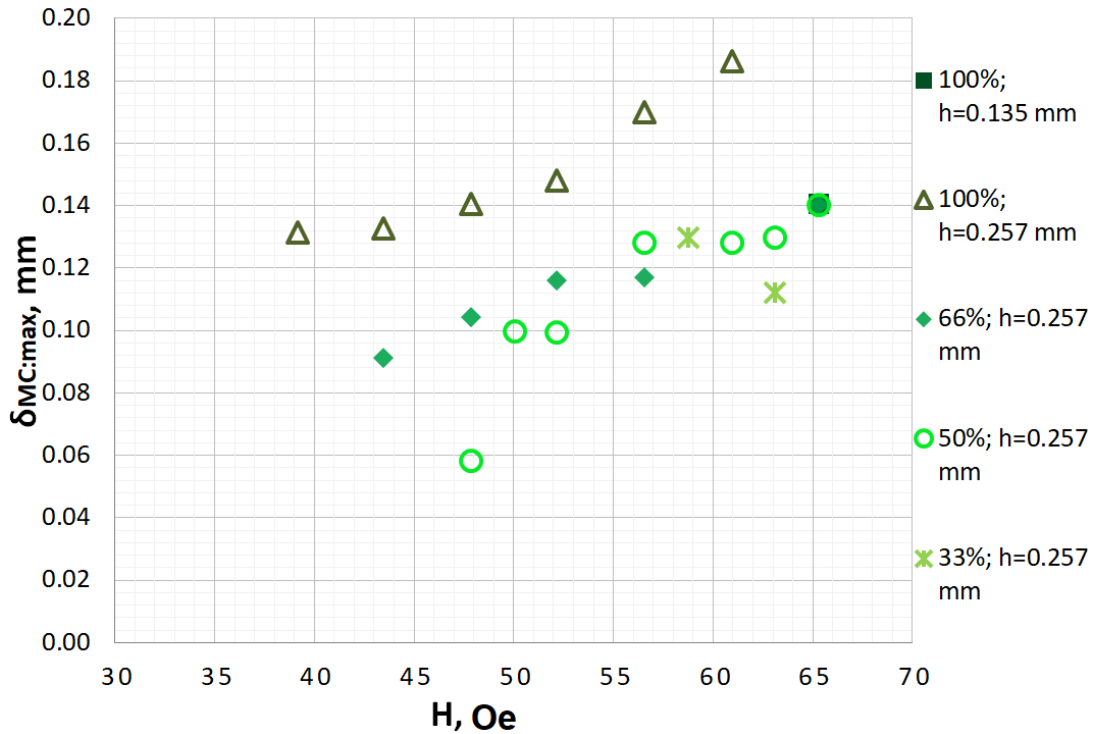
(a) Magnetic fluid: FF09-9
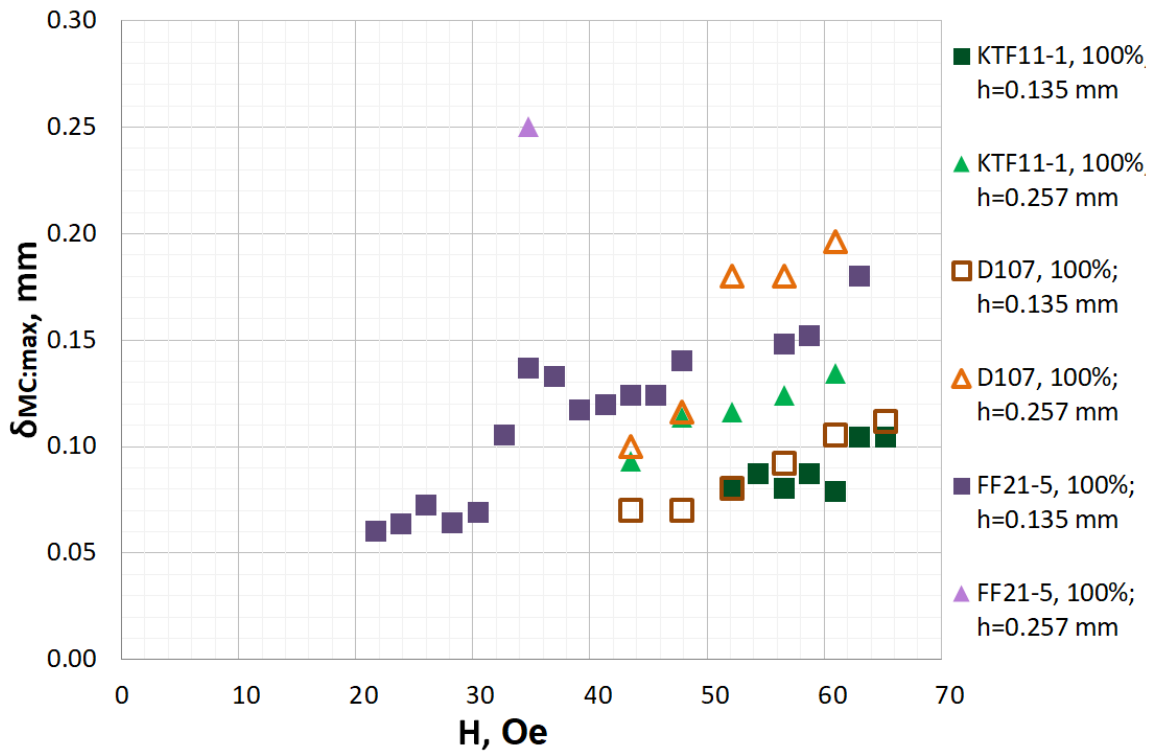
(b) Various magnetic fluids

A.36 Figure: Maximal value of δ_{MC} with respect to external magnetic field for sharp initial interface $\delta_0 = 0$ mm

Micro-convective mixing is more effective for more concentrated magnetic fluids, as the darker markers are above the lighter ones for the same values of external magnetic field. For example, when mixing the fluids with the sharp initial interface between them in the thickest micro-channel ($h_2 = 0.257$ mm) in magnetic field $H = 52.2$ Oe mixing parameter is estimated to be $\delta_{MC:max;100\%} \approx 0.144$ mm for the most concentrated magnetic fluid (triangle shaped markers in fig. A.36a), $\delta_{MC:max;66\%} \approx 0.116$ mm for 66% magnetic fluid dilution (rhombus shaped markers in fig. A.36a), and $\delta_{MC:max;50\%} \approx 0.10$ mm for even more diluted magnetic fluid (round markers in fig. A.36a). In the second graph (fig. A.36b) all of the magnetic fluids represented are with the highest possible concentration (100%) and the effect of the micro-channel thickness is explored. All experiments carried out in the thinnest micro-channel ($h_1 = 0.135$ mm) are represented by square shaped markers and experiments carried out in the thickest micro-channel ($h_2 = 0.257$ mm) are represented by triangle shaped markers.

Experiments carried out with the same magnetic fluid have the same color tonality: green markers for magnetic fluid KTF11-1, orange markers for magnetic fluid D107 and purple markers for magnetic fluid FF21-5. It is visible that for all magnetic fluids the experiments carried out in the thickest micro-channel have larger values of $\delta_{MC:max}$ for the same values of external magnetic field. So, when mixing water and magnetic fluid in a vertical external magnetic field greater mixing thickness can be achieved in a thicker micro-channel. Also, from these magnetic fluids the greater mixing was achieved with FF21-5. The magnetic fluid FF21-5 has the greatest particle volume fraction $\Phi_{Vol} = 5\%$ and the greatest magnetic susceptibility $\chi = 0.0793$ from all of the used magnetic fluids within this study.

Next the dilution ratio effects are explored. In figure A.37 the visual results are demonstrated. The vertical axis here represents the time since the beginning of the experiment and the horizontal axis represents the dilution ratio of the magnetic fluid. One column represents a single experiment dynamics in time. The experiments are carried out with the same magnetic fluid FF09-9 in the same magnetic field $H = 65.3$ Oe. The initial smearing thickness for all three experiments is $\delta_0 = 0.06$ mm. The experiments are carried out in the micro-channel with thickness $h_2 = 0.257$ mm.

Here the fingers have started to form at $t = 1$ s for magnetic fluid FF09-9$_{66\%}$, at $t = 4$ s for FF09-9$_{50\%}$ and only at $t = 10$ s for FF09-9$_{33\%}$. Subsequently after a constant period of time since the beginning of the experiment the fingers of the instability are taller for in experiments with more concentrated magnetic fluids. For example, here in the first column with magnetic fluid FF09-9$_{66\%}$ the fingers of the instability are approximately 0.38 mm tall at $t = 6$ s, while in the second column for FF09-9$_{50\%}$ at the same time point fingers are noticeably shorter: 0.24 mm. In addition to the previous the fingers of the instability are yet to be formed at $t = 6$ s in the last column that represents experiments

with the most diluted magnetic fluid FF09-9$_{33\%}$.

In the experiment with magnetic fluid FF09-9$_{66\%}$ (first column) the fingers have grown more than two times in first five seconds since their appearance: the fingers start to form shortly before $t = 1$ s and at $t = 1$ s they are 0.17 mm tall, and at $t = 6$ s they are 0.38 mm tall. In the second column representing experiments with more diluted magnetic fluid FF09-9$_{50\%}$ the fingers have grown to 0.31 mm in first eight seconds since the emergence of the instability at $t \approx 2$ s. The height of the fingers is smaller and the time of their growth is longer than for FF09-9$_{66\%}$. In fact this height 0.31 mm is also the maximal height of the fingers for this experiment. The fingers do not grow any more after $t = 10$ s, but the mixing length continues to increase due to the diffusion. Micro-convective mixing is more effective for more concentrated magnetic fluids.
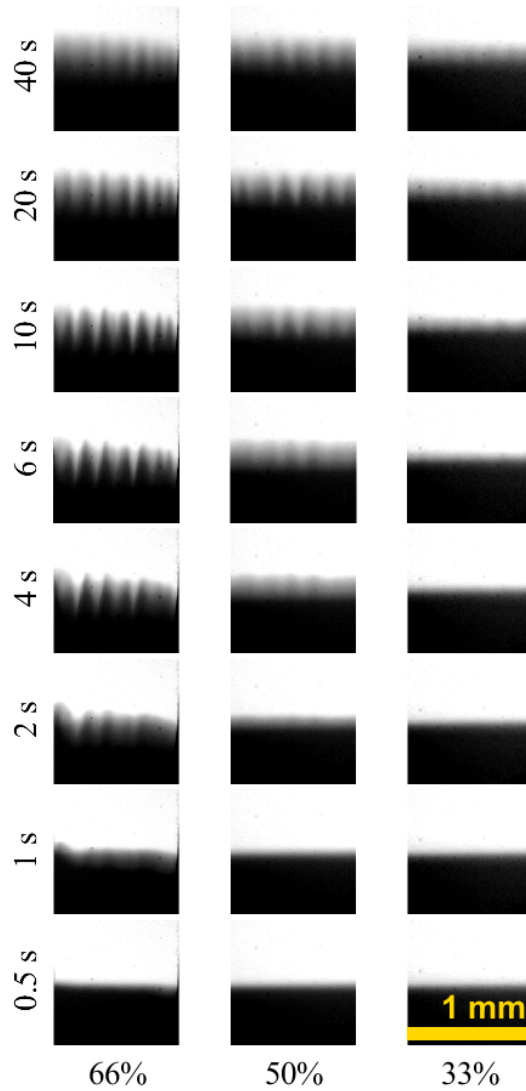
A.37 Figure: Image series of magnetic micro-convection dynamics for various dilution ratios of the same magnetic fluid FF09-9 in the same magnetic field $H = 65.3$ Oe with $\delta_0 = 0.06$ mm in micro-channel with thickness $h_2 = 0.257$ mm. A single image represents 1.0×1.0 mm region.

A.1.5 Comparison of experiments carried out in horizontal and vertical magnetic fields

Here additional experimental data that compliments §4.3. are collected.

Effects of the initial smearing thickness

Here the additional experimental results of micro-convection dynamics with respect to the initial smearing thickness δ_0 is collected.

Comparison of the magnetic field direction for the experiments carried out in the micro-channel with thickness $h_1 = 0.135$ mm is showed in figures A.38 and A.39 For concentrated magnetic fluids KTF11-1$_{100\%}$ and FF09-9$_{100\%}$ accordingly.

In figure A.38 micro-convective mixing length δ_{MC} values are explored. Data is grouped by the value of the external magnetic field. The same magnetic field value is represented by the same marker shape. The experiments carried out in a horizontal magnetic field are represented with blue markers, while the experiments carried out in a vertical magnetic field are represented with orange markers. As the blue markers are above, it is visible that greater δ_{MC} values can be achieved in a horizontal magnetic field for the same initial smearing thickness δ_0 in the same magnetic field intensity.
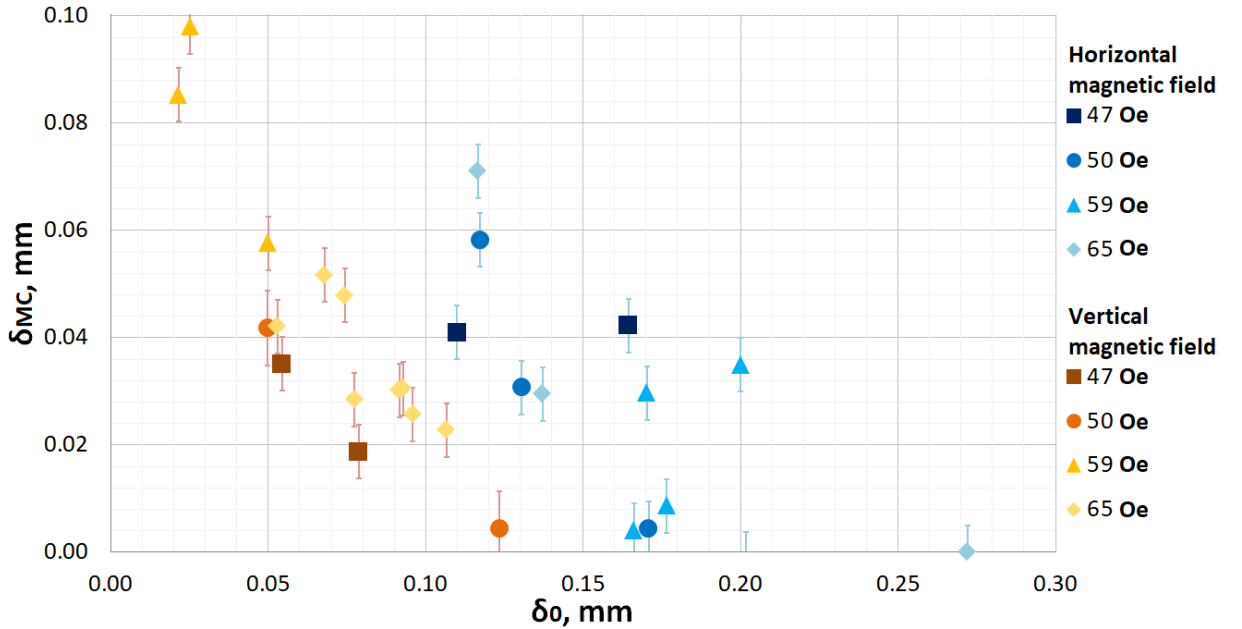
A.38 Figure: Comparison between horizontal and vertical magnetic field's effect on magnetic micro-convection. δ_{MC} with respect to δ_0 for various magnetic fields for magnetic fluid KTF11-1$_{100\%}$ in micro-channel with thickness $h_1 = 0.135$ mm.

In figure A.39 magnetic field values that must be applied to obtain a certain micro-convective mixing length δ_{MC} are explored. The data is grouped by δ_{MC} values, and the same δ_{MC} value is represented with the same marker shape. The experiments carried out

in a horizontal magnetic field are represented with green markers, while the experiments carried out in a vertical magnetic field are represented with red markers. To obtain the same micro-convective mixing length δ_{MC} stronger magnetic fields must be applied if the field direction is vertical, for the experiments with the same initial smearing thickness δ_0.
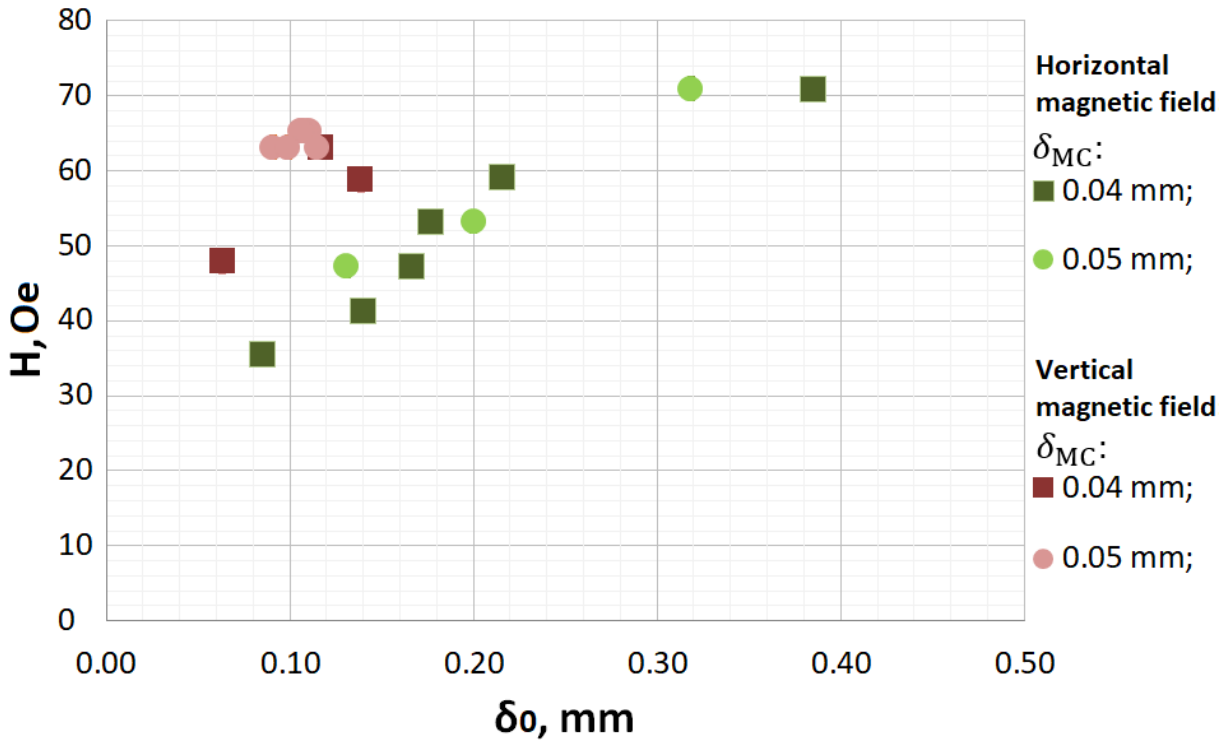
A.39 Figure: Comparison between horizontal and vertical magnetic field's effect on magnetic micro-convection. What value of H must be applied to obtain certain δ_{MC} with respect to δ_0 for magnetic fluid FF09-9$_{100\%}$ in micro-channel with thickness $h_1 = 0.135$ mm.

In figure A.40 micro-convective mixing with respect to the inital smearing thickness δ_0 for various magnetic fields for magnetic fluid FF09-9$_{100\%}$ in micro-channel with thickness $h_2 = 0.257$ mm is explored. Data is grouped by the value of the external magnetic field. The same magnetic field value is represented by the same marker shape. The experiments carried out in a horizontal magnetic field are represented with blue markers, while the experiments carried out in a vertical magnetic field are represented with orange markers. As the blue markers are above, it is visible again that greater δ_{MC} values can be achieved in a horizontal magnetic field for the same initial smearing thickness δ_0 in the same magnetic field intensity.
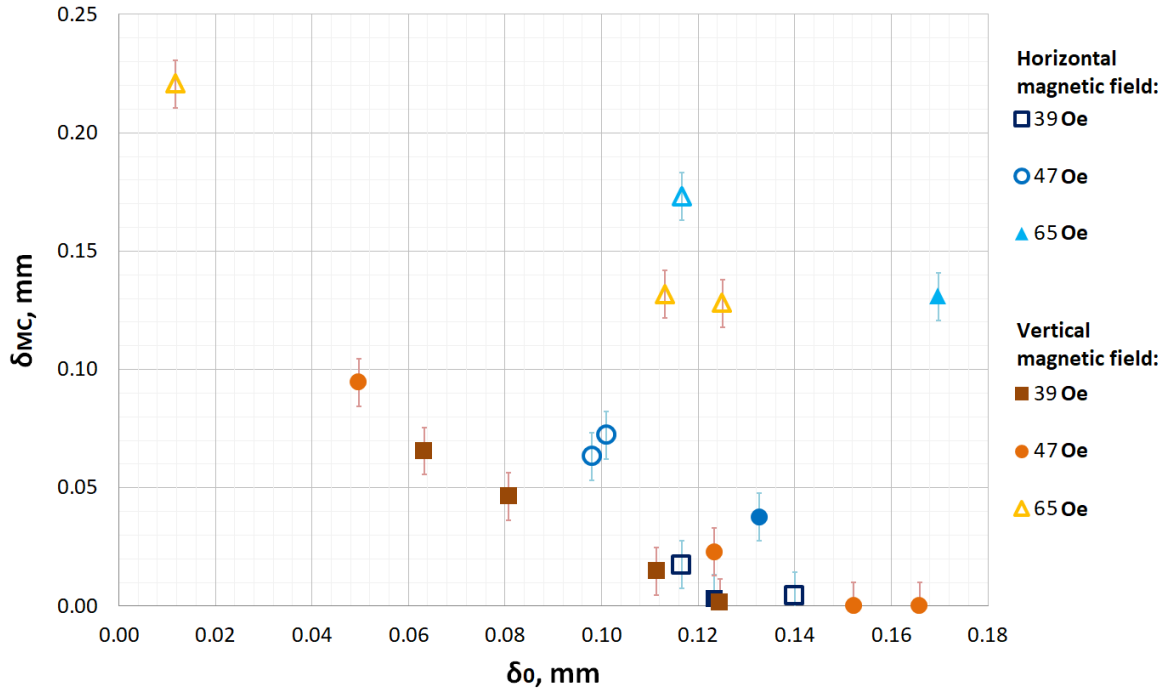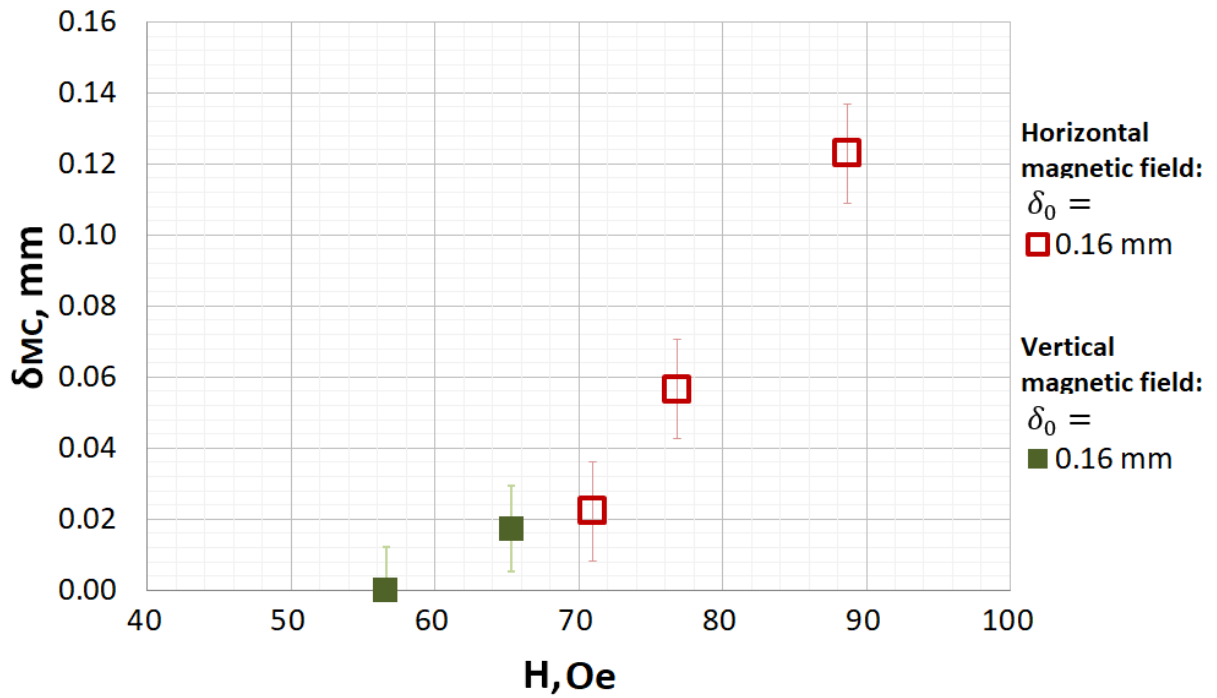
A.40 Figure: Comparison between horizontal and vertical magnetic field's effect on magnetic micro-convection. δ_{MC} with respect to δ_0 for various magnetic fields for magnetic fluid FF09-9$_{100\%}$ in micro-channel with thickness $h_2 = 0.257$ mm.

Effects of the magnetic field intensity

Here the additional experimental results of micro-convection dynamics with respect to the value of the external magnetic field H are collected.

Experiments are visualized by graphs collected in figures A.41 for magnetic fluid KTF11-1$_{100\%}$, in A.42 for magnetic fluid D107$_{100\%}$, in A.43 for magnetic fluid FF09-9$_{100\%}$ in thinnest micro-channel ($h_1 = 0.135$ mm), and in figure A.44 for magnetic fluid FF09-9$_{100\%}$ in thickest micro-channel ($h_2 = 0.257$ mm). In all of these graphs the experiments carried out in a horizontal magnetic field are represented by red markers and experiments carried out in the vertical magnetic field are represented by green ones. The data is grouped by initial smearing thickness δ_0. The same value of δ_0 is represented with the same marker shape per graph. The color of the markers becomes lighter as the value of δ_0 increases.
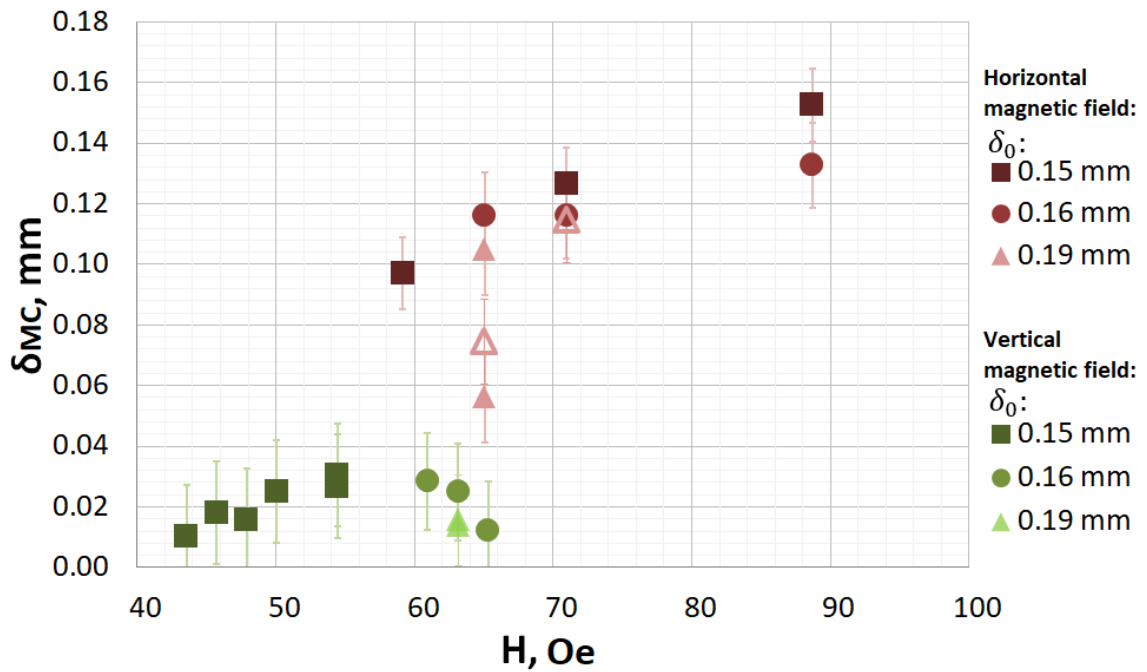
A.41 Figure: Comparison between horizontal and vertical magnetic field's effect on magnetic micro-convection. δ_{MC} with respect to magnetic field for various δ_0 for magnetic fluid KTF11-1$_{100\%}$. Micro-channel with thickness $h_2 = 0.257$ mm. Empty markers represent δ_{MC} obtained with attachment method.
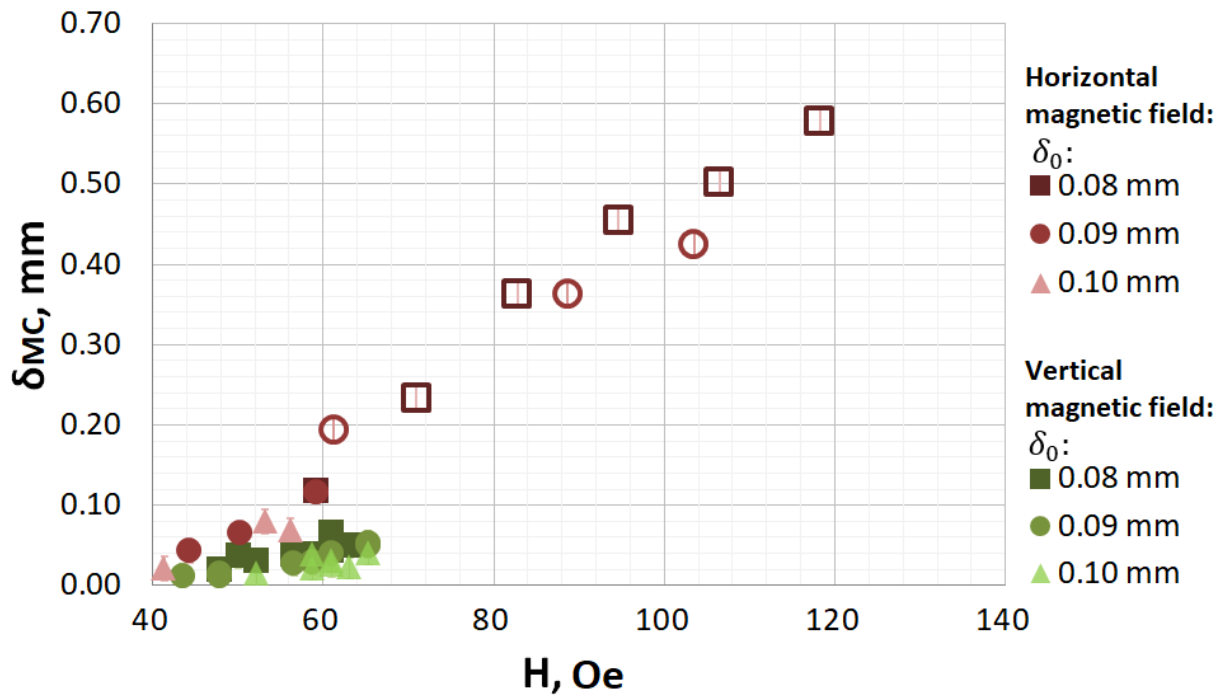
A.42 Figure: Comparison between horizontal and vertical magnetic field's effect on magnetic micro-convection. δ_{MC} with respect to magnetic field for various δ_0 for magnetic fluid D107$_{100\%}$ in micro-channel with thickness $h_1 = 0.135$ mm. Empty markers represent δ_{MC} obtained with attachment method.
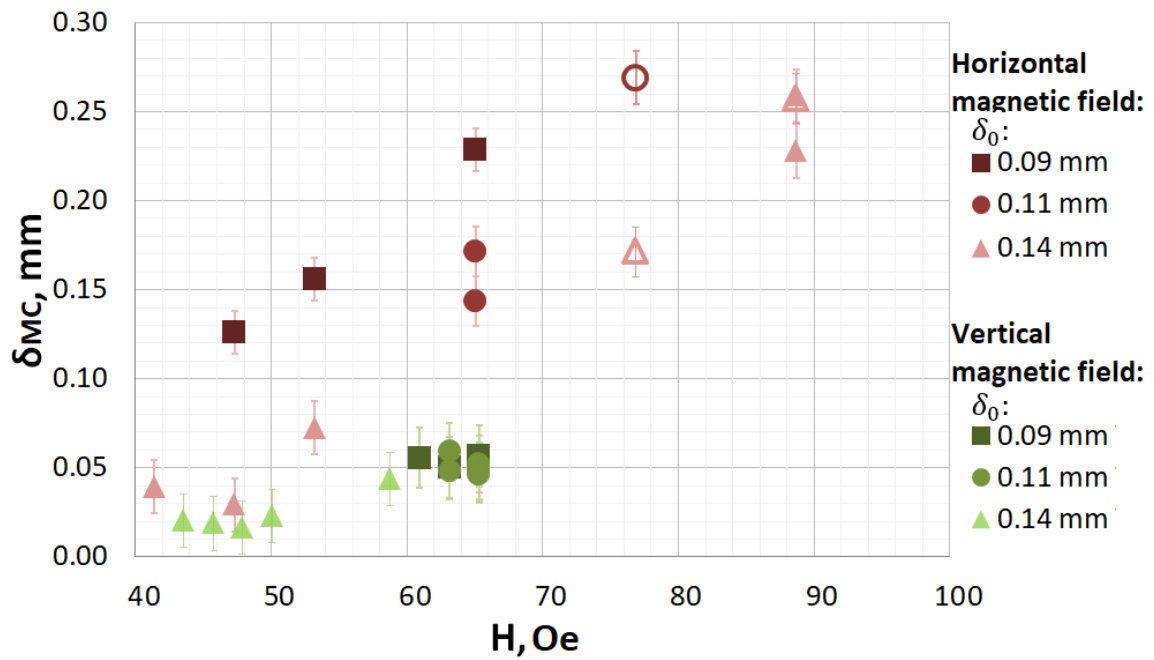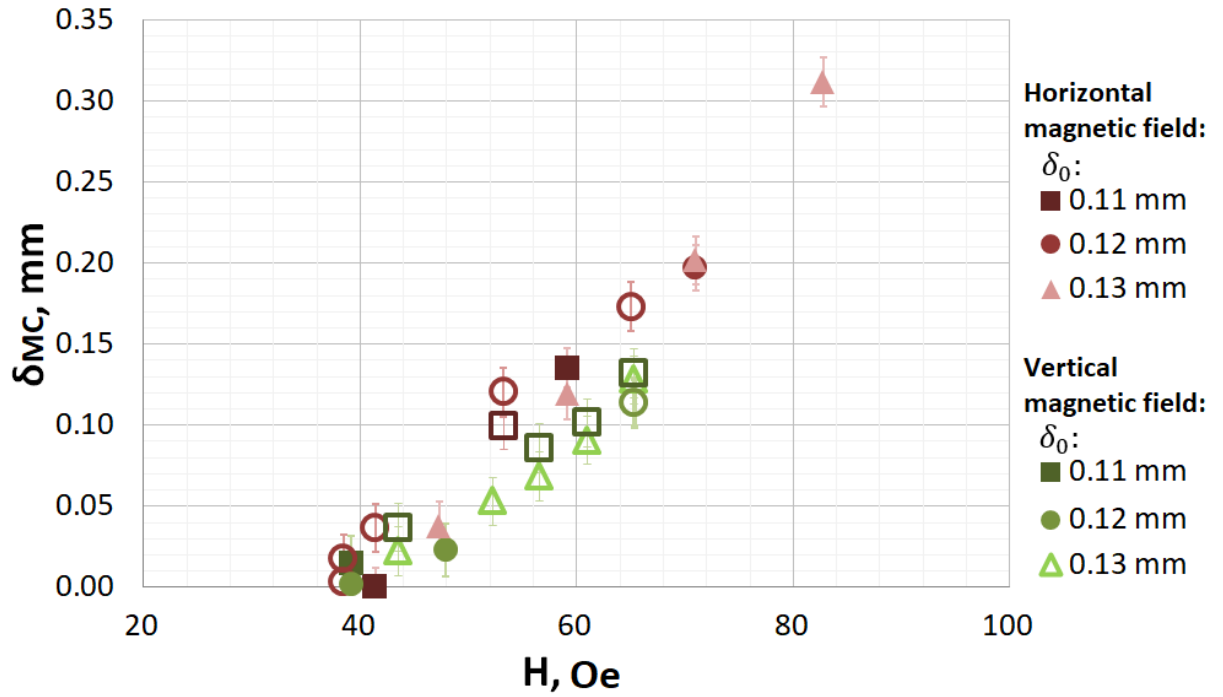
(a) Smaller values of δ_0.

(b) Larger values of δ_0.

A.43 Figure: Comparison between horizontal and vertical magnetic field's effect on magnetic micro-convection. δ_{MC} with respect to magnetic field for various δ_0 for magnetic fluid FF09-9$_{100\%}$ in micro-channel with thickness $h_1 = 0.135$ mm. Empty markers represent δ_{MC} obtained with attachment method.

A.44 Figure: Comparison between horizontal and vertical magnetic field's effect on magnetic micro-convection. δ_{MC} with respect to magnetic field for various δ_0 for magnetic fluid FF09-9$_{100\%}$ in micro-channel with thickness $h_2 = 0.257$ mm. Empty markers represent δ_{MC} obtained with attachment method.

In figure A.43a it seems that the difference between the green and red squared markers representing results with smaller $\delta_0 = 0.09$ mm seems larger than the difference between the green and red triangle markers representing results with larger $\delta_0 = 0.15$ mm. So the differences in obtainable δ_{MC} for the same magnetic field intensity between horizontal and vertical magnetic field direction might be larger if the initial smearing between the mixing fluids is smaller.

In figures A.44 and A.43a magnetic fluid FF09-9$_{100\%}$ with similar δ_0 values is explored. And the difference in absolute values between the red and green markers is undeniably larger in A.43a that represents mixing in thinner micro-channel. For example, the difference of δ_{MC} between the two magnetic field directions, in thinner micro-channel in magnetic field $H = 65$ Oe ($h_1 = 0.135$ mm) is $\delta_{MC,hor} - \delta_{MC,vert} \approx 0.16 - 0.05 = 0.11$ mm, while in thicker micro-channel ($h_2 = 0.257$ mm) for the same values of δ_0 and H this difference is $\delta_{MC,hor} - \delta_{MC,vert} \approx 0.17 - 0.13 = 0.04$ mm.

## A.2 Additional information about data processing

A screen-shot of data processing software made in MATLAB® is visible in figure A.45. Here the graph on the left represents two time-points within the same experiment visible on the left. During the data processing step showed in the figure mixing length 2δ is calculated. Black rectangle on the experimental images represents ROI that is processed. This visual software made by the author of this thesis made the data validation process easier, as graphs could be processed side by side with the images captured by camera.
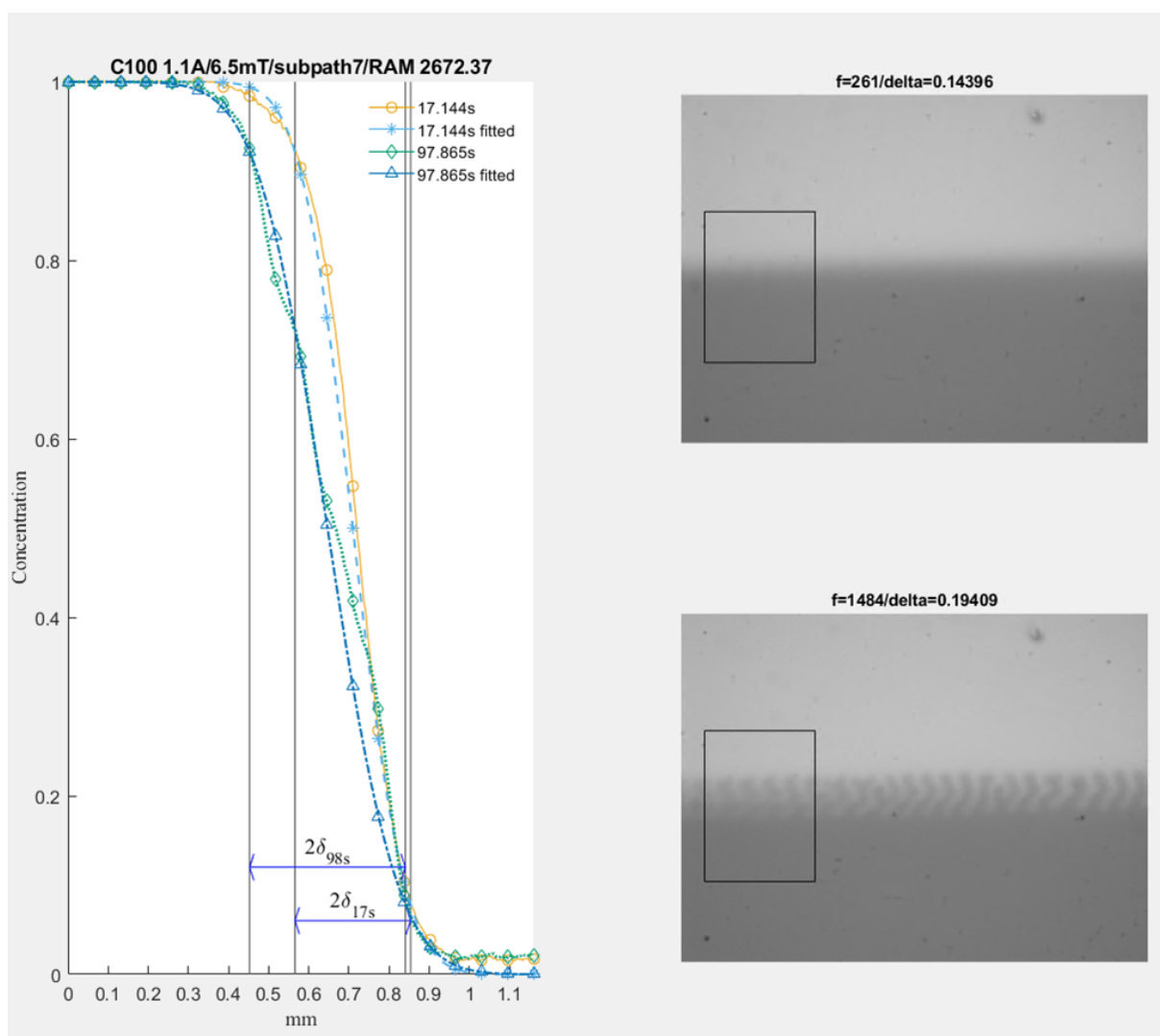
**A.45 Figure:** Data processing.

An example of result validation that D_{exp} for a slope of the linear fit has been achieved when processing the data for the information about δ_{MC} is demonstrated in figure A.46. Here the experiment has been recorded since the syringe pumps have been turned off. Vertical black lines indicate the moments when the magnetic field has been switched on and of. So the actual experiment time is the region between these lines. Before that the fluids have been diffusing. The experiment is fitted linearly over the diffusion period, thus

value of D_exp is obtained. Later the actual experiment is also fitted with linear fit. Here it is visible that optimal time range has been chosen, as both experiment and diffusion fit lines are parallel to each other. If the linear fit for the experiment would have been started earlier, then line with steeper slope would have been obtained, and the value of δ_{MC} would have been underestimated.
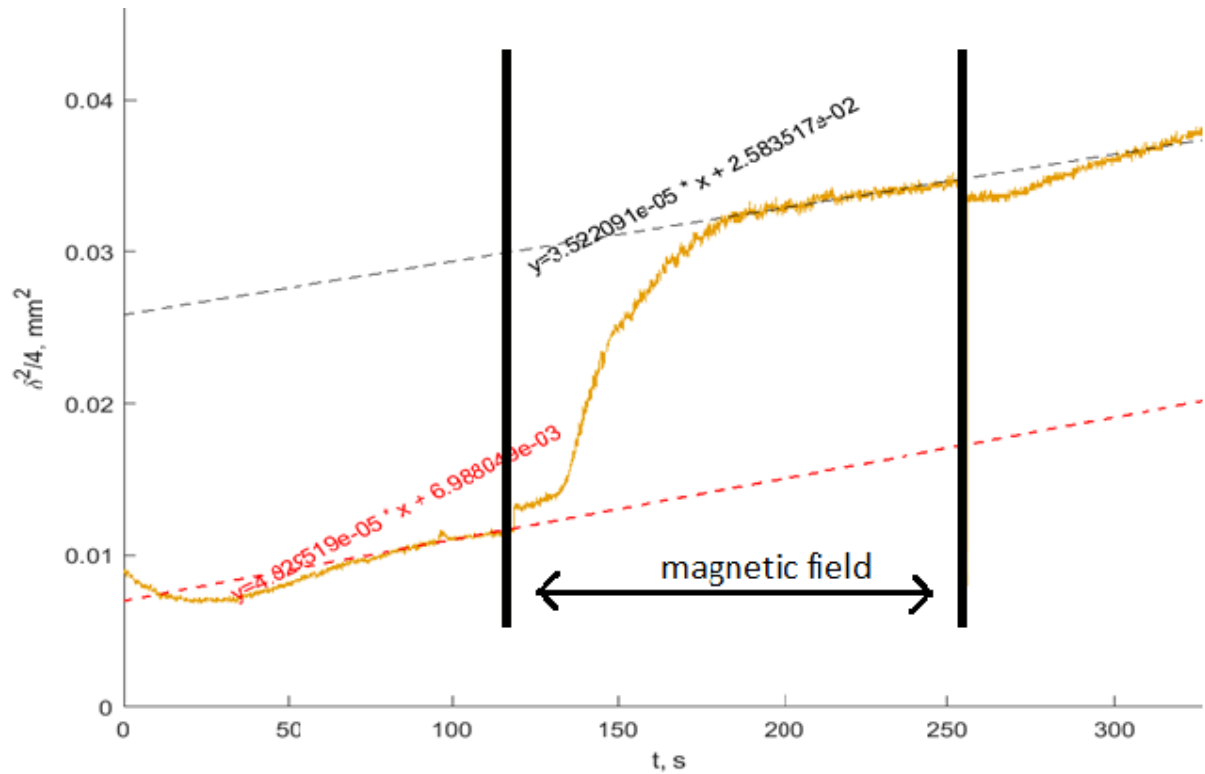
A.46 Figure: Experimental data linear fitting.

An interesting effect can be observed posterizing the picture of an experiment as demonstrated in figure A.47. The original picture is processed so that the regions with the same average pixel intensity are represented with the same tone of gray. Here the original picture is divided in 8 colors. As the intensity plot is associated with concentration plot, the concentration distribution in the fingers can be assumed. It is visible that the tips of the fingers are less concentrated.
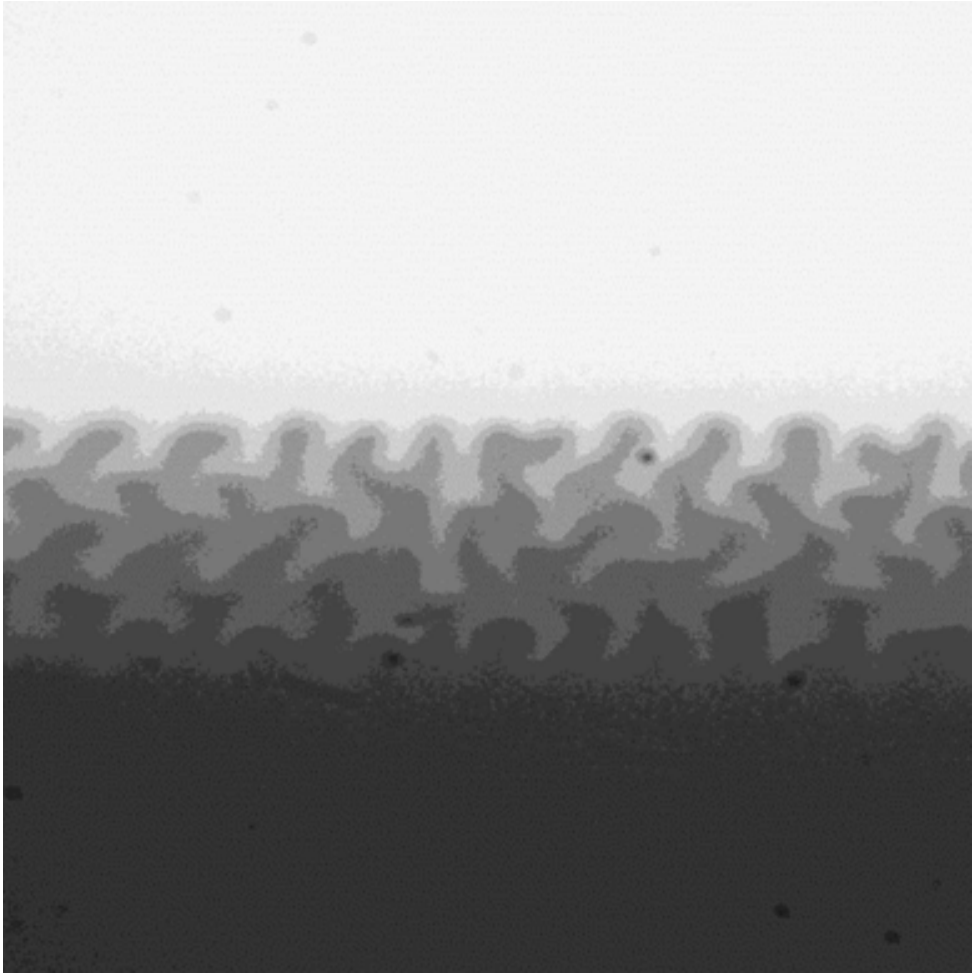
A.47 Figure: Picture of the instability posterized.

A.3 Authors publications

Part of the results of this thesis is included in publication about gravity effects on magnetic micro-convection [25]:

G. Kitenbergs, A. Tatuļčenkovs, L. Puķina, A. Cēbers, "Gravity effects on mixing with magnetic micro-convection in microfluidics", *The European Physical Journal E.*, **2018**, *Vol. 41*, pages 138.

These results are included in the main text of this thesis with kind permission of The European Physical Journal (EPJ).

Another publication that focuses on micro-convective mixing with initially stabilised fluids is prepared [26]:

L. Puķina-Slava, A. Tatuļčenkovs, A. Cēbers, G. Kitenbergs, "How gravity stabilises instability: the case of magnetic micro-convection", *arXiv:2310.15323*, **2023**.

The pre-mixed layer's thickness between the mixing fluids is explored in a publication that is prepared:

L. Puķina-Slava, A. Tatuļčenkovs, A. Cēbers, G. Kitenbergs, "The effects of initially smeared interface on the magnetic micro-convection".